isvr Institute of Sound and Vibration Research

Application and Validation of the TWINS Model for Japanese Railways

T. Kitagawa and D.J. Thompson

ISVR Technical Memorandum 919

September 2003

University of Southampton

SCIENTIFIC PUBLICATIONS BY THE ISVR

Technical Reports are published to promote timely dissemination of research results by ISVR personnel. This medium permits more detailed presentation than is usually acceptable for scientific journals. Responsibility for both the content and any opinions expressed rests entirely with the author(s).

Technical Memoranda are produced to enable the early or preliminary release of information by ISVR personnel where such release is deemed to the appropriate. Information contained in these memoranda may be incomplete, or form part of a continuing programme; this should be borne in mind when using or quoting from these documents.

Contract Reports are produced to record the results of scientific work carried out for sponsors, under contract. The ISVR treats these reports as confidential to sponsors and does not make them available for general circulation. Individual sponsors may, however, authorize subsequent release of the material.

UNIVERSITY OF SOUTHAMPTON

INSTITUTE OF SOUND AND VIBRATION RESEARCH

DYNAMICS GROUP

Application and Validation of the TWINS Model for Japanese Railways

by

T. Kitagawa and D.J. Thompson

ISVR Technical Memorandum No: 919

September 2003

Authorised for issue by
Professor M.J. Brennan
Group Chairman

ABSTRACT

Railway noise is radiated from various track and vehicle components, such as the rail, the wheel, the engine or traction motors and other components. For the conventional narrow-gauge lines in Japan, the noise generated by railway vehicles mainly consists of rolling noise and noise from the driving devices in the motor vehicles (traction-motor fan noise and gear noise). Traction-motor fan noise generally has a much greater contribution to the total noise than rolling noise has. However, by the introduction of a newly developed traction-motor, the traction-motor fan noise has been considerably reduced in new vehicles and the relative contribution of rolling noise for the total noise is therefore larger than before. Now, in order to reduce the noise at the reference point, a better understanding of rolling noise is required.

This report describes the procedures and results of the application and validation of the prediction model of wheel/rail rolling noise generation, the TWINS model, for Japanese railway wheels and tracks. It consists of a main synthesis report of six pages which is provided with 6 appendices presenting the detailed results.

A comparison in terms of noise and rail vibration has been carried out for 6 wheel/rail combinations of Japanese railways. Globally, the TWINS model gives reliable noise predictions in dB(A). The mean difference in noise between the predictions and measurements are in the range of -/+ 1.5 dB. A linear relationship between the predictions and measurements appears in the train speed range considered of 70-120 km/h.

In terms of noise spectra, the TWINS model show good agreement with the measurements. The average difference between the predictions and measurements in 1/3 octave bands is about 1 dB in the frequency range of 250- 8000 Hz.

As supplemental studies, an attempt to estimate the effect of wheel load on noise and rail vibration has been made by using the TWINS model. The TWINS model shows similar trends to the measurements.

Through the validation work, it has shown that the TWINS model is constructed on the basis of robust theories. However, in this report, the validation of the TWINS model has been confirmed only in some cases as a first step. Further tests and studies are required to cover a wider range of rolling stock and track.

CONTENTS

Main report

PAGE

1 INTRODUCTION 1

1.1 BACKGROUND 1

1.2 DESCRIPTION OF TWINS 1

1.2.1 Excitation 3

1.2.2 Wheel-rail interaction 3

1.2.3 Wheel response 3

1.2.4 Rail response 4

1.2.5 Sleeper response 4

1.2.6 Radiation 5

1.3 RECENT RESEARCH ON TRACK VIBRATION 5

1.4 CONTENTS OF THIS REPORT 6

2 MEASUREMENT DESCRIPTION 8

2.1 TRACK AND WHEEL CONDITIONS 8

2.2 MEASUREMENTS 8

2.3 ARRANGEMENT OF MEASUREMENTS 9

3 PARAMETER TUNNING 11

3.1 TUNING OF THE TRACK PARAMETERS 11

3.2 TRACK DECAY RATES 11

3.3 TUNING OF THE WHEEL PARAMETERS 12

4. CALCULATION PARAMETERS 13

4.1 EXCITATION OPTIONS 13

4.2 WHEEL AND RAIL VIBRATION OPTIONS 13

4.3 RADIATION OPTIONS 14

4.4 DISTRIBUTION OF MEASURED RESULTS 14

5 GLOBAL COMPARISONS 16

5.1 NOISE PREDICTED WITH BI-BLOC SLEEPER MODEL 16
5.1.1 Comparison of overall sound levels *16*
5.1.2 Comparison of spectral results *19*
5.2 NOISE PREDICTED WITH MONO-BLOC SLEEPER MODEL 26
5.2.1 Comparison of overall sound levels *26*
5.2.2 Comparison of spectral results *29*
6 INTERMEDIATE COMPARISONS 41
6.1 VIBRATION PREDICTED WITH BI-BLOC SLEEPER MODEL 41
6.2 VIBRATION PREDICTED WITH MONO-BLOC SLEEPER MODEL 44
7 SUPPLEMENTARY STUDIES 47
7.1 MEASUREMENT DESCRIPTION 47
7.2 CALCULATION DESCRIPTION 48
7.3 COMPARISON OF OVERALL LEVELS 50
7.4 COMPARISON OF SPECTRAL RESULTS 52
8 SUMMARY OF THE MAIN RESULTS 56
9 REFERENCES 59
A TRACK CHARACTERIZATION MEASUREMENTS 62
A1 TRACK STUDIED 62
A2 MEASUREMENT PROCEDURE 62
A3 POINT ACCELERANCE 63
A4 TRACK DECAY RATE 64
A5 OTHER PARAMETERS 65
B WHEEL CHARACTERIZATION 85
B1 WHEEL NATURAL FREQUENCIES AND MODE SHAPES 85
B2 FREQUENCY RESPONSE FUNCTION 86
C CALCULATION PROCEDURE 121
C1 CALCULATION PROCEDURE 121

C2 REFERENCE ROUGHNESS 121
C3 CONTACT FILTER 126
C4 TRAIN SPEED 130
C5 DISTRIBUTION OF MEASURED RESULTS 132
C6 CALCULATION PARAMETERS 134
C6.1 Excitation and interaction parameters 134
C6.2 Radiation parameters 134

D GLOBAL COMPARISONS 136

D1 CONTINUOUS TRACK MODEL WITH BI-BLOC SLEEPER 136
D2 PERIODIC TRACK MODEL WITH BI-BLOC SLEEPER 145
D3 CONTINUOUS TRACK MODEL WITH MONO-BLOC SLEEPER 154
D4 PERIODIC TRACK MODEL WITH MODAL SLEEPER 163

E INTERMEDIATE COMPARISONS 172

E1 RAIL VIBRATION PREDICTED WITH RODEL AND TINF MODELS WITH BI-BLOC SLEEPER ... 172
E2 RAIL VIBRATION PREDICTED WITH RODEL AND TINF MODELS WITH MONO-BLOC SLEEPER 181

F SUPPLEMENTARY STUDIES 189

F1 EFFECT OF AXLE LOAD ON CONTACT FILTER EFFECT 189
F2 GLOBAL COMPARISON 193

1 INTRODUCTION

1.1 Background

Railway noise is radiated from various track and vehicle components, such as the rail, the wheel, the engine or traction motors and other components. For the conventional narrow-gauge lines in Japan, the noise generated by railway vehicles mainly consists of rolling noise and noise from the driving devices in the motor vehicles (traction-motor fan noise and gear noise). Rolling noise is generated by a vertical vibration of the wheel and rail, which is induced by a relative displacement between them due to the roughnesses on the wheel and rail surfaces. Traction-motor fan noise is aerodynamic noise generated by the fan that cools the traction motor.

Figure 1.1 shows the contributions of the two noise components at the reference point, which is located at 12.5m away from the centreline of the nearest track [1-3]. The sound power is shown on a linear scale, although the totals are stated in dB. The traction-motor fan noise was the most dominant source in the past (see Figure 1.1, Train A). However, in new vehicles, the traction-motor fan noise has been considerably reduced by the introduction of a newly developed traction-motor, and the relative contribution of rolling noise for the total noise is therefore larger than before (see Figure 1.1, Train C). Now, in order to reduce the noise at the reference point, a better understanding of rolling noise is required.

1.2 Description of TWINS

Theoretical models of wheel/rail rolling noise generation have mainly been developed by Thompson [4-14]. Subsequent research resulted in the implementation of the prediction model in a computer program, TWINS [15]. Figure 1.2 shows a schematic diagram of the theoretical model on which TWINS is based. This model is explained in the following sub-sections.

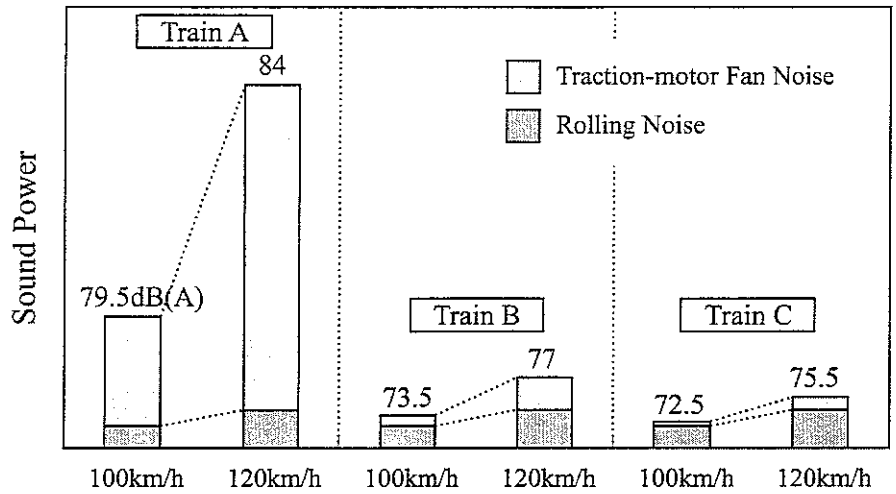

Figure 1.1 Noise of the conventional narrow-gauge lines in Japan [1-3].

(Ground condition: embankment (1.5m in height), ballast track, plain barrier (2m in height).

Car condition: 10 cars (motor vehicle: 6, trailer: 4), gear ratio: 6.

Train A: motors with an outer fan. Train B: motors with an inner fan.

Train C: motors with a high pressure inner fan)

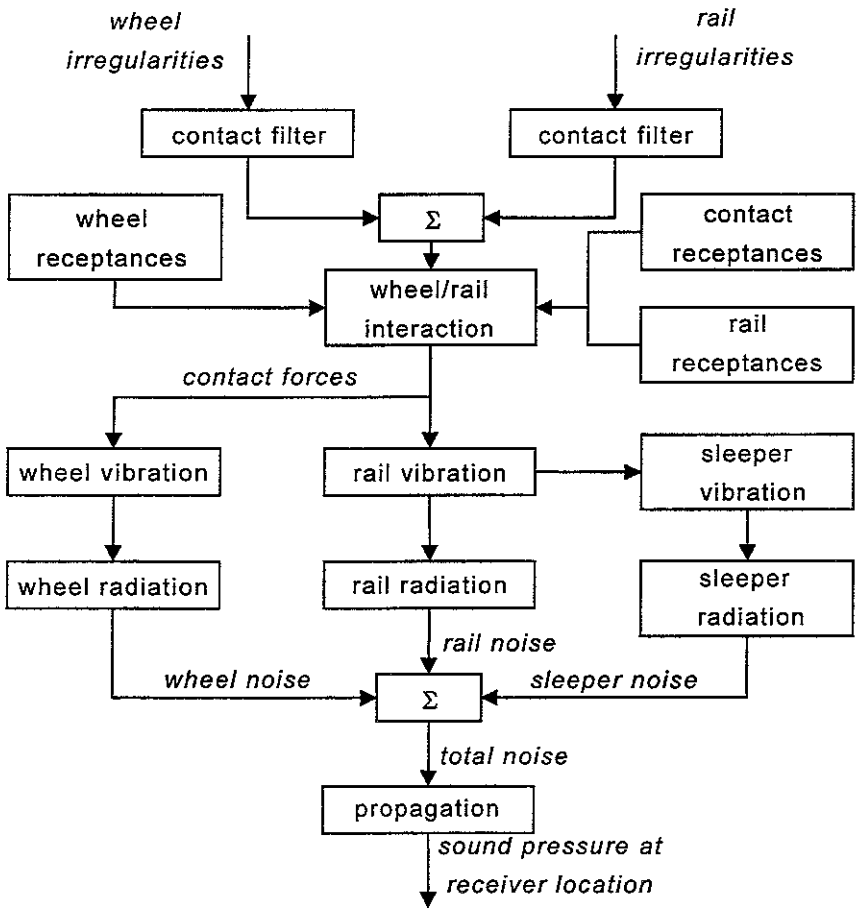

Figure 1.2 Flow diagram of TWINS calculation model [15]

1.2.1 Excitation

The excitation of the wheel-rail system is caused by the surface roughnesses of wheel and rail. In order to estimate the surface roughnesses, the spatial data on a series of multiple parallel lines on the surface of the rail and/or wheel are measured with a point sensor, and an equivalent roughness is calculated by the point-reacting spring model [16-17]. In the model, the wheel and rail surfaces are represented by an array of non-linear springs to simulate dynamic properties in the contact patch. In this model, included in TWINS, the following three features are included in the analysis of the roughness:

(1) the removal of small holes in the surface,

(2) the attenuation for wavelengths shorter than the contact patch length

(3) the correlation of the variations in the roughness across the width of the contact patch.

However, TWINS can also be used to calculate the response to a unit roughness, and previously determined roughness spectra can be combined with these results to give the overall noise in a given situation.

1.2.2 Wheel-rail interaction

The wheel/rail interaction model calculates the vertical and lateral displacements of the wheel and the rail using the roughness estimated by the excitation part of the model. In the model, contact elements linking wheel and rail are derived from

(1) linearized Hertzian contact stiffness in the vertical direction, and

(2) a creep force element in the lateral direction, which is represented by a damper connected to a spring in series.

1.2.3 Wheel response

The modal characteristics of a railway wheel are derived from a finite element model, and the frequency responses of the wheel are predicted in TWINS by combining the modal characteristics using the modal summation theory [18]. Modal damping should be defined either from measurements or based on experience of similar wheels. It is possible to neglect the axle, constraining the inner edge of the hub. However, for the modal damping ratio, the value for the radial mode with one nodal circle should then be set to 1 [19]. Wheel rotation

effects are also included.

1.2.4 Rail response

Three theoretical models of the dynamic behaviour of railway track in the frequency range 50-6000 Hz are considered in TWINS [4, 7, 10-13]. All models have two elastic layers, which correspond to rail pads and ballast. The characteristics of the three models may be stated, as follows.

(1) Continuous supported beam model (rodel model):

The track is considered as a Timoshenko beam on a continuous support, which is composed of a resilient layer (the rail pads), a mass layer (the sleepers) and a second resilient layer (the ballast). The two resilient layers are taken as springs with hysteretic damping. The same model is used for vertical and lateral directions, and the cross-coupling effect between vertical and lateral directions is estimated by using a parameter, X. The cross accelerance A_{xy} can be written as

$$A_{xy} = X\left(A_x A_y\right)^{\frac{1}{2}} \qquad (1.1),$$

where A_x, A_y are vertical and lateral accelerances. The value of X (typically equivalent to -12 dB) is obtained from experimental data from tracks.

(2) Periodically supported beam model (tinf model):

The track is considered as a Timoshenko beam on periodic supports, which consist of spring-mass-spring systems as above. The location of the forcing point can be selected at any point within a sleeper span. The cross accelerance is again expressed by equation (1.1).

(3) Rail model including cross-section deformation (perm model):

The rail is modelled by using multiple finite elements, and the foundation is taken as a continuous support. The rail vibrations are analyzed by combining the finite element method with periodic structure theory [7].

1.2.5 Sleeper response

In either of the first two track models described above, the sleeper vibration can be calculated using a beam model, which accounts for modal sleeper behaviour and frequency dependent ballast properties (stiffness and damping) [20-21]. The results of the calculation

are used as an alternative to the mass-spring description of sleeper and ballast.

1.2.6 Radiation

In TWINS, the sound power is calculated by combining the vibration spectra with radiation efficiencies in one-third octave bands. For the wheel, the radiation efficiencies for both axial and radial vibrations have been derived from boundary element analysis [22]. These have been used to derive simple analytical models that are used in TWINS. For the rail, an equivalent source model (proluf model) has been developed. This is a two-dimensional model, although the three-dimensional effects at low frequency and with high decay rate are included as correction terms [23]. For the sleeper, a model is based on a baffled rectangular piston, and the radiation efficiency obtained is close to 1.

The ground reflection effects that allow for a frequency dependent complex ground impedance can also be introduced in the radiation models in the calculation of sound pressure at a receiver location.

1.3 Recent research on track vibration

Wu and Thompson have developed a methodology for studying rail vibration [24-31], allowing for effects not included in TWINS.

In order to develop a theoretical model for rail vibration, the rail is modelled by taking account of significant cross-sectional deformation of the rail in vertical direction at high frequencies, which is caused by foot flapping [24]. In the model, the rail is considered as two infinite Timoshenko beams in the rail axis direction. The two Timoshenko beams correspond to the head and the foot of the rail, and are connected by continuously distributed springs to allow relative motion between the two beams. The cross-section of the double beam model is simplified to a single-degree-of-freedom system, and the cross-sectional deformation is represented by this double beam model. The results show good agreement with the measurement data in terms of point receptance and vibration decay rate along the rail.

A new model for studying the lateral vibration of a rail has also been developed [25-26]. This model allows for all the essential cross-sectional deformations caused by the lateral

vibration, including rail head bending and torsion, rail foot bending and torsion, and the relative motion between the rail head and foot. In this model, the whole rail is divided into three parts: the head and the foot are represented by two infinite Timoshenko beams which can be subjected to both bending and torsion, and the web are replaced by numerous beams along the rail connecting the head and foot. Using the model, quite good agreement between the predictions and measurement data are given in terms of accelerance.

The sleeper spacing and the ballast stiffness should be treated as random variables within certain limits. The effects of the random sleeper spacing and ballast stiffness on the track vibration have been investigated through numerical simulations [27]. Here, a railway track is simplified to an infinite Timoshenko beam with a finite number of discrete supports in order to represent the vertical vibration behaviour. It is shown that the point receptance and the vibration decay rate of the rail are distributed in a certain region, and that the phenomenon of the pinned-pinned resonance is suppressed by the random sleeper spacing.

Two effects of the presence of multiple wheels on the rail are investigated [28-31]. These effects are the influence of wave reflections in the rail induced by the multiple wheel/rail interactions, and the local stiffening of the railway foundation due to the preload of the vehicle weight. It is shown that the preloading and wave reflections have significant effects on the rail receptance and the wheel/rail interaction force. However, the two effects are much smaller in the overall vibration and noise of the rail. This is due to the fact that the effects of the point receptance and wheel/rail interaction force largely cancel each other out.

These various effects have not yet been included in TWINS, although there are plans to include them in the future.

1.4 Contents of this report

The purpose of this report is to describe the procedures and results of the application and validation of the TWINS model for Japanese railway wheels and tracks.

In section 2, a brief description of the measurement campaign will be given. Then, tuning of the track and wheel models will be described in section 3, and calculation parameters will be given in section 4. In section 5, global comparisons for each wheel/rail

configuration will be presented showing the relative contributions of wheel, rail and sleeper to the total noise. After this, intermediate comparisons (rail vibration) will be carried out in section 6. After confirming the TWINS validation, the effects of wheel load on noise and rail vibration will be discussed as supplemental studies in section 7.

2 MEASUREMENT DESCRIPTION

In this section, the measurement campaign carried out for the validation of the TWINS model is described briefly.

2.1 Track and wheel conditions

Running measurements were carried out for a single track type [32-33], as listed in Table 2.1. This is located on a narrow-gauge line, with track gauge 1.067m.

Table 2.1 Track condition

Track	Location	Rail type	Sleeper	Foundation
JR1	Tokaido Line	60	monobloc concrete	ballast

The measurements were carried out for 6 wheels, as listed in Table 2.2. The tested speeds are also listed in Table 2.2.

Table 2.2 Wheel condition

Wheel	Radius (mm)	Mass (kg)	Braking	Description	Train speed*) (km/h)
A	405	314	disc and tread braked (resin block)	singly curved web	(70), (100) and 110
B	405	332	tread braked (sinter iron block)	singly curved web	(100) and 110
C	430	314	tread braked (cast iron block)	straight web	100, (110) and (120)
AW	430	292	disc and tread braked (resin block)	doubly curved web	(100) and 110
BW	430	307	tread braked (sinter iron block)	doubly curved web	(70), (100), 110 and (120)
CW	430	292	disc and tread braked (resin block)	doubly curved web	70, 100, 110 and 120

* Train speeds put in brackets are used only for overall A-weighted levels.

2.2 Measurements

For the JR1 track, the measurements were made at two positions during a train pass-by:

- 1 accelerometer on the rail,

- 1 microphone at 2 m from the centre of the track (i.e. 1.431 m from the near rail)

Sound pressure measurements were carried out close to the track. The accelerometer was glued stiffly on the end of the foot of a rail at the mid-span between two neighbouring sleepers, and only vertical vibration was measured. These measurement locations are shown in Figure 2.1.

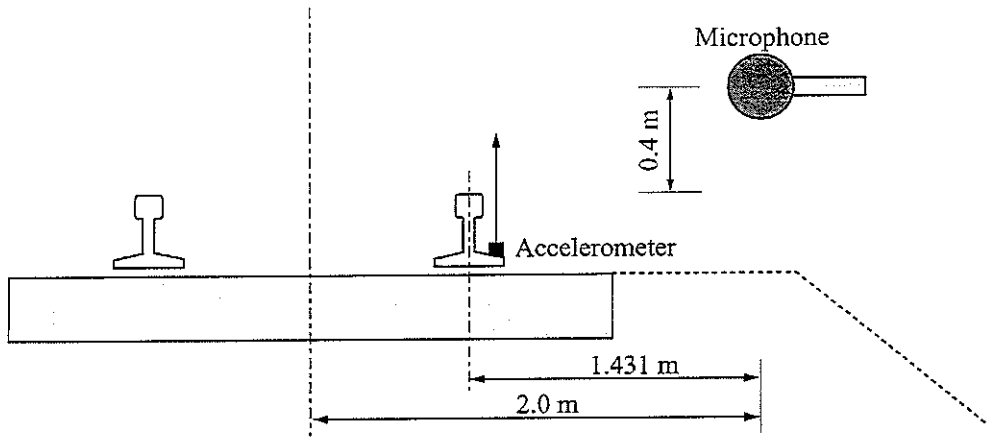

Figure 2.1 Diagram of measuring points

2.3 Arrangement of measurements

Both rail vibration and sound data have been analyzed to give an average level over a distance of travel of 20 m or 10 m. The distance of 20 m corresponds to twice the length of half a coach, and the sound and vibration generated by two adjacent bogies with the same type of wheels are analyzed. The value of 10 m is equal to the length of half a coach, and the sound and vibration data associated with the first bogie of a leading coach or the second bogie of a rear coach are effectively arranged. The averaging length for each wheel type is listed in Table 2.3.

Table 2.3 Averaging length

Wheel	A	B	C	AW	BW	CW
Averaging length*) (m)	10, 20	10, 20	20	20	10, 20	10, 20

* The averaging length is the same as the integration length used in the TWINS calculations.

For the wheel, A-type, C-type, AW-type and CW-type wheels are installed on trailer cars,

and trailer cars radiate mainly rolling noise. Therefore, both noise and rail vibration measurements for each wheel type are suitable for the TWINS validation. B-type and BW-type wheels are installed on motor cars. The noise radiated from motor cars consists of rolling noise and traction-motor fan noise. Traction-motor fan noise generally has a much greater contribution to the total noise than rolling noise has (see Figure 1.1). Therefore, for B-type and BW-type wheels, only rail vibration measurements are considered for the validation.

Regarding with braking system, tread brakes with sinter iron or resin block are not aggressive for the wheel running surface. Therefore, in this report, tread brakes with sinter iron or resin block are assumed to have the same effect on the wheel roughness as disc brakes have. (The actual wheel and rail roughness has not been measured.)

3 PARAMETER TUNNING

3.1 Tuning of the track parameters

Static tests have been performed for five types of Japanese track at the Hino test site [34], in order to determine appropriate calculation parameters. These measurements are described in Appendix A. Of these five tracks, Track B is as used in the running tests.

Figures A2-A11 (Appendix A) show the predicted and measured accelerances in vertical and lateral directions. Calculation parameters are listed in Table A1-A5.

For the vertical accelerance, a comparison of the measured results with the predictions of two models (rodel: continuously supported beam model, tinf: periodically supported beam model) shows good agreement. As the support in the rodel model is continuous, this model cannot predict the behaviour associated with the pinned-pinned effects (where sleeper separation equals half a bending wavelength, about 1000Hz). On the other hand, the tinf model predicts the pinned-pinned resonances and a difference in frequency response between the two measured positions (above a sleeper and at mid-span). Around the pinned-pinned frequency, the rodel model predicts a response which is part way between the response above a sleeper and at mid-span predicted with the tinf model. However, the phenomena associated with the pinned-pinned resonance cannot be seen clearly in the measurements. Therefore, it is not clear whether the tinf model can predict the pinned-pinned effects well for these track types.

For the lateral accelerance, the predictions of both models are lower than the measurements. This is explained by the omission of torsion in the TWINS model. This would be included in the perm track model, but it is not considered here.

3.2 Track decay rates

Figures A12-A16 (Appendix A) show the decay rates of rail vibrations in vertical and lateral directions predicted using the rodel model.

For the vertical vibration, a good agreement is obtained between the predicted and measured decay rates for all tracks. For the decay rate of the lateral vibration, the predicted curve shows a good agreement with the measured results below 400Hz. However, above 500Hz, the predicted decay rates are lower than the measurements. This is due to the fact

that the integral of the measured vibration is carried out over a short length, so that the measured decay rate is not estimated correctly.

3.3 Tuning of the wheel parameters

For eight types of wheel, the modal bases (natural frequencies and mode shape data) have been predicted using the finite element software ANSYS (see Appendix B), and the frequency responses of the wheel are predicted in TWINS by using the modal superposition method. Use is made of the symmetry of the wheel structure, so that the modal bases have been calculated by modelling a quarter wheel with appropriate boundary conditions. Modal frequencies are summarized in Tables B2-B9 in Appendix B. For the modal damping ratio, typical values from a similar wheel are used [4, 6], which are in the range 10^{-2}-10^{-4}. Predicted wheel accelerances are shown in Figures B4-B11 in Appendix B. However, no measured data are available for comparison.

4. CALCULATION PARAMETERS

In this section the options used in the TWINS calculations will be summarized. Full lists of the parameters used for the wheels and tracks are given in Appendix A and B. The other parameters used in this report are listed in Appendix C

4.1 Excitation options

In order to evaluate noise and vibration with the TWINS model, a roughness spectrum is required for input to the calculations. However, rail and wheel roughnesses have not been measured in the measurement campaign. Therefore, the TWINS calculations have been carried out using a "unit roughness" excitation for each frequency. In this excitation, the responses and sound radiation are calculated relative to a unit roughness amplitude (1 m). This means that all calculated parameters have the form of transfer functions. After this, post-processing is carried out using Matlab and Excel, in which a standard roughness spectrum from European railway wheels and rails is added to the noise or vibration spectra predicted with the TWINS model, in 1/3 octave bands. Figures C6-7 (Appendix C) show the reference roughness spectra, in which wheel and rail roughness spectra are combined, including the contact filtering effect [35].

In order to determine the contact positions on the wheel and rail surfaces, their transverse profiles are needed. However, the contact positions have also not been measured for the measurement campaign, so that the exact contact position is unknown. In this report, the nominal contact position on the wheel is chosen as 70 mm from the flange back. For the rail, the centreline might be selected as the nominal contact position. However, it is not necessary that the contact position on the rail should be specified for the rodel and tinf models, since the parameter X (see equation (1.1)) has greater effects in the TWINS calculations.

The calculations have been carried out for train speeds in the range 50-150 km/h, at 10 km/h intervals.

4.2 Wheel and rail vibration options

The wheel responses are calculated including the wheel rotation effects. As mentioned in

section 3.3, the modal bases are predicted using the finite element software ANSYS. For the modal damping, typical values are used in the range 10^{-2}-10^{-4}.

The rail vibrations are predicted with both the rodel and tinf models. For the tinf model, the TWINS calculation is carried out for one excitation position only, which is at mid-span between two neighbouring sleepers. For both models, the rail vibration is accumulated in the range -/+ infinity, and then the track response is averaged over 20 m or 10 m.

4.3 Radiation options

The radiation from each noise component is predicted in the form of sound pressures at one microphone point, corresponding to the position used in the measurements (Figure 2.1).

For the wheel, the sound radiation is calculated using separate radiation efficiencies according to the number of nodal diameters. The rail radiation is predicted with the proluf model. The radiation model is a two-dimensional approach based on replacing the vibrating rail by a series of equivalent line monopoles and dipoles within the surface. For the sleeper, the "baffled plate" option is used.

In TWINS, ground reflections can be included in the radiation models with account of interference between direct and reflected sound. In this report, the reflection effect is neglected, since the sound measurements were made close to the track (see Figure 2.1), and the direct sound has much greater contribution at the microphone point.

4.4 Distribution of measured results

The measured result is not generally constant and the values vary in a certain range, even if the train speed is constant. Before presenting predictions, it is useful to check the standard deviations of the measurement data, which will give the criterion of the accuracy in the predictions. Table 4.1 shows the standard deviations of the measured results for each wheel type. From Table 4.1, it can be seen that the TWINS model can be considered to give adequate predictions as long as differences between measured and predicted levels are smaller than +/-1.5 dB for the noise and +/-2 dB for the rail vibration.

Table 4.1 Standard deviations of measured results (JR1 track, overall A-weighted level)

Wheel type		A	B	C	AW	BW	CW
Standard deviations[a] (dB)	Noise	2.3 (33)[b]	---	1.3 (21)	0.4 (10)	---	1.6 (107)
	Rail vibration[c]	2.3 (33)	2.6 (22)	1.1 (21)	0.4 (10)	1.8 (90)	2.2 (107)

a) See Appendix C

b) Numerical value put in brackets stands for the number of sampled data.

c) The rail vibration is presented in the form of A-weighted velocity levels in the vertical direction.

5 GLOBAL COMPARISONS

In this section the results of the overall and spectral predictions are compared with the measurements.

5.1 Noise predicted with bi-bloc sleeper model

This section presents calculations of noise carried out using:

- the continuous track model (rodel model) and the periodic track model (tinf model)
- bi-bloc sleeper
- calculated track decay rates

In the "bi-bloc" sleeper model, sleeper is regarded as a rigid mass

5.1.1 Comparison of overall sound levels

Figures 5.1-5.2 show the predicted noise levels plotted against the measured levels in terms of A-weighted levels. The individual points represent one of the 4 wheel/track combinations. The solid line corresponds to the mean difference between predictions and measurements (mean -0.9 dB for the rodel model and +1.6 dB for the tinf model). The dashed lines show a range of +/- one standard deviation (standard deviations of 2.6 dB and 2.4 dB respectively). Using either track model, it can be seen that the overall trends are well predicted, although the rodel model gives better predictions than the tinf model does.

Figures 5.3-5.4 show the total noise predicted minus measured noise in dB(A) for each wheel/track combination. In Figures 5.3-5.4, the 'error bar' shows a range of +/- one standard deviation for each condition.

For the rodel model, it can be seen that most of the results for the 12 wheel/track/speed combinations are between +1.5 dB and -1.5 dB. The overall predictions show good agreement with the measured results. However, the results are somewhat under-predicted.

For the tinf model, most of the results are over-predicted, and are greater than +1.5 dB. The results of the tinf model show worse agreement with the measured results than those of the rodel model. This is probably due to the fact that the predictions of the tinf model are carried out at mid-span only, and the fact that the rail decay rates are underestimated at high frequency with this model.

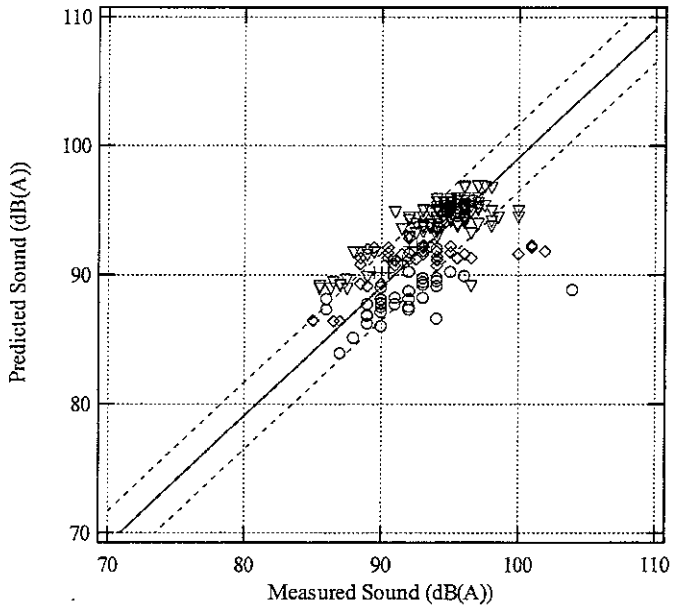

Figure 5.1 Predicted noise plotted against measured noise for all case (rodel, bi-bloc sleeper, ◇: A-type wheel, ○: C-type wheel, +: AW-type wheel, ▽: CW-type wheel)

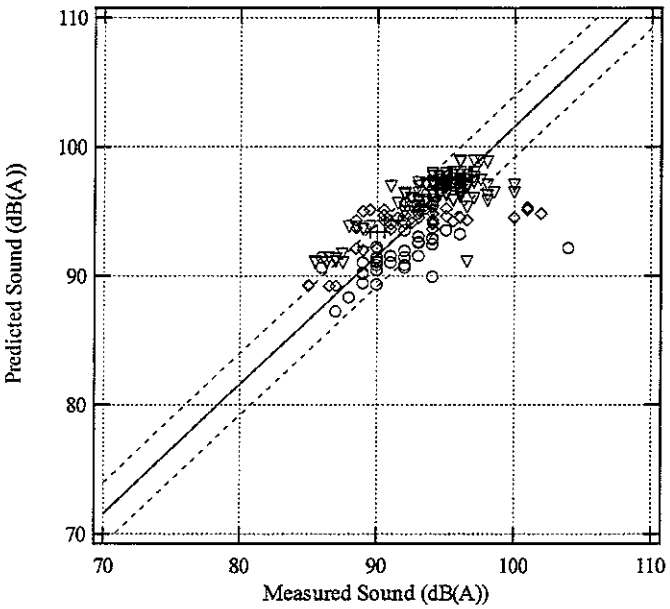

Figure 5.2 Predicted noise plotted against measured noise for all case (tinf, bi-bloc sleeper, ◇: A-type wheel, ○: C-type wheel, +: AW-type wheel, ▽: CW-type wheel)

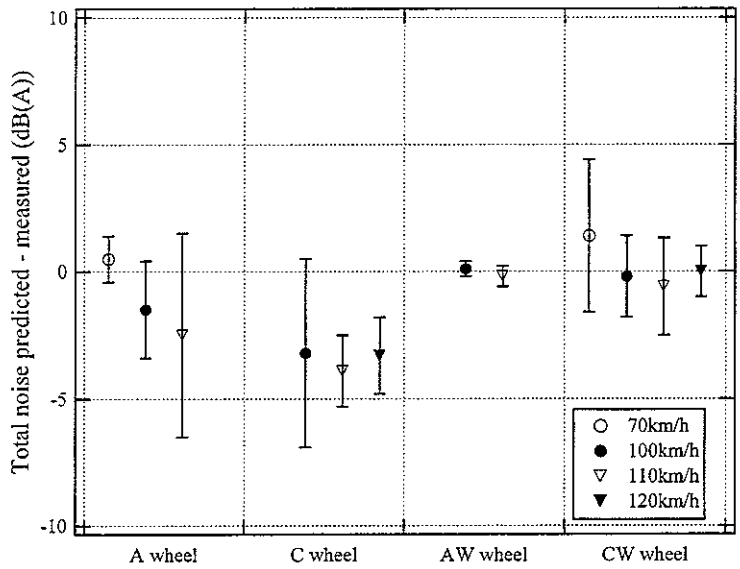

Figure 5.3 Total predicted noise minus measured noise in dB(A)

(rodel, bi-bloc sleeper, results are shown for 70, 100, 110 and 110 km/h)

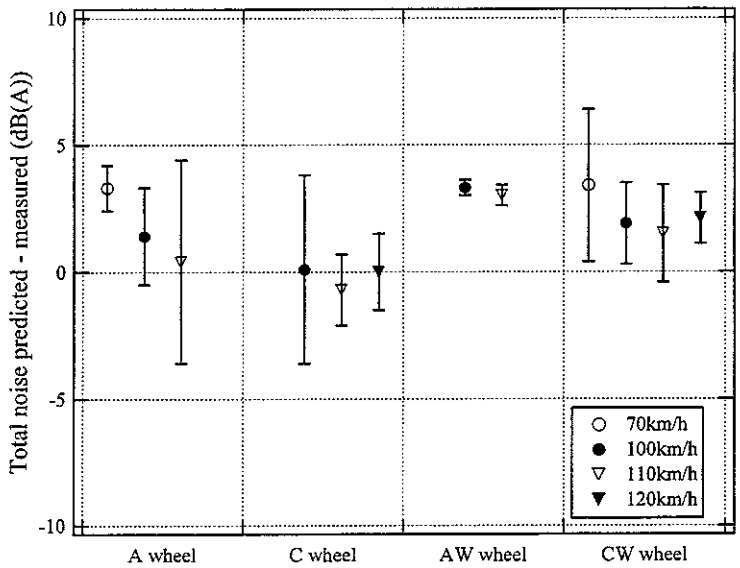

Figure 5.4 Total predicted noise minus measured noise in dB(A)

(tinf, bi-bloc sleeper, results are shown for 70, 100, 110 and 110 km/h)

5.1.2 Comparison of spectral results

Spectral results are only available for 7 of the 12 wheel/track/speed combinations. In order to consider the spectral variation, the difference between predicted and measured noise spectra is constructed for each of the 7 wheel/track/speed combinations. Figures 5.5-5.6 show the spectral differences as the mean and a range of +/- one standard deviation for all cases.

For the rodel model, the predicted results can be seen to be closer to 0. The results are better above 1000 Hz, and are worse below 1000 Hz. The tinf model shows a considerable over-prediction above 1000 Hz, while, below 1000 Hz, the tinf model shows the trends with a peak around 315 Hz and a trough around 630 Hz. These features below 1000 Hz, also seen in the results of the rodel model, occur because the sleeper vibration is not modelled adequately (at these frequencies the sleeper vibration is the dominant source). Figures 5.5-5.6 show a large under-prediction below 250 Hz. This is mainly due to the fact that, as the sound measurements were made close to the track, the measured results were contaminated by wind noise, which is generated during train pass-by, at the low frequencies.

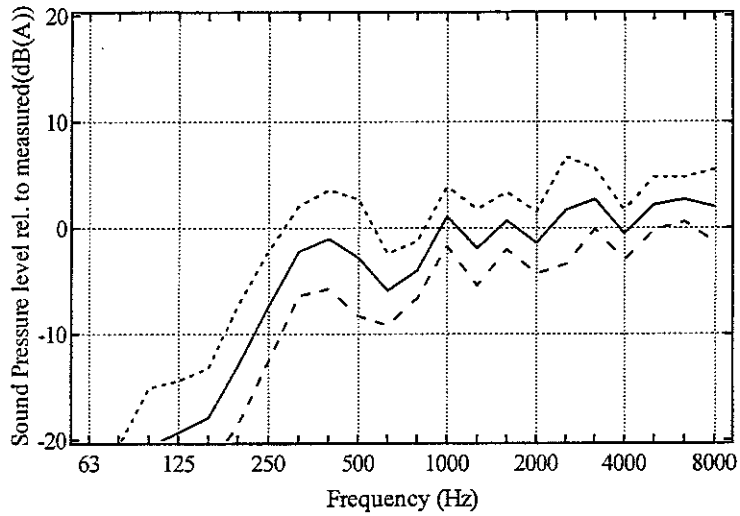

Figure 5.5 Average differences between predicted and measured noise spectra for all cases. (rodel, bi-bloc sleeper, ——: mean, ……: mean +std deviation, - - - - - :mean-std deviation)

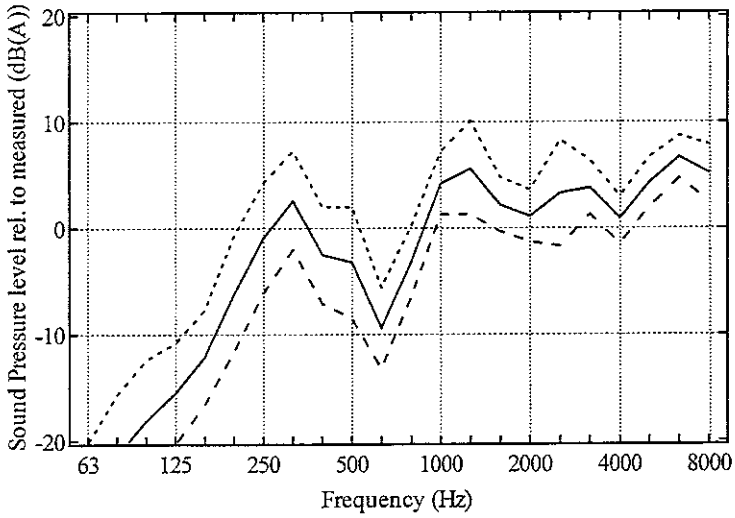

Figure 5.6 Average differences between predicted and measured noise spectra for all cases. (tinf, bi-bloc sleeper, ———: mean, ……: mean +std deviation, ------: mean-std deviation)

Figures 5.7-5.8 show the total predicted sound pressure level minus measured level for each wheel/track combination and each train speed.

For the rodel model, it can be seen that there are some differences between the results for the different wheels. The results for the C-type wheel can be seen to be close to 0 dB in the frequency range 250-8000 Hz, whereas the results of the other wheels show an under-prediction below 2000 Hz.

For the tinf model, it can be seen that the predictions for the four wheels show similar trends with a peak around 315 Hz and a trough around 630 Hz. This is again due to the fact that the sleeper vibration is not modelled appropriately. The result is worse below 250 Hz. This is again because the measured results were affected by wind noise.

Figures 5.7(d) and 5.8(d) show the results of the only wheel type for which different speeds are available. It can be seen that the difference does not depend on train speed.

Figures 5.9-5.10 show the separate contributions of noise from rail, wheel and sleeper to the total prediction in the form of absolute spectra. The measured spectra are also shown for comparison.

For the rodel model, it can be seen that the sleeper is the important source below around 500 Hz, whilst the wheel is the predominant source above 2000 Hz. In the middle frequencies, the dominant component in the total noise depends on the wheel type. For A

and C wheels, the rail becomes dominant in the middle frequencies. On the other hand, for AW and CW wheels, the wheel has almost the same contribution to the total noise as the rail has between 1000 and 2000 Hz, due to their lower radial natural frequencies (see Appendix B).

For the tinf model, the results show the same trends as above with a peak around 315 Hz and a trough around 630 Hz. This is again due to the inadequacy in modelling of the sleeper vibration. For the contributions of each noise components, the same trends are found that, in the middle frequencies, the dominant component in the total noise depends on the wheel type. It is clear that the sleeper is dominant below around 400 or 500 Hz, whilst the wheel has larger contribution to the total noise above 2000 Hz.

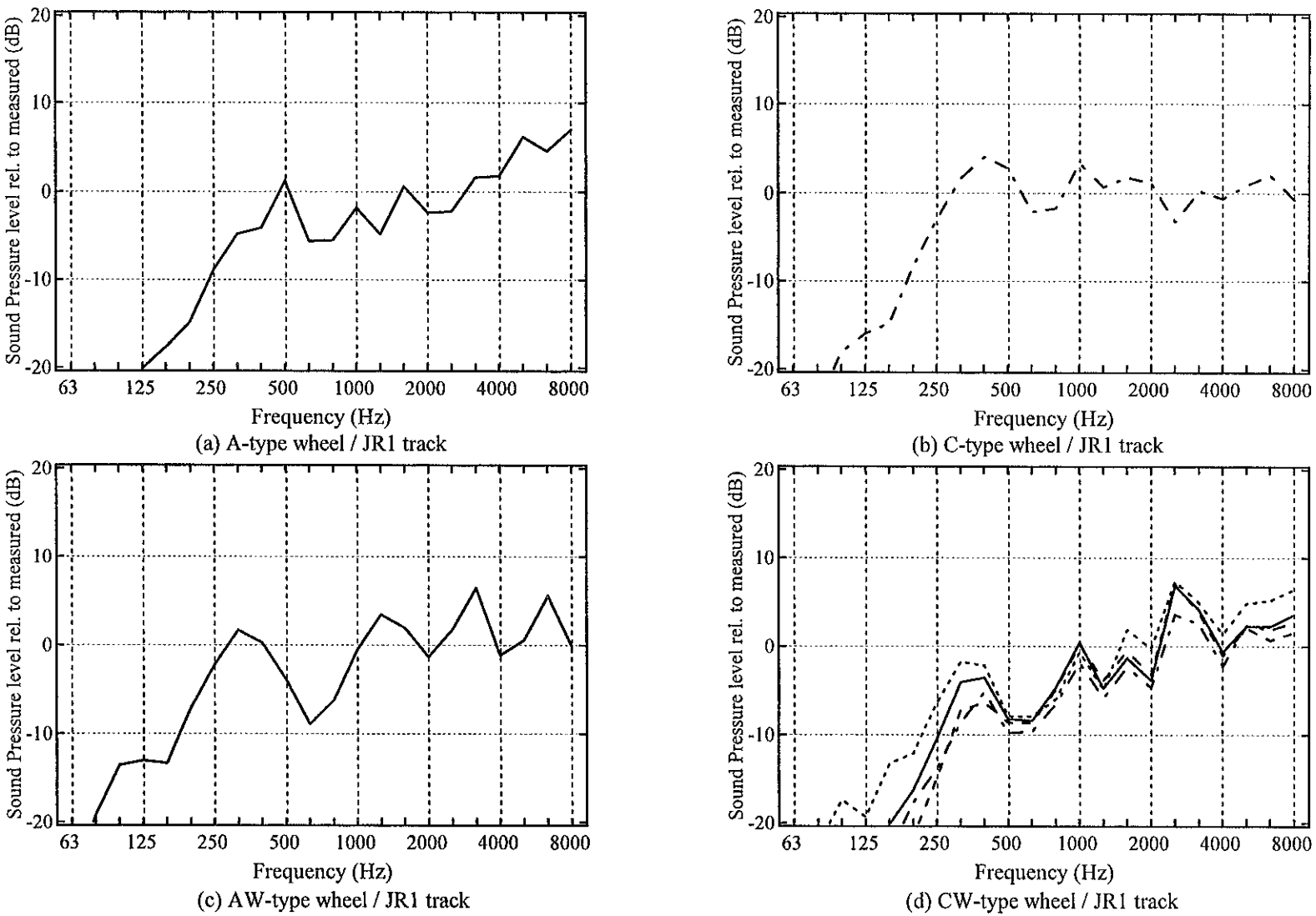

(a) A-type wheel / JR1 track

(b) C-type wheel / JR1 track

(c) AW-type wheel / JR1 track

(d) CW-type wheel / JR1 track

Figure 5.7 Predicted noise minus measured noise for each wheel using rodel model
(JR1 track, bi-bloc sleeper,····· :70 km/h,– – – :100 km/h,—— :110 km/h,– – – :120 km/h)

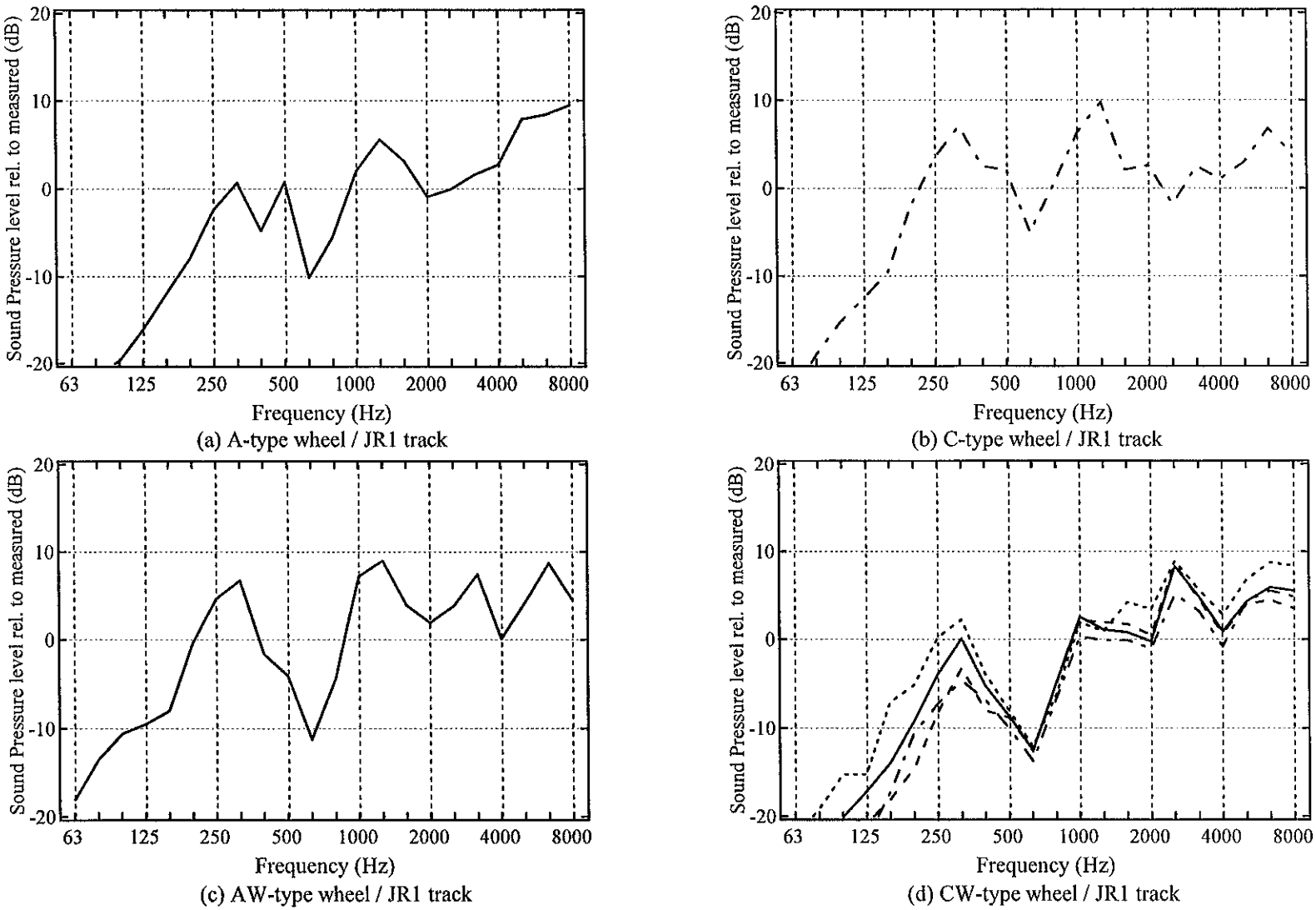

(a) A-type wheel / JR1 track

(b) C-type wheel / JR1 track

(c) AW-type wheel / JR1 track

(d) CW-type wheel / JR1 track

Figure 5.8 Predicted noise minus measured noise for each wheel using rodel model
(JR1 track, bi-bloc sleeper;····· :70 km/h,– – – :100 km/h,——— :110 km/h,– – – :120 km/h)

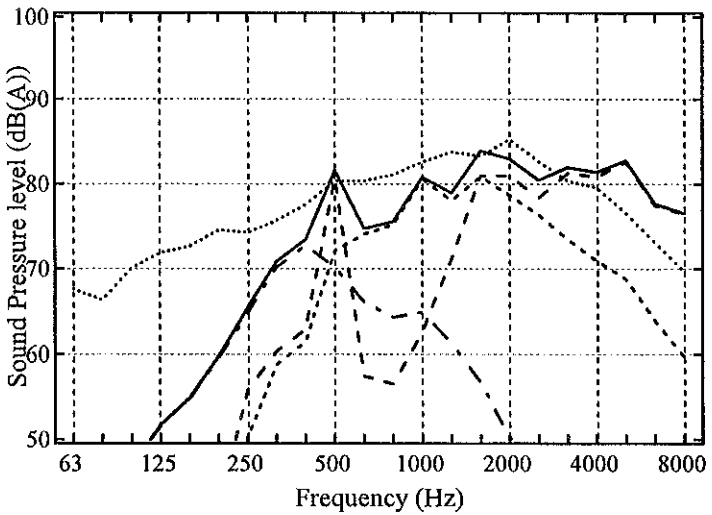

(a) A-type wheel / JR1 track (110km/h)

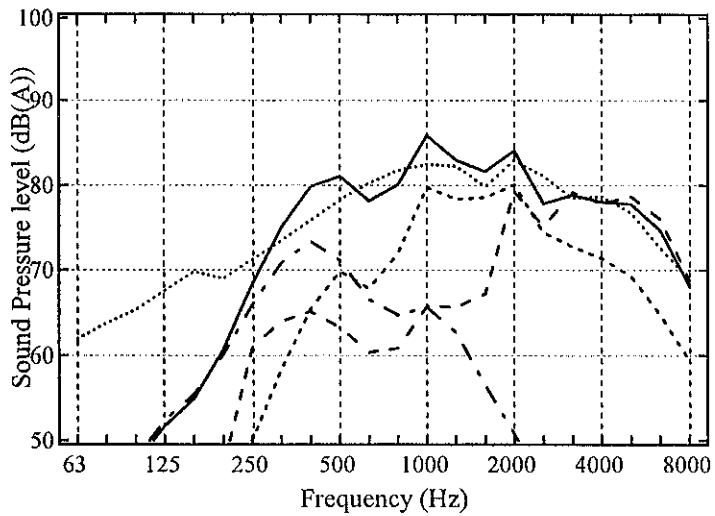

(b) C-type wheel / JR1 track (100 km/h)

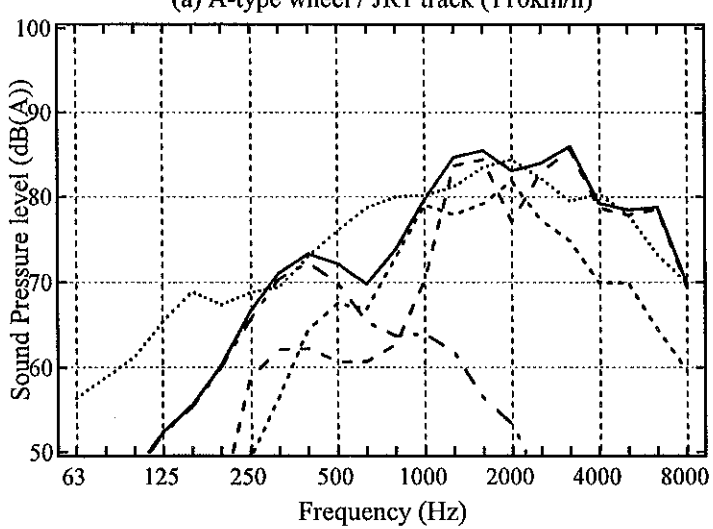

(c) AW-type wheel / JR1 track (110 km/h)

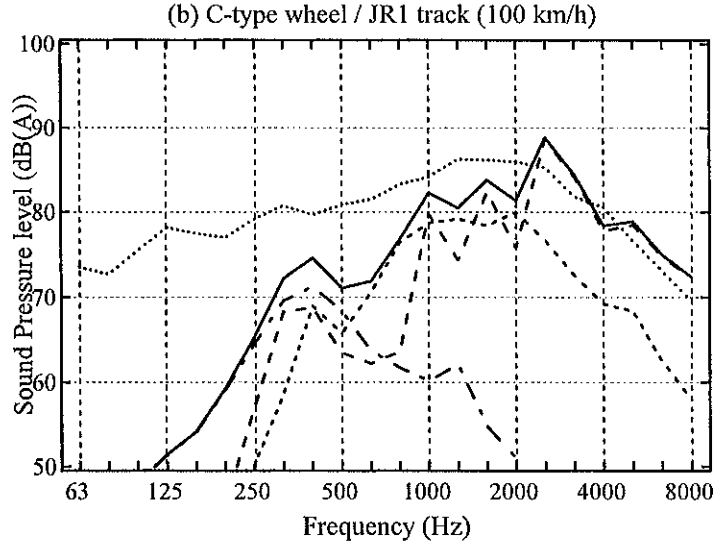

(d) CW-type wheel / JR1 track (110 km/h)

Figure 5.9 Predicted noise and measured noise for each wheel using rodel model

(JR1 track, bi-bloc sleeper, ····· :measured noise, —— :predicted noise, ------ :rail, - - :wheel, - - :sleeper)

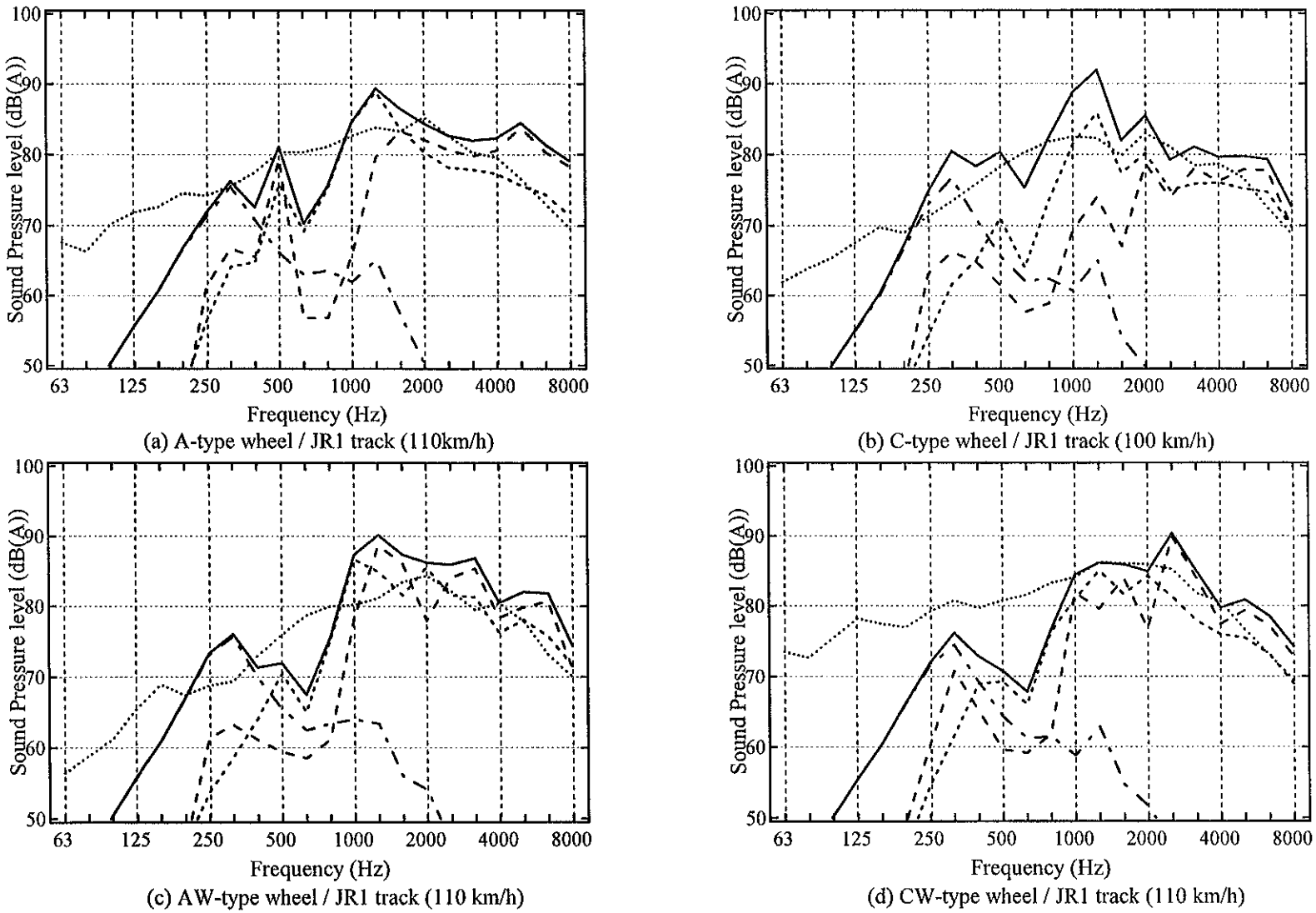

(a) A-type wheel / JR1 track (110km/h)

(b) C-type wheel / JR1 track (100 km/h)

(c) AW-type wheel / JR1 track (110 km/h)

(d) CW-type wheel / JR1 track (110 km/h)

Figure 5.10 Predicted noise and measured noise for each wheel using tinf model

(JR1 track, bi-bloc sleeper, ····· :measured noise, —— :predicted noise,- - - - :rail, - - :wheel, - - :sleeper)

5.2 Noise predicted with mono-bloc sleeper model

In this section, the "mono-bloc" sleeper model is introduced as an alternative of the bi-bloc sleeper model. In the mono-bloc sleeper model, sleeper is considered as a beam. This sleeper model introduces modal sleeper behaviour and frequency dependent ballast properties. Use of this model should improve the prediction at low frequencies (where the sleeper vibration is the dominant source). This section presents calculations of noise carried out using:

- the continuous track model (rodel model) and the periodic track model (tinf model)
- mono-bloc sleeper
- calculated track decay rates

5.2.1 Comparison of overall sound levels

Figures 5.11-5.12 show the predicted noise levels plotted against the measured levels in terms of A-weighted levels. The individual points represent one of the 4 wheel/track combinations. The solid line corresponds to the mean difference between predictions and measurements (mean +0.3 dB for the rodel model and +1.7 dB for the tinf model). The dashed lines show a range of +/- one standard deviation (standard deviations of 2.4 dB and 2.4 dB respectively). For the improved rodel model, the mean value is closer to zero than previously. It is clear that the improved rodel model gives better overall predictions than the rodel model with bi-bloc sleeper does. The introduction of the mono-bloc sleeper model could make the predictions of the rodel model better. For the improved tinf model, the overall predictions cannot be seen to be different from those obtained using the tinf model with bi-bloc sleeper.

Figures 5.13-5.14 show the total noise predicted minus measured noise in dB(A) for each wheel/track combination, with error bars representing the range of +/- one standard deviation.

For the improved rodel model, it can be seen that most of the results for the 12 wheel/track/ speed combinations are in the range +/-1.5 dB. The overall predictions show good agreement with the measured results. Comparing Figure 5.13 with Figure 5.3, it is found that the predictions of the improved rodel model are closer to the measurements than

those of the rodel model with bi-bloc sleeper. Therefore, it is confirmed that, by introducing the mono-bloc sleeper model, the rodel model gives better predictions.

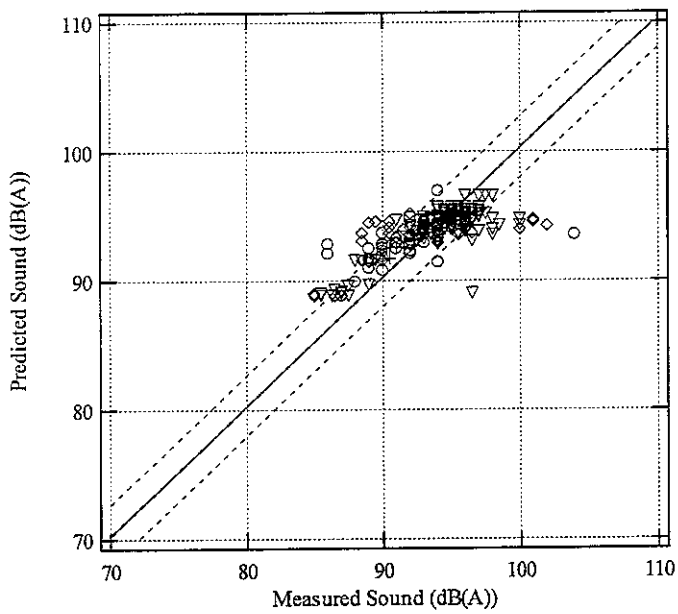

Figure 5.11 Predicted noise plotted against measured noise for all case (rodel, mono-bloc sleeper, ◇: A-type wheel, ○: C-type wheel, +: AW-type wheel, ▽: CW-type wheel)

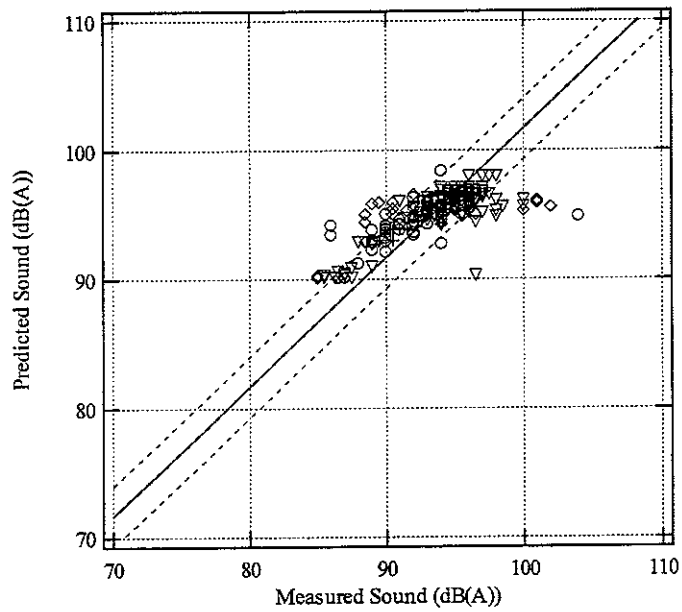

Figure 5.12 Predicted noise plotted against measured noise for all case (tinf, mono-bloc sleeper, ◇: A-type wheel, ○: C-type wheel, +: AW-type wheel, ▽: CW-type wheel)

For the tinf model with mono-bloc sleeper, most of the predictions are still over-predicted. The predictions show poor agreement with the measurements. A comparison of Figures 5.4 and 5.14 shows that the influence of the introduction of the mono-bloc sleeper model depends on wheel/track combination. The results of AW and CW wheels are improved, but the results of A and C wheels become worse.

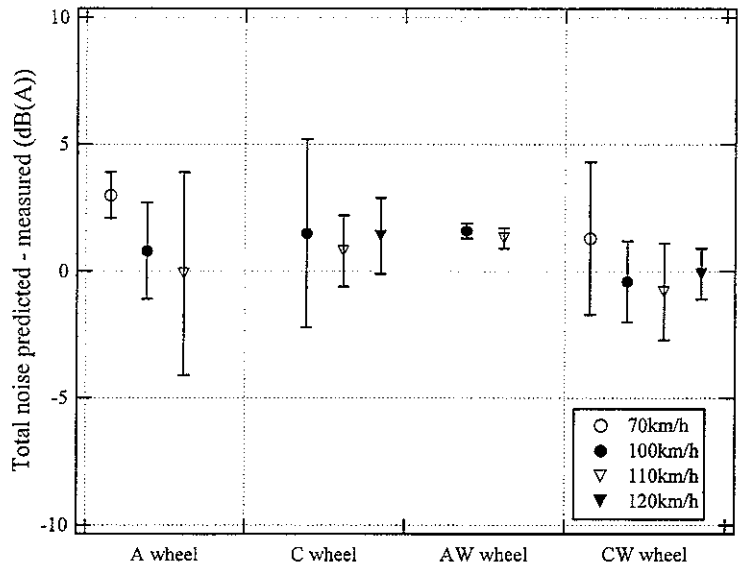

Figure 5.13 Total predicted noise minus measured noise in dB(A)

(rodel, mono-bloc sleeper, results are shown for 70, 100, 110 and 110 km/h)

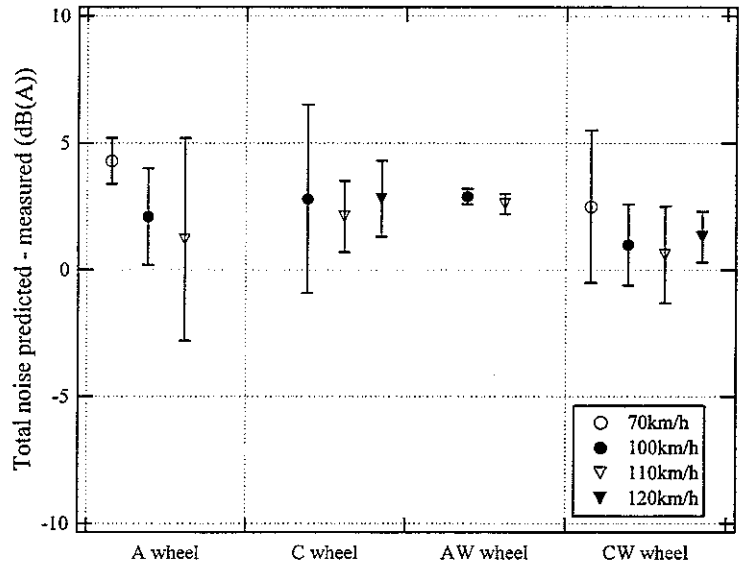

Figure 5.14 Total predicted noise minus measured noise in dB(A)

(tinf, mono-bloc sleeper, results are shown for 70, 100, 110 and 110 km/h)

5.2.2 Comparison of spectral results

In order to consider the spectral variation, the difference between predicted and measured noise spectra is constructed for each of the 7 wheel/track/speed combinations. Figures 5.15-5.16 show the spectral differences as the mean and a range of +/- one standard deviation for all cases.

For the improved rodel model, the results can be seen to be closer to zero, compared with Figure 5.5. The average difference is slightly reduced from -0.9 to -0.8 dB in the whole frequency range of 250-8000 Hz, while the average standard deviation of the results is not changed (3.5 dB). The shape of the results is improved above 250 Hz. The trends with a peak around 315 Hz and a trough around 630 Hz are removed by using the mono-bloc sleeper model. However, the results show a slight under-prediction below 1000 Hz. This is probably because the rail vibration is not predicted correctly. Below 250 Hz, the result is still poor, since the measured results were contaminated by wind noise.

For the tinf model with mono-bloc sleeper, the shape of the results is improved, and the peak at 315 Hz has been eliminated. The average difference is reduced from 1.3 to 0.1 dB in the whole frequency range of 250-8000 Hz. However, the results are under-predicted below 1000 Hz, and over-predicted at high frequencies.

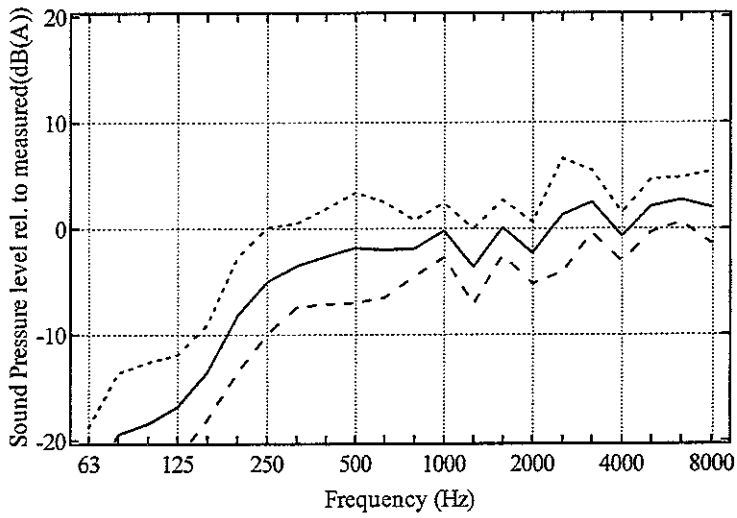

Figure 5.15 Average differences between predicted and measured noise spectra for all cases.

(rodel, mono-bloc sleeper, ——— : mean, ... : mean +std deviation,

------ :mean-std deviation)

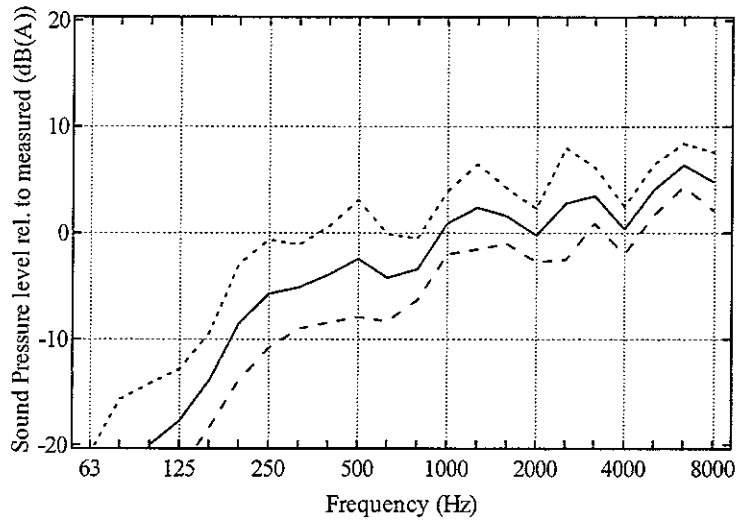

Figure 5.16 Average differences between predicted and measured noise spectra for all cases. (tinf, mono-bloc sleeper,———: mean,.....: mean +std deviation, ------:mean-std deviation)

Figures 5.17-5.18 show the total predicted sound pressure level minus measured level for each wheel/track combination and each train speed.

For the rodel model, it can be seen that there are some differences between the results for the different wheels below 1000 Hz. The results for the C-type and AW-type wheels can be seen to be close to 0 dB in the frequency range above 250 Hz, whereas the results of the other wheels show an under-prediction below 1000 Hz. At high frequencies above 1000 Hz, the results of AW-type wheel vary significantly. This is probably related to the fact that the wheel resonances do not necessarily lie in the correct 1/3 octave band.

For the tinf model, it can be seen that the trends with a peak around 315 Hz and a trough around 630 Hz are also eliminated by introducing the mono-bloc sleeper model. It can be seen that the results of the C-type wheel are close to 0 dB in the frequency range above 250 Hz, whereas the results of the other wheels show an under-prediction below 1000 Hz and an over-prediction above 1000 Hz.

In Figures 5.17(d) and 5.18(d), it is again found that the difference does not depend on train speed.

Figures 5.19-5.20 show the separate contributions of noise from rail, wheel and sleeper to the total prediction in the form of absolute spectra. The measured spectra are also shown

for comparison.

For the two models, it can be seen that the sleeper is the important source below around 400 Hz, whilst the wheel is the predominant source above 2000 Hz. In the middle frequencies, the dominant component in the total noise depends on the wheel type. For A-type and C-type wheels, the rail becomes dominant in the middle frequencies. On the other hand, for AW-type and CW-type wheels, the wheel has almost the same contribution to the total noise as the rail has between 1000 and 2000 Hz.

In Figures 5.17-5.18, the results of A-type, AW-type and CW-type wheels are over-predicted above 2500 Hz, whilst the predictions of C-type wheel show good agreement with the measurements. Some causes may be responsible for this.

(a) As the wheel has greater contribution to the total noise in this frequency range, the wheel radiation model may not give appropriate predictions for the wheels with a singly or doubly curved web. However, the radiation efficiencies above 2000 Hz are equal to 1. The predictions depend on the modal bases (natural frequencies and mode shape data). The over-prediction may occur because the modal bases of the wheels with a singly or doubly curved web have not been predicted well by using the FE model.

(b) In order to predict wheel radiation, the wheel response is calculated at up to six specified positions. The mode shape of the wheels with a singly or doubly curved web is so complicated that the positions chosen may not be appropriate to calculate the average wheel response.

(c) The roughness spectra used may not be suitable at these frequencies, due to the assumed roughness spectra and contact filter used.

The results of the wheels with a singly curved web have previously been well predicted by the TWINS module [19]. Therefore, it is considered that the TWINS model gives reliable predictions at least for the Japanese wheels with a singly curved web. However, it is not clear whether the TWINS model is suitable for the radiation predictions of the wheels with a doubly curved web, although actually one of the wheels in the original validation was also a doubly curved wheel [19]. For (b) and (c), as the wheel characterisation measurements have not been carried out, it is not possible to compare the FEM predictions with the measurements in terms of modal bases. It is necessary to carry out wheel characterisation

measurements in order to confirm the modal bases of the wheels with a singly or doubly curved web.

Figures 5.21-22 show the relative noise levels of each wheel compared with the results of C-type wheel in the form of the transfer function from roughness to noise. These relative noise levels therefore do not include roughness effects. In Figures 5.21-22, it can be seen that C-type wheel is quieter than the other wheels. The results of AW-type and CW-type wheels have similar trends, whereas these trends are not found in the results of A-type wheel. This suggests that the noise radiation of wheel depends roughly on wheel web configuration. Above 2500 Hz, it is seen that, for AW-type and CW-type wheels, the variations of the relative noise levels are large (up to 15 dB). For A-type wheel, the variations of the relative levels are up to about 5 dB above 2500 Hz. Figure 5.23-24 show the relative noise of each wheel to the results of A-type wheel in dB(A). In order to estimate the relative noise of each wheel, the TWINS calculations were carried out for the same roughness spectra. In Figures 5.23-24, the changes in relative noise levels of each wheel do not depend on train speed. C-type wheel is quieter than the others by about 4 dB. It can be seen that the noise of AW-type and CW-type wheels (the wheels with a doubly web) are greater than the other wheels. This is probably due to the fact that these wheels have thin webs.

In Figures 5.21-5.22, the over-predictions above 2500 Hz might occur due to the roughness spectra or the contact filter effects. By changing the contact filter, the attenuation given at each frequency band could be changed, but the relative levels between any wheels will be kept the same as before. This means that, if only the contact filter is arranged in order to make the predictions corresponding to A-type wheel close to the measurements, the predictions of C-type wheel will be worse. Therefore, the over-prediction above 2500 Hz may occur mainly due to the inadequacy of the roughness spectra used for A-type wheel.

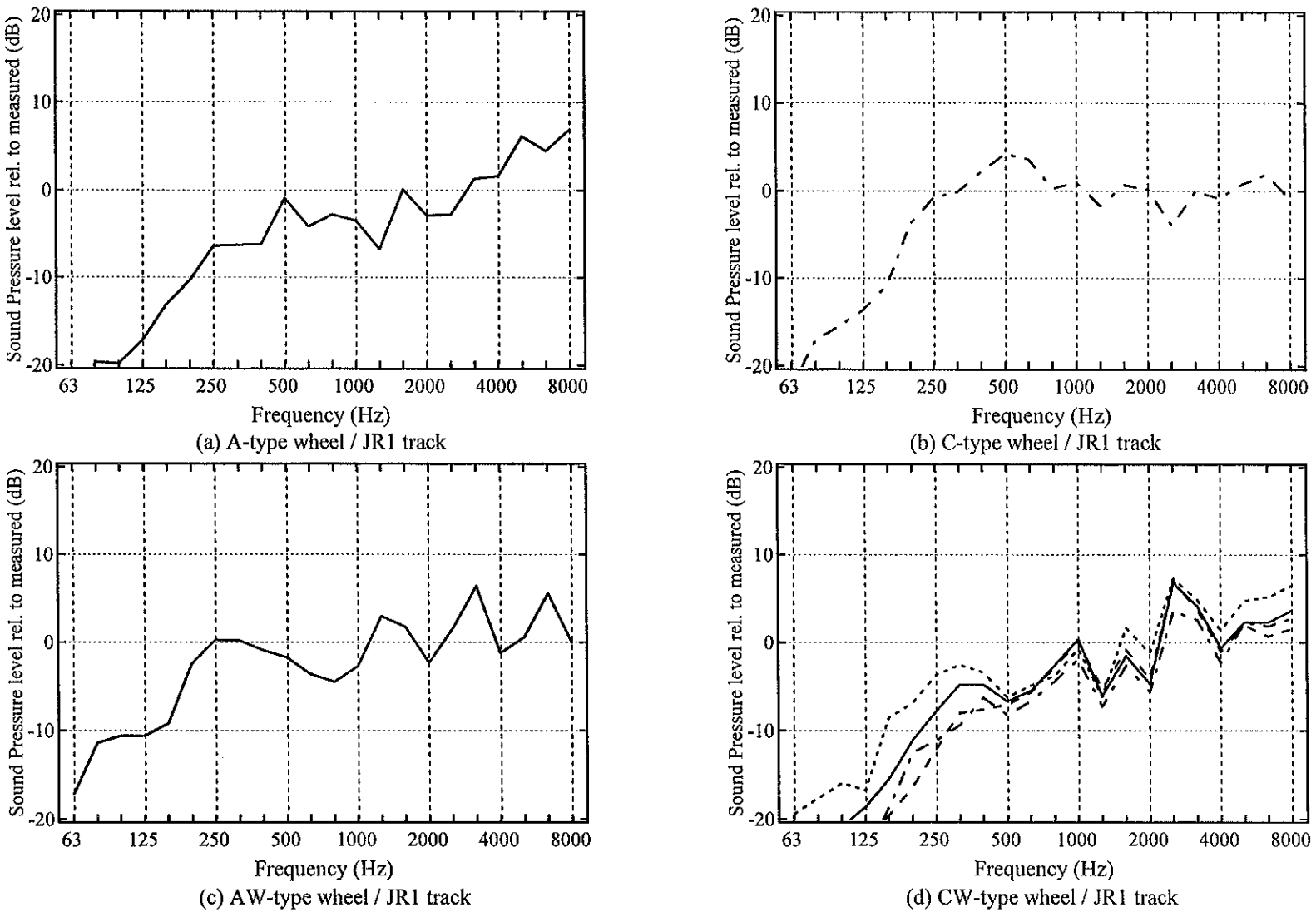

(a) A-type wheel / JR1 track

(b) C-type wheel / JR1 track

(c) AW-type wheel / JR1 track

(d) CW-type wheel / JR1 track

Figure 5.17 Predicted noise minus measured noise for each wheel using rodel model (JR1 track, mono-bloc sleeper;····· :70 km/h,– – – :100 km/h,—— :110 km/h,- - - :120 km/h)

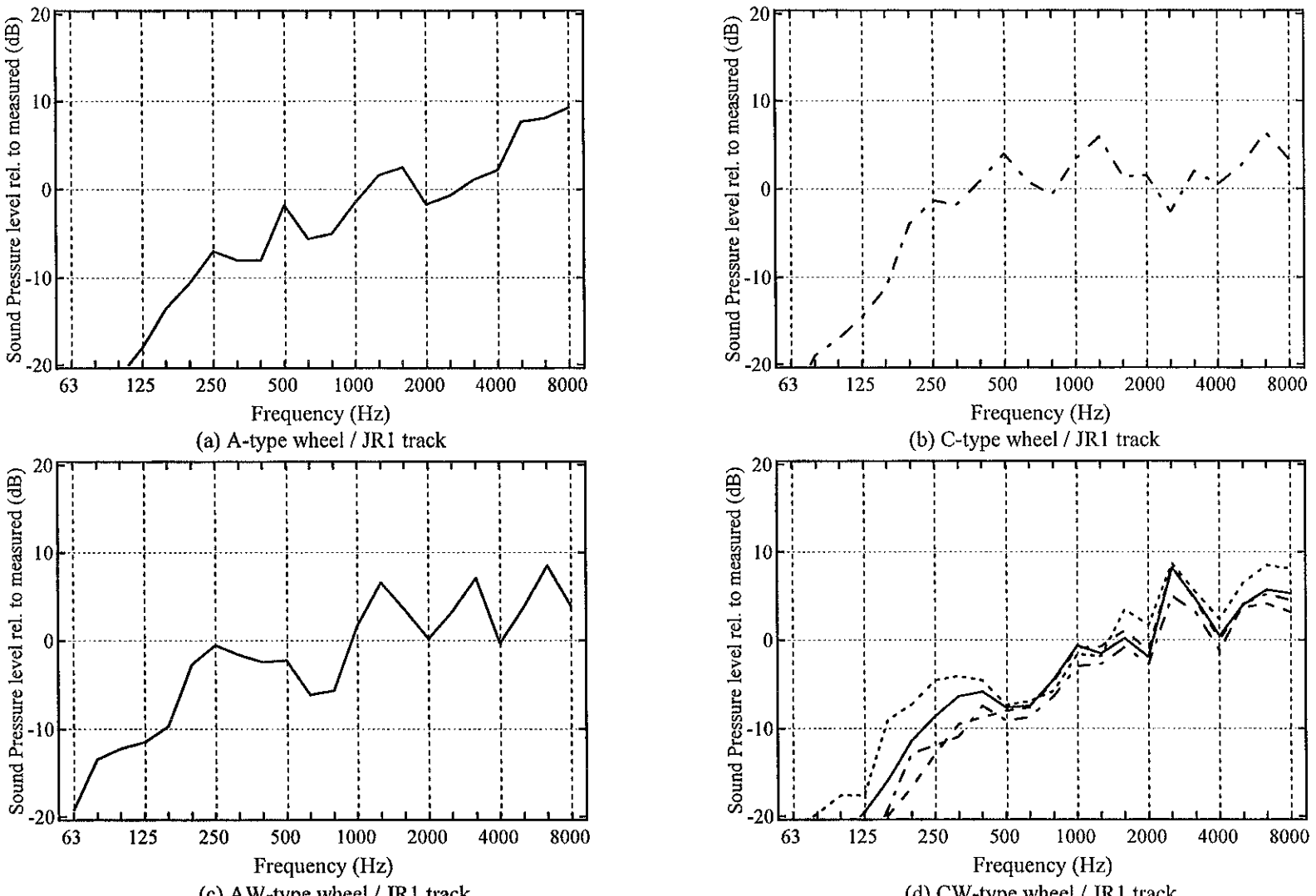

Figure 5.18 Predicted noise minus measured noise for each wheel using rodel model
(JR1 track, mono-bloc sleeper, ------ :70 km/h, – – – :100 km/h, ——:110 km/h, - - - :120 km/h)

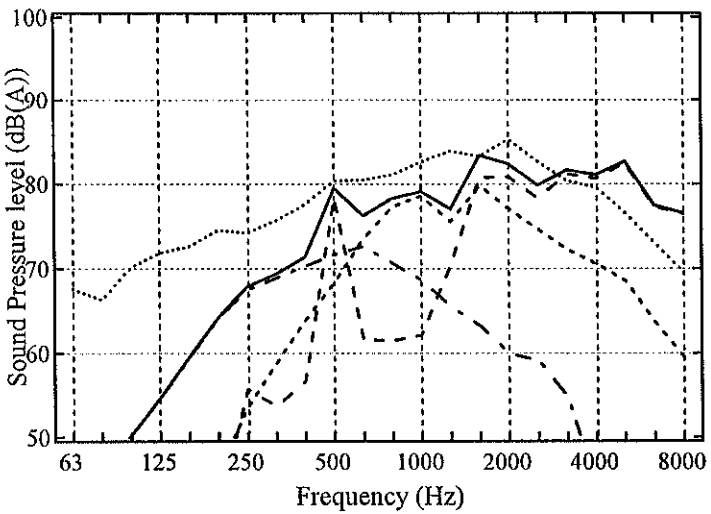

(a) A-type wheel / JR1 track (110km/h)

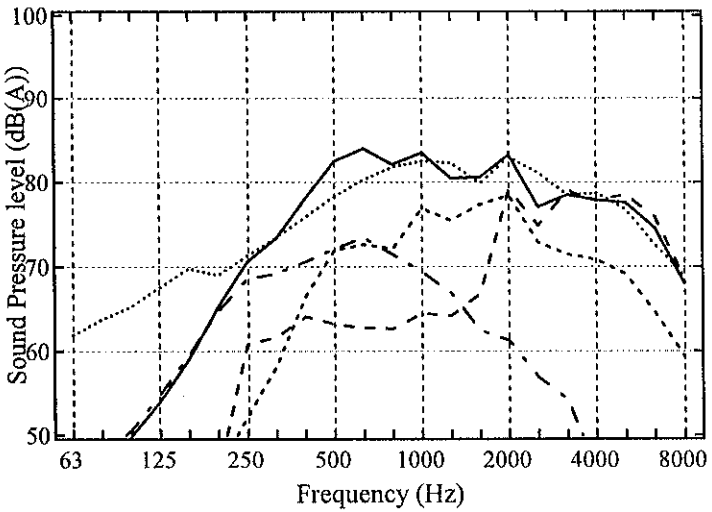

(b) C-type wheel / JR1 track (100 km/h)

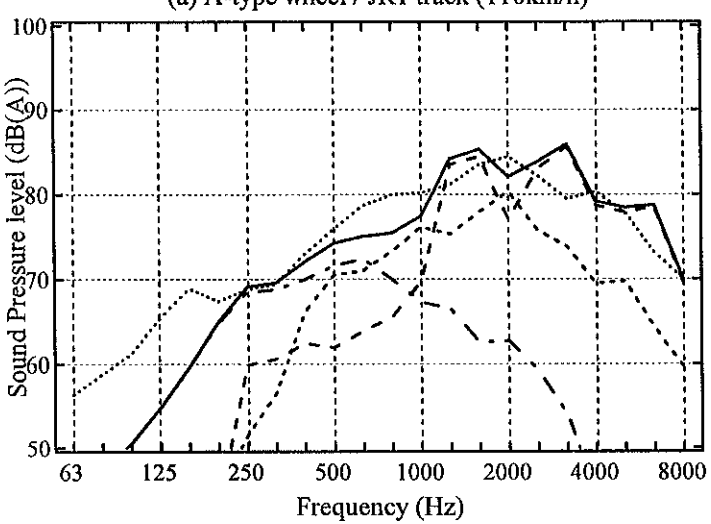

(c) AW-type wheel / JR1 track (110 km/h)

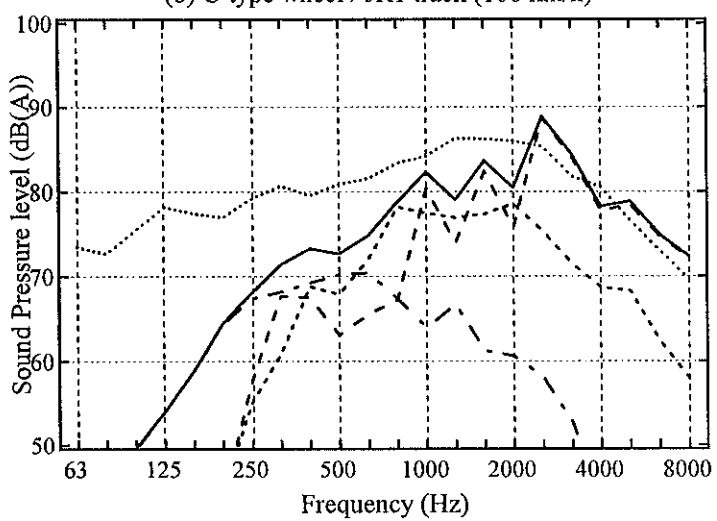

(d) CW-type wheel / JR1 track (110 km/h)

Figure 5.19 Predicted noise and measured noise for each wheel using rodel model

(JR1 track, mono-bloc sleeper, ····· :measured noise, —— :predicted noise, ----- :rail, - - :wheel, - - - :sleeper)

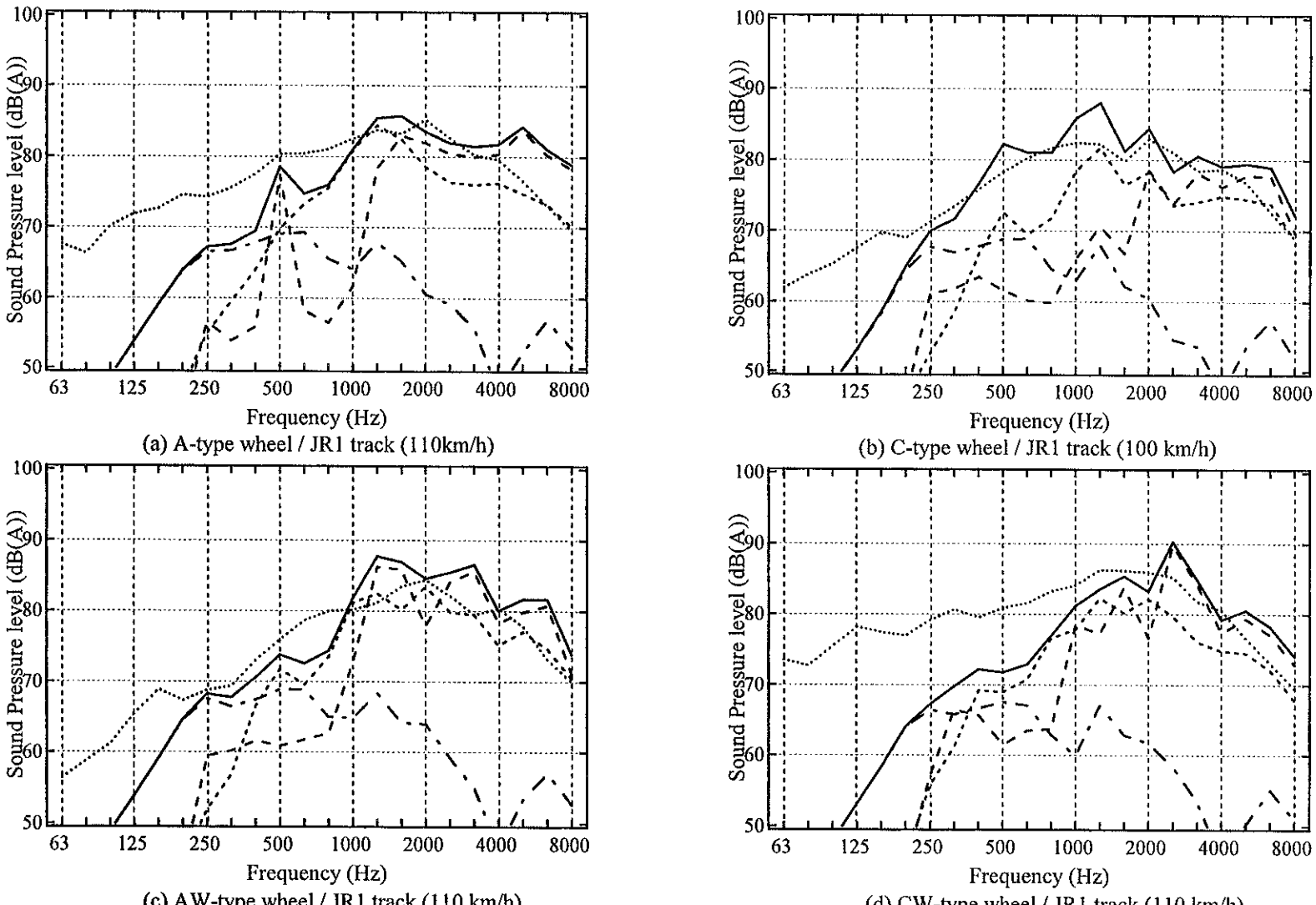

(a) A-type wheel / JR1 track (110km/h)

(b) C-type wheel / JR1 track (100 km/h)

(c) AW-type wheel / JR1 track (110 km/h)

(d) CW-type wheel / JR1 track (110 km/h)

Figure 5.20 Predicted noise and measured noise for each wheel using tinf model

(JR1 track, mono-bloc sleeper, ····· :measured noise, —— :predicted noise, ····· :rail, - - - :wheel, - - - :sleeper)

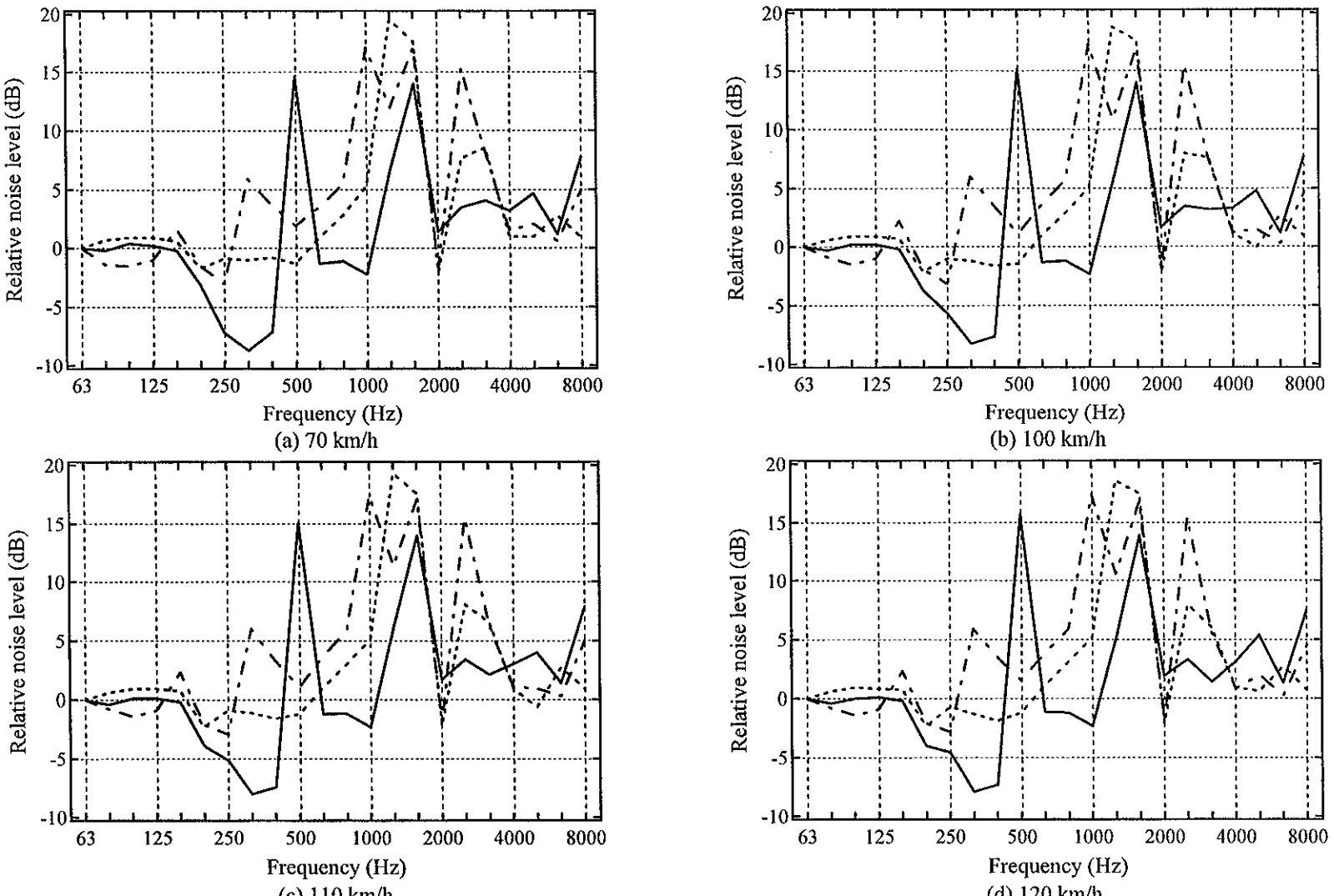

Figure 5.21 Relative noise levels of each wheel compared with the results of C-type wheel
(JR1 track, rodel, mono-bloc sleeper; —— :A-type wheel, ·····:AW-type wheel, – – –:CW-type wheel)

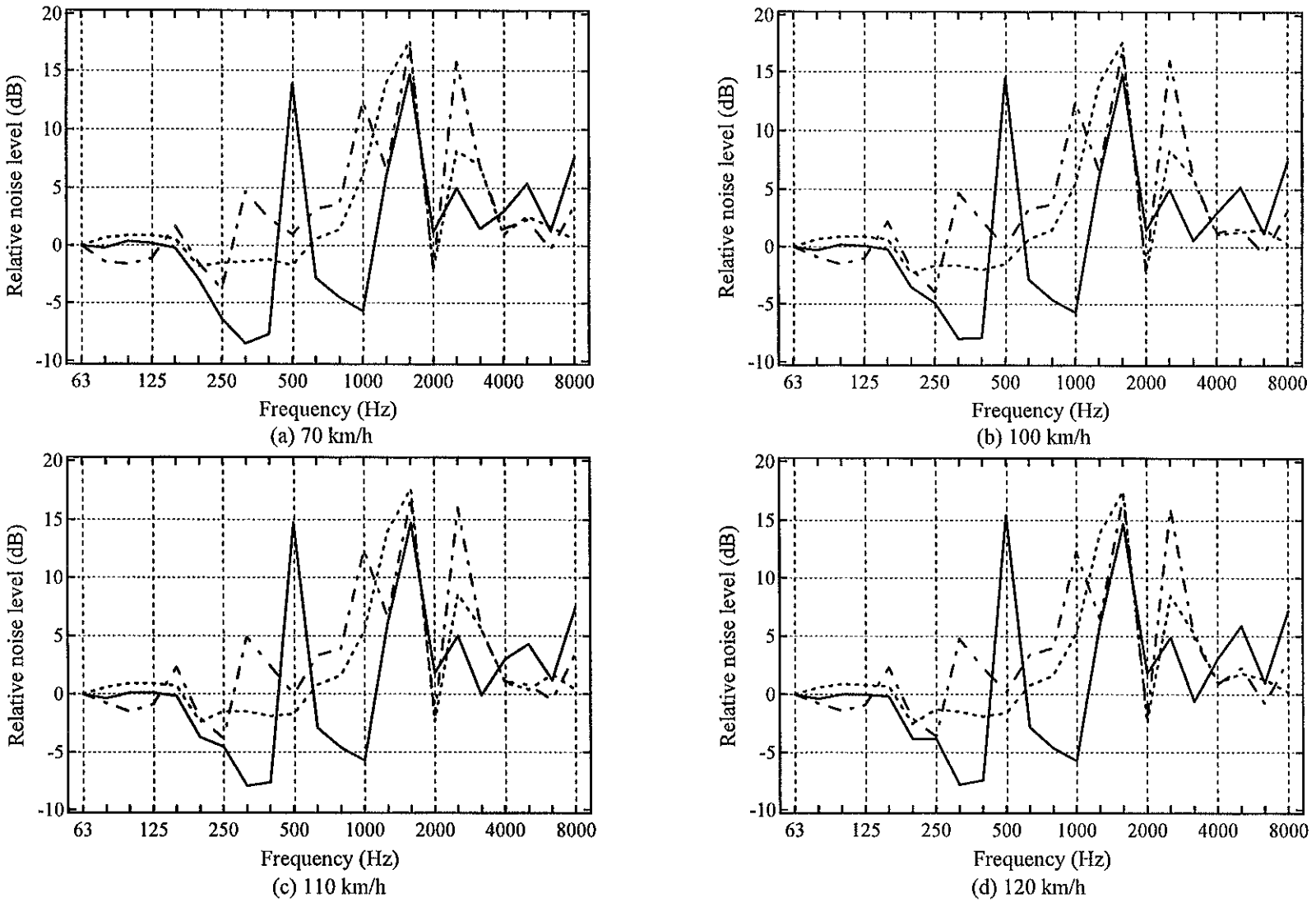

Figure 5.22 Relative noise levels of each wheel compared with the results of C-type wheel (JR1 track, tinf, mono-bloc sleeper, ——:A-type wheel, ------:AW-type wheel, – - –:CW-type wheel)

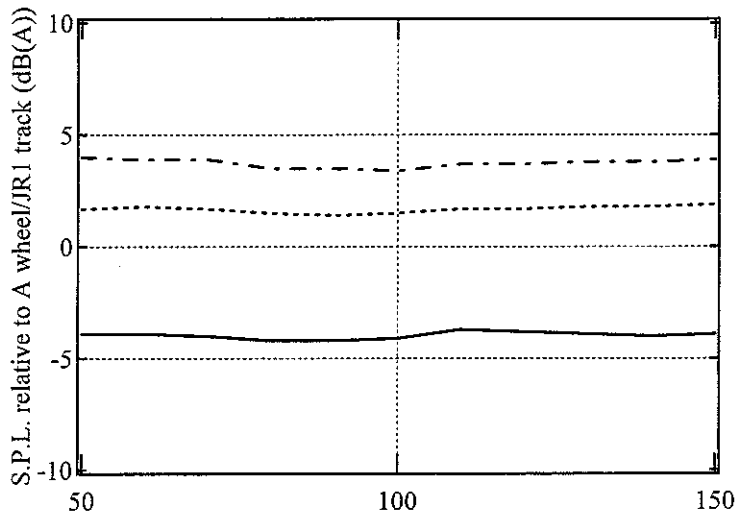

(a) Disk braked wheel/ JR1 track

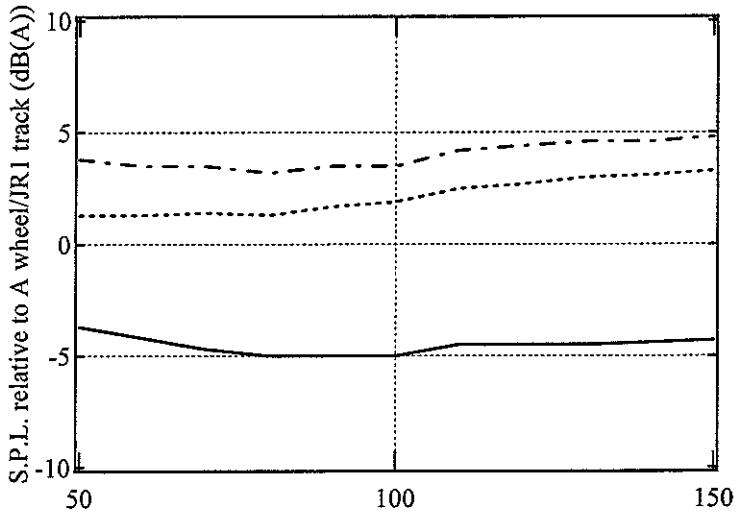

(b) Tread braked wheel/ JR1 track

Figure 5.23 Predicted wheel noise relative to A-wheel/JR1-track

(rodel, mono-bloc sleeper, ——— :C wheel, ------- :AW wheel, – – – :CW wheel)

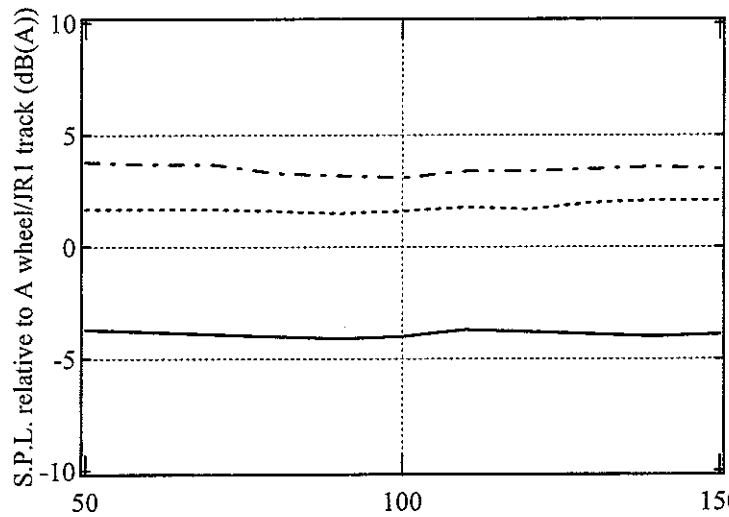

(a) Disk braked wheel/ JR1 track

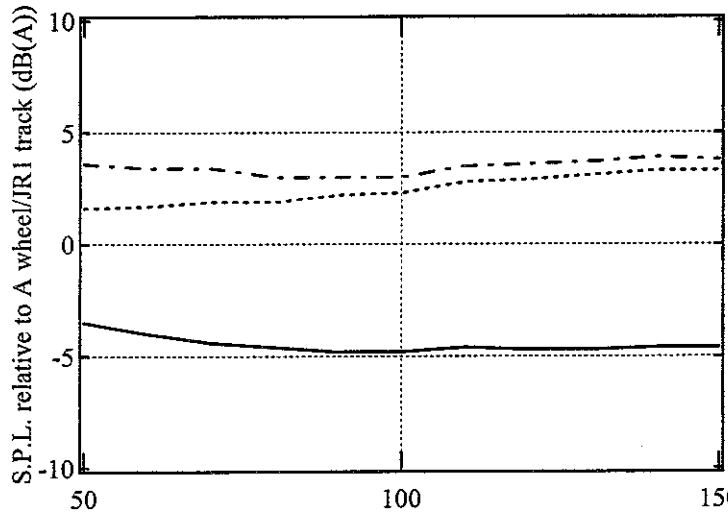

(b) Tread braked wheel/ JR1 track

Figure 5.24 Predicted wheel noise relative to A-wheel/JR1-track

(tinf, mono-bloc sleeper, —— :C wheel, ····· :AW wheel, – – – :CW wheel)

6 INTERMEDIATE COMPARISONS

In this part of this report, the track vibration predicted with the TWINS model is compared with the measured results in order to obtain a deeper understanding of the discrepancies between the predicted and measured sound levels in Section 5.

6.1 Vibration predicted with bi-bloc sleeper model

This section presents calculations of rail vibration carried out using:

- the continuous track model (rodel model) and the periodic track model (tinf model)
- bi-bloc sleeper
- calculated track decay rates

Figures 6.1-6.2 show predicted rail vibration plotted against measured level in the vertical direction in dB(A). Both the measured and predicted vibrations are presented in the form of velocity levels. The individual points represent one of the 6 wheel/track combinations. The solid line corresponds to the mean difference between predictions and measurements (mean + 0.9 dB for the rodel model and 4.8 dB for the tinf model). The dashed lines show a range of +/- one standard deviation (standard deviations of 2.8 dB in both cases). The rodel model gives better predictions than the tinf model does. However, most of the predictions are somewhat over-predicted. Although the tinf model calculations are carried out for the same position where the measurements are performed, the predictions show poor agreement with measured results. This is due to the omission of rail loss factor in the tinf model.

Figures 6.3-6.4 show the spectral differences as the mean and a range of +/- one standard deviation for all cases.

The rodel model show the same trends found in the noise results with an over-prediction around 250 Hz and an under-prediction around 630 Hz. These features are related to the poor modelling of the sleeper vibration at low frequencies, and could be improved by introducing the mono-bloc sleeper model, which accounts for the modal sleeper behaviour and frequency dependent ballast properties.

For the tinf model, it is found that the predictions are over-predicted, and the mean is between about +3 dB(A) and +13 dB(A). The tinf model gives the same trends with a peak

around 250 Hz and a trough around 630 Hz. This is also mainly due to the inadequacy of the model of the sleeper vibration.

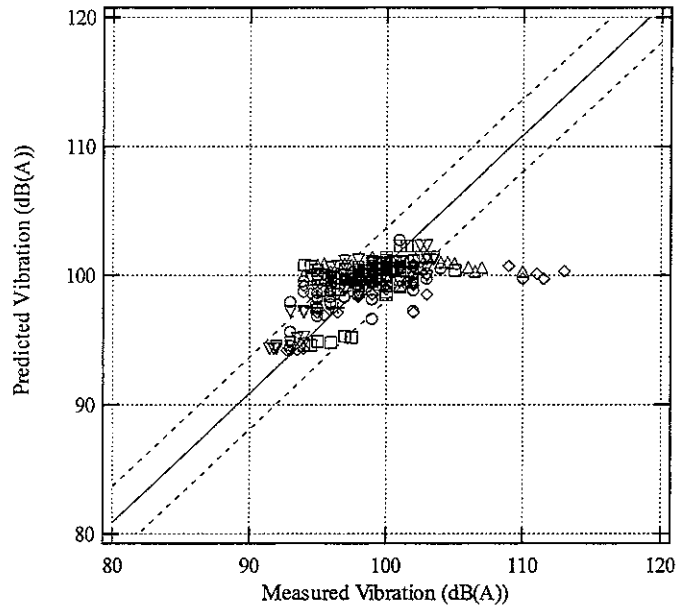

Figure 6.1 Predicted rail vibration velocity level plotted against measured rail vibration velocity level for all case (rodel, bi-bloc sleeper, ◇: A-type wheel, △: B-type wheel, ○: C-type wheel, +: AW-type wheel, □: BW-type wheel, ▽: CW-type wheel)

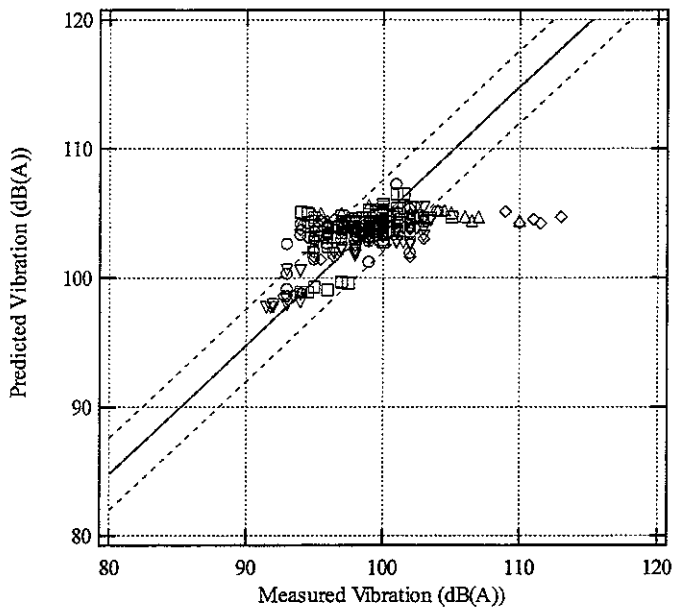

Figure 6.2 Predicted rail vibration velocity level plotted against measured rail vibration velocity level for all case (tinf, bi-bloc sleeper, ◇: A-type wheel, △: B-type wheel, ○: C-type wheel, +: AW-type wheel, □: BW-type wheel, ▽: CW-type wheel)

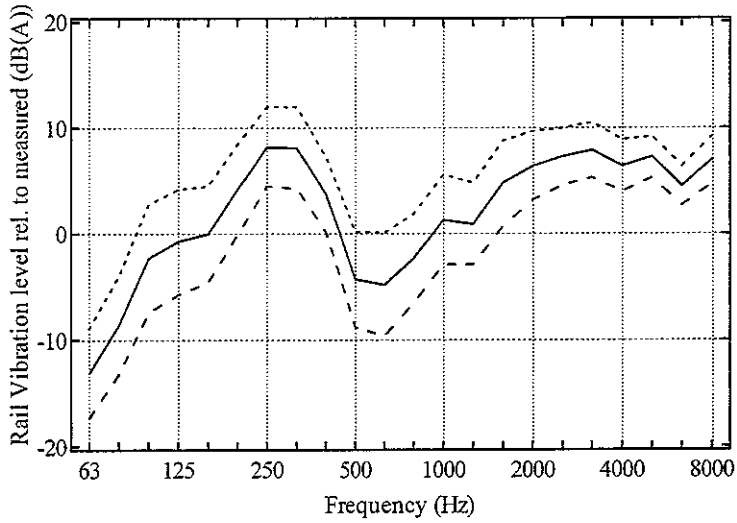

Figure 6.3 Average differences between predicted and measured rail vibration velocity spectra for all cases. (rodel, bi-bloc sleeper,———: mean,·····: mean +std deviation, ------:mean-std deviation)

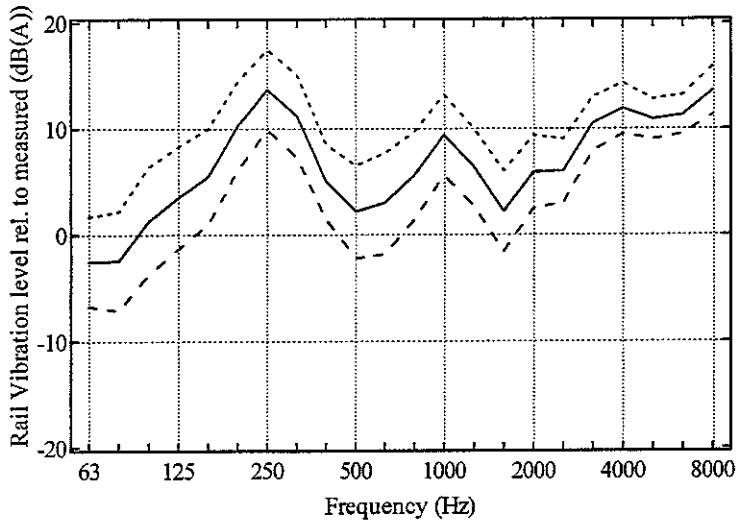

Figure 6.4 Average differences between predicted and measured rail vibration velocity spectra for all cases. (tinf, bi-bloc sleeper,———: mean,·····: mean +std deviation, ------:mean-std deviation)

6.2 Vibration predicted with mono-bloc sleeper model

This section presents calculations of rail vibration carried out using:

- the continuous track model (rodel model) and the periodic track model (tinf model)
- mono-bloc sleeper
- calculated track decay rates

Figures 6.5-6.6 show predicted vertical rail vibration velocity level plotted against measured level in terms of overall A-weighted levels. The individual points represent one of the 6 wheel/track combinations. The solid line corresponds to the mean difference between predictions and measurements (mean -0.5 dB for the rodel model and +2.6 dB for the tinf model). The dashed lines show a range of +/- one standard deviation (standard deviations of 2.8 dB in each case). It is clear that the results of both models are improved by using the mono-bloc sleeper model. Comparing Figure 6.5 with Figure 6.6, it can be seen that the improved rodel model gives better predictions than the improved tinf model does. This is also because rail loss factor is neglected in the tinf model.

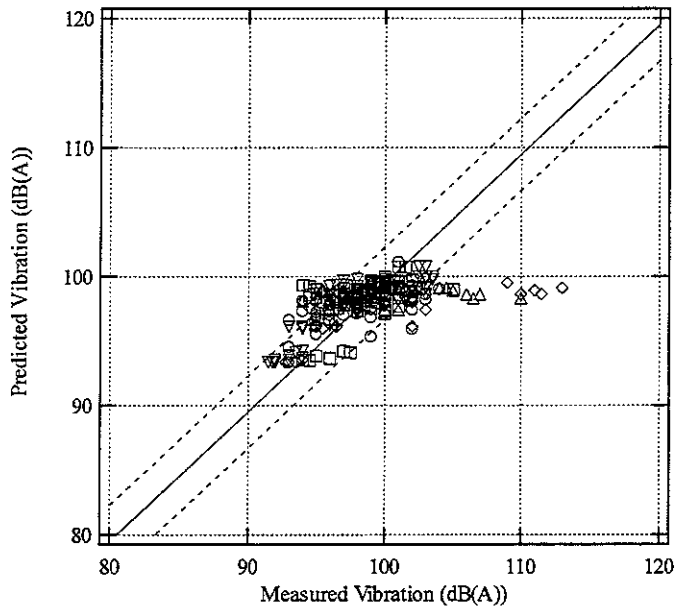

Figure 6.5 Predicted rail vibration velocity level plotted against rail vibration velocity level for all case (rodel, mono-bloc sleeper, ◇: A-type wheel, △: B-type wheel, ○: C-type wheel, +: AW-type wheel, □: BW-type wheel, ▽: CW-type wheel)

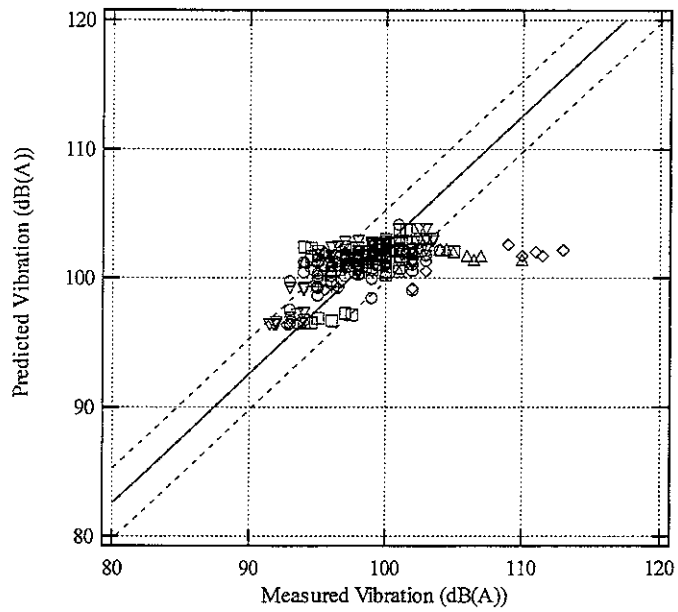

Figure 6.6 Predicted rail vibration velocity level plotted against measured rail vibration velocity level for all case (tinf, mono-bloc sleeper, ◇: A-type wheel, △: B-type wheel, ○: C-type wheel, +: AW-type wheel, □: BW-type wheel, ▽: CW-type wheel)

Figures 6.7-6.8 show the spectral differences as the mean and a range of +/- one standard deviation for all cases.

It can be seen that the shape of the results is much improved and the peak at 250 Hz has been eliminated by using the mono-bloc sleeper model. However, the results of the two models are over-predicted.

The results of the rodel model show that an under-prediction appears in the frequency range 800-1250 Hz. This under-prediction is probably related to the phenomena associated with the pinned-pinned resonance around 1000 Hz. The rodel model cannot predict the pinned-pinned resonance correctly, since the foundation is taken as a continuous support in the rodel model.

The overall results of the rodel model show an under-prediction in Figure 6.5, although, in Figure 6.7, the spectral results are over-predicted in most of 1/3 octave bands. These features occur because, in the measurements, the spectra in velocity levels have trends with a peak around 1000 Hz. For the measurements, the vibration components in the range of 800-1250 Hz have greater contribution to the overall levels. However, for the predictions,

the spectral results show an under-prediction in the frequency range.

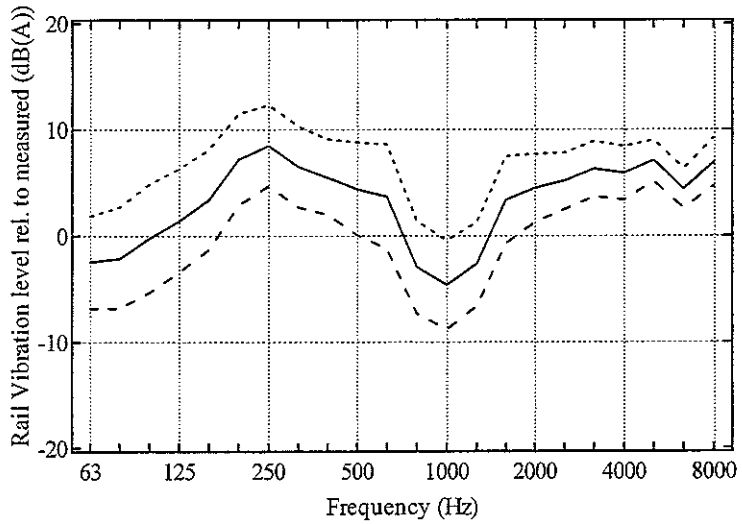

Figure 6.7 Average differences between predicted and measured rail vibration velocity spectra for all cases. (rodel, mono-bloc sleeper,———: mean,·····: mean +std deviation, - - - - - -:mean-std deviation)

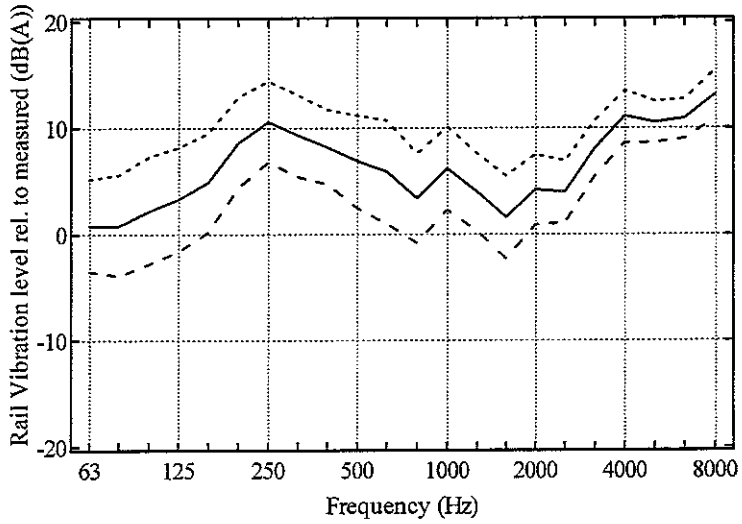

Figure 6.8 Average differences between predicted and measured rail vibration velocity spectra for all cases. (tinf, mono-bloc sleeper,———: mean,·····: mean +std deviation, - - - - - -:mean-std deviation)

7 SUPPLEMENTARY STUDIES

The validity of the TWINS model has been confirmed throughout Sections 5-6. In this section, an attempt to estimate the effect of wheel load on noise and rail vibration will be made by using the TWINS model. The measurement campaign performed will be described briefly. Then, the effect of the wheel load will be predicted with the TWINS model.

7.1 Measurement description

Running measurements were carried out for a single track type [36-37], as listed in Table 7.1. This is located on a narrow-gauge line, with track gauge 1.067m. The measurements were made for A-type and B-type freight cars with A-type wheels, as listed in Table 2.2. The tested speeds are 80, 100 and 110 km/h. For the braking system of A-type and B-type freight cars, tread brakes with sinter iron are used. Therefore, the TWINS calculations are carried out using the reference roughness spectra representing the combination of disc braked wheel and rail (see Figure C7). The wheel load conditions are listed in Table 7.2.

Table 7.1 Track condition

Track	Location	Rail type	Sleeper	Foundation
JR2	Tokaido Line	60	monobloc concrete	ballast

Table 7.2 wheel load condition

Freight Car	Integration length	Condition 1	Condition 2
A	20 m	23500 N	64000 N
B	16 m	21500 N	81500 N

For the JR2 track, the measurements were made at two positions:

- 1 accelerometer on the rail,
- 1 microphone at 2.53 m from the centre of the track (i.e. 1.96 m from the near rail)

Sound pressure measurements were carried out close to the track. The accelerometer was glued on the end of the foot of a rail at the mid-span between two neighbouring sleepers, and only vertical vibration was measured. These measurement positions are shown in Figure 7.1.

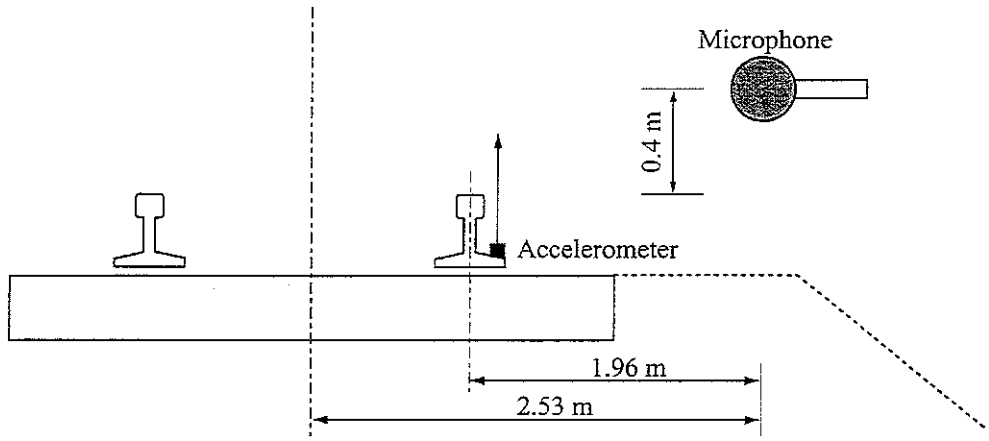

Figure 7.1 Diagram of measuring points

7.2 Calculation description

The TWINS calculations of noise and rail vibration are carried out using:

- the continuous track model (rodel model)
- modal sleeper model
- a "unit roughness" excitation
- frequency dependent ballast stiffness model.
- calculated track decay rates
- calculating with a single speed (100 km/h)

TWINS calculations have been carried out using a "unit roughness" excitation for each frequency, since rail and wheel roughnesses have not been measured during the running tests. The 'standard' roughness spectrum is added afterwards for each speed.

The rodel model with mono-bloc sleeper model has been used. This is due to the fact the rodel model gives better predictions than the other models (see Chapters 5-6). In order to save computational efforts, the TWINS calculations have been carried out for a single speed (100km/h, see Appendix C), although the roughness added corresponds to several speeds.

In order to estimate the effect of the wheel load, two effects should be considered in the TWINS calculations.

- normal load effect
- contact filter effect

For the normal load effect, it is only necessary that the static load equivalent to the wheel

load is entered in the "Interaction" option. This determines the contact stiffness.

For the contact filter effect, the wheel load has effects on determining the size of the contact zone between the wheel and rail. Roughness with wavelengths that are small in comparison with the contact patch length is attenuated, and does not excite the wheel/track system as well as long wavelength roughness. The contact patch length determines the wavelength at which the contact filter rolls off. Therefore, it is necessary that the contact filter effect corresponding to the wheel load should be determined in order to make the TWINS predictions correctly. Figure 7.2 shows the contact filtering effect for each wheel load condition relative to the results of a wheel load of 50000 N (see Appendix F). These relative differences should be included in the TWINS calculations.

Post-processing is carried out using a standard roughness spectrum which includes the contact filtering effect corresponding to each wheel load condition.

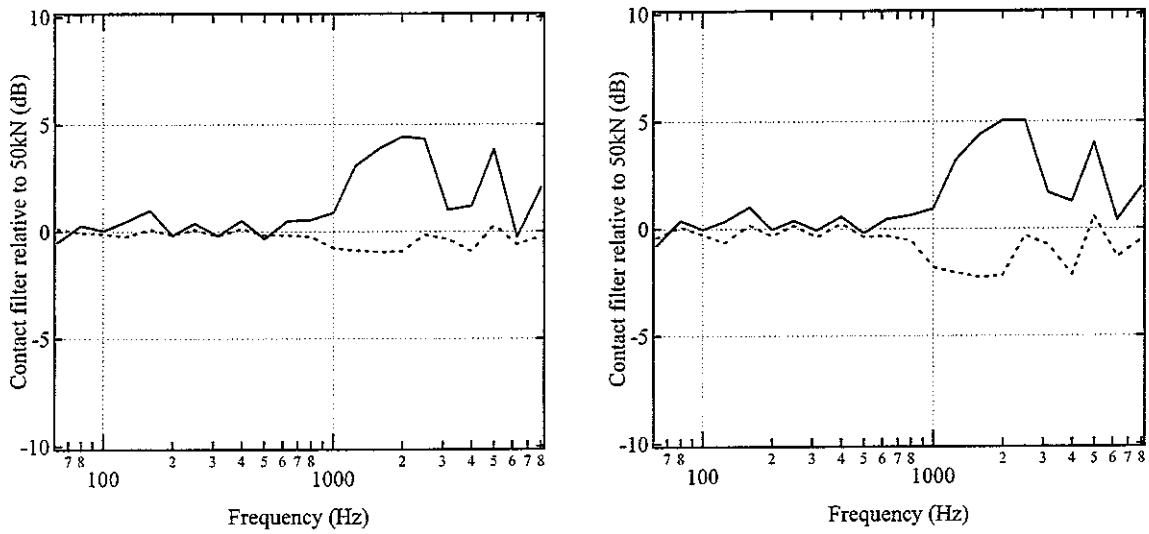

(a) Freight A (b) Freight B

Figure 7.2 Predicted contact filter effect (wheel load: 50000 N)

(Freight A: 23000N (———), 64000N (·····), Freight B: 21500N (———), 81500N (·····))

7.3 Comparison of overall levels

Figure 7.3 shows the overall noise in dB(A) plotted against train speed. It can be seen that all the predicted results show a noise increase of about 8 dB for a doubling of train speed. The predictions corresponding to the heavier wheel load condition are lower. The difference between the two wheel load conditions appears to be constant, and independent of train speed. Comparing with the measurements, the global trends are predicted well. However, the predictions are somewhat too high. This is probably because the standard roughness spectrum used (see Figure C7) is not appropriate for the TWINS calculation. (The standard roughness spectrum is different from the roughness spectrum based on the actual wheel/rail roughnesses in JR2 track.)

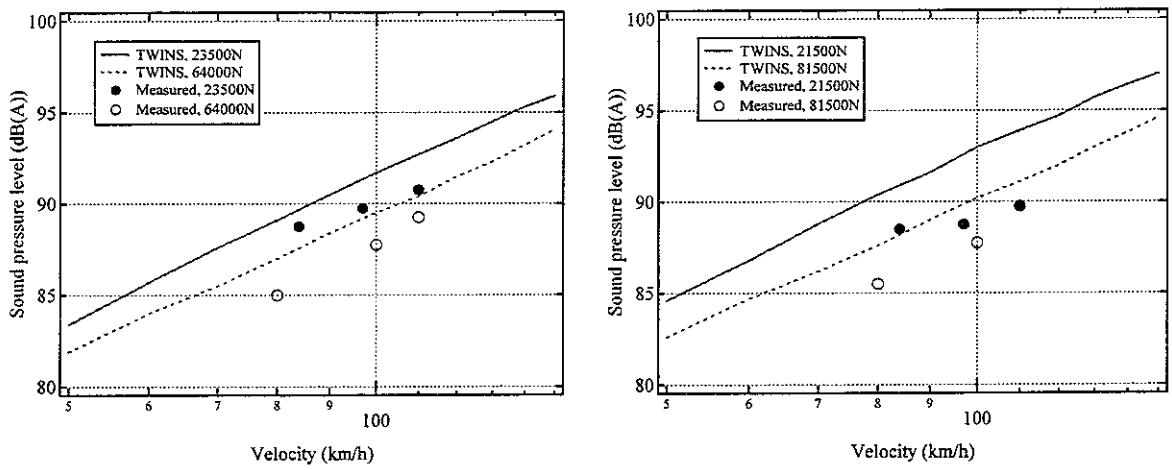

(a) Freight A (b) Freight B

Figure 7.3 Overall levels plotted against train speed (rodel, mono-bloc sleeper, JR2 track)

Figure 7.3 shows the differences in dB(A) between the two wheel load conditions. For the measurements, the differences are reduced as the wheel load is increased, and the average difference is about 2 dB. For the predictions, the same trends are found that the differences are also smaller as the wheel load increases, and the differences are in the range 1-2.5 dB. However, the measured difference between the two wheel load conditions appears to depend on train speed, whilst the predicted difference is independent of train speed. Some factors may be responsible for this.

- the wheel/rail roughness profile may have changed gradually during the running tests (the

running tests were carried out over a period of two weeks).

- the noise radiated from other vehicle components (e.g. rattling noise from bogies and goods on cars) may have changed.
- track non-linearities may modify the track noise under preload.

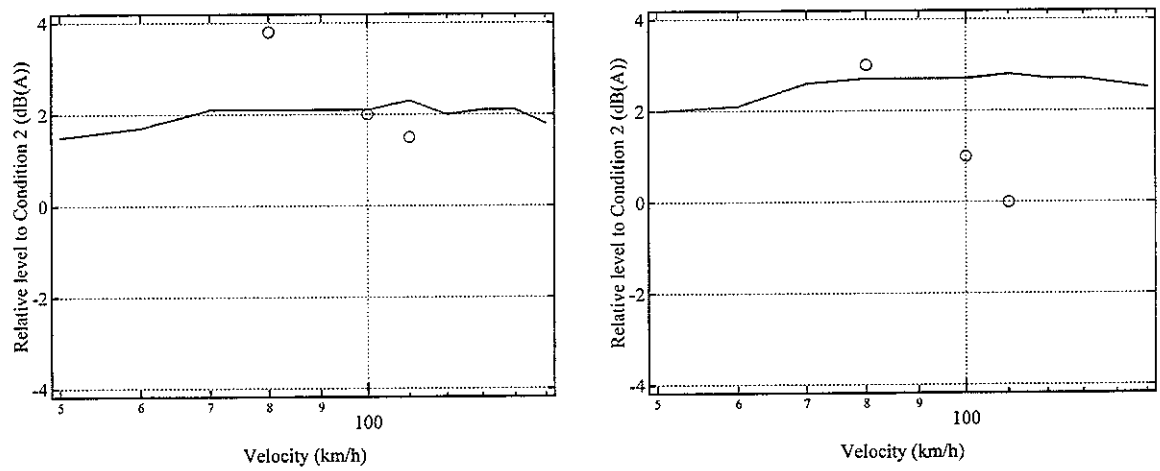

(a) Freight A (b) Freight B

Figure 7.3 Difference in dB(A) between two wheel load conditions (rodel, mono-bloc sleeper, —— :TWINS, ○: Measured results, JR2 track, Freight A:23500N(Cond.1), 64000N(Cond.2), Freight B:21500N(Cond.1), 81500N(Cond.2))

7.4 Comparison of spectral results

Figures 7.4 shows the predicted and measured results in the form of absolute spectra for a single speed (100 km/h). It is clear that the results are under-predicted below 1600 Hz, and are over-predicted above 1600 Hz. This is again due to the fact that the standard roughness spectrum does not match the spectrum calculated from the actual wheel/rail roughnesses in JR2 track. Below 125 Hz, the predictions become worse. This is because, as the sound measurements were made close to the track, the measured results would be contaminated by wind noise.

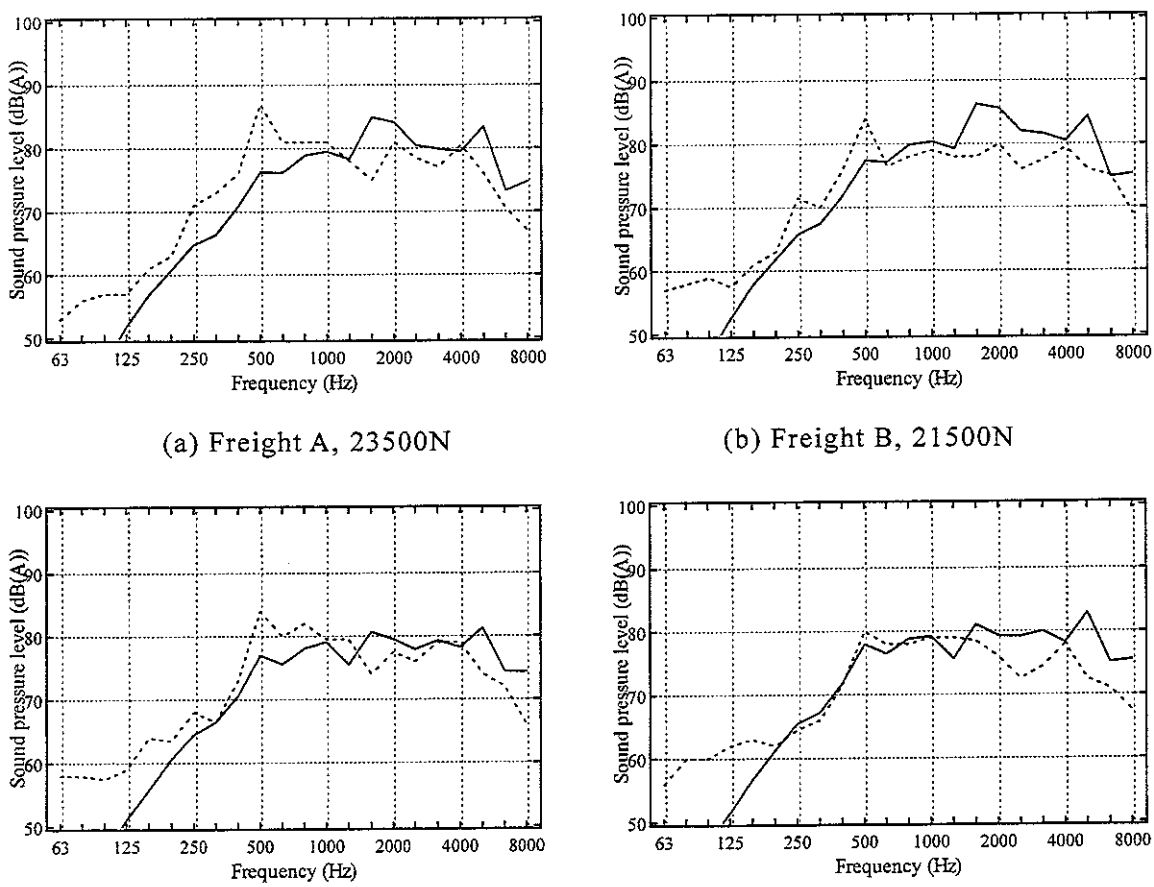

(a) Freight A, 23500N

(b) Freight B, 21500N

(c) Freight A, 64000N

(d) Freight B, 81500N

Figure 7.4 Predicted noise and measured noise for a speed of 100km/h (rodel, mono-bloc sleeper, JR2 track, ——: predicted, - - - - -:measured)

In order to illustrate the spectral variation, the differences between the two wheel load conditions should be constructed for a given train speed. It is noted that, in the TWINS calculations, the effect of the wheel/rail roughnesses on the differences will be removed, if

the differences are calculated at one speed. This indicates that the spectral differences between the two wheel load conditions depend only on the contact filter and normal load effects, and are composed of the superposition of the two effects. In the measurements, the differences in frequency spectra between the two wheel load conditions could also be equal to the differences due to the contact and normal load conditions, if the wheel/rail roughness profile remained unchanged during the running tests.

Before presenting comparisons of the predictions and measurements, it is useful to check the compact filter and normal load effects, which will give better understanding of the two effects on noise and rail vibration.

Figure 7.5 shows the predicted difference in contact filter and normal load effects between the two wheel load conditions. Below 800 Hz, the contact filter and normal load effects give no significant influence on the noise components. Above 1000 Hz, it is clear that the contact filter effect has greater influence on the noise components. As the wheel load is increased, the whole contact filter curve is shifted to the left (see Figure F1.2). The effective frequency at which the contact filter rolls off is shifted lower as the wheel load is increased. Therefore, the wheel/rail system is significantly influenced due to the contact filtering effect above 1000 Hz, and the increase of the wheel load could lead to the noise reduction.

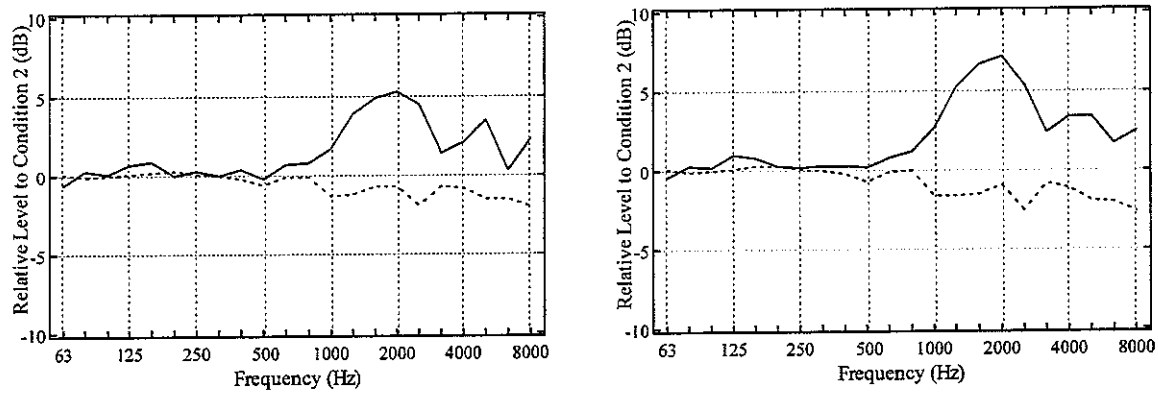

(a) Freight A (b) Freight B

Figure 7.5 Predicted difference in contact filter and normal load effects (100 km/h, rodel, mono-bloc sleeper, ——: Contact filter, - - - -: Normal load, Freight A:23500N(Cond.1), 64000N(Cond.2), Freight B:21500N(Cond.1), 81500N(Cond.2))

Figure 7.6(a) shows the measured and predicted differences in noise between the two wheel load conditions for Freight A at a speed of 100 km/h. These results are presented in 1/3 octave bands. As the measured results were affected by wind noise below 125 Hz, it is better to focus on the results from 125 Hz upwards. For the predictions, the differences can be seen to be less than 1 dB below 1000 Hz, and up to 6 dB above 1000 Hz. Above 1000 Hz, the predictions show good agreement with the measurements. In Figures 7.6(a), the predictions are of a similar order of magnitude to the measurements above 1000 Hz. This indicates that the contact filter and normal load effects are predicted correctly, and that the contact filter has a significant effect on the wheel/rail system in this frequency range.

However, below 1000 Hz, the predictions are poor. These points may be responsible for this.

- the wheel/rail roughness profile may have changed.
- the noise radiated from other vehicle components may have changed.
- track non-linearities may have an influence.

Figure 7.6(b) shows the predicted differences between the two wheel load conditions in the form of spectra of rail vibration velocity. The measured results are also shown for comparison. It is clear that the global trends are well predicted above 125 Hz. This indicates that the wheel/rail roughness profile remained unchanged during the running tests, and other vehicle components of Freight A are more likely to be responsible for effects in the noise below 1000 Hz.

Figure 7.7(a) shows the differences in noise between the two wheel load conditions for Freight B at a speed of 100 km/h. The predictions show poor agreement with the measurements above 125 Hz. Figure 7.7(b) shows the differences in rail vibration velocity between the two wheel load conditions. It is clear that the predictions are also poor above 125 Hz. This suggests that the wheel roughness profile may have changed during the running test (from the results of Freight A, it could be expected that the rail roughness profile remained unchanged) or track preload effects on the track may have an influence on the track noise.

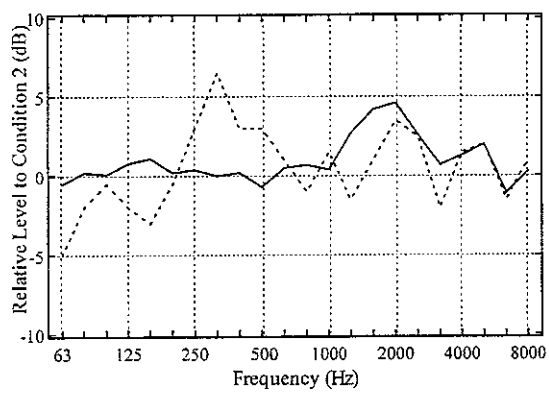

(a) Noise

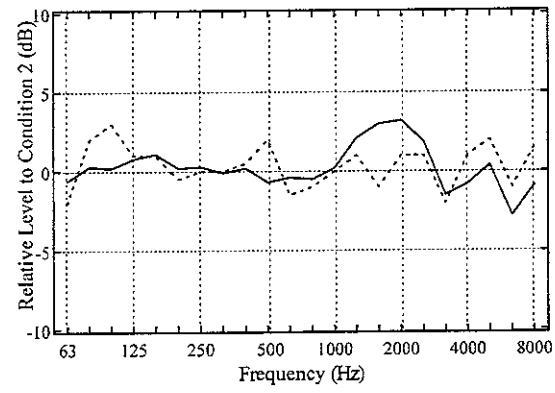

(b) Rail vibration velocity

Figure 7.6 Difference in frequency between two wheel load conditions

(Freight A, 100 km/h, rodel, mono-bloc sleeper, ——: TWINS, -----: Measured results, Condition 1: 23500N, Condition 2: 64000N)

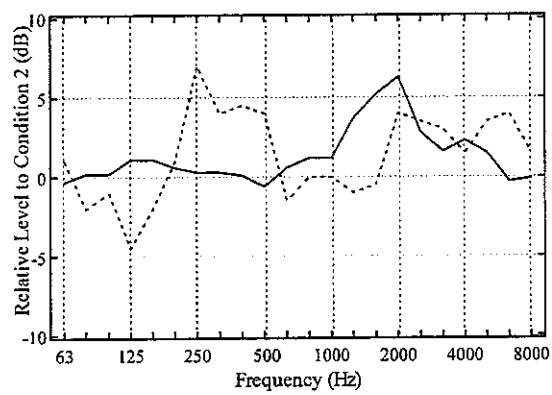

(a) Noise

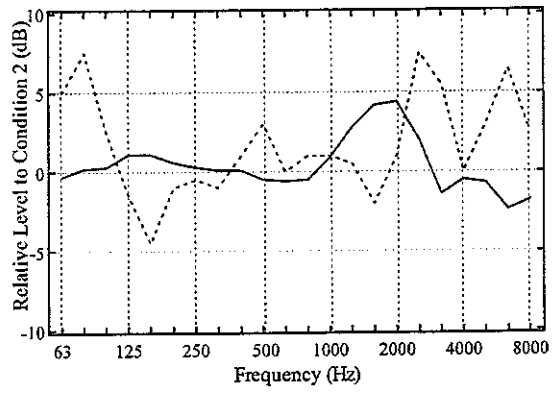

(b) Rail vibration velocity

Figure 7.7 Difference in frequency between two wheel load conditions

(Freight B, 100 km/h, rodel, mono-bloc sleeper, ——: TWINS, -----: Measured results, Condition 1: 21500N, Condition 2: 81500N)

8 SUMMARY OF THE MAIN RESULTS

In order to validate the TWINS software for rolling noise prediction, a comparison in terms of noise and rail vibration has been carried out for 6 wheel/rail combinations of Japanese railways. The main results are summarized as follows.

- Globally, the TWINS model gives reliable noise predictions, provided that the mono-bloc sleeper model is introduced in the TWINS model. A linear relationship between the predictions and measurements appears in the train speed range considered of 70-120 km/h. It is found that the mean difference in noise between the predictions and measurements are in the range of -/+ 1.5 dB. For the rodel model, the predictions are somewhat under-predicted, and the results of the tinf model show an over-prediction. This is probably due to the fact that the calculations of the tinf model are carried out at mid-span only, and that rail loss factor is omitted in the tinf model.

- In terms of noise spectra, the predictions are somewhat under-predicted in the frequency range of 63- 8000 Hz. By introducing the mono-bloc sleeper model, the results are improved, and show an under-prediction below 1000 Hz and an over-prediction above 1000 Hz. The under-prediction below 1000 Hz occurs due to the fact that the rail vibration is not predicted correctly. The over-prediction above 2000 Hz may be caused by the inadequacy of the wheel radiation model or the inaccuracy of the modal bases calculated by FE model or more likely due to the roughness spectra and contact filter used. Below 250 Hz, there is a significant under-prediction, since the measurements are contaminated by wind noise. The rodel model with the mono-bloc sleeper model gives the most reliable predictions. For the rodel model, the average difference between the predictions and measurements in 1/3 octave bands is about 1 dB, while the standard deviation is about 2-4 dB above 250 Hz.

The rail vibration is somewhat over-predicted. This may be due to the roughness used being higher than applicable for Japanese situations. In the noise predictions this may be offset by ignoring ground reflections and sound radiation from the far rail/wheels.

- An attempt to estimate the effect of wheel load on noise and rail vibration has been made

by using the TWINS model. The TWINS model shows similar trends to the measurements. For the predictions and measurements, the overall levels are reduced by about 1-2 dB(A) as the wheel load is increased from 21-24 kN to 64-82 kN. The spectral results show that, above 1000 Hz, the predictions show good agreement with the measurements and that the predictions are of a similar order of magnitude to the measurements above 1000 Hz. This indicated that the contact filter effect is predicted correctly, since the contact filter effect has a significant effect on wheel/rail system above 1000 Hz.

The validation of the TWINS model has been carried out for six types of wheel and one track type. Through the validation work, it has shown that the TWINS model is constructed on the basis of robust theories.

Further tests and studies are required to cover a wider range of rolling stock and track. In this report, the validation of the TWINS model has been confirmed only in some cases as a first step. In order to make a deeper understanding of rolling noise, the measured data are needed to characterize the vibratory behaviour of the track and wheel.

- Roughness measurement

For the roughness, in this report, the TWINS calculations have been carried out by using a "unit roughness" excitation and reference wheel/rail roughness spectra. This means that the wheel and rail roughness profiles of Japanese railway are not used, since the wheel and rail roughnesses have not been measured during the running tests. It should be necessary that the TWINS calculations are carried out directly by using wheel and rail roughness profiles of Japanese railway. However, care should be taken to ensue that these measurements are compatible with the requirements of TWINS.

- Track and wheel measurements

It is necessary to obtain a better understanding of the vibratory behaviour of the tracks and wheels by performing characterisation measurements. In this report, the vibratory behaviour of the tracks is confirmed only below 1250 Hz. It is important to make a clear confirmation of the vibratory behaviour of the tracks from some experimental investigation covering in the whole frequency range of 63-8000 Hz. More extensive measurements of track decay rate are required as part of these. For the wheel measurements, it is necessary

to compare the FEM predictions with the measurements in terms of modal characteristics, particularly natural frequencies.

9 REFERENCES

[1] Kitagawa, T. et al. Sound Radiated by Vibration of Railway Wheels. *Proceeding of Inter Noise 2001*, Hague (Netherlands).

[2] Kitagawa, T. Murata, K. Zenda, Y. Analysis about Vibration and Sound Generated by Wheels *RTRI Report* Vol.15 (2001), No.5, 47-52 (in Japanese).

[3] Kitagawa, T. Nagakura, K. Ogata, S. Noise Prediction Method for Conventional Railways. *RTRI Report*, Vol.13 (1998), No.12, 41-46 (in Japanese).

[4] Thompson, D.J. & Jones, C.J.C. A review of the modelling of wheel/rail noise generation. *Journal of Sound and Vibration*, **231**(3), 2000, 519-536.

[5] Thompson, D.J. Wheel-Rail Noise Generation, Part I: Introduction and Interaction Model. *Journal of Sound and Vibration*, **161**(3), 1991, 387-400.

[6] Thompson, D.J. Wheel-Rail Noise Generation, Part II: Wheel Vibration. *Journal of Sound and Vibration*, **161**(3), 1991, 401-419.

[7] Thompson, D.J. Wheel-Rail Noise Generation, Part III: Rail Vibration. *Journal of Sound and Vibration*, **161**(3), 1991, 420-446.

[8] Thompson, D.J. Wheel-Rail Noise Generation, Part IV: Contact Zone and Resultsl. *Journal of Sound and Vibration*, **161**(3), 1991, 447-466.

[9] Thompson, D.J. Wheel-Rail Noise Generation, Part V: Inclusion of Wheel Rotation. *Journal of Sound and Vibration*, **161**(3), 1991, 467-482.

[10] Thompson, D.J. Hemsworth, B. Vincent, N. Experimental Validation of the TWINS Prediction Program for Rolling Noise, Part 1: Description of the Model and Method. *Journal of Sound and Vibration*, **193**(3), 1996, 123-135.

[11] Thompson, D.J. Fodiman, P. Mahé, H. Experimental Validation of the TWINS Prediction Program for Rolling Noise, Part 2: Results. *Journal of Sound and Vibration*, **193**(3), 1996, 137-147.

[12] Thompson, D.J., Vincent, N. Track Dynamic Behaviour at High Frequencies. Part 1: Theoretical Models and Laboratory Measurements. *Vehicle System Dynamics Supplement*, **24**, 1995, 86-99.

[13] Vincent, N. Thompson, D. J. Track Dynamic Behaviour at High Frequencies. Part 2: Experimental Results and Comparisons. *Vehicle System Dynamics Supplement*, **24**, 1995,

100-114.

[14] Thompson, D.J. On thed relationship between wheel and rail surface roughness and rolling noise. *Journal of Sound and Vibration*, **193**(1), 1996, 149-160.

[15] Thompson, D.J. & Janssens, M.H.A. TWINS: Track-Wheel Interaction Noise Software. Theoretical manual, version2.4. *TNO Report.* TPD-HAG-RPT-93-0214, revision Jan 1997.

[16] Remington, P.J. & Webb, J. Estimation of wheel/rail interaction forces in the contact area due to roughness. *Journal of Sound and Vibration*, **193**(1), 1996, 83-102.

[17] Thompson, D.J. The influence of the contact zone the excitation of wheel/rail noise. *Proceeding of 8th International Workshop on Railway Noise.* 2001.

[18] Thompson, D.J. Mace, B.R., High frequency structural vibration, *ISVR lecture notes*, University of Southampton, 2003

[19] Jones, C.J.C. & Thompson, D.J. Extended validation of a theoretical model for railway rolling noise using novel wheel and track design. *Proceeding of 8th International Workshop on Railway Noise.* 2001.

[20] Grassie, S.L. Dynamic modeling of concrete railway sleepers. *Journal of Sound and Vibration*, **187**(5), 1995, 799-813.

[21] Jones, C.J.C. Thompson, D.J. Toward M.G.R. The Dynamic Stiffness of the Ballast Layer in Railway Track. *Seventh International Conference on Recent Advances in Structural Dynamics*, 2002, 1037-1048.

[22] Thompson, D.J. & Jones, C.J.C. Sound radiation from vibrating railway wheel. *Journal of Sound and Vibration*, **253**(2), 2002, 401-419.

[23] Thompson, D.J. Jones, C.J.C. & Turner, N. Investigation into the validity of two-dimensional models for sound radiation from waves in rails. *Journal of the Acoustical Society of America*, **113**(4), Part 1, 2003, 1965-1974.

[24] Wu, T.X. & Thompson, D.J. A double beam Timoshenko beam model for vertical vibration analysis of railway track at high frequencies. *Journal of Sound and Vibration*, **224**(2), 1999, 329-348.

[25]Wu, T.X. & Thompson, D.J. Analysis of lateral vibration behavior of railway track at high frequencies using a continuously supported multiple beam model. *Journal of the*

Acoustical Society of America, **106**(3), Part 1, 1999, 1369-1376.

[26] Wu, T.X. & Thompson, D.J. Application of a multiple-beam model for lateral vibration analysis of a discretely supported rail at high frequencies. *Journal of the Acoustical Society of America*, **108**(3), Part 1, 2000, 1341-1344.

[27] Wu, T.X. & Thompson, D.J. The influence of random sleeper spacing and ballast stiffness on the vibration behaviour of railway track. *Acustica*, **84**, 2000, 313-321.

[28] Wu, T.X. & Thompson, D.J. The effects of local preload on the foundation stiffness and vertical vibration of railway track. *Journal of Sound and Vibration*, **219**(5), 1999, 881-904.

[29] Wu, T.X. & Thompson, D.J. Vibration analysis of railway track with multiple wheels on the rail. *Journal of Sound and Vibration*, **239**(1), 2001, 69-97.

[30] Wu, T.X. & Thompson, D.J. The effects on railway rolling noise of wave reflections in the rail and support stiffing sue to the presense of multiple wheels. *Applied Acoustics*, **62**, 2001, 1249-1266.

[31] Wu, T.X. & Thompson, D.J. The vibration behaviour of railway track at high frequencies under multiple preloads and wheel interactions. *Journal of the Acoustical Society of America*, **108**(3), Part 1, 2000, 1048-1053.

[32] Zenda, Y. Kitagawa, T. Ogata, Y. Abe, Y. & Watanabe, K. Noise characterization of 313 series train Part I, *RTRI Report,* 2001 (in Japanese)

[33] Ogata, Y. et al. Noise characterization of 313 series train Part II, *RTRI Report*, 2002 (in Japanese)

[34] Manabe, K. and Takigawa, M. Modal behaviour of a track, *RTRI Report*, 2001 (in Japanese).

[35] Thompson, D.J. Definition of the reference roughness. *ISVR contract report*, 1997.

[36] Ogata, Y. et al. Noise characterization of freight cars, *RTRI contract report*, 1998

[37] Kitagawa, T. et al. Study on Relationship between Axle Load and Noise. *J-RAIL'99*, Kawasaki (Japan), 1999.12, 109-112 (in Japanese)

A TRACK CHARACTERIZATION MEASUREMENTS

A1 Track studied

In order to characterize the vibratory behaviour of tracks, field tests have been carried out for five types of track at the Hino test site [A1]. The test section for each track type is 25m long, and concrete monobloc sleepers are used with a spacing of 0.5-0.65m. The track gauge is 1.067 m. The main features of each track are listed in Table A1. The measurements include two different rails and five different rail pads. Figure A1 shows the configurations of 50N-type and 60-type rails.

These measurements are compared with predictions using the TWINS model. The parameters used for the TWINS model are presented in Tables A2-A5. In this TWINS calculation, the "bi-bloc" sleeper model is used, in which the sleeper is regarded as a rigid mass. In Table A3, the values of the rail-pad stiffness and damping listed have been chosen to obtain a good tuning for the track resonance behaviour between measurements and predictions in both vertical and lateral directions. For the properties of the ballast, typical values from European railway tracks are chosen.

A2 Measurement procedure

The following measurements have been carried out on each track, as shown in Figure A2.

(1) vertical and lateral point accelerances on the railhead, above a sleeper and at mid-point between two sleepers,

(2) vibration decay rates along the rail in vertical and lateral directions,

These data have been obtained on unloaded tracks by hitting the railhead with an instrumented impact hammer, and installing accelerometers on the railhead, rail foot and sleeper. In the measurements it has been ensured that the coherence curve remains above 0.8. Data were recorded and analyzed by using FFT (Matlab) in the frequency range 0-1250 Hz.

For the decay measurements, the position of the excitation was moved along the rail, and

cross sections A and B were used for the response position.

A3 Point accelerance

The frequency response function of a structure is the response level due to a unit force input, as a function of excitation frequency. It is known as "accelerance" if the response is expressed as acceleration. Each accelerance curve is obtained by averaging 10-20 impacts. The results of two types of accelerance measurements are presented.

(1) vertical accelerance at the railhead

(2) lateral accelerance at the railhead

These point accelerances were all measured above a sleeper and at mid-span between two sleepers.

Figures A3-A7 show vertical frequency response functions measured at A and B for each track. In figures A3-A7, the results predicted with TWINS models (rodel and tinf models) are also shown. For the vertical accelerance, a comparison of the measured results with the prediction of the rodel model shows good agreement. In figures A3-A7, the following resonance behaviour can be seen, which is responsible for the relative motion of the rail and sleeper.

- $f \fallingdotseq 250$ Hz: the combined mass of the rail and sleeper moves on the ballast stiffness
- $f \fallingdotseq 700$ Hz: the mass of the sleeper moves on the stiffness of the pad and ballast
- $f \fallingdotseq 1000$ Hz: the rail moves on the pad stiffness (out of phase with the sleeper)

As the support in the rodel model is continuous, this model cannot predict the behaviour associated with the pinned-pinned effects (where sleeper separation equals half a bending wavelength, about 1000 Hz). On the other hand, the tinf model predicts the pinned-pinned resonances and a difference in frequency response between the two measured positions. However, it is found that the phenomena associated with the pinned-pinned resonance cannot be seen clearly in the measurements. Therefore, it is not clear whether the tinf model can predict the pinned-pinned effects well for these tracks. Some points may be responsible for

this.

- the pinned-pinned modes may be out of the measured frequency range (0-1250 Hz),
- the pinned-pinned modes may be mitigated by sleeper bending modes,
- the sleepers of the tracks are randomly spaced in a certain range, and this may make the pinned-pinned resonance less distinct.
- the rail pads are modelled as point springs but occurs over a certain length in practice - this may introduce more damping to the pinned-pinned mode.

Figures A8-A12 show lateral response functions of the tracks. It is found that the predictions are lower than the measurements. This is because torsion is neglected in the TWINS models (see also [9]). The measured results do not clearly show the periodicity effect, which is associated with the pinned-pinned resonance. Therefore, although the tinf model predicts the pinned-pinned resonance, it is not clear that the tinf model gives good predictions for the pinned-pinned resonance.

A4 Track decay rate

The measured decay rate is calculated from an integral of squared vibration over the length of the rail [A2]. If the transfer accelerance from x=0 to position x is $A(x)$, its amplitude can be approximated by

$$|A(x)| \approx |A(0)|e^{-\beta x}$$

where β is the imaginary (decaying) part of the wave number. Then the integral

$$\int_0^\infty |A(x)|^2 dx \approx |A(0)|^2 \int_0^\infty e^{-2\beta x} dx = |A(0)|^2 \frac{1}{2\beta}$$

from which the decay rate, Δ (dB/m), can be estimated:

$$\Delta = 8.686\beta \approx \frac{4.343}{\int_0^\infty \frac{|A(x)|^2}{|A(0)|^2} dx} \approx \frac{4.343}{\sum_{i=1}^{N} \frac{|A(x_i)|^2}{|A(0)|^2} \Delta x_i}$$

where N measurement positions are used and Δx_i is the distance between adjacent

measurement positions. This method gives more reliable results than fitting a straight line to the curves of amplitude versus distance, although it is sensitive to the value of the point accelerance, $A(0)$.

In order to estimate the decay rates using this method, measurements should be performed at many positions along a rail, since it is necessary that the integral of squared vibration is carried out over a long distance. However, in the field measurements, the position of the excitation was moved only up to 1.0 or 1.2 m (1.0 m: three positions, 1.2 m: four positions). This length is not sufficient to estimate low decay rates accurately.

Figure A13 shows predicted decay rate plotted against measured decay rate for all track conditions. Each symbol represents values at 1/3 octave bands. For the decay rate of vertical vibration, it can be seen that the overall trends are predicted reasonably well. For the lateral decay rate, the measured result shows a poor agreement with the predicted results, when the predicted decay rates are less than 3 dB/m. This is caused by the measured length not being long enough to estimate low decay rates.

The decay rates of vertical and lateral vibration obtained from the measurements are compared with the results of the rodel model in figures A14-A18. (The decay rate from the tinf model is not shown since the damping of the rail is neglected in this model.) The decay rate of the vertical vibration is well predicted for all tracks. For the lateral decay rate, the predicted curve shows a good agreement with the measured results below 400 Hz. Above 500Hz, the measured decay rate is much higher than the predicted results. This is due to the fact that the integral of the measured vibration is carried out over a short length, and the decay rate is not estimated correctly.

A5 Other parameters

Apart from the parameters listed in Tables A1-A5, the following parameters were used throughout.

Other parameters used for rodel

- •Minimum frequency: 50 Hz
- •Maximum frequency: 9000 Hz
- •spacing type: log
- •spacing parameter: 1.059

Other parameters used for tinf

- •Excitation point: z=0.25 (sleeper spacing=0.5),
  0.3125 (sleeper spacing=0.6-0.65)
- •Minimum frequency: 50 Hz
- •Maximum frequency: 9000 Hz
- •spacing type: log
- •spacing parameter: 1.059

References

[A1] Manabe, K. and Takigawa, M. Modal behaviour of a track, *RTRI Report*, 2001 (in Japanese).

[A2] Thompson, D.J. Jones, C. J. C. Wu, T. X. & France, G. The influence of the non-linear stiffness behaviour of rail pads on the component of rolling noise, *Proc. Instn. Mech. Enginrs.*, Vol. 213 Part F, 1999, pp233-241.

Table A1 Main features of tracks

Track	Rail	Sleeper	Sleeper spacing	Rail pad	Roadbed
A	50N	Concrete monobloc	0.5m	Pandrol	Ballast
B	60	Concrete monobloc	0.6-0.65m	5N-type	Ballast
C	60	Concrete monobloc	0.6-0.65m	T-type	Ballast
D	60	Concrete monobloc	0.63m	5-type	Ballast
E	50N	Concrete monobloc	0.6m	10-type	Ballast

Table A2 Rail parameters

Rail	50N-type	60-type
Bending stiffness (ver)	4.034×10^{6}	5.320×10^{6}
Shear coefficient (ver)	0.4	0.4
Rail loss factor (ver)	0.01	0.01
Bending stiffness (lat)	0.685×10^{6}	1.05×10^{6}
Shear coefficient (lat)	0.4	0.4
Rail loss factor (lat)	0.01	0.01
Mass per length	50	60
Cross receptance level	-12	-12
Cross receptance sign	+1	+1

Table A3 Rail pad parameters

Fastener	Pandrol	5N-type	T-type	5-type	10-type
Vertical stiffness	1.1×10^{9}	0.7×10^{9}	0.26×10^{9}	0.75×10^{9}	0.6×10^{9}
Vertical loss factor	0.25	0.25	0.25	0.25	0.25
Lateral stiffness	1.2×10^{8}	0.85×10^{8}	0.35×10^{8}	1.0×10^{8}	0.85×10^{8}
Lateral loss factor	0.25	0.25	0.25	0.25	0.25

Table A4 Sleeper parameters

Track	A	B	C	D	E
Mass (1/2 sleeper)	80	80	80	80	80
Distance between sleepers	0.5	0.625 (0.6-0.65)	0.625 (0.6-0.65)	0.63	0.6
Length (1/2 sleeper)	1.0	1.0	1.0	1.0	1.0
Width	0.156	0.156	0.156	0.156	0.156

Table A5 Ballast parameters

Vertical stiffness	6.7×10^{7}
Vertical loss factor	2.0
Lateral stiffness	3.4×10^{7}
Lateral loss factor	2.0

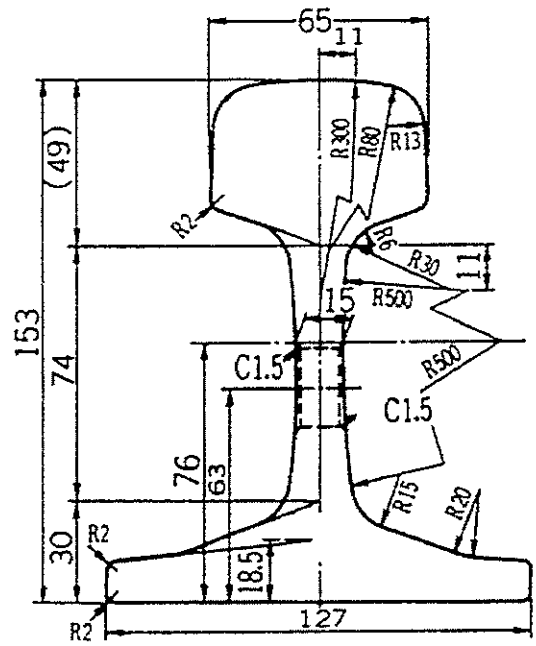

(a) 50N-type Rail

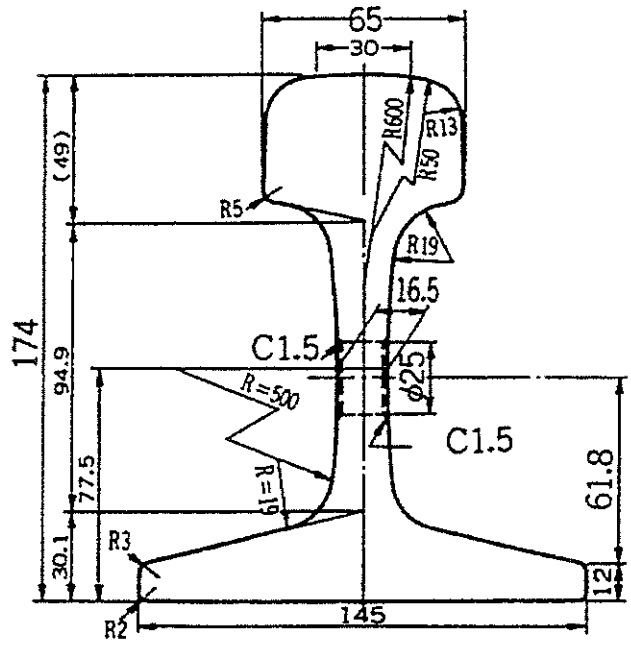

(b) 60-type Rail

Figure A1 Configuration of 50N-type and 60-type rails

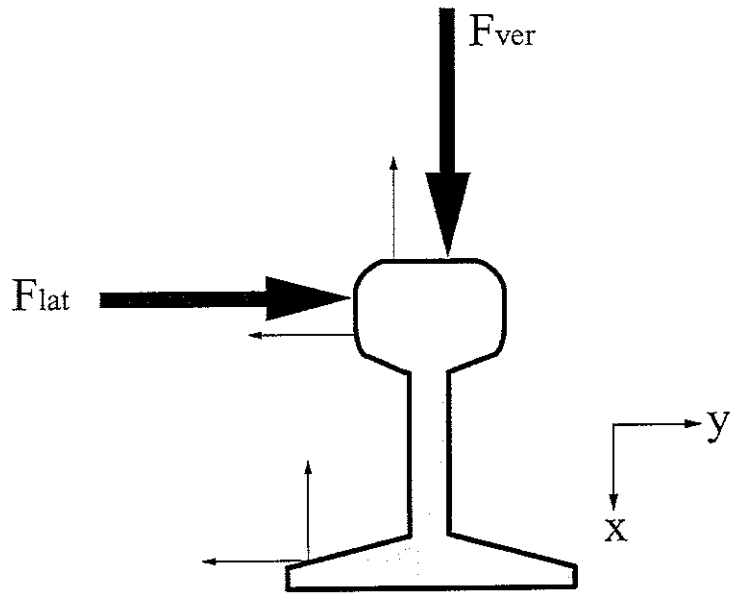

(a) Accelerometer and force positions on rail cross-section at A and B

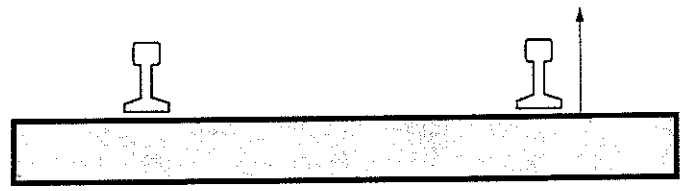

(b) Accelerometer position on sleeper at B

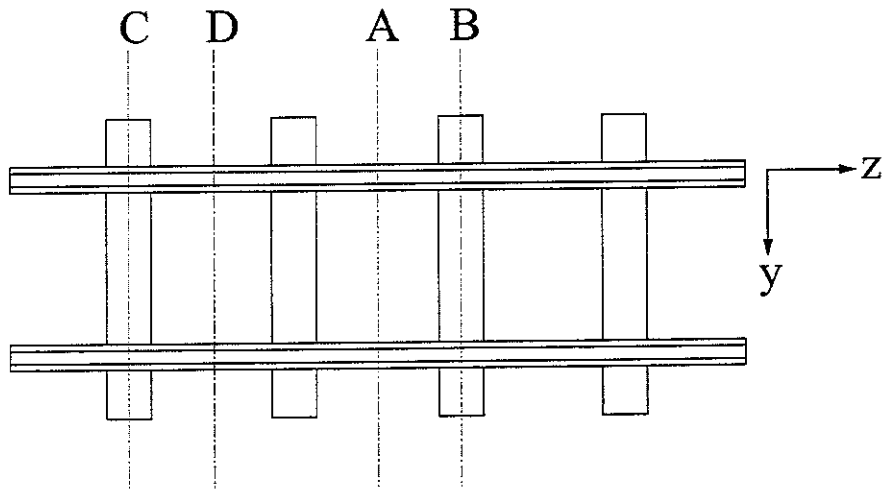

(c) Global positions on track

Figure A2 Measurement positions used for track characterization

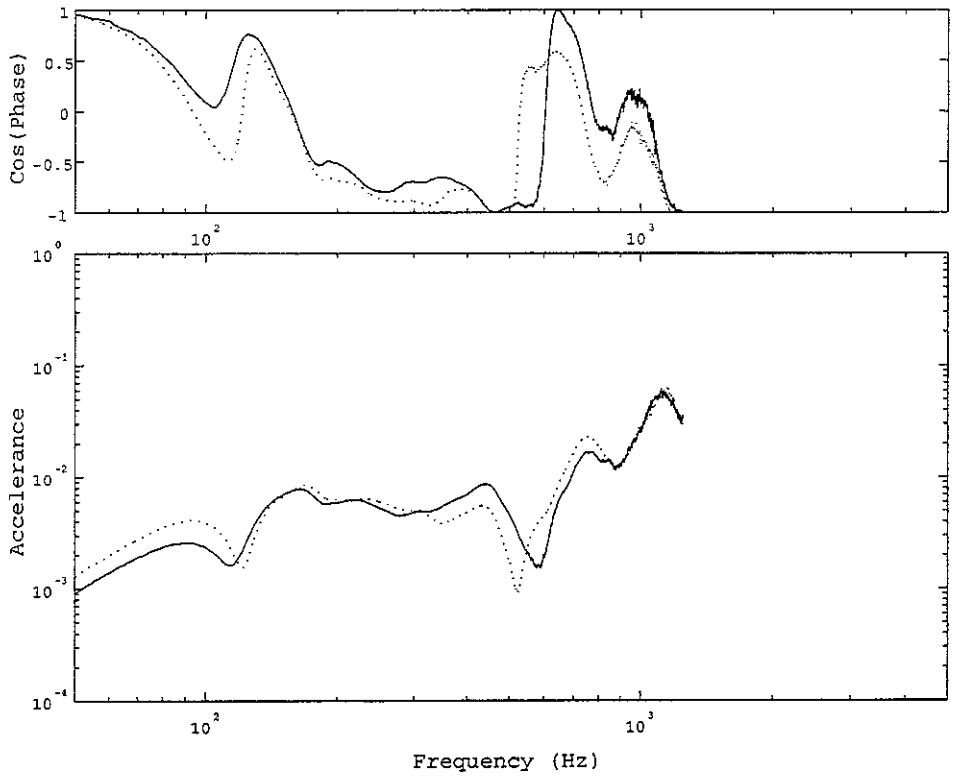

(a) Measured accelerance

(——: above sleeper, ------: between sleepers)

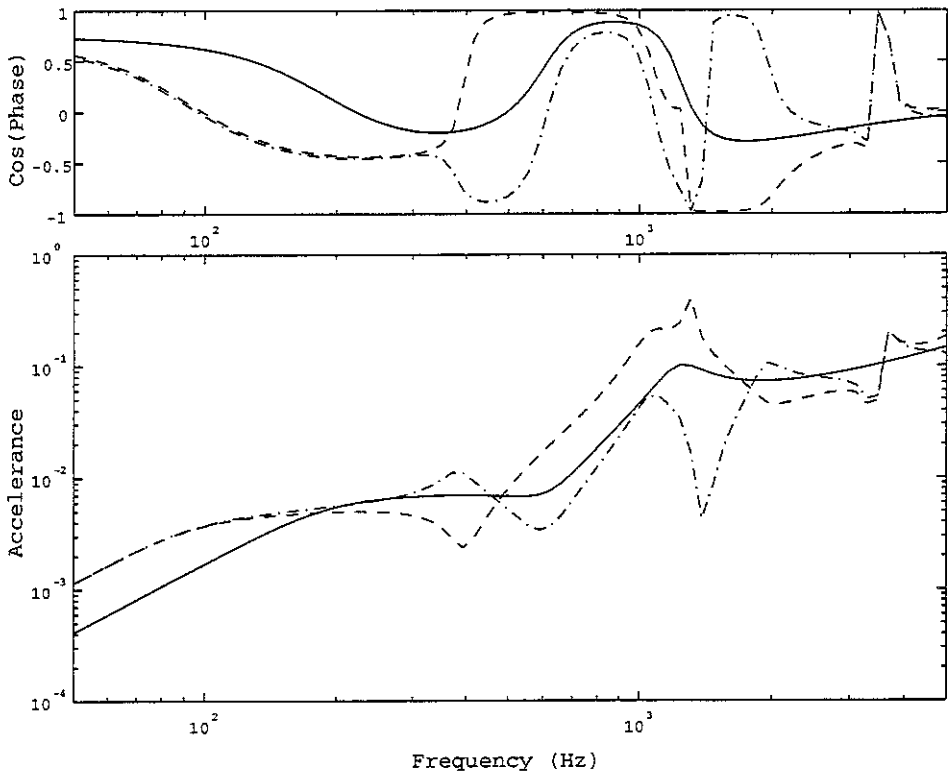

(b) Predicted accelerance

(——: rodel model, — · —: above sleeper (tinf model), ------: between sleepers(tinf model))

Figure A3 Vertical point accelerance of Track A

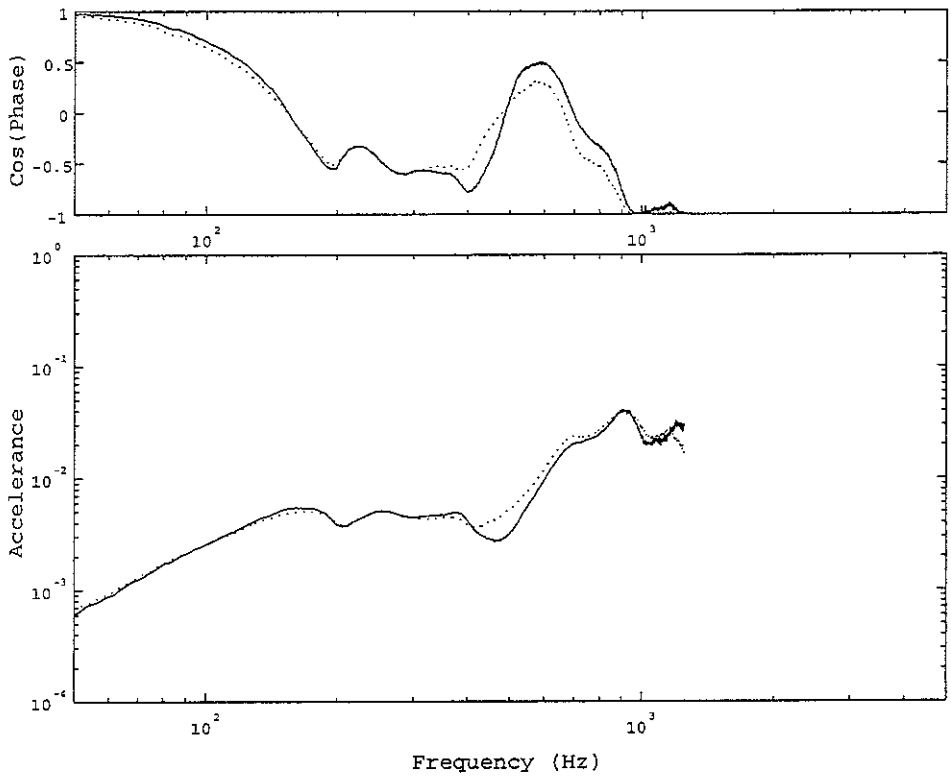

(a) Measured accelerance

(——: above sleeper, ------: between sleepers)

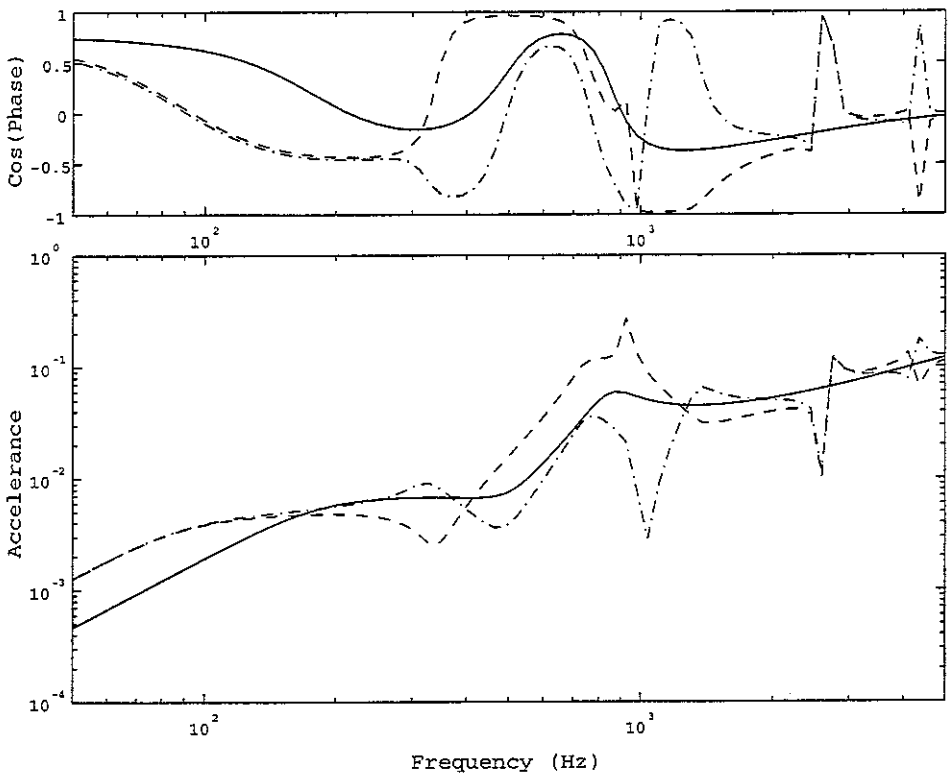

(b) Predicted accelerance

(——: rodel model, — · —: above sleeper (tinf model), ------: between sleepers(tinf model))

Figure A4 Vertical point accelerance of Track B

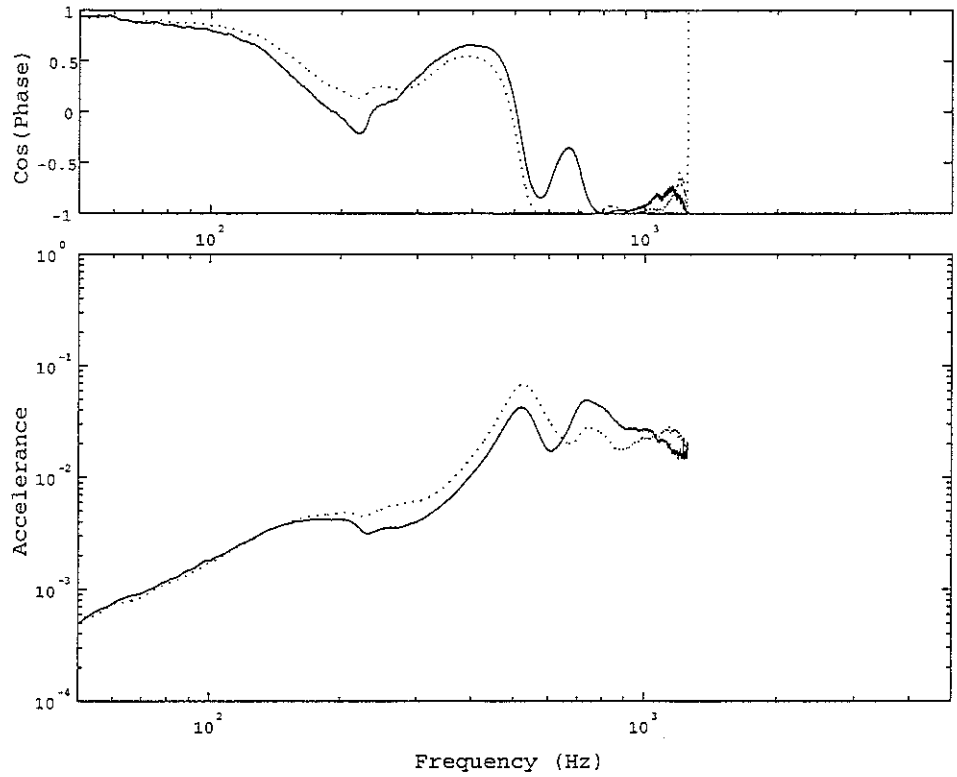

(a) Measured accelerance

(——: above sleeper, ------: between sleepers)

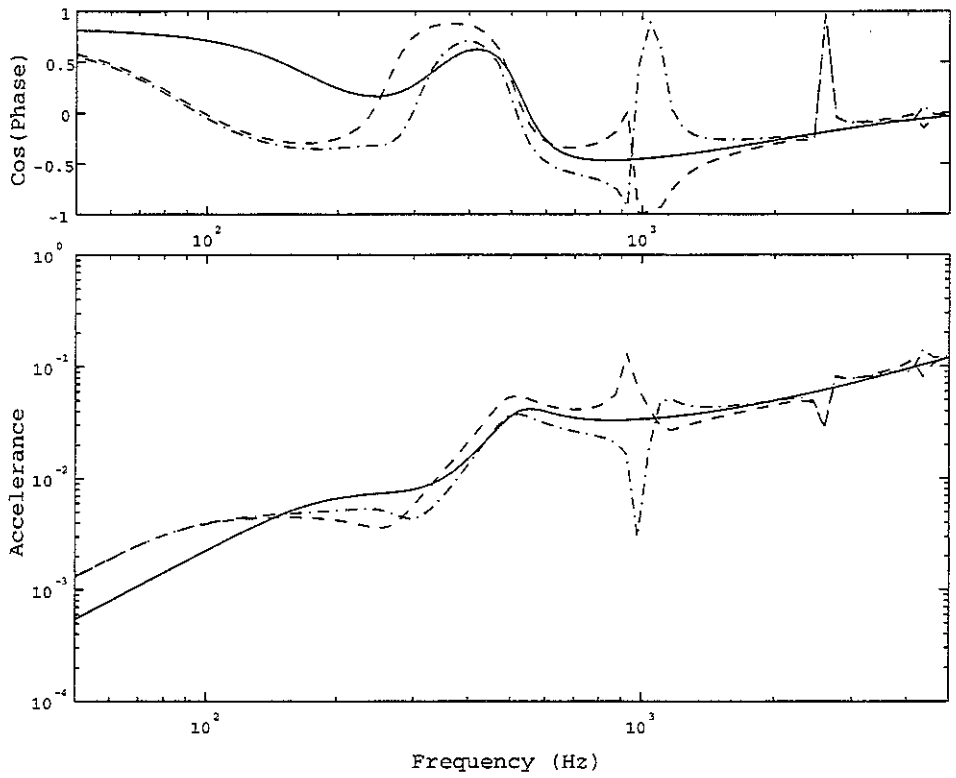

(b) Predicted accelerance

(——: rodel model, — · —: above sleeper (tinf model), ------: between sleepers(tinf model))

Figure A5 Vertical point accelerance of Track C

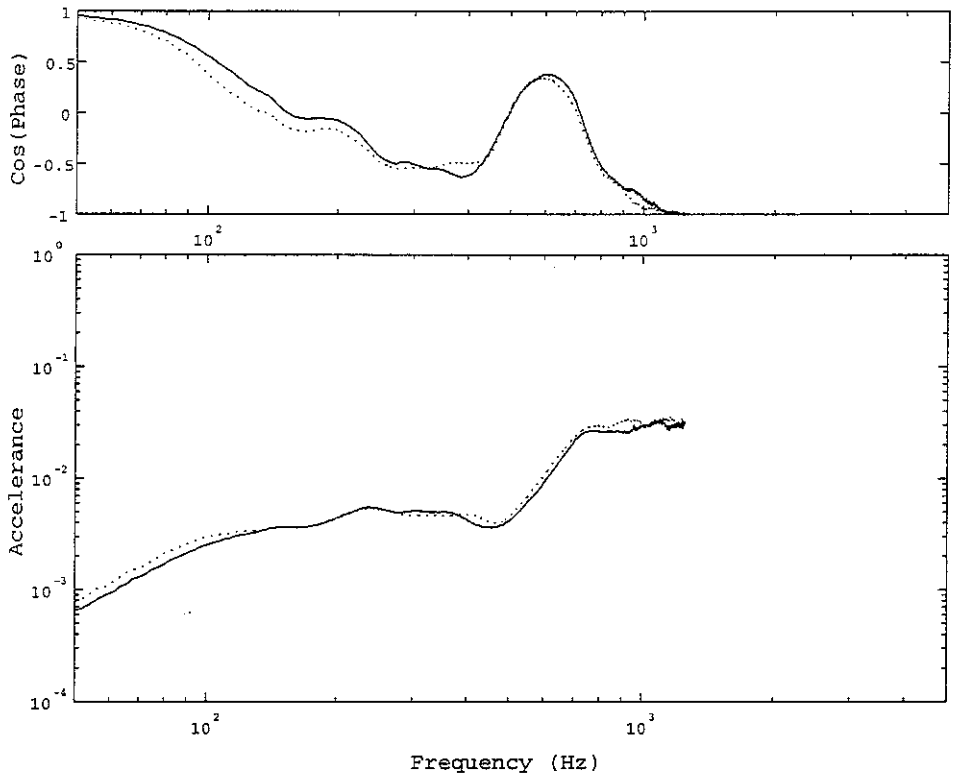

(a) Measured accelerance

(——: above sleeper, ------: between sleepers)

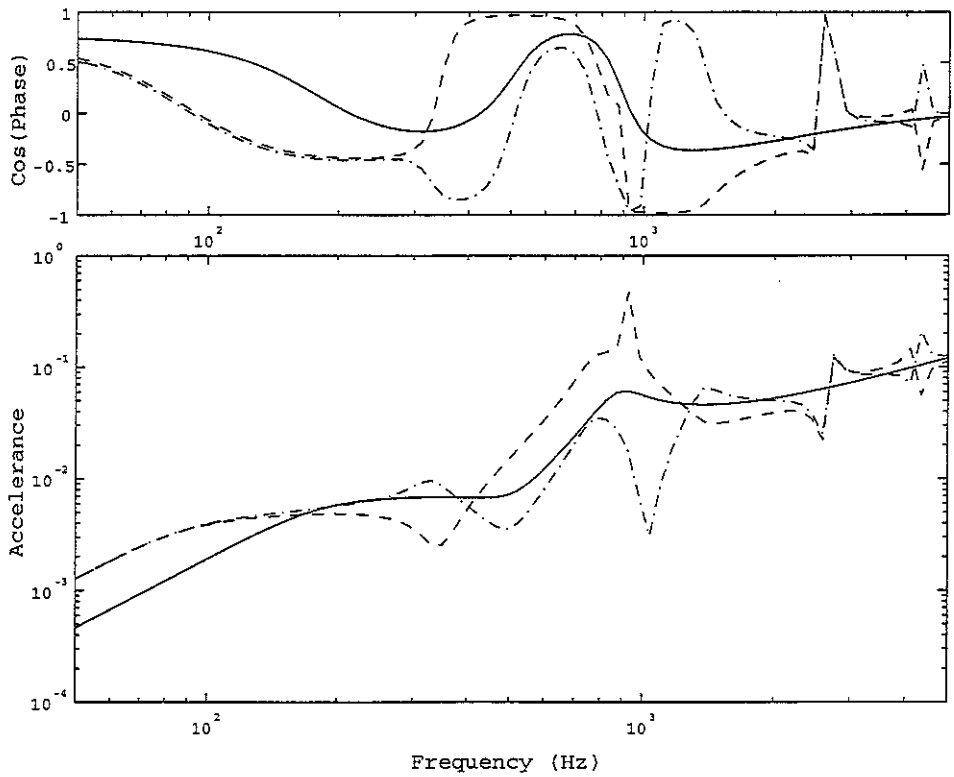

(b) Predicted accelerance

(——: rodel model, — · —: above sleeper (tinf model), ------: between sleepers(tinf model))

Figure A6 Vertical point accelerance of Track D

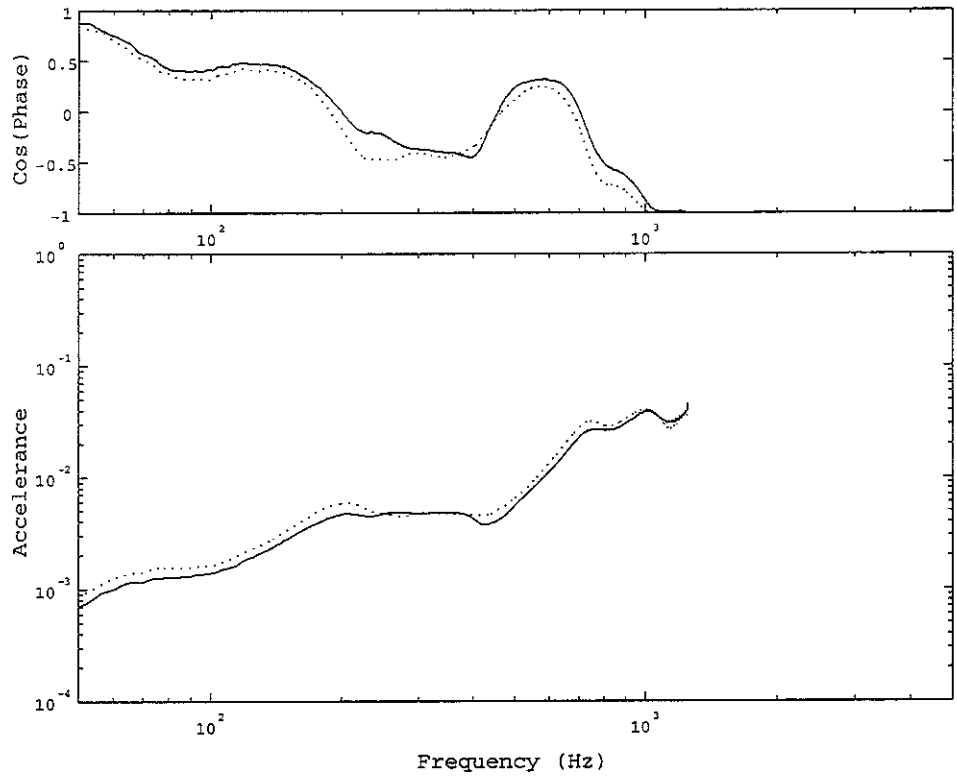

(a) Measured accelerance

(——: above sleeper, ------: between sleepers)

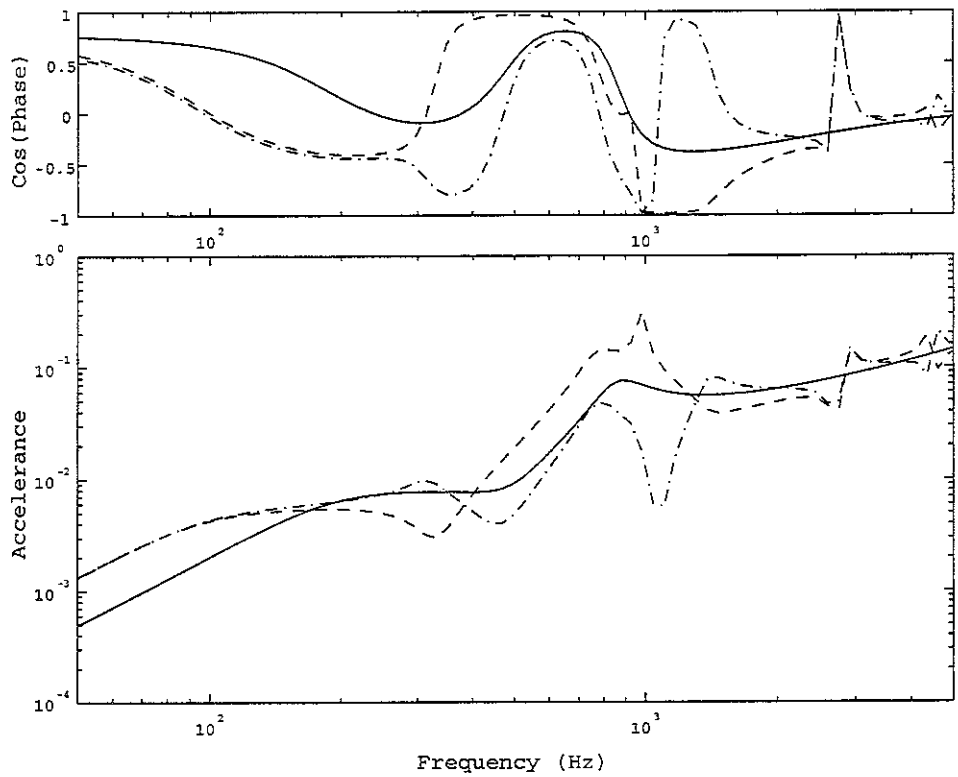

(b) Predicted accelerance

(——: rodel model, — · —: above sleeper (tinf model), ------: between sleepers(tinf model))

Figure A7 Vertical point accelerance of Track E

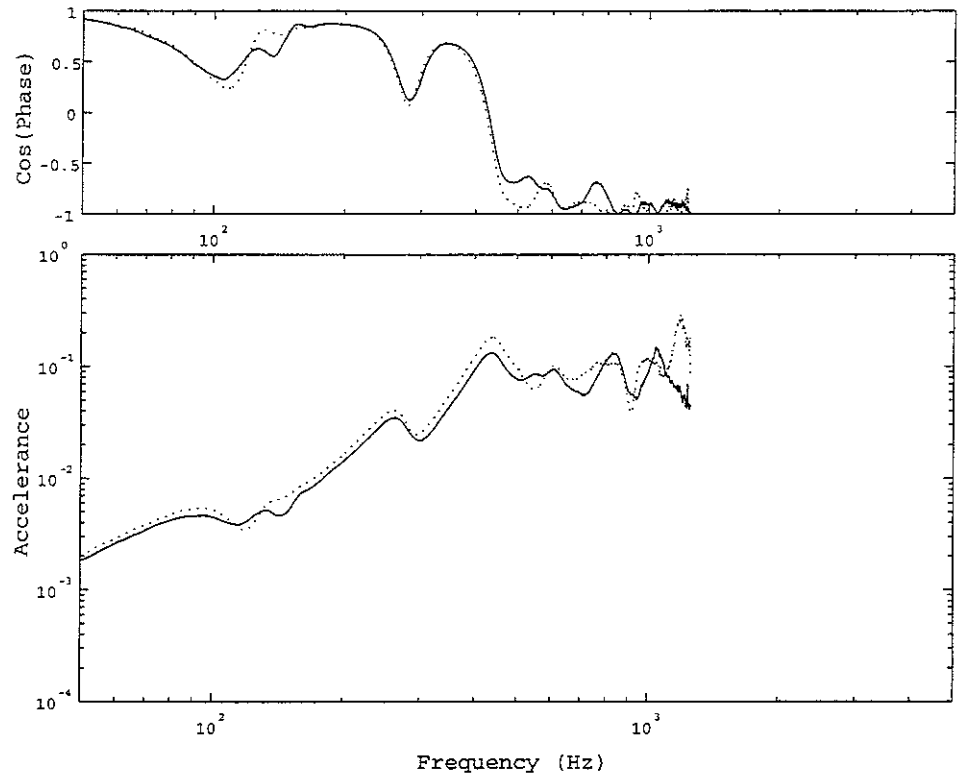

(a) Measured accelerance

(——: above sleeper, ------: between sleepers)

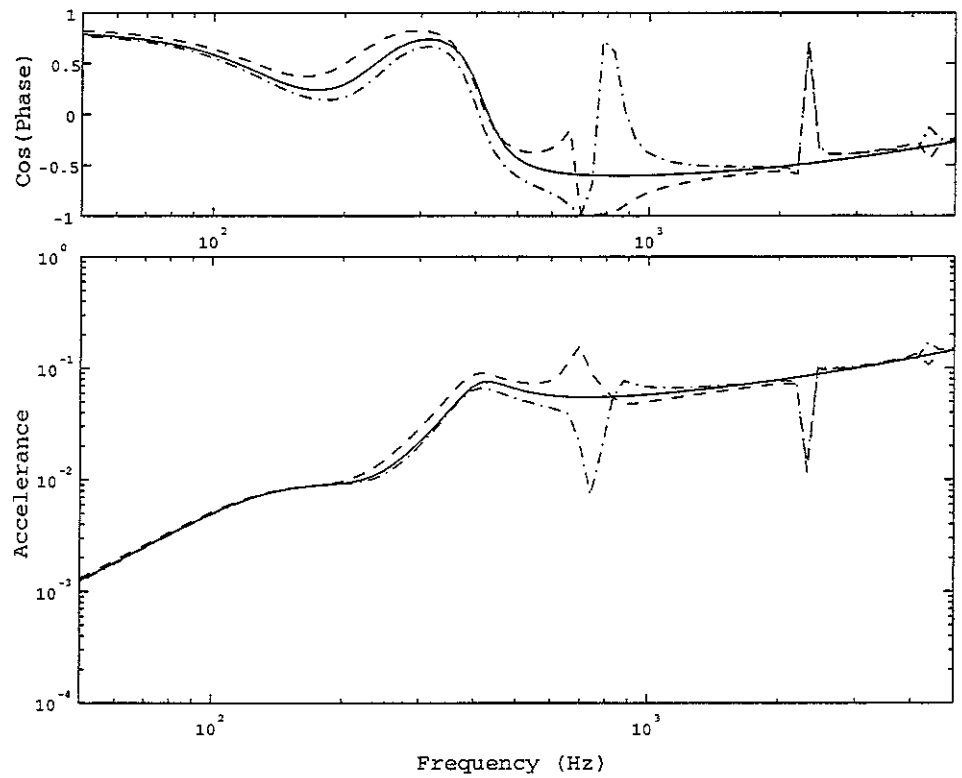

(b) Predicted accelerance

(——: rodel model, — · —: above sleeper (tinf model), ------: between sleepers(tinf model))

Figure A8 Lateral point accelerance of Track A

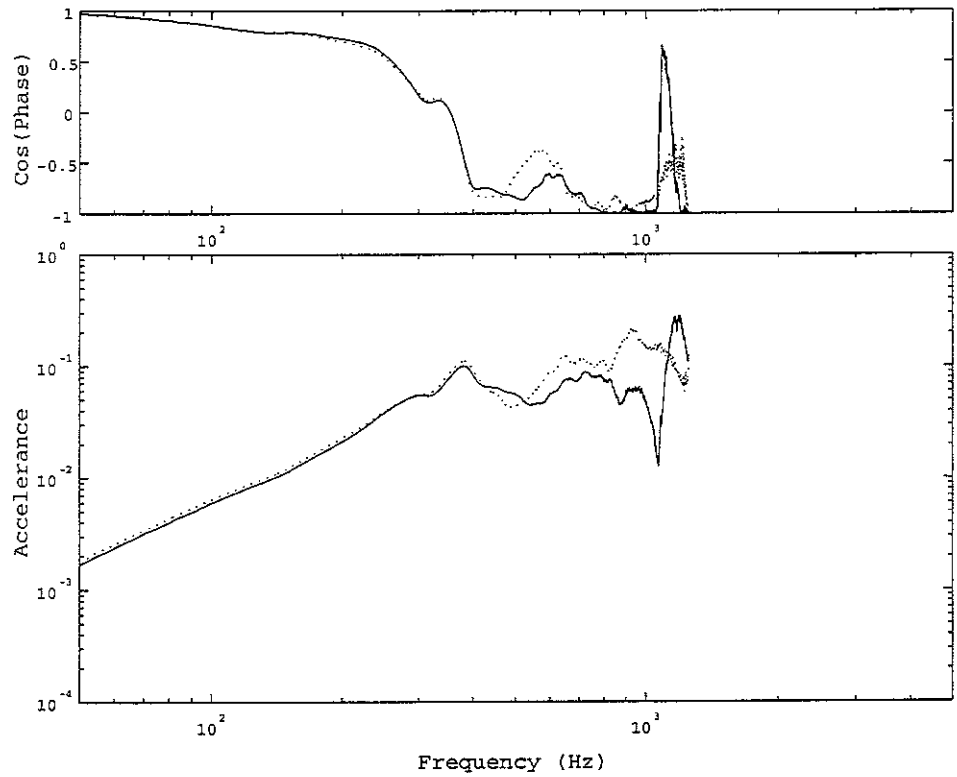

(a) Measured accelerance

(——: above sleeper, ------: between sleepers)

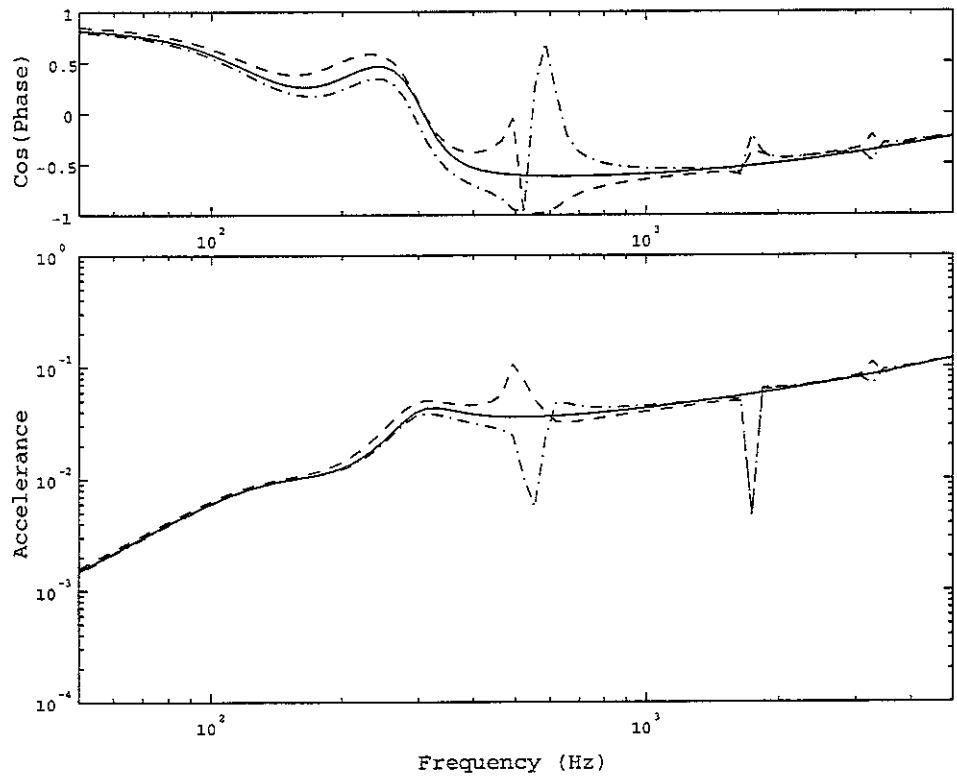

(b) Predicted accelerance

(——: rodel model, — · —: above sleeper (tinf model), ------: between sleepers(tinf model))

Figure A9 Lateral point accelerance of Track B

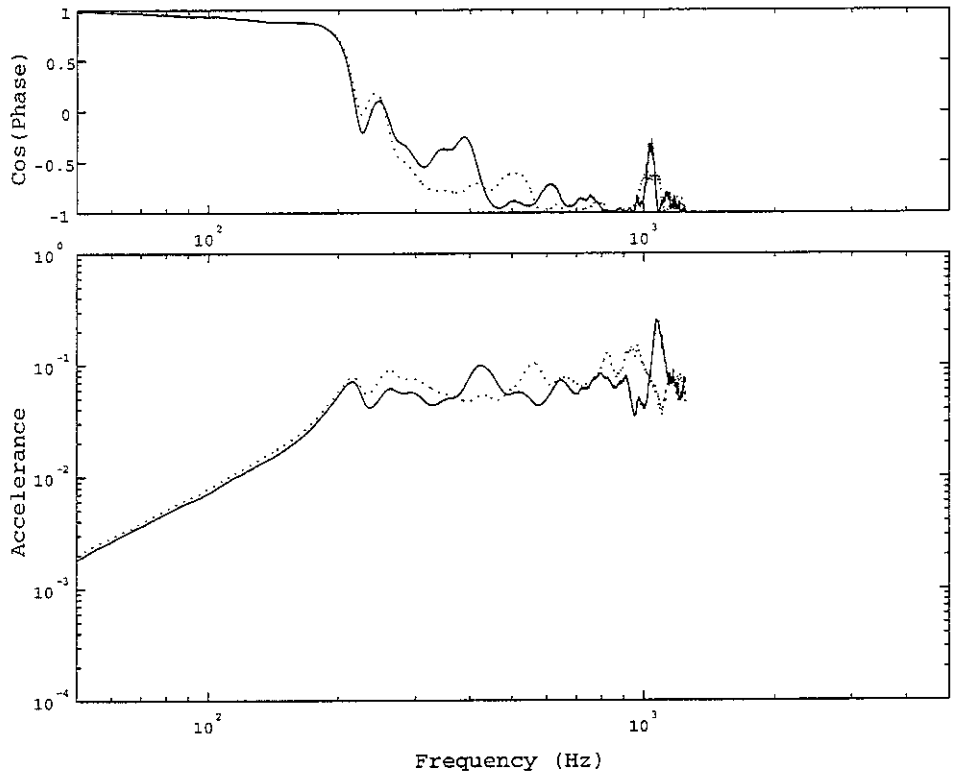

(a) Measured accelerance

(——: above sleeper, ------: between sleepers)

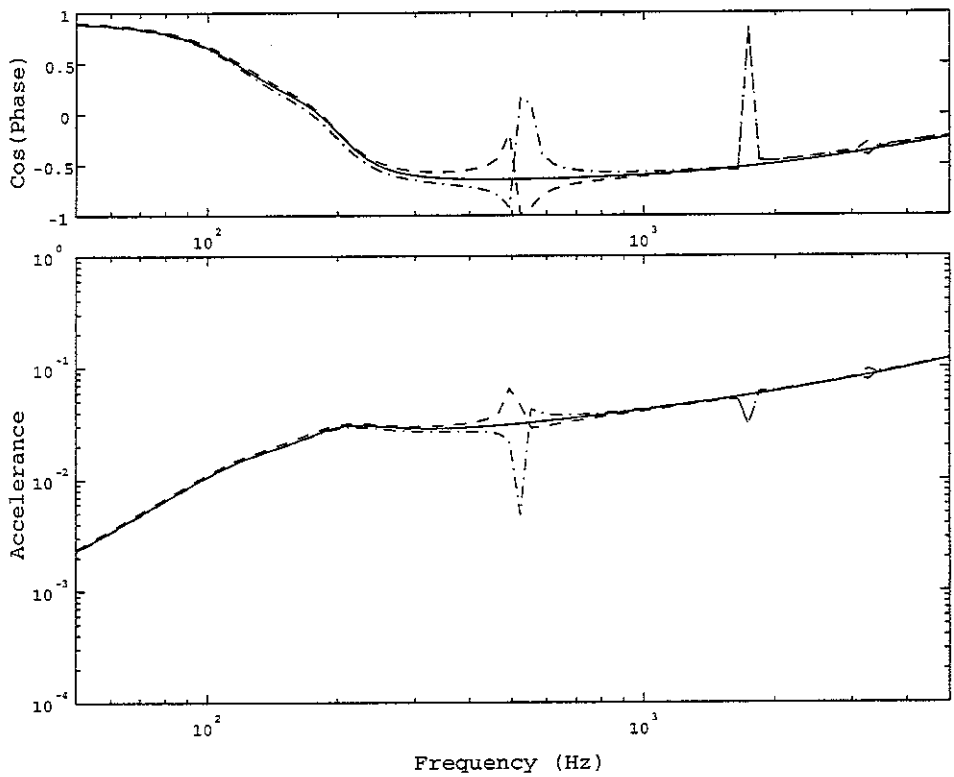

(b) Predicted accelerance

(——: rodel model, — · —: above sleeper (tinf model), ------: between sleepers(tinf model))

Figure A10 Lateral point accelerance of Track C

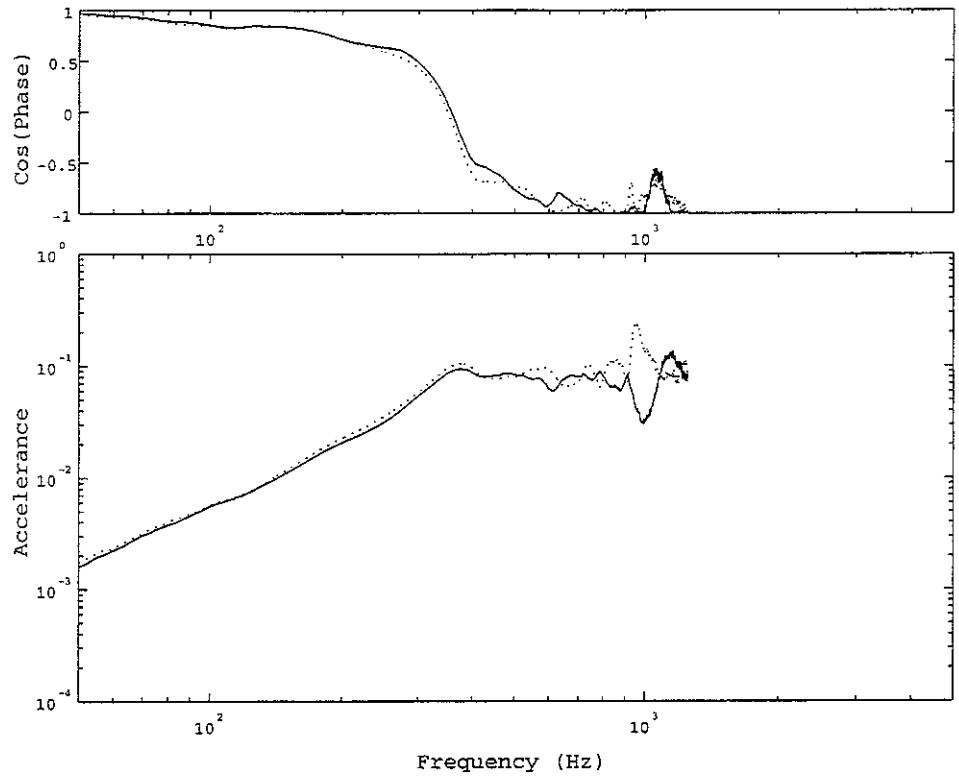

(a) Measured accelerance

(——: above sleeper, ------: between sleepers)

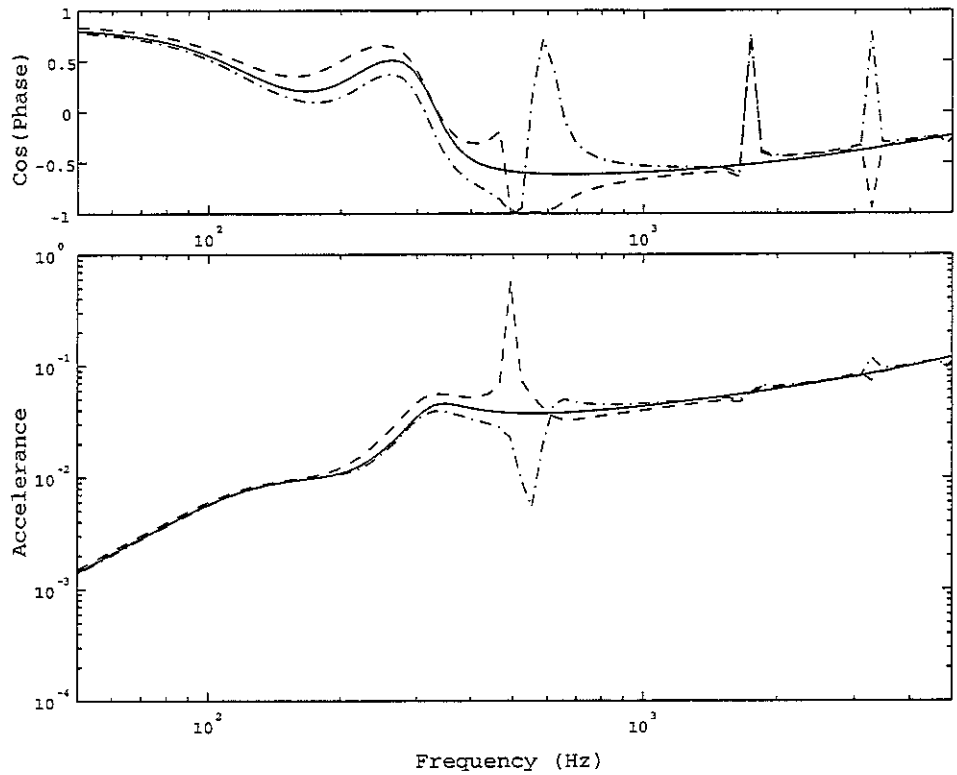

(b) Predicted accelerance

(——: rodel model, — · —: above sleeper (tinf model), ------: between sleepers(tinf model))

Figure A11 Lateral point accelerance of Track D

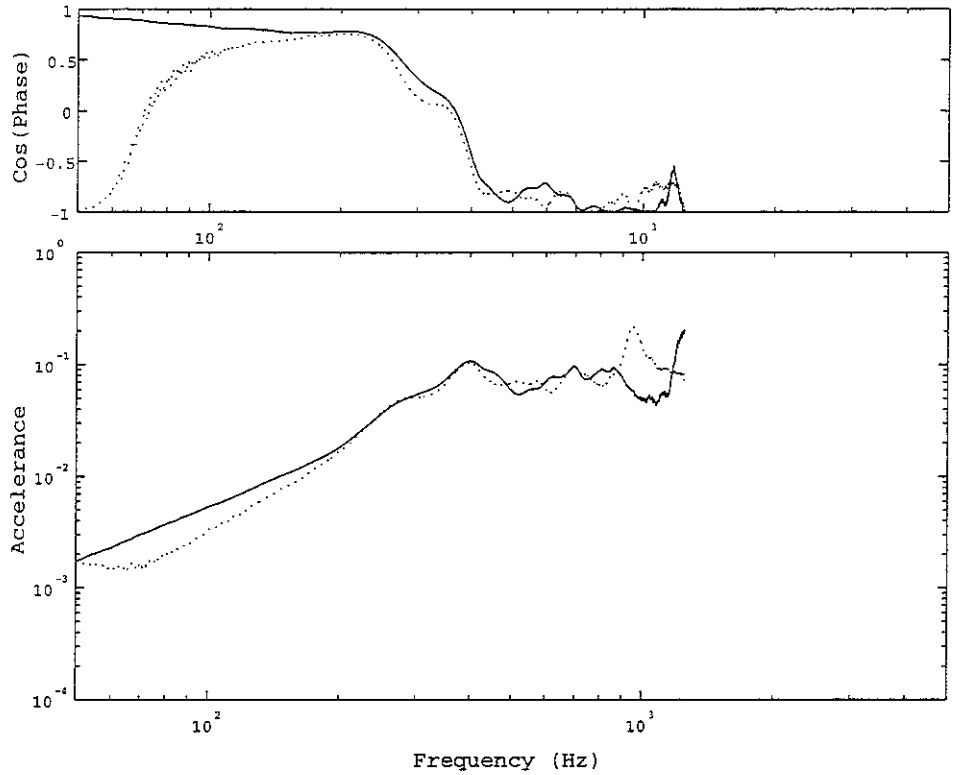

(a) Measured accelerance

(——: above sleeper, ------: between sleepers)

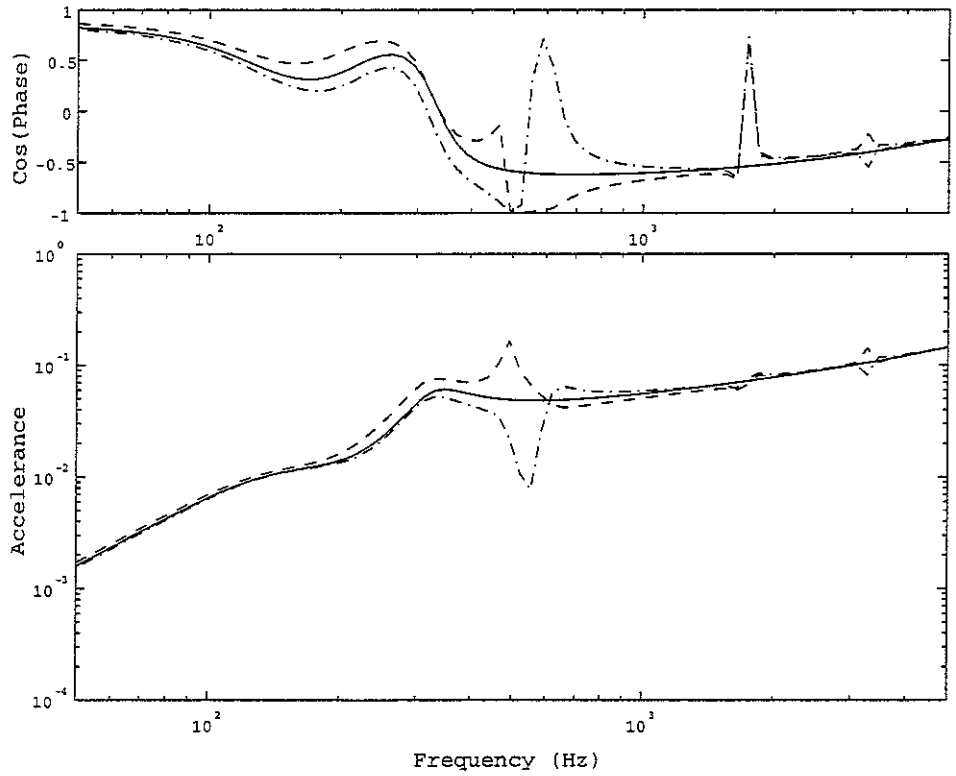

(b) Predicted accelerance

(——: rodel model, — · —: above sleeper (tinf model), ------: between sleepers(tinf model))

Figure A12 Lateral point accelerance of Track E

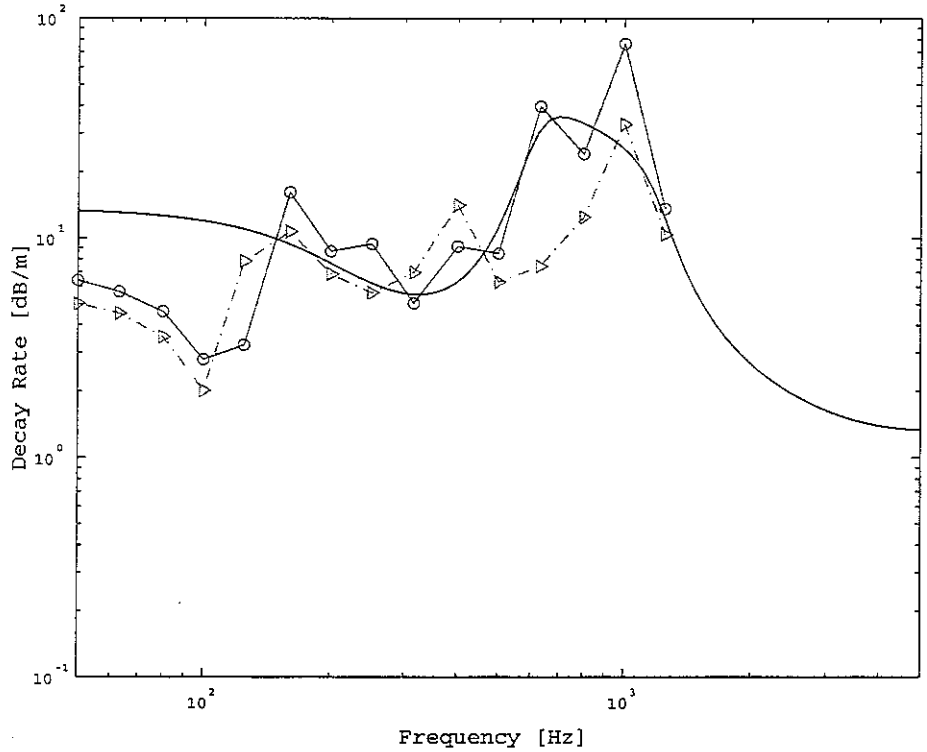

(a) Vertical direction

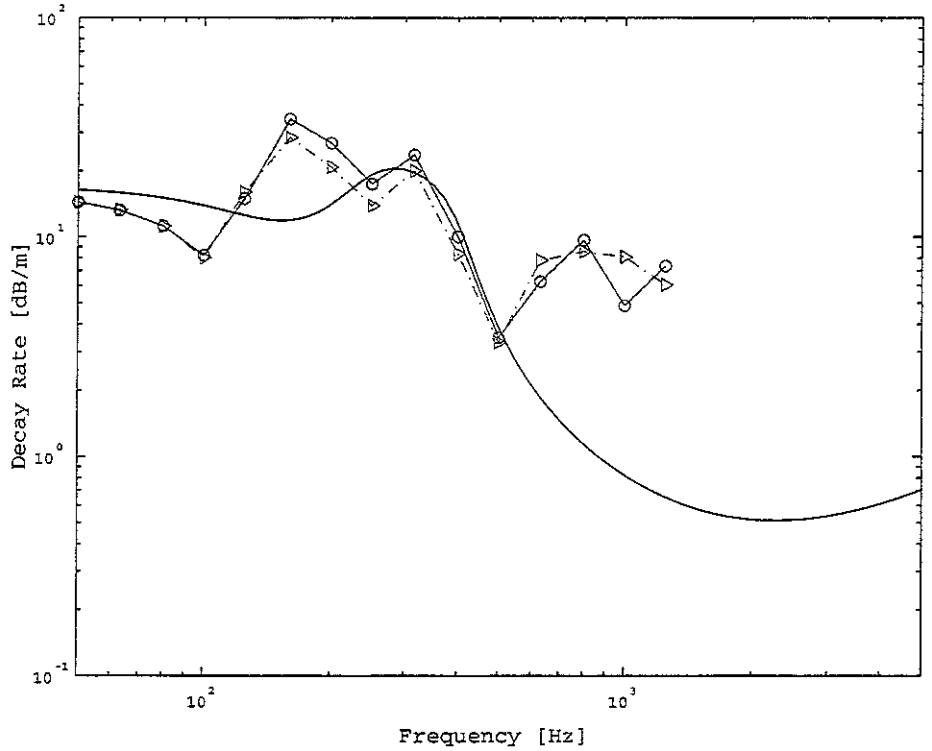

(b) Lateral direction

Figure A14 Decay rate with distance of Track A

(——: propagating wave (rodel model), —○—: measured wave (cross-section A), —△—: measured wave (cross section B))

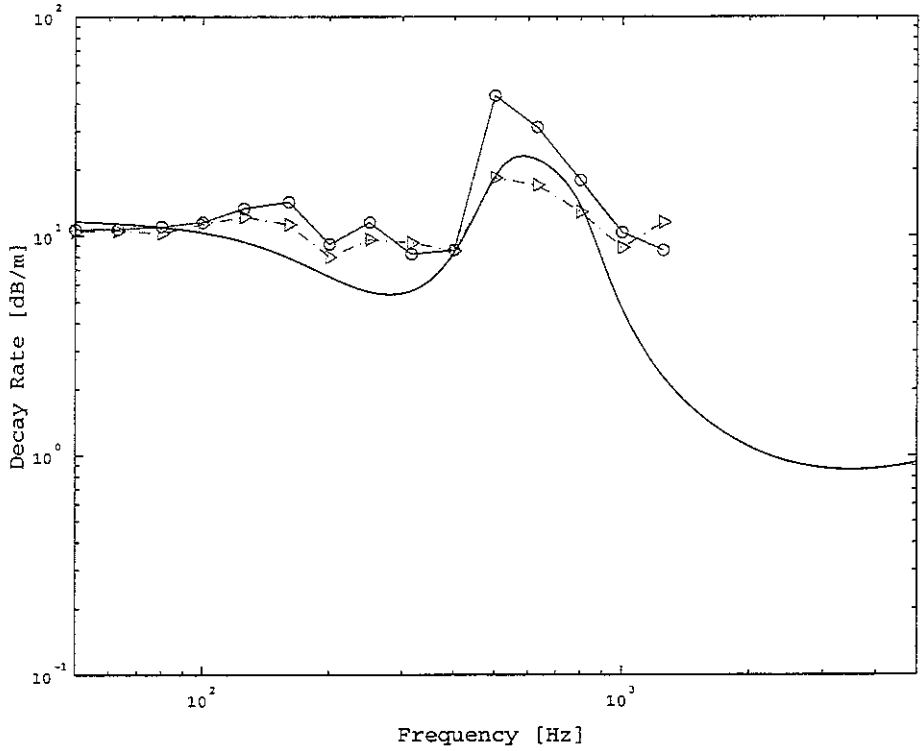

(a) Vertical direction

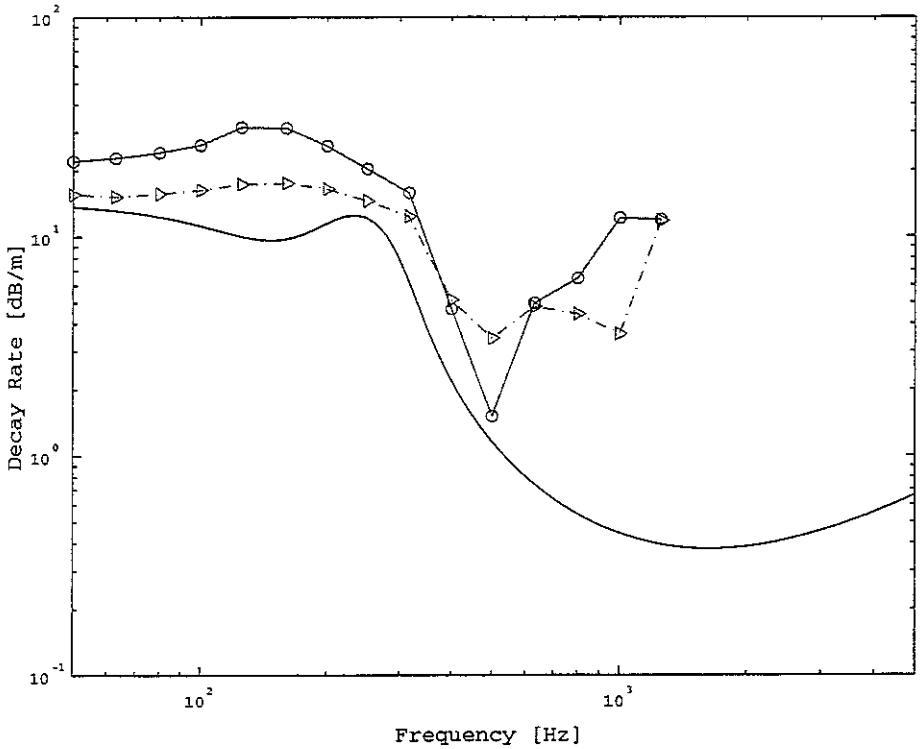

(b) Lateral direction

Figure A15 Decay rate with distance of Track B

(——: propagating wave (rodel model), —○—: measured wave (cross-section A), —△—: measured wave (cross section B))

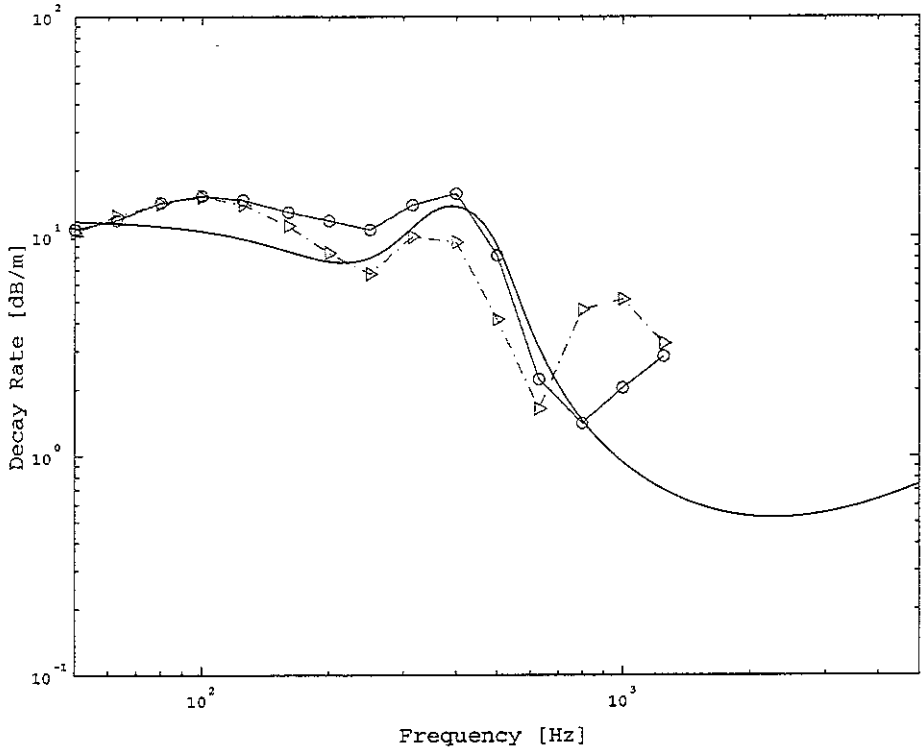

(a) Vertical direction

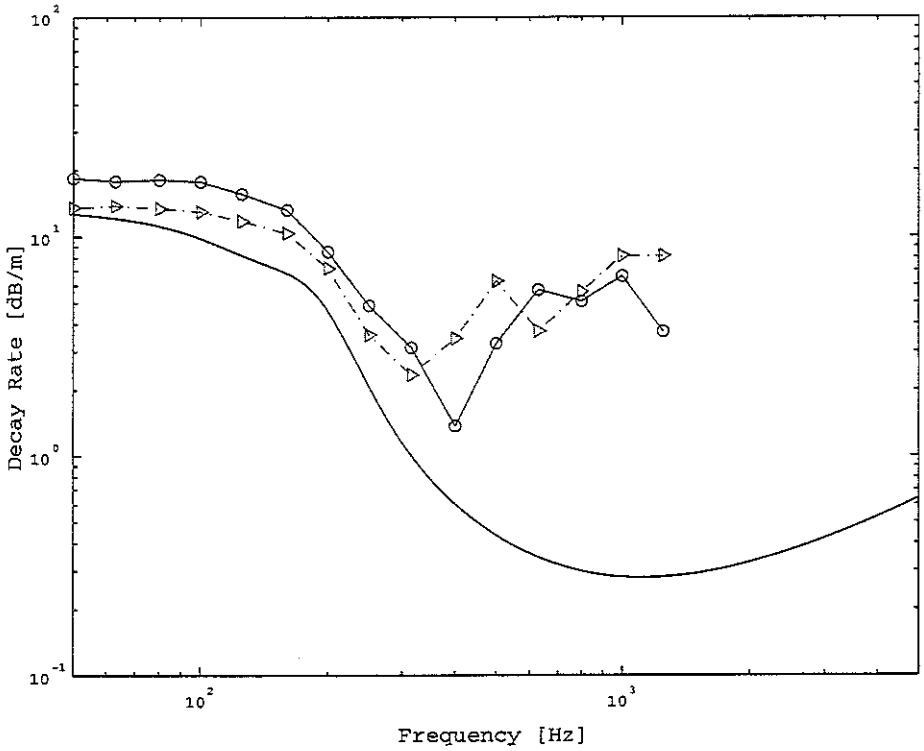

(b) Lateral direction

Figure A16 Decay rate with distance of Track C

(——: propagating wave (rodel model), —○—: measured wave (cross-section A), —△—: measured wave (cross section B))

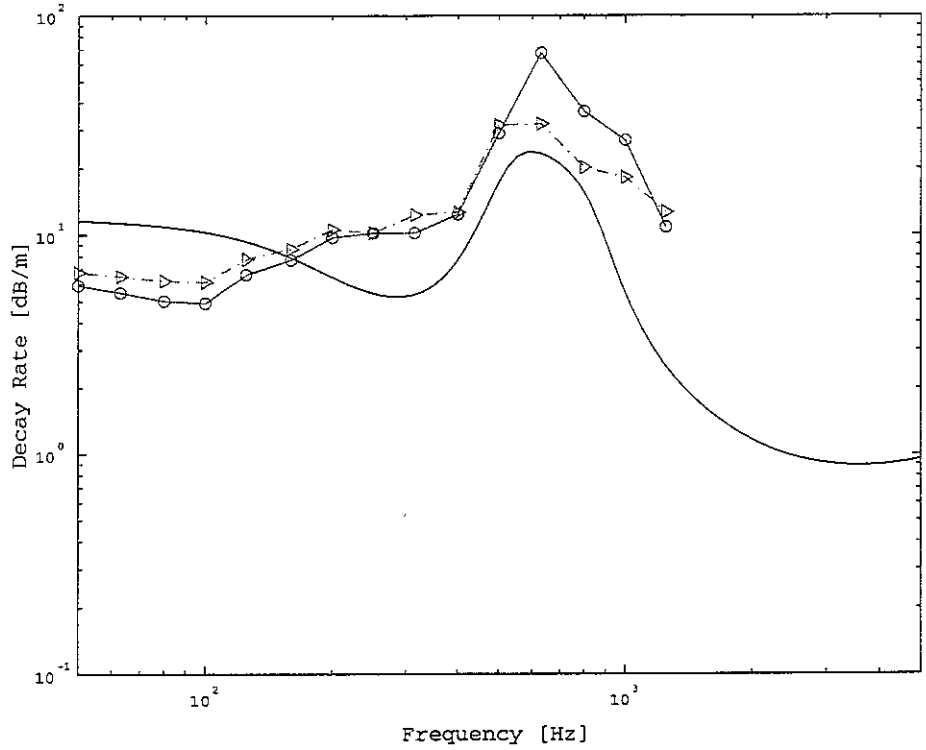

(a) Vertical direction

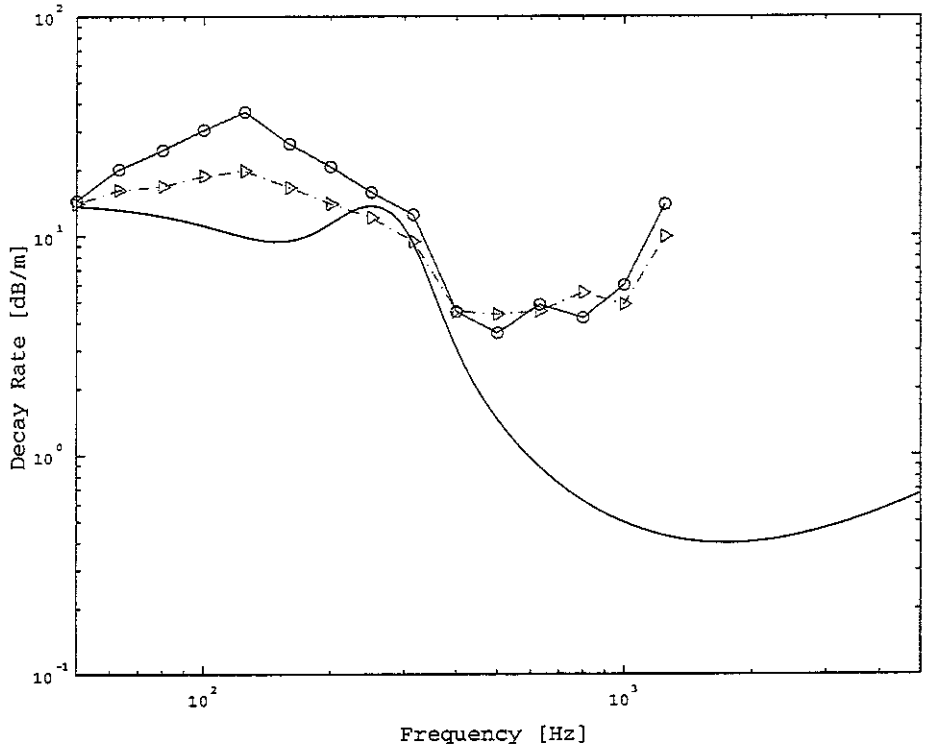

(b) Lateral direction

Figure A17 Decay rate with distance of Track D

(——: propagating wave (rodel model), —○—: measured wave (cross-section A), —△—: measured wave (cross section B))

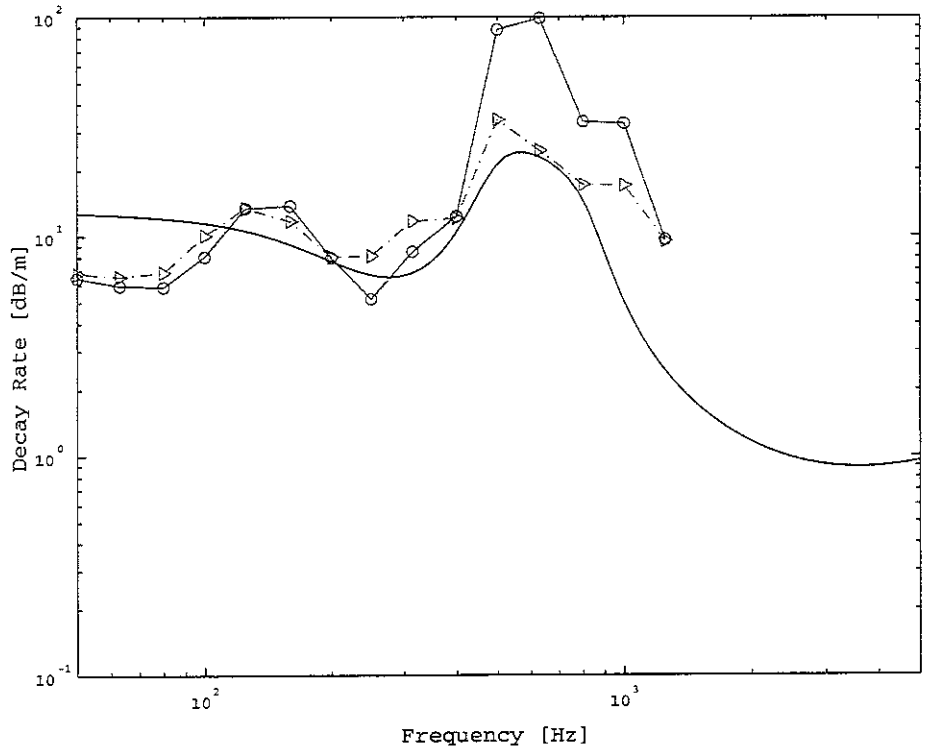

(a) Vertical direction

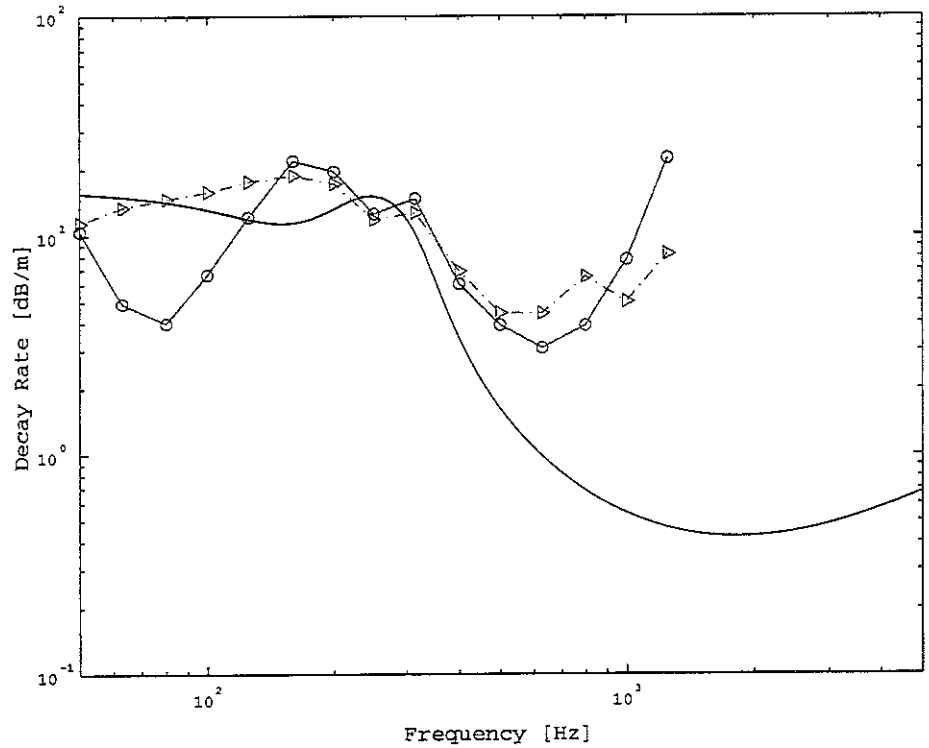

(b) Lateral direction

Figure A18 Decay rate with distance of Track E

(——: propagating wave (rodel model), —○—: measured wave (cross-section A), —△—: measured wave (cross section B))

B WHEEL CHARACTERIZATION

B1 Wheel natural frequencies and mode shapes

Eight types of wheel have been modelled using TWINS, of which six are used for the validation tests. Wheel conditions are listed in Table B1. Figures B1-B2 show the cross-section details of the eight wheels.

Table B1 Wheel condition

Wheel	Description	Diameter (mm)	Mass (kg)
A	A-type solid wheel with curved web	810	314
B	B-type solid wheel with curved web	810	332
C	C-type solid wheel with straight web	860	314
D	EC4489-type solid wheel with curved web	860	314
E	A86D-type solid wheel with curved web	860	314
AW	A-type solid wheel with doubly curved web	860	292
BW	B-type solid wheel with doubly curved web	860	307
CW	NA-type solid wheel with doubly curved web	860	292

For each of these eight wheel types, modal bases (natural frequencies and mode shape data) have been obtained using the finite element software ANSYS. Use is made of the symmetry of the wheel structure, so that a quarter wheel is modelled by using solid elements. Axisymmetric models were not used as some wheels are doubly curved. Figure B3 shows an example of the finite element model. The wheel axle is ignored, and the wheel model is clamped at the inner edge of the hub. The modal bases have been calculated up to 9000 Hz, since an upper limit frequency on 8000 Hz in 1/3 octave bands corresponds to 8900 Hz. The calculations have been carried out by using symmetric/anti-symmetric boundary conditions (two symmetry boundary conditions give modes with an even number of nodal

diameters, and symmetric and anti-symmetric boundary conditions give modes with an odd number of nodal diameters). Predicted natural frequencies for the eight wheel types are listed in Tables B2-B9. Wheel principle modes of vibration are categorized by two numbers: the number of nodal diameters (n) and the number of nodal circle. In-plane (radial) modes are categorized similarly, except that only one such set (m=0) is found within the frequency range of interest. No measured values are available for comparison.

In Tables B2-B9, it can be seen that wheels AW, BW and CW have lower radial natural frequencies than the other wheels due to the fact that these wheels have thin webs.

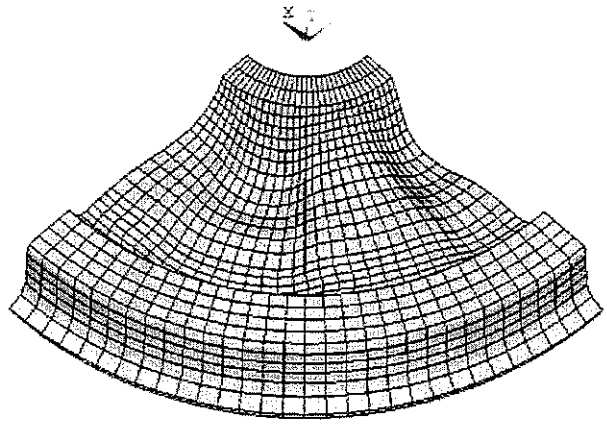

Figure B3 Finite element model of wheel AW

B2 Frequency response function

The accelerance of a structure can be derived from its natural frequencies, the corresponding mode shapes and the damping loss factor, using the modal superposition method [B1]. The natural frequencies and mode shapes of a wheel can be predicted with the finite element idealization. It might be better that the modal damping ratios are determined from wheel characterization measurements, but such measurements have not been carried out for the present measurement campaign. It is difficult to estimate the modal damping ratios, even if the measurements are carried out. This is because the estimation of modal damping ratios depends on frequency resolution of the FFT analyzer. Therefore,

typical values from a similar wheel are used [B2-B3], which are in the range 10^{-2}-10^{-4}. For modes including axle vibration (0 and 1 nodal diameter modes), the modal damping ratios should be chosen in the range 0.001-0.1 to give good agreement with measurements [B2]. Therefore, the modal damping ratios corresponding to 0 and 1 nodal diameter modes are set to 0.001 and 0.01 respectively. For modes with 2 or more nodal diameters, a nominal value of 10^{-4} is used here for the damping loss factor. This is due to the fact that, in all-steel wheels, the modal damping ratios of the modes are typically 10^{-4}. These damping ratios are acceptable since they are considerably smaller than the damping induced by the coupling with a track, and therefore exact values are not required for the TWINS calculations. Also the 1 nodal diameter radial mode is given a damping ratio of 1 [B3]. The modal parameter file corresponding to each wheel type is listed on the pages 103-120.

Predicted frequency response functions for the eight wheel types at the contact position are shown in Figures B4-B11. In figures B4-B11, axle bending modes are not included.

In Figures B4-B11, it can be seen that the radial accelerance has the behaviour of a mass at low frequencies, a dip at around 500 Hz, and then above 1000 Hz a series of peaks which are the one-nodal circle modes and the radial modes. In the absence of axial-radial coupling only the radial modes can be seen. For the axial accelerance, the strong peaks correspond to the zero-nodal-circle modes.

The parameters used in the TWINS calculations are presented in Table B10.

References

[B1] Thompson, D.J. Mace, B.R., High frequency structural vibration, *ISVR lecture notes*, University of Southampton, 2003

[B2] Thompson, D.J. Wheel-Rail Noise Generation, Part II: Wheel Vibration. *Journal of Sound and Vibration*, **161**(3), 1991, 401-419.

[B3] Thompson, D.J. & Jones, C.J.C. A review of the modelling of wheel/rail noise generation. *Journal of Sound and Vibration*, **231**(3), 2000, 519-536.

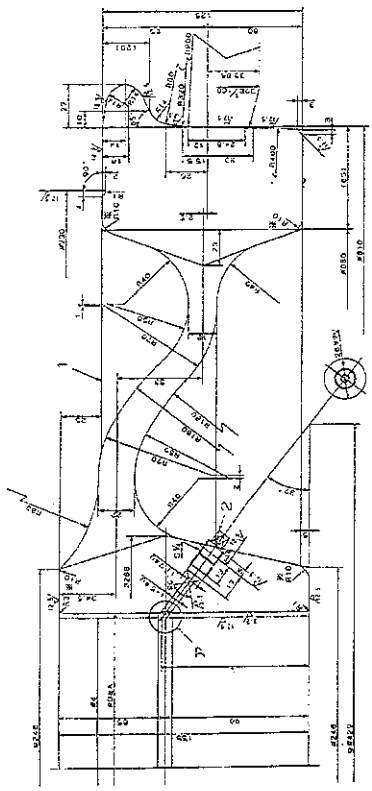

(a) wheel A

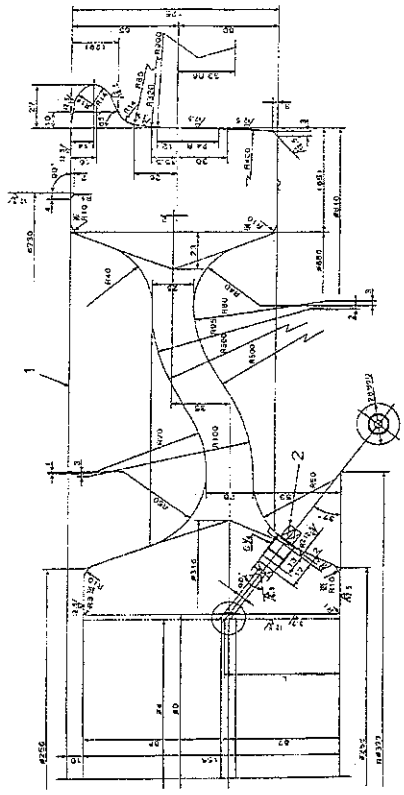

(b) wheel B

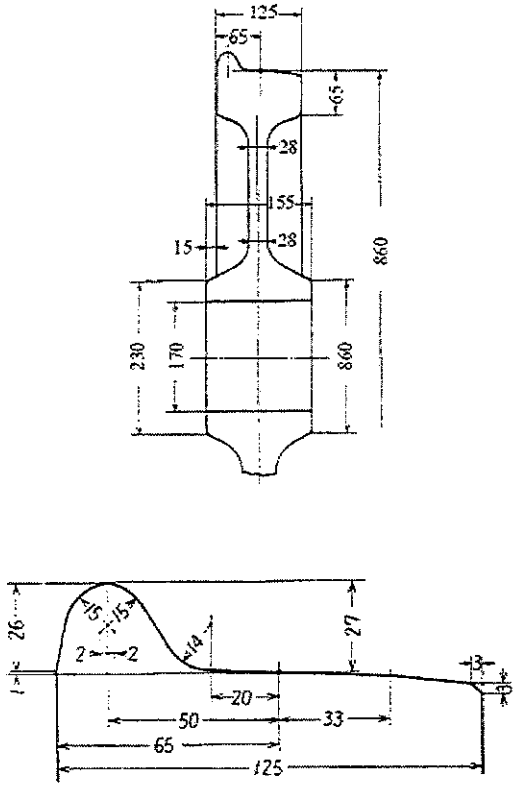

(a) wheel C

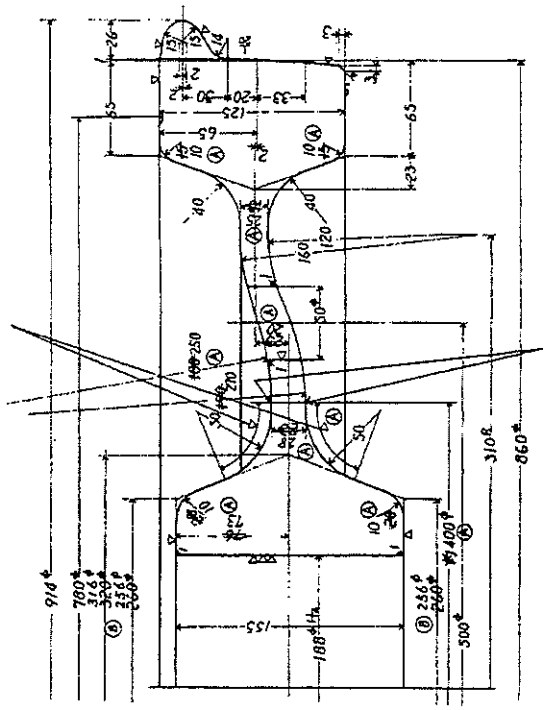

(b) wheel D

Figure B1 Cross-section details of wheel

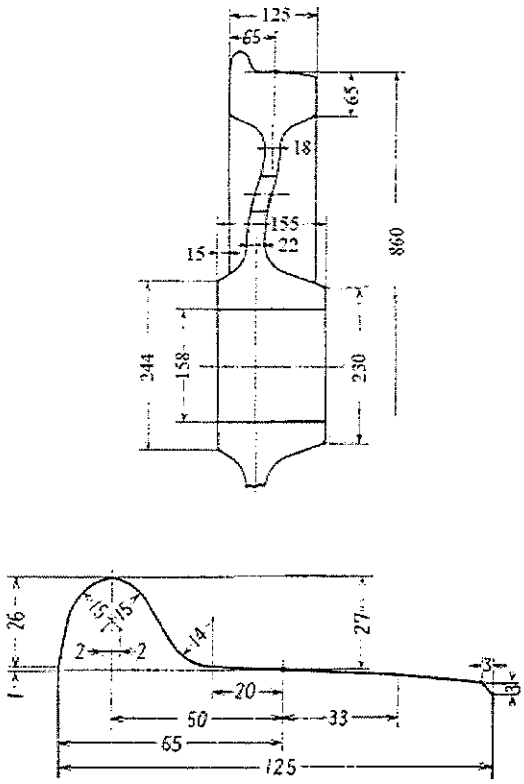

(a) wheel E

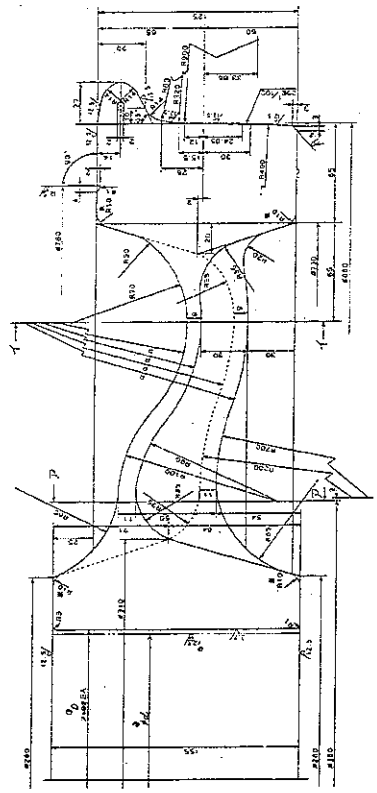

(b) wheel AW

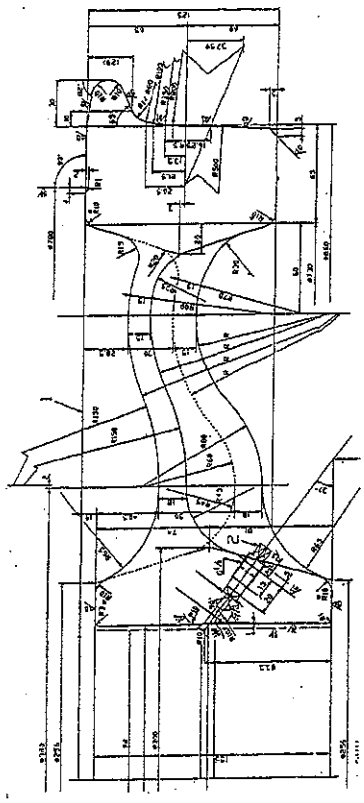

(c) wheel BW

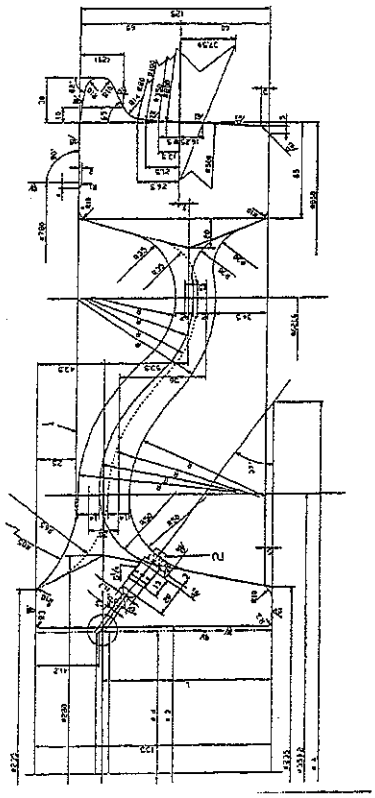

(d) wheel CW

Figure B2 Cross-section details of wheel

Table B2 Natural frequencies for wheel A

n	Zero-nodal-circle	Radial	One-nodal-circle	Two-nodal-circle	Three-nodal-circle	Circum-ferential
0	466	2740	1802	4782	---	---
1	246	1082	2190	4826	---	3307
2	498	1554	2934	5165	---	4772
3	1279	2199	3822	5386	---	6914
4	2274	3044	4686	6099	---	8908
5	3393	4046	5484	7067	---	---
6	4590	5153	6303	8197	---	---
7	5837	6313	7238	---	---	---
8	7120	7488	8339	---	---	---
9	8430	8692	---	---	---	---

Table B3 Natural frequencies for wheel B

n	Zero-nodal-circle	Radial	One-nodal-circle	Two-nodal-circle	Three-nodal-circle	Circum-ferential
0	473	3260	1932	5611	---	---
1	284	1430	2266	5660	---	3636
2	500	2034	2994	5872	---	5044
3	1253	2711	3867	6234	---	6987
4	2235	3567	4805	6882	---	8965
5	3351	4568	5762	7720	---	---
6	4551	5680	6743	8729	---	---
7	5807	6881	7781	---	---	---
8	7102	8157	8904	---	---	---
9	8427	---	---	---	---	---

Table B4 Natural frequencies for wheel C

n	Zero-nodal-circle	Radial	One-nodal-circle	Two-nodal-circle	Three-nodal-circle	Circum-ferential
0	275	3277	1704	4341	8624	---
1	195	1389	1925	4416	8681	3544
2	429	2103	2465	4688	8919	4801
3	1123	2819	3149	5221	---	6558
4	2022	3658	3930	6003	---	8430
5	3049	4594	4827	6977	---	---
6	4161	5618	5859	8093	---	---
7	5329	6721	7023	---	---	---
8	6538	7895	8306	---	---	---
9	7775	---	---	---	---	---

Table B5 Natural frequencies for wheel D

n	Zero-nodal-circle	Radial	One-nodal-circle	Two-nodal-circle	Three-nodal-circle	Circum-ferential
0	279	2823	1578	3800	8088	---
1	162	1200	1878	3876	8224	3216
2	423	1750	2452	3961	8190	4764
3	1126	2349	3058	4507	8525	6524
4	2028	3059	3662	5298	---	8378
5	3054	4378	3815	6254	---	---
6	4159	5289	4579	7298	---	---
7	5308	6354	5408	8396	---	---
8	6520	7520	6311	---	---	---
9	7741	8761	7342	---	---	---
10	8987	---	8484	---	---	---

Table B6 Natural frequencies for wheel E

n	Zero-nodal-circle	Radial	One-nodal-circle	Two-nodal-circle	Three-nodal-circle	Circum-ferential
0	453	2714	1793	4909	---	---
1	239	1081	2159	4951	---	3296
2	496	1563	2906	5240	---	4815
3	1278	2216	3822	5493	---	6911
4	2274	3063	4724	6179	---	8905
5	3394	4066	5550	7118	---	---
6	4590	5178	6377	8233	---	---
7	5838	6348	7301	---	---	---
8	7121	7539	8382	---	---	---
9	8432	8753	---	---	---	---

Table B7 Natural frequencies for wheel AW

n	Zero-nodal-circle	Radial	One-nodal-circle	Two-nodal-circle	Three-nodal-circle	Circum-ferential
0	276	2521	1813	3602	8305	---
1	192	871	2176	3751	7804	3065
2	425	1211	2846	3911	8077	4582
3	1100	1695	3470	4312	8406	6411
4	1942	2413	4186	4898	---	8241
5	2885	3276	5767	6213	---	---
6	3937	4560	6385	7011 7053	---	---
7	4975	5518	7625	8219	---	---
8	6112	6807	8395	---	---	---
9	7168	7907	---	---	---	---
10	8302	---	---	---	---	---

Table B8 Natural frequencies for wheel BW

n	Zero-nodal-circle	Radial	One-nodal-circle	Two-nodal-circle	Three-nodal-circle	Circum-ferential
0	344	2683	1883	3756	8686	---
1	241	1070	2187	3983	---	3160
2	437	1467	2811	4169	---	6274
3	1103	1950	3425	4784	---	6404
4	1956	2664	4317	5258	---	7543
5	2920	3485	5929	6617	---	8422
6	3996	4770	6767	7452	---	---
7	5044	5652	7679	8239	---	---
8	6094	6936	---	---	---	---
9	7168	8023	---	---	---	---
10	8188	---	---	---	---	---

Table B9 Natural frequencies for wheel CW

n	Zero-nodal-circle	Radial	One-nodal-circle	Two-nodal-circle	Three-nodal-circle	Circum-ferential
0	313	2266	1627	2785	8000	---
1	163	744	1912	2750	8147	3047
2	418	1072	2475	3182	8301	4574
3	1086	1679	2847	3959	8342	6326
4	1922	2354	3921	4911	8861	8881
5	2843	3322	4461	5904	---	---
6	3842	4441	5449	6980	---	---
7	4848	5210	5955	7957	---	---
8	6010	6891	7257	---	---	---
9	7060	8064	8188	---	---	---
10	8085	8123	---	---	---	---

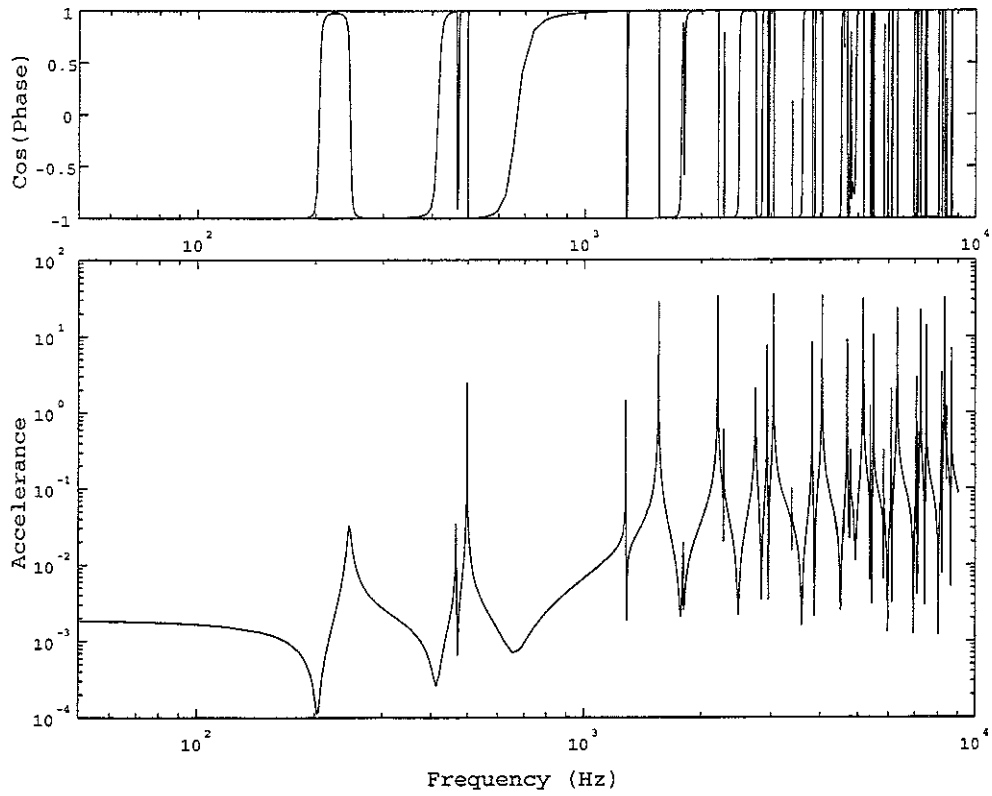

(a) Radial direction

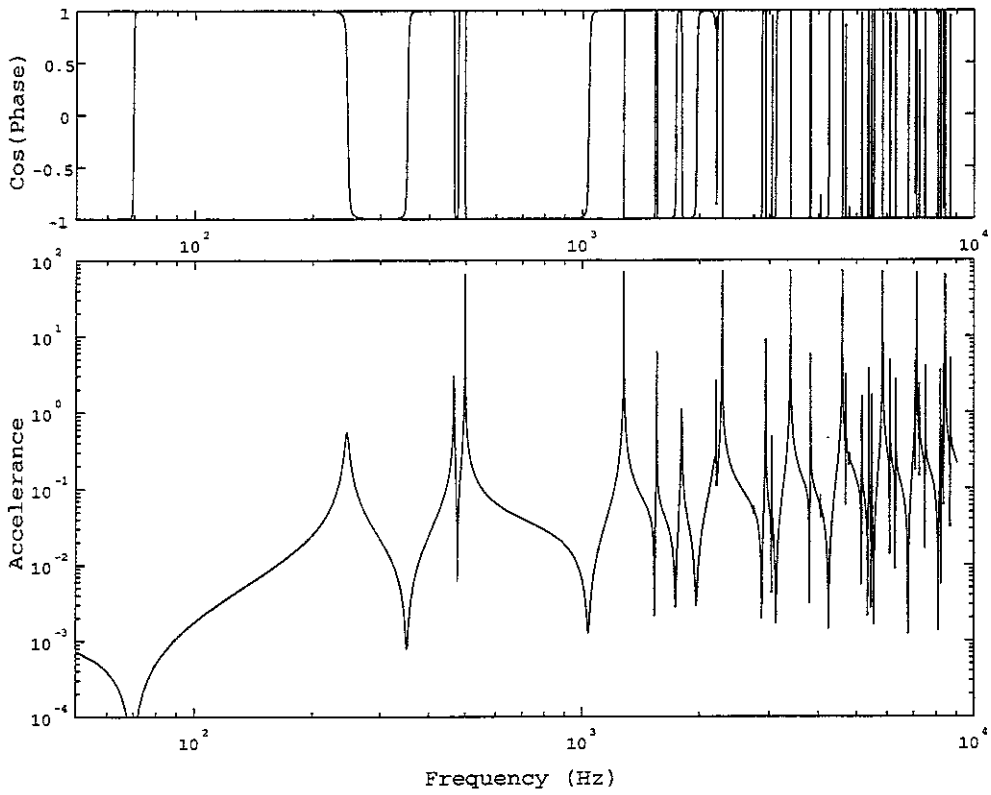

(b) Axial direction

Figure B4 Wheel accelerance (wheelA, 0km/h)

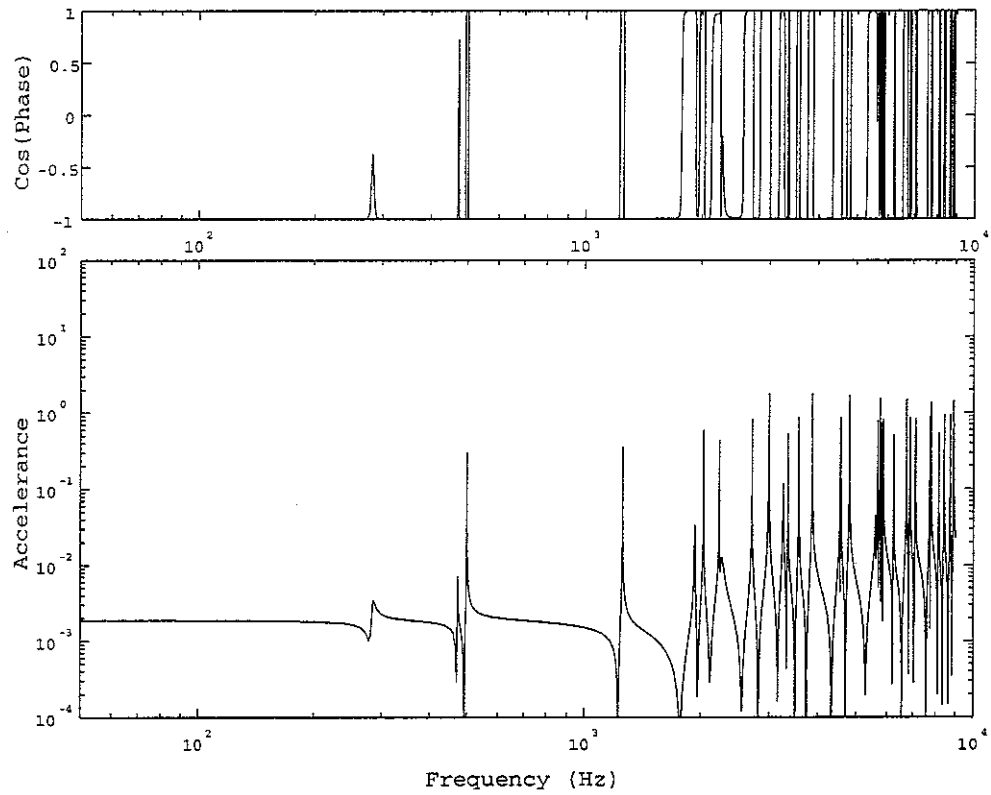

(a) Radial direction

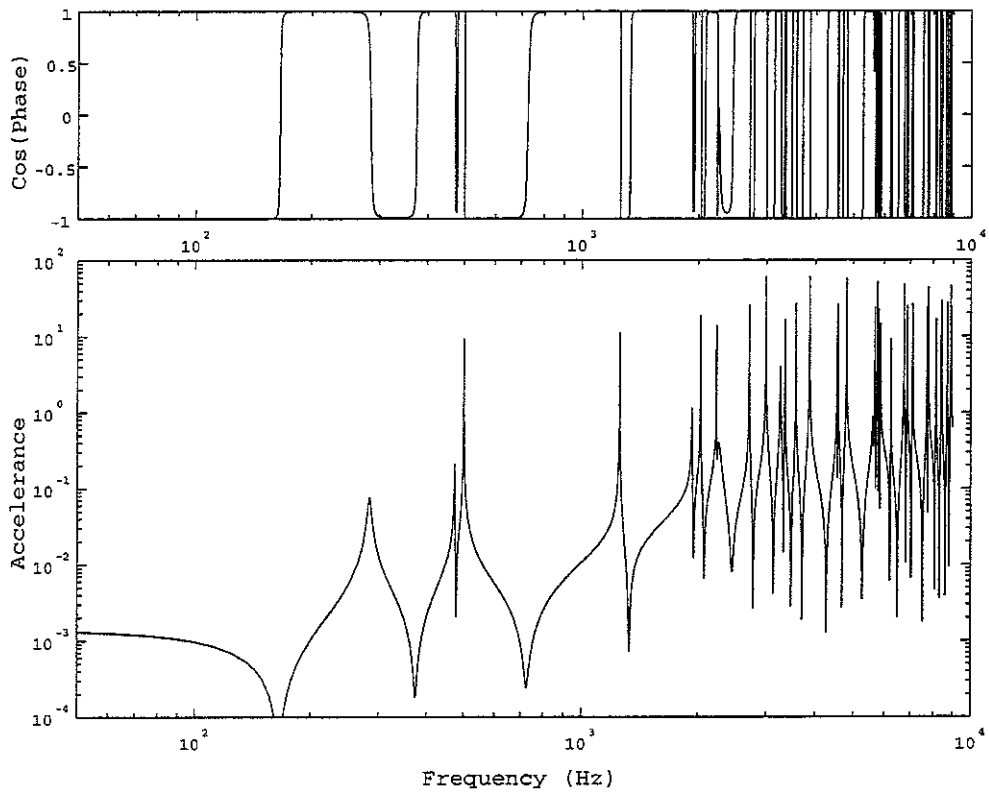

(b) Axial direction

Figure B5 Wheel accelerance (wheel B, 0km/h)

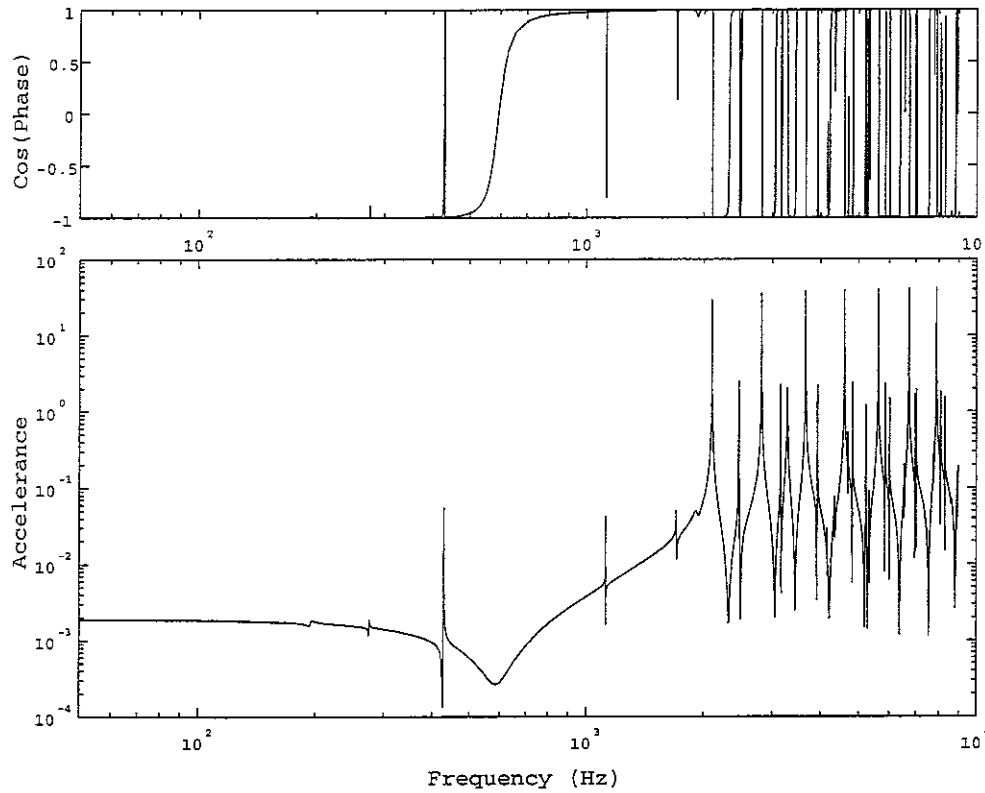

(a) Radial direction

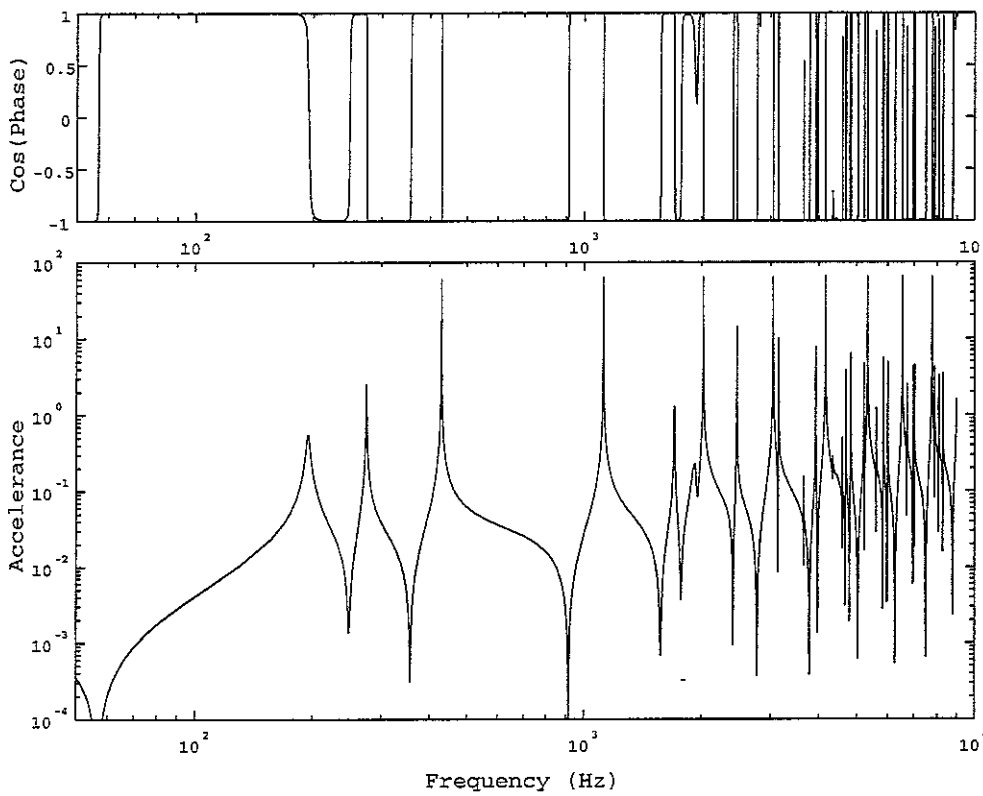

(b) Axial direction

Figure B6 Wheel accelerance (wheel C, 0km/h)

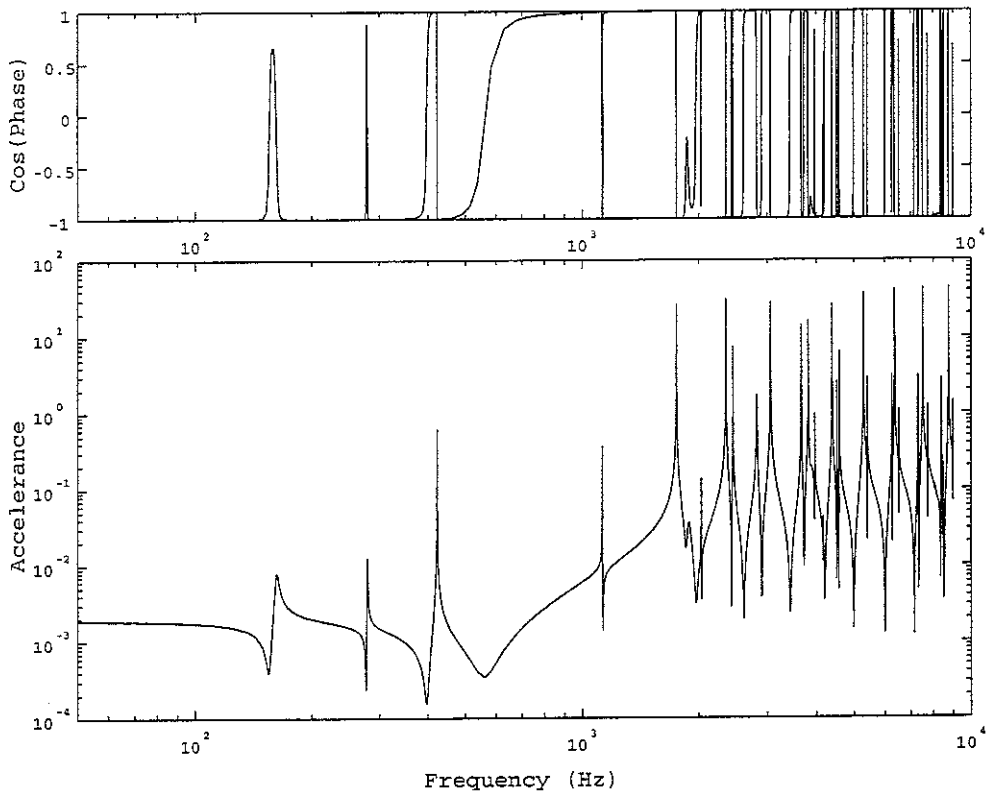

(a) Radial direction

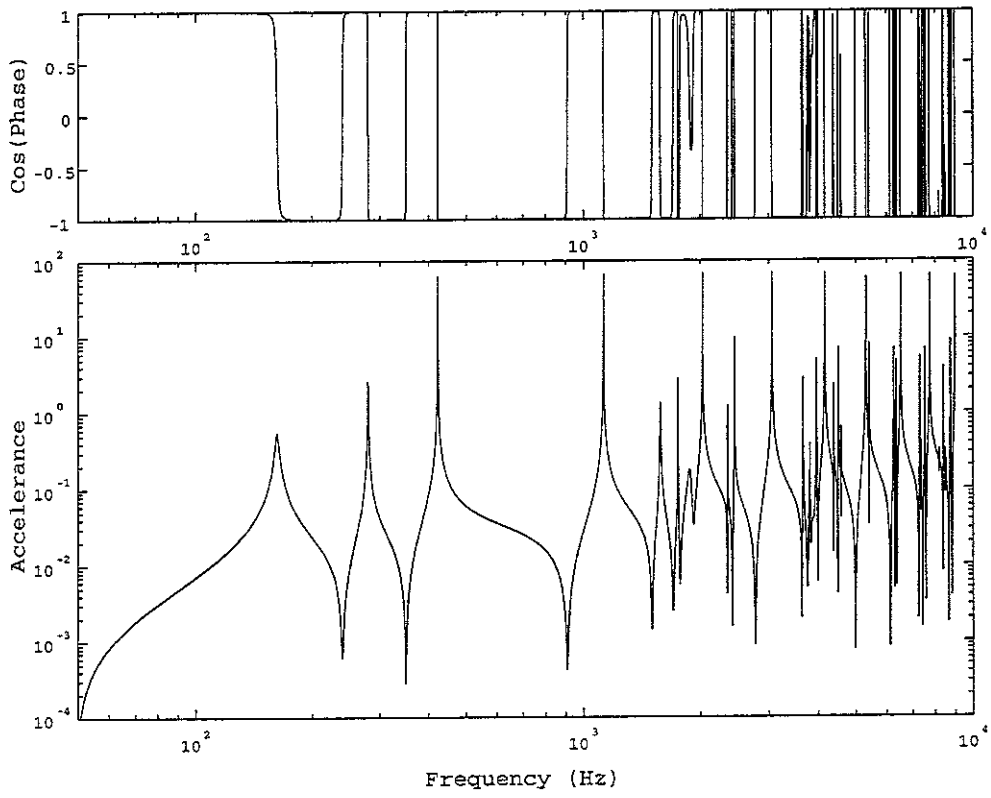

(b) Axial direction

Figure B7 Wheel accelerance (wheel D, 0km/h)

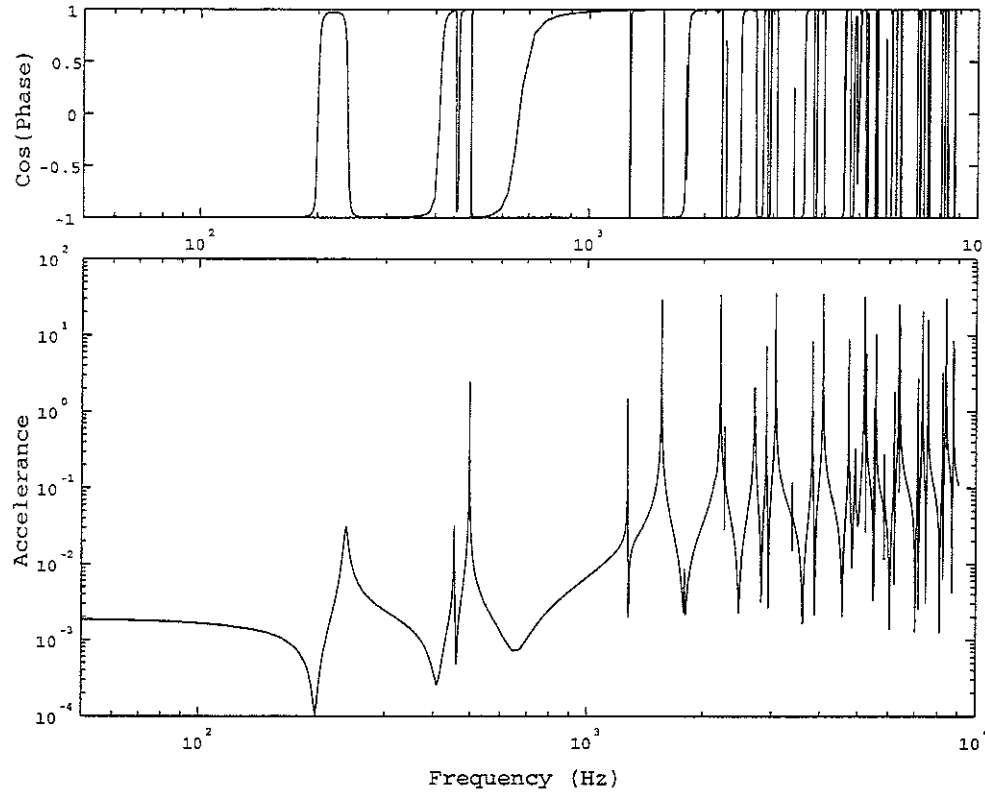

(a) Radial direction

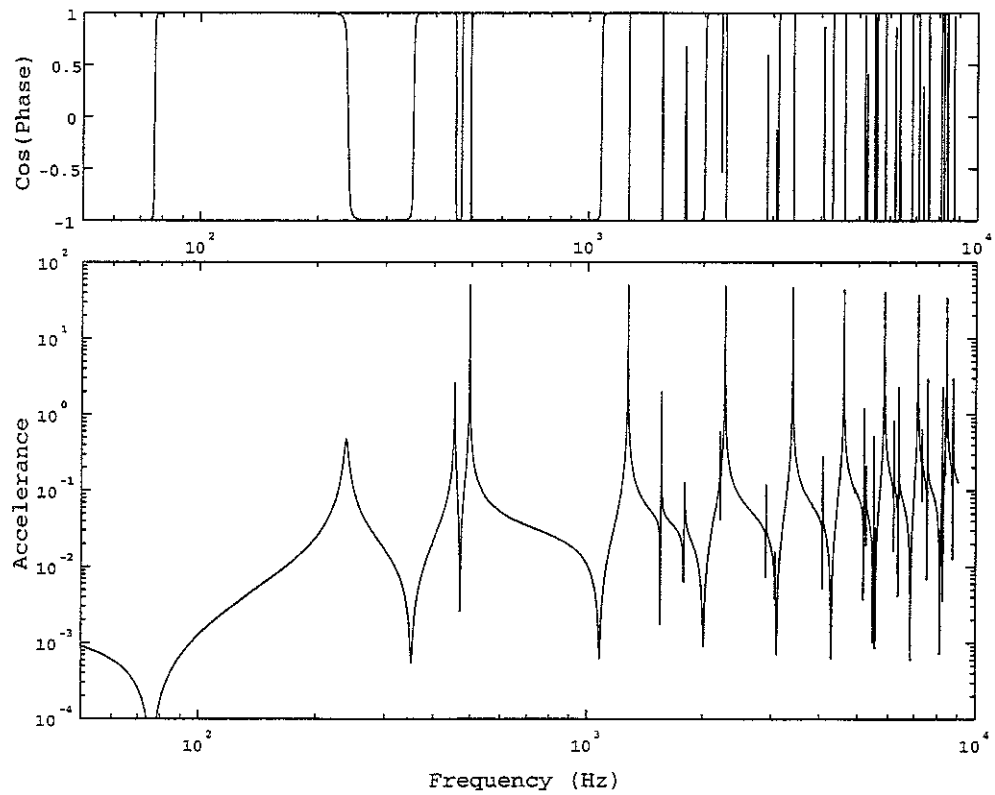

(b) Axial direction

Figure B8 Wheel accelerance (wheel E, 0km/h)

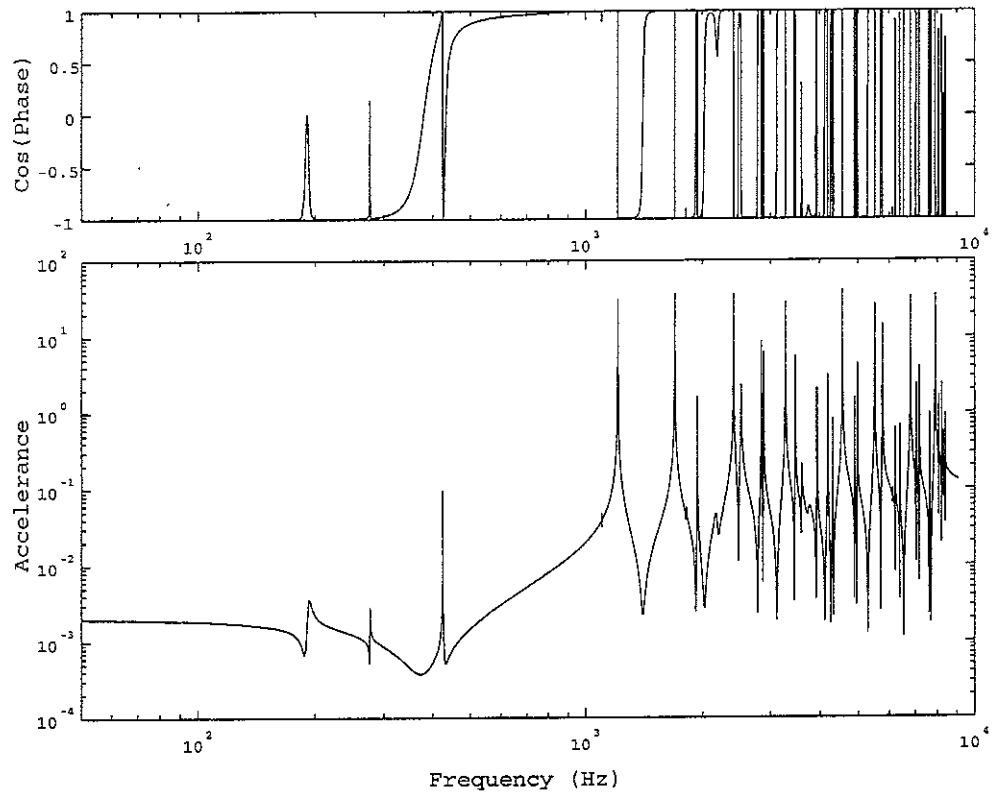

(a) Radial direction

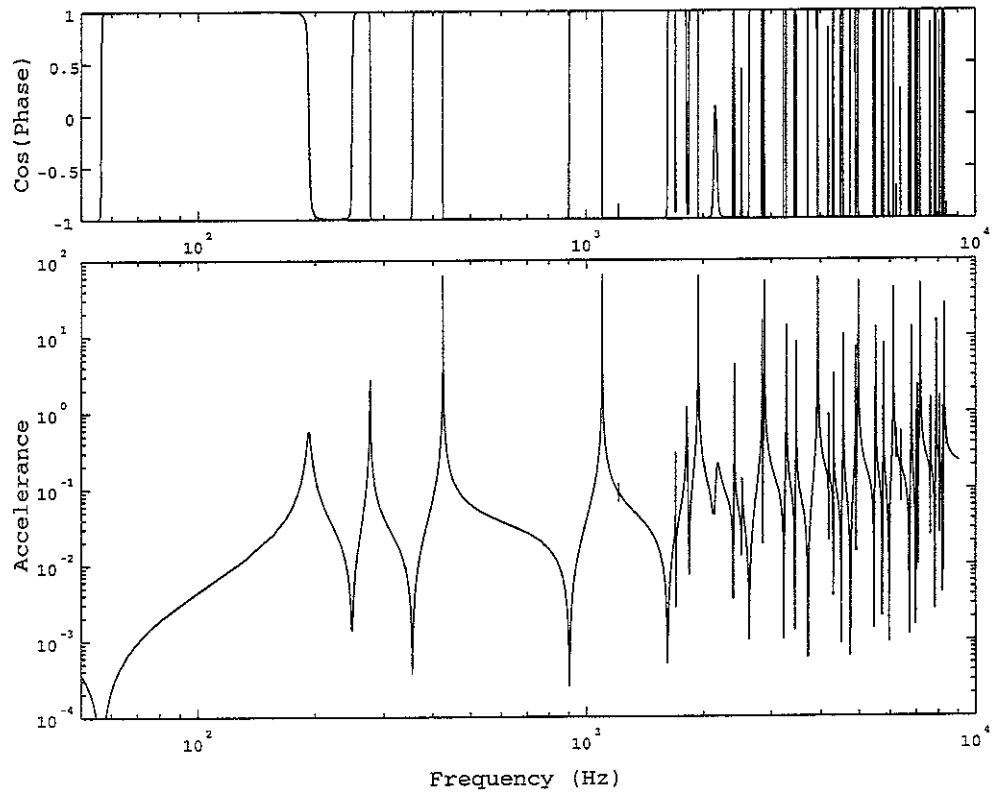

(b) Axial direction

Figure B9 Wheel accelerance (wheel AW, 0km/h)

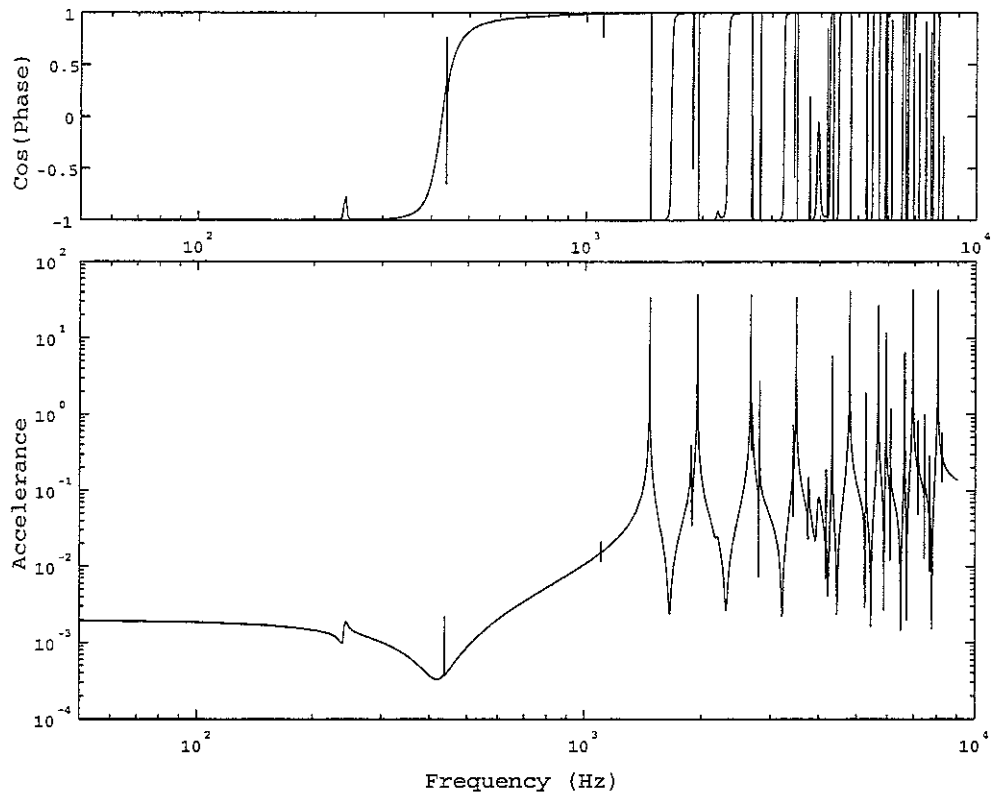

(a) Radial direction

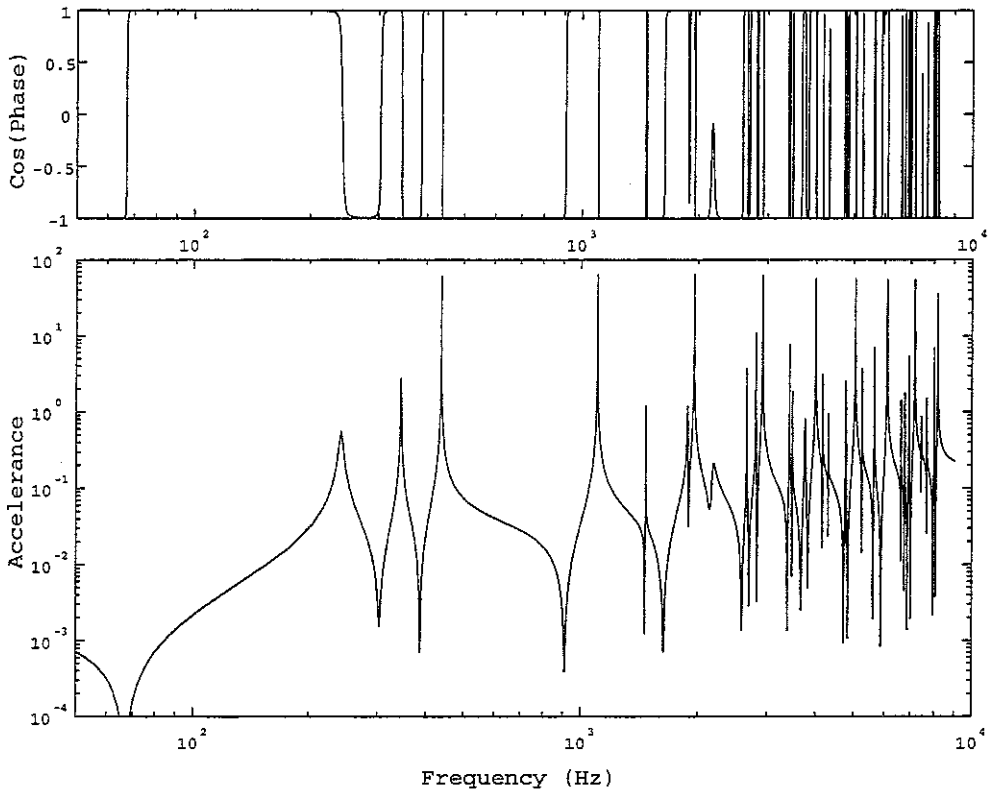

(b) Axial direction

Figure B10 Wheel accelerance (wheel BW, 0km/h)

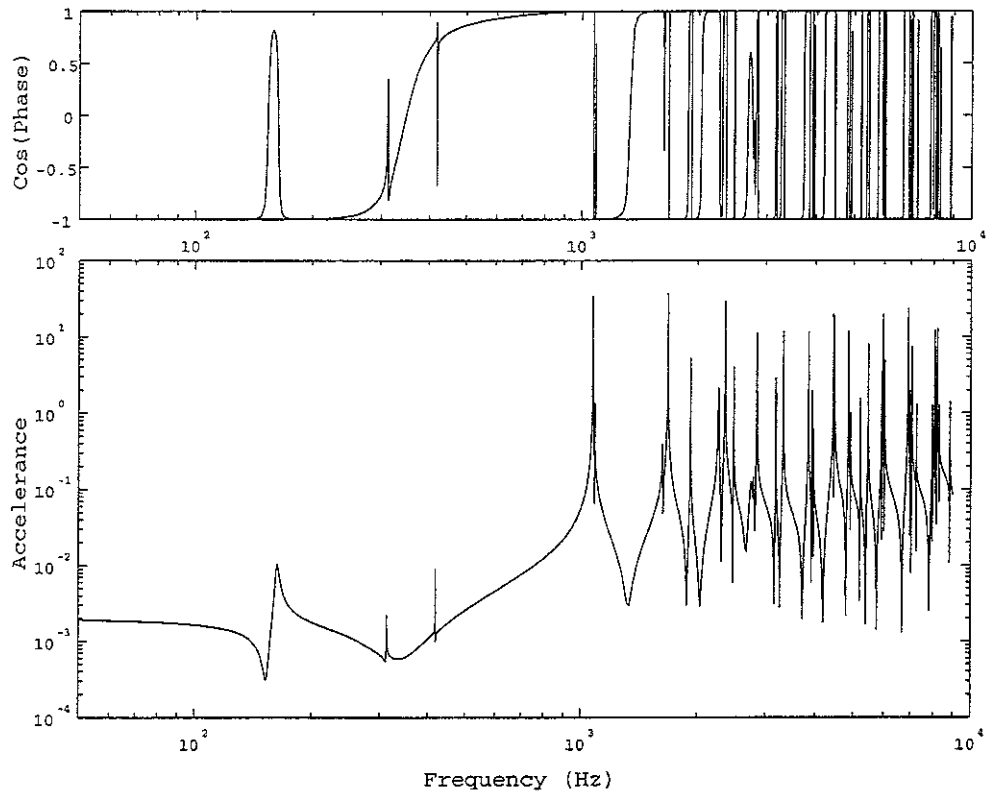

(a) Radial direction

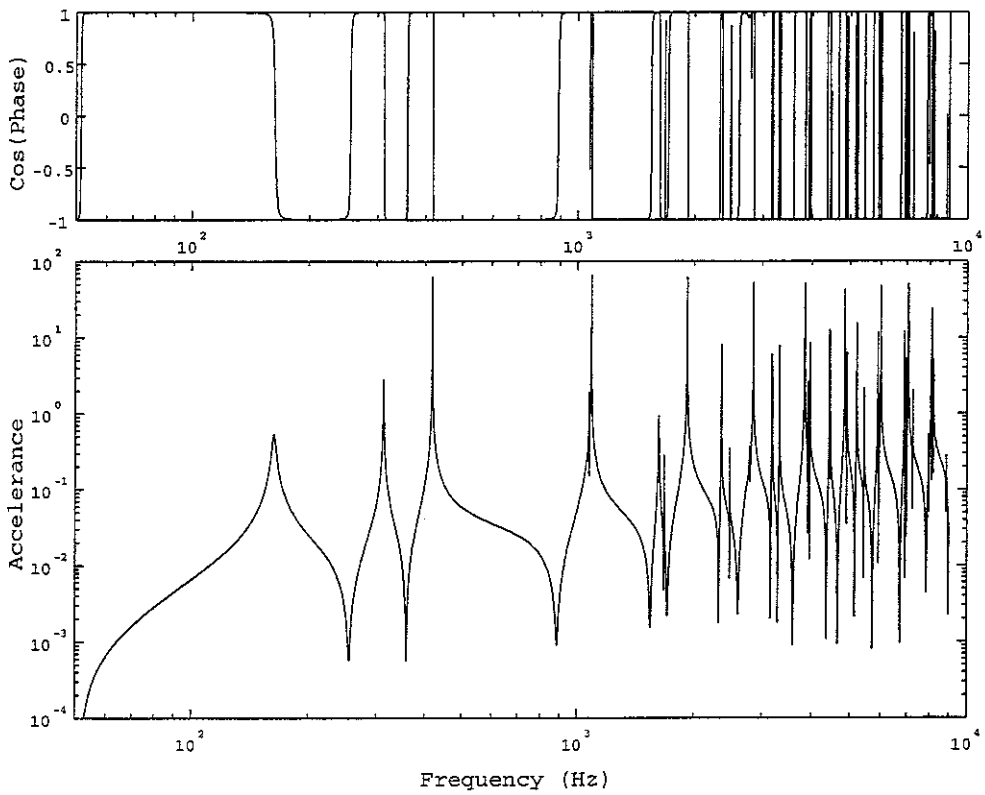

(b) Axial direction

Figure B11 Wheel accelerance (wheel CW, 0km/h)

Table B10 Wheel parameters used for TWINS calculation

Wheel	A	B	C	D	E	AW	BW	CW
Receptance								
Contact position	0.0	0.0	0.0	0.0	0.0	0.0	0.0	0.0
Radius (R_{11})	0.405	0.405	0.43	0.43	0.43	0.43	0.43	0.43
Trans. radius (R_{12})	0.9	0.9	0.8	0.8	0.8	0.8	0.8	0.8
Dof	LX, LY	LX, LY	LX, LY	LX, LY	LX, LY	LX, LY	LX, LY	LX, LY
Start frequency	50	50	50	50	50	50	50	50
End frequency	9000	9000	9000	9000	9000	9000	9000	9000
Max level increment	3	3	3	3	3	3	3	3
Max freq. step	50	50	50	50	50	50	50	50
Response								
Max level increment	5	5	5	5	5	5	5	5
Max frequency step	50	50	50	50	50	50	50	50
Max n for separate response	2	2	2	2	2	2	2	2
Static load (N)	50000	50000	50000	50000	50000	50000	50000	50000
Radiation								
hub	0.123	0.128	0.115	0.125	0.115	0.130	0.128	0.118
web 1	0.161	0.190	0.174	0.182	0.163	0.180	0.174	0.162
web 2	0.197	0.230	0.210	0.219	0.200	0.221	0.225	0.204
web 3	0.230	0.264	0.246	0.255	0.237	0.258	0.254	0.246
web 4	0.259	0.305	0.282	0.291	0.272	0.300	0.287	0.287
web 5	0.292	0.333	0.318	0.327	0.311	0.334	0.322	0.327
tyre inner	0.340	0.340	0.365	0.365	0.365	0.365	0.365	0.365
tyre outer	0.405	0.405	0.430	0.430	0.430	0.430	0.430	0.430
tyre width	0.125	0.125	0.125	0.125	0.125	0.125	0.125	0.125
web width	0.020	0.027	0.028	0.020	0.020	0.010	0.017	0.013
Axial position	1-6	1-6	1-6	1-6	1-6	1-6	1-6	1-6
Radial position	7	7	7	7	7	7	7	7
Rocking position	9	9	9	9	9	9	9	9

AW.mp

AW modal parameters file created 28-2-03 by TK (A-type wheel)
FACTOR MASS 4.000 ! web response positions
FACTOR DAMPING 1.000 ! 2 @ 0.1612 3 @ 0.1974 4 @ 0.2297
MIN DAMPING 0.5000E-04 ! 5 @ 0.2586 6 @ 0.2924
NODE POINT 0.40471 0.37300E-2
*MODES
A 0 0.000 259.250 0.100E-03
0.000 1.000 0.000 0.000 0.000 0.000
1.000 1.000 1.000 1.000 1.000 1.000
S 1 0.000 259.250 0.100E-03
1.000 0.000 -1.000 0.000 0.000 0.000
0.000 0.000 0.000 0.000 0.000 0.000
A 1 0.000 81.301 0.100E-03
-.5600 0.4047 -.5600 1.000 0.000 1.000
0.1612 0.1974 0.2297 0.2586 0.2924 0.3705
A 1 245.710 1.000 0.100E-01
0.5347E-010.2115 0.000 0.000 0.000 -.6751
0.5324E-020.3281E-010.6789E-010.9802E-010.1315 0.1887
A 0 465.580 1.000 0.100E-02
0.1823E-010.1558 0.000 0.000 0.000 -.4599
0.7302E-020.3390E-010.5764E-010.7321E-010.9661E-010.1408
A 2 498.320 1.000 0.100E-03
-.4880E-01-.2288 0.000 0.000 0.000 1.125
-.4624E-02-.2606E-01-.5243E-01-.7531E-01-.1071 -.1899
A 1 1081.700 1.000 0.100E+01
0.1010 -.9888E-01 0.000 0.000 0.000 1.206
-.1341E-01-.2377E-010.1044E-010.5477E-010.4986E-01-.5882E-0
1
A 3 1278.600 1.000 0.100E-03
0.3950E-010.2372 0.000 0.000 0.000 -1.464
0.4391E-020.2245E-010.4212E-010.5847E-010.8922E-010.1858
A 2 1553.800 1.000 0.100E-03
0.1460 -.7056E-01 0.000 0.000 0.000 1.176
-.1284E-01-.9398E-020.4856E-010.1043
0.8428E-01-.3075E-01
A 0 1802.000 1.000 0.100E-02
0.2307E-02-.9411E-01 0.000 0.000 0.000 2.528
0.2066E-010.1064 0.1906 0.2237 0.1974
-.8038E-02
A 1 2190.400 1.000 0.100E-01
-.6092E-01-.1072 0.000 0.000 0.000 3.372
0.4691E-010.2070 0.3317 0.3486 0.2831
0.6369E-02
A 3 2198.900 1.000 0.100E-03
0.1605 -.4496E-01 0.000 0.000 0.000 0.9457
-.5692E-020.2119E-010.9828E-010.1485
0.9724E-01-.1239E-01
A 4 2273.900 1.000 0.100E-03
0.2824E-010.2419 0.000 0.000 0.000 -1.745
0.3642E-020.1790E-010.3118E-010.4252E-010.7490E-010.1802
A 0 2739.600 1.000 0.100E-02
-.1297 -.9884E-02 0.000 0.000 0.000 0.3957
0.4407E-010.1587 0.1877 0.1163
0.3825E-01-.3020E-02
A 2 2934.300 1.000 0.100E-03
0.8925E-010.8618E-01 0.000 0.000 0.000 -3.079
-.5809E-01-.2506 -.3935 -.3895 -.2819
-.1527E-01
A 4 3044.200 1.000 0.100E-03
0.1654 -.1984E-01 0.000 0.000 0.000 0.6810
0.1966E-020.5638E-010.1550 0.1960 0.1083
0.4308E-02
A 5 3393.300 1.000 0.100E-03
0.1566E-010.2438 0.000 0.000 0.000 -1.986
0.2436E-020.1102E-010.1667E-010.2428E-010.6149E-010.1733
A 3 3822.400 1.000 0.100E-03
-.9195E-01-.6888E-01 0.000 0.000 0.000 2.628
0.6120E-010.2912 0.4708 0.4443 0.2686
0.1575E-01
A 5 4045.900 1.000 0.100E-03
0.1646 0.5655E-02 0.000 0.000 0.000 0.3962
0.8153E-020.9366E-010.2199 0.2500 0.1206
0.2082E-01
A 6 4589.500 1.000 0.100E-03
0.3291E-020.2429 0.000 0.000 0.000 -2.183
0.1051E-020.1772E-02-.2223E-020.2960E-020.4825E-010.1651
A 4 4686.400 1.000 0.100E-03
-.9206E-01-.5030E-01 0.000 0.000 0.000 1.905
0.5980E-010.3320 0.5572 0.4975 0.2314
0.9113E-02
A 0 4782.100 1.000 0.100E-02
0.5480E-010.2967E-01 0.000 0.000 0.000 -1.613
0.3994E-010.2323 0.4043 0.3198
-.1614E-01-.2075E-01
A 1 4826.300 1.000 0.100E-01
0.7113E-010.4286E-01 0.000 0.000 0.000 -2.305
0.5565E-010.3269 0.5653 0.4390
-.3134E-01-.2864E-01
A 6 5152.900 1.000 0.100E-03
-.1567 -.2908E-01 0.000 0.000 0.000 -.1166

-.1320E-01-.1370 -.3025 -.3197 -.1360
-.3550E-01
A 2 5164.900 1.000 0.100E-03
0.7943E-010.3637E-01 0.000 0.000 0.000 -1.834
0.2161E-010.1928 0.3759 0.3031
-.3325E-01-.8702E-02
A 3 5386.200 1.000 0.100E-03
0.4216E-010.5574E-01 0.000 0.000 0.000 -2.988
0.5056E-010.3007 0.4955 0.3303 -.1201
-.4197E-01
A 5 5483.800 1.000 0.100E-03
-.9622E-01-.3708E-01 0.000 0.000 0.000 1.226
0.5276E-010.3442 0.5992 0.5130 0.1826
-.8408E-03
A 7 5836.600 1.000 0.100E-03
-.7234E-020.2396 0.000 0.000 0.000 -2.337
-.2964E-03-.9621E-02-.2601E-01-.2204E-010.3496E-010.1560
A 4 6099.400 1.000 0.100E-03
0.5312E-010.6275E-01 0.000 0.000 0.000 -3.486
0.3330E-010.2286 0.3797 0.2148 -.1879
-.4779E-01
A 6 6303.200 1.000 0.100E-03
0.1107 0.3456E-01 0.000 0.000 0.000 -.8489
-.4273E-01-.3253 -.5871 -.4903 -.1401
0.1169E-01
A 7 6312.900 1.000 0.100E-03
0.1373 0.4674E-01 0.000 0.000 0.000 -.1206
0.1728E-010.1879 0.4086 0.4109 0.1547
0.4560E-01
A 5 7066.500 1.000 0.100E-03
-.6195E-01-.6175E-01 0.000 0.000 0.000 3.754
-.2135E-01-.1646 -.2666 -.1038 0.2410
0.5392E-01
A 8 7119.700 1.000 0.100E-03
-.1510E-010.2344 0.000 0.000 0.000 -2.447
-.1481E-02-.2319E-01-.5614E-01-.5278E-010.2087E-010.1462
A 7 7237.600 1.000 0.100E-03
-.1360 -.4248E-01 0.000 0.000 0.000 0.7324
0.3180E-010.2810 0.5251 0.4303 0.1003
-.2515E-01
A 8 7488.300 1.000 0.100E-03
0.1062 0.5712E-01 0.000 0.000 0.000 -.2973
0.1887E-010.2307 0.5110 0.5030 0.1715
0.4978E-01
A 6 8197.100 1.000 0.100E-03
0.6619E-010.5427E-01 0.000 0.000 0.000 -3.818
0.1658E-010.1321 0.1999 0.3172E-01-.2735
-.5967E-01
A 8 8339.200 1.000 0.100E-03
-.1635 -.5759E-01 0.000 0.000 0.000 0.7953
0.2125E-010.2176 0.4199 0.3364
0.6060E-01-.4079E-01
A 9 8429.900 1.000 0.100E-03
-.2001E-010.2279 0.000 0.000 0.000 -2.515
-.2321E-02-.3761E-01-.9167E-01-.8977E-010.5464E-020.1361
A 9 8691.600 1.000 0.100E-03
0.7584E-010.6387E-01 0.000 0.000 0.000 -.4396
0.1702E-010.2454 0.5692 0.5651 0.1825
0.5091E-01
A 7 9420.600 1.000 0.100E-03
-.6753E-01-.4364E-01 0.000 0.000 0.000 3.791
-.1563E-01-.1234 -.1704 0.1236E-010.2966
0.6568E-01
A 9 9598.000 1.000 0.100E-03
-.1822 -.7284E-01 0.000 0.000 0.000 0.9474
0.1320E-010.1579 0.3155 0.2468
0.3017E-01-.5435E-01
A 10 9762.600 1.000 0.100E-03
0.2078E-01-.2219 0.000 0.000 0.000 2.554
0.2253E-020.4317E-010.1109 0.1130 0.5730E-02-.1270
A 0 9763.500 1.000 0.100E-02
0.2656E-010.6481E-02 0.000 0.000 0.000
-.7667E-01
0.3839 0.4008 -.5516E-01-.2127
-.3712E-010.1177E-01
A 1 9795.700 1.000 0.100E-01
0.3485E-010.8685E-02 0.000 0.000 0.000
-.9680E-01
0.5399 0.5680 -.7696E-01-.3040
-.5491E-010.1624E-01
A 2 9845.100 1.000 0.100E-03
-.6120E-01-.1672E-01 0.000 0.000 0.000 0.8906
-.1827 -.8025E-010.5026E-01-.1513 -.1259
-.2699E-02
A 10 9967.100 1.000 0.100E-03
-.5536E-01-.6438E-01 0.000 0.000 0.000 0.5017
-.1342E-01-.2377 -.5895 -.6041 -.1921
-.4856E-01
A 3 10484.000 1.000 0.100E-03
0.2246E-010.9502E-02 0.000 0.000 0.000
0.1589E-01
0.4932 0.6396 -.3046E-01-.3634
-.9140E-010.2173E-01
A 8 10874.000 1.000 0.100E-03

0.1046E-01-.1468E-01 0.000 0.000 0.000 0.3791
0.9990E-010.2183 0.4835E-01-.1163
-.4625E-01-.5109E-01
*END

BW.mp

BW modal parameters file created 28-2-03 by TK (B-type wheel)
FACTOR MASS 4.000 ! web response positions
FACTOR DAMPING 1.000 ! 2 @ 0.1900 3 @ 0.2302 4 @ 0.2644
MIN DAMPING 0.5000E-04 ! 5 @ 0.3050 6 @ 0.3333
NODE POINT 0.42997 -.44500E-2
*MODES
A 0 0.000 268.250 0.100E-03
0.000 1.000 0.000 0.000 0.000 0.000
1.000 1.000 1.000 1.000 1.000 1.000
S 1 0.000 268.250 0.100E-03
1.000 0.000 -1.000 0.000 0.000 0.000
0.000 0.000 0.000 0.000 0.000 0.000
A 1 0.000 84.123 0.100E-03
-.5600 0.4300 -.5600 1.000 0.000 1.000
0.1900 0.2302 0.2644 0.3050 0.3333 0.4027
A 1 284.210 1.000 0.100E-01
-.8670E-040.3160E-03 0.000 0.000 0.000 3.125
0.000 0.000 0.000 0.1672 0.1275 0.1980
A 0 472.850 1.000 0.100E-02
-.8843E-040.3575E-03 0.000 0.000 0.000 1.646
0.6054E-030.3583E-030.1446E-020.1264 0.9719E-010.1457
A 2 499.760 1.000 0.100E-03
0.6824E-04-.2441E-03 0.000 0.000 0.000 -3.481
0.5014E-030.2573E-030.8799E-03-.1555 -.1083 -.1990
A 3 1253.100 1.000 0.100E-03
-.5794E-040.1909E-03 0.000 0.000 0.000 3.801
0.000 0.000 0.000 0.1467 0.9824E-010.1994
A 1 1430.200 1.000 0.100E+01
-.9201E-040.5713E-03 0.000 0.000 0.000 -2.824
0.000 0.000 0.000
0.1070E-01-.5183E-010.5657E-01
A 0 1931.700 1.000 0.100E-02
-.3903E-030.1717E-02 0.000 0.000 0.000 -3.757
0.3270E-020.1752E-020.4206E-020.7396E-010.1921
-.3622E-01
A 2 2033.800 1.000 0.100E-03
0.7216E-04-.5150E-03 0.000 0.000 0.000 4.882
0.8151E-030.5190E-030.2571E-020.1100E-010.9069E-01-.4530E-01
A 4 2235.200 1.000 0.100E-03
-.4864E-040.1385E-03 0.000 0.000 0.000 4.184
0.3791E-030.1441E-030.3970E-030.1373 0.9308E-010.1963
A 1 2265.600 1.000 0.100E-01
-.7354E-030.3200E-02 0.000 0.000 0.000 -7.003
0.000 0.000 0.000 0.1160 0.2722
-.2993E-01
A 3 2711.200 1.000 0.100E-03
0.3051E-040.6628E-04 0.000 0.000 0.000 -5.743
0.000 0.000 0.000
-.1074E-01-.9645E-010.4178E-01
A 2 2994.200 1.000 0.100E-03
0.9961E-03-.3988E-02 0.000 0.000 0.000 8.644
0.8663E-020.4065E-020.1017E-01-.1185 -.2687
0.1293E-01
A 0 3259.500 1.000 0.100E-02
-.6654E-030.2651E-02 0.000 0.000 0.000 -7.023
0.5500E-020.2701E-020.1362E-010.1144E-010.2320E-010.1211E-01
A 5 3350.700 1.000 0.100E-03
-.3745E-040.8664E-04 0.000 0.000 0.000 4.628
0.000 0.000 0.000 0.1280 0.8942E-010.1929
A 4 3567.500 1.000 0.100E-03
0.1328E-03-.2919E-03 0.000 0.000 0.000 -5.909
-.1083E-02-.3003E-03-.7887E-03-.5889E-02-.1009
0.4409E-01
A 3 3867.500 1.000 0.100E-03
0.1049E-02-.3636E-02 0.000 0.000 0.000 8.676
0.000 0.000 0.000 -.1146 -.2671
0.4626E-02
A 6 4550.600 1.000 0.100E-03
0.2896E-04-.5812E-04 0.000 0.000 0.000 -5.058
0.2560E-030.5112E-040.1869E-03-.1186 -.8693E-01-.1890
A 5 4567.700 1.000 0.100E-03
0.1632E-03-.3516E-03 0.000 0.000 0.000 -5.836
0.000 0.000 0.000 -.2386E-03-.1064
0.4898E-01
A 4 4805.500 1.000 0.100E-03
-.9245E-030.2710E-02 0.000 0.000 0.000 -8.449
0.7561E-020.2712E-020.6467E-020.1052 0.2589
0.2369E-02
A 0 5610.800 1.000 0.100E-02
-.2664E-020.1266E-01 0.000 0.000 0.000 3.238
0.2853E-010.1323E-010.2109E-01-.6580E-01-.1275E-01-.1350E-01
A 1 5659.700 1.000 0.100E-01
-.3877E-020.1715E-01 0.000 0.000 0.000 4.737
0.000 0.000 0.000
-.9703E-01-.2841E-01-.1877E-01
A 6 5679.700 1.000 0.100E-03
-.1583E-030.3438E-03 0.000 0.000 0.000 5.556

-.1031E-02-.1161E-03-.8058E-03-.4448E-020.1145
-.5424E-01
A 5 5762.000 1.000 0.100E-03
-.7669E-030.2023E-02 0.000 0.000 0.000 -8.058
0.000 0.000 0.000 0.8962E-010.2433
0.6556E-02
A 7 5806.900 1.000 0.100E-03
-.1985E-040.2180E-04 0.000 0.000 0.000 5.390
0.000 0.000 0.000 0.1101 0.8666E-010.1847
A 2 5871.700 1.000 0.100E-03
-.3622E-020.1400E-01 0.000 0.000 0.000 4.909
-.3314E-01-.1375E-01-.2551E-01-.1003
-.4068E-01-.1950E-01
A 3 6234.500 1.000 0.100E-03
-.2952E-020.9898E-02 0.000 0.000 0.000 3.852
0.000 0.000 0.000 -.1200
-.7184E-01-.1579E-01
A 6 6743.200 1.000 0.100E-03
0.4492E-03-.9361E-03 0.000 0.000 0.000 7.845
0.4186E-020.9070E-030.3067E-02-.8069E-01-.2284
-.1467E-01
A 7 6880.700 1.000 0.100E-03
0.1306E-03-.2596E-03 0.000 0.000 0.000 -5.235
0.000 0.000 0.000 0.6636E-02-.1259
0.5867E-01
A 4 6882.100 1.000 0.100E-03
-.1980E-020.5656E-02 0.000 0.000 0.000 4.718
0.1612E-010.5366E-020.1290E-01-.1325 -.1039
-.1950E-01
A 8 7102.400 1.000 0.100E-03
-.6931E-050.4036E-05 0.000 0.000 0.000 5.810
0.9857E-04-.2277E-050.6955E-040.1003 0.8152E-010.1800
A 5 7719.800 1.000 0.100E-03
-.1180E-020.2874E-02 0.000 0.000 0.000 5.653
0.000 0.000 0.000 -.1498 -.1489
-.2600E-01
A 7 7781.100 1.000 0.100E-03
-.3145E-030.6165E-03 0.000 0.000 0.000 -7.482
0.000 0.000 0.000 0.6624E-010.2080
0.2112E-01
A 8 8157.200 1.000 0.100E-03
-.8915E-040.1847E-03 0.000 0.000 0.000 4.656
0.8597E-030.5423E-040.6224E-03-.6118E-020.1413
-.5997E-01
A 9 8426.600 1.000 0.100E-03
-.2946E-050.7189E-05 0.000 0.000 0.000 6.132
0.000 0.000 0.000 0.9068E-010.7563E-010.1748
A 6 8729.200 1.000 0.100E-03
0.6875E-03-.1479E-02 0.000 0.000 0.000 -5.981
0.5514E-020.1097E-020.4121E-020.1602 0.1757
0.3337E-01
A 8 8903.900 1.000 0.100E-03
-.1906E-030.4260E-03 0.000 0.000 0.000 -7.642
0.1584E-020.1492E-030.1115E-020.6302E-010.1992
0.3093E-01
A 9 9504.900 1.000 0.100E-03
-.9313E-040.2860E-03 0.000 0.000 0.000 4.234
0.000 0.000 0.000 -.3769E-020.1577
-.5897E-01
A 10 9771.700 1.000 0.100E-03
0.1931E-05-.8116E-05 0.000 0.000 0.000 -6.374
0.6317E-05-.1062E-040.1770E-05-.8139E-01-.6746E-01-.1691
A 7 9872.900 1.000 0.100E-03
-.4936E-030.1259E-02 0.000 0.000 0.000 6.210
0.000 0.000 0.000 -.1684 -.1978
-.4278E-01
A 9 10125.000 1.000 0.100E-03
0.2929E-03-.1136E-02 0.000 0.000 0.000 7.539
0.000 0.000 0.000 -.6361E-01-.1941
-.3964E-01
*END

CW.mp

CW modal parameters file created 28-2-03 by TK (Plane web wheel)
FACTOR MASS 4.000 ! web response positions
FACTOR DAMPING 1.000 ! 2 @ 0.1738 3 @ 0.2098 4 @ 0.2458
MIN DAMPING 0.5000E-04 ! 5 @ 0.2817 6 @ 0.3177
NODE POINT 0.43005 0.40000E-2
*MODES
A 0 0.000 259.250 0.100E-03
0.000 1.000 0.000 0.000 0.000 0.000
1.000 1.000 1.000 1.000 1.000 1.000
S 1 0.000 259.250 0.100E-03
1.000 0.000 -1.000 0.000 0.000 0.000
0.000 0.000 0.000 0.000 0.000 0.000
A 1 0.000 81.301 0.100E-03
-.5600 0.4300 -.5600 1.000 0.000 1.000
0.1738 0.2098 0.2458 0.2817 0.3177 0.4042
A 1 194.590 1.000 0.100E-01
0.7466E-020.2105 0.000 0.000 0.000 -.6511
0.9802E-020.3381E-010.6703E-010.1023 0.1342 0.1939
A 0 275.440 1.000 0.100E-02
0.3643E-020.1428 0.000 0.000 0.000 -.2929
0.8622E-020.2935E-010.5691E-010.8410E-010.1057 0.1356
A 2 429.360 1.000 0.100E-03
-.1057E-01-.2199 0.000 0.000 0.000 0.9827
-.7325E-02-.2523E-01-.5131E-01-.8182E-01-.1144 -.1938
A 3 1122.900 1.000 0.100E-03
0.1063E-010.2244 0.000 0.000 0.000 -1.230
0.6814E-020.2250E-010.4511E-010.7215E-010.1031 0.1906
A 1 1388.900 1.000 0.100E+01
0.9727E-01-.5791E-02 0.000 0.000 0.000 0.2161
0.5260E-020.1193E-010.1823E-010.2109E-010.1864E-01-.2012E-02
A 0 1704.400 1.000 0.100E-02
-.2697E-01-.1013 0.000 0.000 0.000 2.311
0.4495E-010.1209 0.1866 0.2055 0.1658
-.4380E-01
A 1 1925.500 1.000 0.100E-01
-.4794E-01-.1288 0.000 0.000 0.000 3.170
0.7085E-010.1855 0.2807 0.3029 0.2407
-.4992E-01
A 4 2022.000 1.000 0.100E-03
0.8876E-020.2268 0.000 0.000 0.000 -1.436
0.7084E-020.2264E-010.4410E-010.6871E-010.9674E-010.1862
A 2 2103.100 1.000 0.100E-03
-.1519 0.4950E-02 0.000 0.000 0.000 -.2814
-.8640E-02-.1999E-01-.2963E-01-.3269E-01-.2761E-01-.2334E-02
A 2 2464.700 1.000 0.100E-03
0.5655E-010.1070 0.000 0.000 0.000 -2.911
-.8922E-01-.2214 -.3193 -.3255 -.2428
0.3533E-01
A 3 2819.400 1.000 0.100E-03
0.1679 0.2820E-02 0.000 0.000 0.000 0.2017
0.9116E-020.2174E-010.3168E-010.3367E-010.2750E-010.1012E-01
A 5 3049.200 1.000 0.100E-03
0.6147E-020.2283 0.000 0.000 0.000 -1.628
0.7109E-020.2296E-010.4438E-010.6748E-010.9226E-010.1814
A 3 3149.100 1.000 0.100E-03
-.5275E-01-.9044E-01 0.000 0.000 0.000 2.578
0.1089 0.2630 0.3647 0.3490 0.2364
-.2795E-01
A 0 3277.300 1.000 0.100E-02
0.1275 0.7145E-02 0.000 0.000 0.000
-.6361E-01
-.3950E-02-.1378E-01-.1756E-01-.1195E-01-.2480E-020.1196E-01
A 4 3657.800 1.000 0.100E-03
0.1737 0.1079E-01 0.000 0.000 0.000 0.1456
0.1128E-010.2814E-010.4078E-010.4176E-010.3213E-010.1862E-01
A 4 3929.700 1.000 0.100E-03
-.5111E-01-.7877E-01 0.000 0.000 0.000 2.261
0.1181 0.2901 0.3996 0.3688 0.2284
-.2497E-01
A 6 4160.700 1.000 0.100E-03
-.2932E-02-.2292 0.000 0.000 0.000 1.812
-.6388E-02-.2179E-01-.4328E-01-.6574E-01-.8788E-01-.1763
A 0 4340.800 1.000 0.100E-02
0.2729E-010.3512E-01 0.000 0.000 0.000 -1.456
0.1811 0.3345 0.3120 0.1212
-.6189E-01-.6358E-03
A 1 4416.400 1.000 0.100E-01
0.3724E-010.5146E-01 0.000 0.000 0.000 -2.144
0.2555 0.4676 0.4319 0.1613
-.9548E-01-.1015E-02
A 5 4594.300 1.000 0.100E-03
0.1767 0.1989E-01 0.000 0.000 0.000
0.7622E-01
0.1337E-010.3538E-010.5239E-010.5305E-010.3876E-010.2809E-01

A 2 4688.100 1.000 0.100E-03
0.2927E-010.5554E-01 0.000 0.000 0.000 -2.365
0.2466 0.4470 0.4037 0.1331 -.1174
-.3956E-02
A 5 4826.900 1.000 0.100E-03
-.5175E-01-.7145E-01 0.000 0.000 0.000 2.041
0.1141 0.2953 0.4182 0.3859 0.2260
-.2397E-01
A 3 5221.300 1.000 0.100E-03
0.4182E-010.6136E-01 0.000 0.000 0.000 -2.674
0.2290 0.4189 0.3701 0.9858E-01-.1462
-.2780E-02
A 7 5329.300 1.000 0.100E-03
-.3687E-030.2293 0.000 0.000 0.000 -1.986
0.4989E-020.1866E-010.3947E-010.6181E-010.8248E-010.1709
A 6 5617.900 1.000 0.100E-03
-.1794 -.3128E-01 0.000 0.000 0.000
0.4986E-01
-.1240E-01-.3566E-01-.5579E-01-.5823E-01-.4234E-01-.3882E-01
A 6 5858.700 1.000 0.100E-03
0.5076E-010.6619E-01 0.000 0.000 0.000 -1.922
-.1011 -.2833 -.4239 -.4036 -.2323
0.2263E-01
A 4 6002.600 1.000 0.100E-03
0.4615E-010.6255E-01 0.000 0.000 0.000 -2.899
0.2038 0.3856 0.3383 0.6965E-01-.1698
-.5246E-02
A 8 6537.700 1.000 0.100E-03
-.3395E-020.2286 0.000 0.000 0.000 -2.145
0.3368E-020.1429E-010.3318E-010.5523E-010.7559E-010.1651
A 7 6720.900 1.000 0.100E-03
0.1829 0.4457E-01 0.000 0.000 0.000 -.2338
0.8789E-020.2821E-010.4806E-010.5367E-010.4097E-010.5052E-
01
A 5 6976.800 1.000 0.100E-03
0.4875E-010.5894E-01 0.000 0.000 0.000 -3.019
0.1788 0.3581 0.3211 0.5693E-01-.1833
-.9529E-02
A 7 7022.600 1.000 0.100E-03
-.4672E-01-.6029E-01 0.000 0.000 0.000 1.864
0.8369E-010.2598 0.4199 0.4225 0.2469
-.1910E-01
A 9 7774.600 1.000 0.100E-03
-.5849E-020.2267 0.000 0.000 0.000 -2.277
0.1978E-020.9813E-020.2573E-010.4673E-010.6737E-010.1587
A 8 7894.700 1.000 0.100E-03
0.1865 0.5791E-01 0.000 0.000 0.000 -.4407
0.5242E-020.1925E-010.3661E-010.4494E-010.3731E-010.6228E-
01
A 6 8092.700 1.000 0.100E-03
-.5022E-01-.5144E-01 0.000 0.000 0.000 3.063
-.1549 -.3362 -.3192 -.6214E-010.1868
0.1553E-01
A 8 8305.700 1.000 0.100E-03
-.4221E-01-.5270E-01 0.000 0.000 0.000 1.834
0.6523E-010.2289 0.4069 0.4402 0.2671
-.1325E-01
A 0 8624.400 1.000 0.100E-02
-.1527E-01-.1010E-01 0.000 0.000 0.000 0.8672
0.3498 0.2375 -.1317 -.2686
-.7322E-010.1131E-01
A 1 8681.000 1.000 0.100E-01
-.2532E-01-.1506E-01 0.000 0.000 0.000 1.246
0.4917 0.3330 -.1873 -.3800 -.1032
0.1500E-01
A 2 8918.800 1.000 0.100E-03
0.1520E-010.1216E-01 0.000 0.000 0.000 -1.261
-.4835 -.3440 0.1752 0.3812 0.1065
-.1952E-01
A 10 9032.800 1.000 0.100E-03
0.7531E-02-.2234 0.000 0.000 0.000 2.375
-.1021E-02-.6109E-02-.1851E-01-.3751E-01-.5837E-01-.1515
A 9 9131.000 1.000 0.100E-03
0.1901 0.7008E-01 0.000 0.000 0.000 -.6453
0.2834E-020.1220E-010.2643E-010.3629E-010.3333E-010.7348E-
01
A 7 9317.800 1.000 0.100E-03
0.5127E-010.4100E-01 0.000 0.000 0.000 -3.063
0.1310 0.3153 0.3275 0.8333E-01-.1811
-.2323E-01
A 3 9427.000 1.000 0.100E-03
-.2160E-01-.1152E-01 0.000 0.000 0.000 1.339
0.4711 0.3729 -.1542 -.3938 -.1182
0.2064E-01
A 9 9693.500 1.000 0.100E-03
-.3902E-01-.4362E-01 0.000 0.000 0.000 1.817
0.4799E-010.1941 0.3856 0.4540 0.2905
-.5698E-02
*END

DW.mp

DW modal parameters file created 28-2-03 by TK (EC4499 wheel)
FACTOR MASS 4.000 ! web response positions
FACTOR DAMPING 1.000 ! 2 @ 0.1822 3 @ 0.2187 4 @ 0.2549
MIN DAMPING 0.5000E-04 ! 5 @ 0.2913 6 @ 0.3269
NODE POINT 0.42989 -.27400E-2
*MODES
A 0 0.000 259.250 0.100E-03
0.000 1.000 0.000 0.000 0.000 0.000
1.000 1.000 1.000 1.000 1.000 1.000
S 1 0.000 259.250 0.100E-03
1.000 0.000 -1.000 0.000 0.000 0.000
0.000 0.000 0.000 0.000 0.000 0.000
A 1 0.000 81.301 0.100E-03
-.5600 0.4299 -.5600 1.000 0.000 1.000
0.1822 0.2187 0.2549 0.2913 0.3269 0.4036
A 1 161.650 1.000 0.100E-01
0.2327E-010.2112 0.000 0.000 0.000 -.5967
0.8412E-020.3771E-010.7672E-010.1166 0.1481 0.1958
A 0 279.360 1.000 0.100E-02
0.9230E-020.1443 0.000 0.000 0.000 -.2449
0.9026E-020.3563E-010.6610E-010.9506E-010.1163 0.1383
A 2 422.920 1.000 0.100E-03
-.1955E-01-.2244 0.000 0.000 0.000 1.021
-.6431E-02-.2763E-01-.5595E-01-.8828E-01-.1230 -.1969
A 3 1125.600 1.000 0.100E-03
0.1353E-010.2301 0.000 0.000 0.000 -1.301
0.6588E-020.2532E-010.4764E-010.7400E-010.1087 0.1937
A 1 1199.500 1.000 0.100E+01
0.1019 -.6260E-01 0.000 0.000 0.000 1.049
-.1220E-01-.2686E-020.4976E-010.8525E-010.5501E-01-.3690E-0
1
A 0 1577.600 1.000 0.100E-02
0.3265E-02-.1034 0.000 0.000 0.000 2.483
0.3725E-010.1325 0.2118 0.2262 0.1644
-.4014E-01
A 2 1749.600 1.000 0.100E-03
0.1478 -.4763E-01 0.000 0.000 0.000 1.070
-.9728E-020.1776E-010.9468E-010.1308
0.7856E-01-.1934E-01
A 1 1878.500 1.000 0.100E-01
-.4075E-01-.1178 0.000 0.000 0.000 3.220
0.7524E-010.2393 0.3439 0.3312 0.2306
-.3594E-01
A 4 2028.100 1.000 0.100E-03
-.6163E-02-.2331 0.000 0.000 0.000 1.515
-.7396E-02-.2647E-01-.4579E-01-.6722E-01-.1001 -.1892
A 3 2349.200 1.000 0.100E-03
0.1587 -.3146E-01 0.000 0.000 0.000 0.8547
0.9047E-020.7270E-010.1630 0.1696
0.8118E-01-.6325E-02
A 2 2452.100 1.000 0.100E-03
0.6928E-010.8868E-01 0.000 0.000 0.000 -2.706
-.1078 -.3224 -.4283 -.3567 -.2117
0.2167E-01
A 0 2822.700 1.000 0.100E-02
-.1171 0.1271E-02 0.000 0.000 0.000
-.9446E-01
0.8610E-010.2063 0.1832
0.5787E-01-.7060E-02-.7645E-02
A 5 3054.100 1.000 0.100E-03
-.2142E-020.2344 0.000 0.000 0.000 -1.693
0.8611E-020.3039E-010.4925E-010.6565E-010.9433E-010.1838
A 3 3057.600 1.000 0.100E-03
-.7705E-01-.6483E-01 0.000 0.000 0.000 1.984
0.1352 0.4014 0.5122 0.3705 0.1682
-.1754E-01
A 4 3058.700 1.000 0.100E-03
0.1493 -.2095E-01 0.000 0.000 0.000 0.7293
0.4453E-010.1779 0.2915 0.2433
0.9189E-010.2919E-02
A 4 3661.700 1.000 0.100E-03
-.1023 -.4762E-01 0.000 0.000 0.000 1.283
0.1414 0.4246 0.5258 0.3370 0.1120
-.2015E-01
A 0 3799.900 1.000 0.100E-02
0.6284E-010.3608E-01 0.000 0.000 0.000 -1.602
0.1085 0.3098 0.3586 0.1337
-.8969E-010.2957E-03
A 5 3814.700 1.000 0.100E-03
0.1145 -.1719E-01 0.000 0.000 0.000 0.6684
0.8788E-010.3168 0.4644 0.3403 0.1040
0.5542E-02
A 1 3875.900 1.000 0.100E-01
0.8978E-010.5134E-01 0.000 0.000 0.000 -2.274
0.1435 0.4091 0.4717 0.1673 -.1305
0.2688E-02
A 2 3961.000 1.000 0.100E-03
0.1973E-010.6292E-01 0.000 0.000 0.000 -2.737
0.1749 0.4570 0.4655 0.1058 -.1779
-.7356E-02

A 6 4158.600 1.000 0.100E-03
0.1010E-01-.2339 0.000 0.000 0.000 1.831
-.1176E-01-.4293E-01-.6666E-01-.7478E-01-.9162E-01-.1774
A 5 4378.300 1.000 0.100E-03
-.1428 -.4324E-01 0.000 0.000 0.000 0.8649
0.1161 0.3552 0.4272 0.2452
0.5822E-01-.3018E-01
A 3 4507.000 1.000 0.100E-03
0.3657E-010.7576E-01 0.000 0.000 0.000 -3.328
0.1489 0.3844 0.3655 0.1492E-01-.2324
-.5203E-02
A 6 4579.300 1.000 0.100E-03
-.7291E-010.2230E-01 0.000 0.000 0.000 -.6385
-.1093 -.4011 -.5785 -.4021 -.1037
0.1135E-02
A 6 5289.100 1.000 0.100E-03
0.1691 0.5001E-01 0.000 0.000 0.000 -.7577
-.7868E-01-.2460 -.2859 -.1435
-.1926E-010.4415E-01
A 4 5298.300 1.000 0.100E-03
0.3973E-010.7874E-01 0.000 0.000 0.000 -3.605
0.1251 0.3138 0.2602 -.7487E-01-.2693
-.6688E-02
A 7 5308.400 1.000 0.100E-03
-.7513E-020.2193 0.000 0.000 0.000 -1.750
0.3801E-010.1485 0.2249 0.1823 0.1097 0.1638
A 7 5407.900 1.000 0.100E-03
0.5061E-01-.8016E-01 0.000 0.000 0.000 1.048
0.1016 0.3968 0.5883 0.4020
0.7772E-01-.4642E-01
A 5 6253.900 1.000 0.100E-03
-.4020E-01-.7433E-01 0.000 0.000 0.000 3.653
-.1149 -.2808 -.1959 0.1389 0.2905
0.9852E-02
A 8 6310.600 1.000 0.100E-03
0.2534E-010.3307E-01 0.000 0.000 0.000
0.2809E-01
0.9620E-010.4102 0.6443 0.4670 0.1219
0.3364E-01
A 7 6353.700 1.000 0.100E-03
0.1784 0.6196E-01 0.000 0.000 0.000 -.8598
-.5238E-01-.1699 -.1928
-.8293E-010.2422E-030.5795E-01
A 8 6519.600 1.000 0.100E-03
-.3503E-010.2288 0.000 0.000 0.000 -2.123
-.1364E-01-.5777E-01-.8597E-01-.3675E-010.5446E-010.1590
A 6 7297.700 1.000 0.100E-03
0.3944E-010.6630E-01 0.000 0.000 0.000 -3.585
0.1156 0.2796 0.1646 -.1880 -.3049
-.1383E-01
A 9 7342.300 1.000 0.100E-03
0.1855E-010.1720E-01 0.000 0.000 0.000 0.1344
0.8203E-010.3894 0.6575 0.4979 0.1239
0.2087E-01
A 8 7520.400 1.000 0.100E-03
0.1819 0.7411E-01 0.000 0.000 0.000 -1.042
-.3597E-01-.1234 -.1398
-.5185E-010.9062E-020.7024E-01
A 9 7741.200 1.000 0.100E-03
-.3723E-010.2277 0.000 0.000 0.000 -2.183
-.6517E-02-.2998E-01-.4524E-01-.9898E-020.5705E-010.1533
A 0 8088.500 1.000 0.100E-02
0.1267E-01-.5794E-02 0.000 0.000 0.000 0.5494
0.4026 0.3323 -.1836 -.3091
-.2888E-010.1200E-01
A 2 8189.700 1.000 0.100E-03
-.3606E-020.1167E-01 0.000 0.000 0.000 -.9609
-.5409 -.4710 0.2558 0.4538
0.3877E-01-.1518E-01
A 1 8224.500 1.000 0.100E-01
0.3657E-01-.2112E-02 0.000 0.000 0.000 0.4412
0.4982 0.3918 -.2169 -.3397
-.3248E-010.1903E-01
A 7 8396.000 1.000 0.100E-03
-.3801E-01-.5649E-01 0.000 0.000 0.000 3.449
-.1216 -.2989 -.1552 0.2305 0.3169
0.1817E-01
A 10 8483.600 1.000 0.100E-03
-.1330E-01-.1412E-01 0.000 0.000 0.000 -.1389
-.6635E-01-.3576 -.6597 -.5315 -.1330
-.1767E-01
A 3 8524.600 1.000 0.100E-03
0.6736E-02-.1100E-01 0.000 0.000 0.000 1.005
0.5307 0.5000 -.2478 -.4700
-.3999E-010.1928E-01
A 9 8761.200 1.000 0.100E-03
0.1838 0.8420E-01 0.000 0.000 0.000 -1.241
-.2504E-01-.9287E-01-.1080
-.3613E-010.1245E-010.8059E-01
A 10 8986.800 1.000 0.100E-03
-.3909E-010.2249 0.000 0.000 0.000 -2.226
-.4873E-02-.2479E-01-.3962E-01-.8572E-020.5272E-010.1459
*END

EW.mp

EW modal parameters file created 28-2-03 by TK (A86D wheel)
FACTOR MASS 4.000 ! web response positions
FACTOR DAMPING 1.000 ! 2 @ 0.1628 3 @ 0.2002 4 @ 0.2372
MIN DAMPING 0.5000E-04 ! 5 @ 0.2720 6 @ 0.3333
NODE POINT 0.40471 0.37300E-2
*MODES
A 0 0.000 259.250 0.100E-03
0.000 1.000 0.000 0.000 0.000 0.000
1.000 1.000 1.000 1.000 1.000 1.000
S 1 0.000 259.250 0.100E-03
1.000 0.000 -1.000 0.000 0.000 0.000
0.000 0.000 0.000 0.000 0.000 0.000
A 1 0.000 81.301 0.100E-03
-.5600 0.4047 -.5600 1.000 0.000 1.000
0.1628 0.2002 0.2372 0.2720 0.3333 0.4316
A 1 238.830 1.000 0.100E-01
0.5213E-010.2118 0.000 0.000 0.000 -.6691
0.7492E-020.3782E-010.7766E-010.1131 0.1638 0.2298
A 0 453.020 1.000 0.100E-02
0.1746E-010.1548 0.000 0.000 0.000 -.4324
0.1010E-010.3916E-010.6524E-010.8494E-010.1233 0.1666
A 2 496.000 1.000 0.100E-03
-.4813E-01-.2287 0.000 0.000 0.000 1.120
-.6320E-02-.2955E-01-.5938E-01-.8791E-01-.1506 -.2573
A 1 1081.100 1.000 0.100E+01
0.1028 -.9487E-01 0.000 0.000 0.000 1.134
-.1866E-01-.2895E-010.1401E-010.5363E-01-.1212E-01-.1268
A 3 1277.900 1.000 0.100E-03
0.3949E-010.2370 0.000 0.000 0.000 -1.460
0.5895E-020.2509E-010.4709E-010.6953E-010.1388 0.2736
A 2 1562.800 1.000 0.100E-03
-.1473 0.6871E-01 0.000 0.000 0.000 -1.137
0.1786E-010.1210E-01-.5687E-01-.1004 -.1264E-010.1040
A 0 1792.700 1.000 0.100E-02
-.2172E-02-.9623E-01 0.000 0.000 0.000 2.552
0.2802E-010.1198 0.2055 0.2225 0.9280E-01-.1716
A 1 2158.600 1.000 0.100E-01
-.6171E-01-.1107 0.000 0.000 0.000 3.411
0.6053E-010.2246 0.3428 0.3324 0.1405 -.2110
A 3 2215.800 1.000 0.100E-03
0.1611 -.4483E-01 0.000 0.000 0.000 0.9405
-.8301E-020.2255E-010.1089 0.1353
0.1980E-01-.7983E-01
A 4 2274.000 1.000 0.100E-03
0.2876E-010.2417 0.000 0.000 0.000 -1.741
0.4886E-020.1992E-010.3484E-010.5343E-010.1290 0.2871
A 0 2713.500 1.000 0.100E-02
-.1298 -.8004E-02 0.000 0.000 0.000 0.3208
0.5475E-010.1621 0.1642
0.7097E-010.1086E-01-.1054E-01
A 2 2906.300 1.000 0.100E-03
0.8726E-010.8862E-01 0.000 0.000 0.000 -3.126
-.7351E-01-.2669 -.3964 -.3543 -.1397 0.1790
A 4 3063.500 1.000 0.100E-03
0.1659 -.2065E-01 0.000 0.000 0.000 0.6930
0.1720E-020.6080E-010.1653 0.1692
0.2404E-01-.5532E-01
A 5 3393.800 1.000 0.100E-03
0.1655E-010.2438 0.000 0.000 0.000 -1.982
0.3323E-020.1250E-010.1955E-010.3660E-010.1200 0.3009
A 3 3821.800 1.000 0.100E-03
-.9118E-01-.7137E-01 0.000 0.000 0.000 2.717
0.7716E-010.3082 0.4669 0.3803 0.1256 -.1480
A 5 4066.300 1.000 0.100E-03
0.1657 0.4365E-02 0.000 0.000 0.000 0.4157
0.9621E-020.1001 0.2278 0.2055
0.2849E-01-.2956E-01
A 6 4590.400 1.000 0.100E-03
0.4415E-020.2431 0.000 0.000 0.000 -2.182
0.1566E-020.2847E-020.5950E-030.1852E-010.1112 0.3157
A 4 4723.700 1.000 0.100E-03
-.9220E-01-.5349E-01 0.000 0.000 0.000 2.054
0.7561E-010.3542 0.5522 0.3993 0.9460E-01-.1064
A 0 4908.900 1.000 0.100E-02
0.5448E-010.2898E-01 0.000 0.000 0.000 -1.605
0.5286E-010.2620 0.4105 0.1970
-.8677E-010.8322E-01
A 1 4951.500 1.000 0.100E-01
0.7021E-010.4176E-01 0.000 0.000 0.000 -2.290
0.7375E-010.3694 0.5737 0.2664 -.1230 0.1184
A 6 5177.600 1.000 0.100E-03
-.1593 -.2763E-01 0.000 0.000 0.000 -.1389
-.1593E-01-.1449 -.3063 -.2510
-.3313E-010.4091E-02
A 2 5240.300 1.000 0.100E-03
0.7529E-010.3920E-01 0.000 0.000 0.000 -2.042
0.4157E-010.2685 0.4479 0.2040 -.1011
0.9610E-01
A 3 5493.100 1.000 0.100E-03
0.4075E-010.5329E-01 0.000 0.000 0.000 -2.916

0.6747E-010.3441 0.5023 0.1656 -.1580 0.1592
A 5 5550.500 1.000 0.100E-03
-.9549E-01-.3963E-01 0.000 0.000 0.000 1.366
0.6753E-010.3750 0.6027 0.3932
0.5926E-01-.6527E-01
A 7 5837.700 1.000 0.100E-03
-.5876E-020.2401 0.000 0.000 0.000 -2.337
-.8747E-04-.8504E-02-.2187E-01-.7125E-030.1026 0.3324
A 4 6179.000 1.000 0.100E-03
0.5063E-010.6024E-01 0.000 0.000 0.000 -3.406
0.4586E-010.2718 0.3945 0.7205E-01-.1823 0.1833
A 7 6348.500 1.000 0.100E-03
0.1428 0.4526E-01 0.000 0.000 0.000
-.9491E-01
0.2123E-010.1989 0.4098 0.3116
0.3693E-010.1892E-01
A 6 6377.400 1.000 0.100E-03
0.1077 0.3565E-01 0.000 0.000 0.000 -.9456
-.5557E-01-.3617 -.6008 -.3657
-.3403E-010.3978E-01
A 5 7118.200 1.000 0.100E-03
0.5979E-010.6017E-01 0.000 0.000 0.000 -3.712
0.2961E-010.1995 0.2763 -.2197E-01-.1998 0.1968
A 8 7121.100 1.000 0.100E-03
-.1334E-010.2354 0.000 0.000 0.000 -2.451
-.1456E-02-.2094E-01-.4783E-01-.2149E-010.9400E-010.3518
A 7 7300.900 1.000 0.100E-03
-.1308 -.4198E-01 0.000 0.000 0.000 0.7907
0.4244E-010.3203 0.5500 0.3182
0.1724E-01-.2960E-01
A 8 7539.300 1.000 0.100E-03
0.1141 0.5462E-01 0.000 0.000 0.000 -.2539
0.2417E-010.2501 0.5208 0.3778
0.3877E-010.3857E-01
A 6 8233.400 1.000 0.100E-03
0.6476E-010.5331E-01 0.000 0.000 0.000 -3.802
0.2242E-010.1581 0.1984 -.8646E-01-.2081 0.1986
A 8 8381.600 1.000 0.100E-03
-.1587 -.5619E-01 0.000 0.000 0.000 0.8256
0.2936E-010.2550 0.4519 0.2482
0.4835E-02-.3078E-01
A 9 8431.700 1.000 0.100E-03
-.1766E-010.2299 0.000 0.000 0.000 -2.527
-.2321E-02-.3244E-01-.7461E-01-.4284E-010.8558E-010.3751
A 9 8752.600 1.000 0.100E-03
0.8323E-010.5765E-01 0.000 0.000 0.000 -.3511
0.2295E-010.2747 0.5969 0.4284
0.3858E-010.5538E-01
A 7 9450.700 1.000 0.100E-03
-.6656E-01-.4290E-01 0.000 0.000 0.000 3.788
-.2058E-01-.1435 -.1586 0.1288 0.2121 -.1953
A 9 9622.600 1.000 0.100E-03
-.1794 -.7167E-01 0.000 0.000 0.000 0.9634
0.1872E-010.1877 0.3437 0.1782
-.3183E-02-.3734E-01
A 10 9764.300 1.000 0.100E-03
-.1834E-010.2247 0.000 0.000 0.000 -2.573
-.2240E-02-.3578E-01-.8690E-01-.5486E-010.7795E-010.4043
A 0 9828.900 1.000 0.100E-02
0.2840E-010.7120E-02 0.000 0.000 0.000 -.1079
0.4103 0.3396 -.1413 -.1379
0.5219E-03-.1696E-01
A 1 9856.100 1.000 0.100E-01
0.3496E-010.8938E-02 0.000 0.000 0.000 -.1167
0.5753 0.4815 -.2003 -.2046
0.1675E-02-.2681E-01
A 10 10030.000 1.000 0.100E-03
0.6128E-010.5486E-01 0.000 0.000 0.000 -.3728
0.1896E-010.2725 0.6338 0.4641
0.3643E-010.6384E-01
*END

AWW.mp

AWW modal parameters file created 15-8-03 by TK (AW-type wheel)
FACTOR MASS 4.000 ! web response positions
FACTOR DAMPING 1.000 ! 2 @ 0.1800 3 @ 0.2212 4 @ 0.2582
MIN DAMPING 0.5000E-04 ! 5 @ 0.3000 6 @ 0.3339
NODE POINT 0.42992 -.28300E-2
*MODES
A 0 0.000 248.250 0.100E-03
0.000 1.000 0.000 0.000 0.000 0.000
1.000 1.000 1.000 1.000 1.000 1.000
S 1 0.000 248.250 0.100E-03
1.000 0.000 -1.000 0.000 0.000 0.000
0.000 0.000 0.000 0.000 0.000 0.000
A 1 0.000 77.851 0.100E-03
-.5600 0.4299 -.5600 1.000 0.000 1.000
0.1800 0.2212 0.2582 0.3000 0.3339 0.3955
A 1 192.690 1.000 0.100E-01
0.1370E-010.2142 0.000 0.000 0.000 -.6239
0.1037E-010.3945E-010.6217E-010.1151 0.1528 0.1928
A 0 276.360 1.000 0.100E-02
0.3680E-020.1468 0.000 0.000 0.000 -.2623
0.8773E-020.3131E-010.4627E-010.9088E-010.1194 0.1381
A 2 425.050 1.000 0.100E-03
-.5798E-02-.2243 0.000 0.000 0.000 1.051
-.8957E-02-.3206E-01-.4422E-01-.8380E-01-.1262 -.1877
A 1 871.190 1.000 0.100E+01
0.1158 -.3632E-01 0.000 0.000 0.000 0.6531
-.2955E-030.3242E-010.1191 0.1059
0.3360E-01-.1457E-01
A 3 1099.900 1.000 0.100E-03
0.7357E-02-.2277 0.000 0.000 0.000 1.333
-.8154E-02-.2595E-01-.2732E-01-.6157E-01-.1096 -.1804
A 2 1211.400 1.000 0.100E-03
-.1583 0.6479E-02 0.000 0.000 0.000 -.4078
-.6218E-02-.6566E-01-.1847 -.1433
-.4314E-01-.7866E-02
A 3 1694.900 1.000 0.100E-03
0.1708 0.1529E-01 0.000 0.000 0.000
0.9345E-01
0.1743E-010.1049 0.2362 0.1605
0.3870E-010.2010E-01
A 0 1813.500 1.000 0.100E-02
0.2014E-01-.9617E-01 0.000 0.000 0.000 2.707
0.3195E-010.1205 0.1978 0.2449 0.1753
-.3187E-02
A 4 1942.400 1.000 0.100E-03
0.3989E-01-.2218 0.000 0.000 0.000 1.473
-.3913E-02-.3906E-020.1845E-01-.2725E-01-.9551E-01-.1681
A 1 2175.600 1.000 0.100E-01
-.3924E-01-.1238 0.000 0.000 0.000 3.974
0.6057E-010.2050 0.2845 0.3540 0.2731
0.1116E-01
A 4 2413.100 1.000 0.100E-03
0.1694 0.5804E-01 0.000 0.000 0.000 -.3357
0.3321E-010.1573 0.2984 0.1913
0.4858E-010.4921E-01
A 0 2520.900 1.000 0.100E-02
0.1323 0.3201E-01 0.000 0.000 0.000 -1.204
-.3468E-01-.7824E-01-.1772E-01-.5173E-01-.8619E-01-.2455E-02
A 2 2846.100 1.000 0.100E-03
-.7245E-01-.1132 0.000 0.000 0.000 3.992
0.7850E-010.2657 0.3527 0.3909 0.2849
0.1995E-01
A 5 2885.200 1.000 0.100E-03
0.7413E-01-.2044 0.000 0.000 0.000 1.416
0.5803E-020.3900E-010.9162E-010.1392E-01-.8661E-01-.1499
A 5 3276.200 1.000 0.100E-03
0.1475 0.1050 0.000 0.000 0.000 -1.128
0.7301E-010.2945 0.4547 0.2310
0.3009E-010.6958E-01
A 3 3469.900 1.000 0.100E-03
-.5775E-01-.8135E-01 0.000 0.000 0.000 3.048
0.9432E-010.3381 0.4613 0.3957 0.2268
0.1876E-01
A 0 3602.400 1.000 0.100E-02
0.3688E-01-.6690E-02 0.000 0.000 0.000 -.5766
0.1426 0.5230 0.6705 0.2283
-.4990E-01-.2528E-01
A 1 3751.300 1.000 0.100E-01
-.4609E-01-.3762E-02 0.000 0.000 0.000 -.8769
0.1855 0.6584 0.7922 0.2225
-.8232E-01-.3658E-01
A 2 3911.000 1.000 0.100E-03
0.2545E-02-.2121E-01 0.000 0.000 0.000 1.362
-.1690 -.6158 -.7817 -.2236
0.9940E-010.2446E-01
A 6 3936.600 1.000 0.100E-03
-.4602E-010.2145 0.000 0.000 0.000 -1.854
0.2658E-010.8462E-010.8053E-010.4217E-010.6555E-010.1449
A 4 4185.600 1.000 0.100E-03

0.4776E-010.2727E-01 0.000 0.000 0.000 -.8398
-.7576E-01-.2695 -.3579 -.2192
-.6105E-010.3832E-02
A 3 4311.700 1.000 0.100E-03
-.1826E-01-.5034E-01 0.000 0.000 0.000 2.627
-.1115 -.4098 -.5139 -.3469E-010.1988
0.3692E-01
A 6 4560.400 1.000 0.100E-03
-.1769 -.9114E-01 0.000 0.000 0.000 0.7623
0.3392E-010.7610E-01-.2181E-01-.1102
-.5576E-01-.7504E-01
A 4 4898.000 1.000 0.100E-03
-.2518E-01-.7605E-01 0.000 0.000 0.000 3.608
-.3577E-01-.8564E-01-.2371E-010.2636 0.2806
0.4488E-01
A 7 4975.200 1.000 0.100E-03
-.6444E-010.2034 0.000 0.000 0.000 -1.876
0.2473E-02-.1912E-01-.7805E-01-.4580E-010.4949E-010.1309
A 7 5518.200 1.000 0.100E-03
-.1436 -.1020 0.000 0.000 0.000 0.5536
-.1891E-02-.9923E-01-.3118 -.3080 -.1076
-.9090E-01
A 5 5767.500 1.000 0.100E-03
-.9819E-01-.7934E-01 0.000 0.000 0.000 3.131
0.2285E-010.2332 0.4752 0.4438 0.2303
0.1726E-01
A 8 6111.500 1.000 0.100E-03
-.1020E-010.1850 0.000 0.000 0.000 -1.696
-.2546E-01-.2943 -.5041 -.1566 0.5111E-010.1235
A 5 6213.400 1.000 0.100E-03
0.2781E-01-.1670E-01 0.000 0.000 0.000 1.980
-.7317E-01-.5539 -.9664 -.2803 0.1651
0.4954E-01
A 6 6385.200 1.000 0.100E-03
0.2092E-010.1999E-01 0.000 0.000 0.000 -.7874
-.1935E-01-.2888 -.6917 -.4947
-.8387E-01-.4796E-02
A 8 6806.600 1.000 0.100E-03
-.1604 -.1021 0.000 0.000 0.000 1.080
0.1363E-01-.5847E-01-.2216 -.1977
-.6121E-01-.7751E-01
A 6 7011.000 1.000 0.100E-03
0.8985E-020.2844E-01 0.000 0.000 0.000 -1.989
0.2489E-010.5296 0.9856 0.2442 -.1495
-.3666E-01
A 6 7053.300 1.000 0.100E-03
-.3504E-01-.4282E-01 0.000 0.000 0.000 2.942
-.2974E-010.1201 0.3889 0.4577 0.2663
0.4804E-01
A 9 7168.500 1.000 0.100E-03
0.6177E-01-.1957 0.000 0.000 0.000 1.828
-.5011E-02-.2931E-01-.3516E-01-.2549E-01-.5691E-01-.1221
A 7 7625.500 1.000 0.100E-03
-.2145E-01-.3481E-01 0.000 0.000 0.000 2.284
-.6220E-01-.2661E-010.4303 0.6769 0.2364
0.3744E-01
A 1 7803.900 1.000 0.100E-01
-.1038E-010.3115E-02 0.000 0.000 0.000 -.1636
-.6203E-010.1874 0.6416 0.3892
0.1489E-01-.4860E-02
A 9 7906.800 1.000 0.100E-03
0.1642 0.1131 0.000 0.000 0.000 -1.409
-.1196E-010.6696E-020.1403 0.1884
0.5322E-010.8133E-01
A 2 8076.900 1.000 0.100E-03
0.3677E-01-.3573E-01 0.000 0.000 0.000 0.2474
0.6511E-010.4221E-01-.2358 -.3046
-.4399E-01-.1142E-01
A 7 8219.300 1.000 0.100E-03
-.3566E-01-.3060E-01 0.000 0.000 0.000 2.792
0.1990E-01-.2509E-01-.2622 -.2213E-010.2286
0.5369E-01
A 10 8301.600 1.000 0.100E-03
-.2493E-010.1448 0.000 0.000 0.000 -1.782
-.1329E-010.5096E-010.7242E-01-.7603E-01-.8757E-020.9628E-0
1
A 0 8304.800 1.000 0.100E-02
0.4732E-02-.7982E-02 0.000 0.000 0.000 -.2514
-.9238E-01-.4192 -.3270 0.1433
-.8228E-02-.1777E-01
A 8 8395.400 1.000 0.100E-03
-.2499E-010.1444E-01 0.000 0.000 0.000 0.9147
-.4417E-01-.1599 0.1334 0.4635 0.1501
0.5137E-01
A 3 8406.100 1.000 0.100E-03
-.2973E-020.1334E-02 0.000 0.000 0.000 -.1932
-.9323E-01-.6120 -.7406
-.3163E-01-.1718E-02-.8432E-02
*END

BWW.mp

BWW modal parameters file created 28-2-03 by TK (BW-type wheel)
FACTOR MASS 4.000 ! web response positions
FACTOR DAMPING 1.000 ! 2 @ 0.1736 3 @ 0.2249 4 @ 0.2541
MIN DAMPING 0.5000E-04 ! 5 @ 0.2871 6 @ 0.3223
NODE POINT 0.42997 -.44500E-2
*MODES
A 0 0.000 255.750 0.100E-03
0.000 1.000 0.000 0.000 0.000 0.000
1.000 1.000 1.000 1.000 1.000 1.000
S 1 0.000 255.750 0.100E-03
1.000 0.000 -1.000 0.000 0.000 0.000
0.000 0.000 0.000 0.000 0.000 0.000
A 1 0.000 80.203 0.100E-03
-.5600 0.4300 -.5600 1.000 0.000 1.000
0.1736 0.2249 0.2541 0.2871 0.3223 0.4027
A 1 241.620 1.000 0.100E-01
0.1196E-010.2132 0.000 0.000 0.000 0.6824
0.9200E-020.4126E-010.5981E-010.9198E-010.1339 0.1948
A 0 344.390 1.000 0.100E-02
0.1815E-020.1489 0.000 0.000 0.000 0.3646
0.7565E-020.3150E-010.4311E-010.6741E-010.1019 0.1392
A 2 437.610 1.000 0.100E-03
-.5839E-02-.2220 0.000 0.000 0.000 -1.040
-.8256E-02-.3559E-01-.4993E-01-.7418E-01-.1120 -.1929
A 1 1070.000 1.000 0.100E+01
0.1163 -.5222E-01 0.000 0.000 0.000 -.7755
0.2031E-030.3123E-010.8217E-010.1070
0.5216E-01-.3128E-01
A 3 1102.900 1.000 0.100E-03
-.8563E-02-.2258 0.000 0.000 0.000 -1.288
-.9106E-02-.3848E-01-.5427E-01-.7377E-01-.1019 -.1885
A 2 1466.700 1.000 0.100E-03
0.1615 -.3110E-01 0.000 0.000 0.000 -.7642
0.9348E-020.7179E-010.1480 0.1739
0.8473E-01-.1239E-01
A 0 1882.800 1.000 0.100E-02
0.4292E-01-.9759E-01 0.000 0.000 0.000 -2.634
0.2987E-010.1253 0.1818 0.2268 0.1943
-.2950E-01
A 3 1950.000 1.000 0.100E-03
0.1692 -.3948E-01 0.000 0.000 0.000 -.7462
0.1950E-010.1049 0.1881 0.2013
0.8121E-01-.2283E-01
A 4 1956.100 1.000 0.100E-03
-.3724E-02-.2284 0.000 0.000 0.000 -1.502
-.1081E-01-.4256E-01-.5739E-01-.7251E-01-.9414E-01-.1836
A 1 2187.000 1.000 0.100E-01
0.8781E-02-.1194 0.000 0.000 0.000 -3.692
0.5342E-010.2052 0.2744 0.3262 0.2866
-.2361E-01
A 4 2663.900 1.000 0.100E-03
0.1682 -.5504E-01 0.000 0.000 0.000 -1.153
0.3731E-010.1707 0.2695 0.2770 0.1185
-.2999E-01
A 0 2683.400 1.000 0.100E-02
0.1030 0.2232E-01 0.000 0.000 0.000 0.9936
-.3991E-01-.1115 -.9788E-01-.7678E-01-.8065E-01-.9534E-02
A 2 2811.100 1.000 0.100E-03
-.6229E-01-.9304E-01 0.000 0.000 0.000 -3.408
0.5660E-010.2113 0.2645 0.3042 0.2786
-.2291E-02
A 5 2919.600 1.000 0.100E-03
0.6112E-020.2230 0.000 0.000 0.000 1.601
0.1934E-010.7176E-010.9225E-010.9856E-010.9585E-010.1744
A 3 3425.000 1.000 0.100E-03
0.3667E-010.7893E-01 0.000 0.000 0.000 2.968
-.5925E-01-.2422 -.3202 -.3488 -.2662
0.2379E-04
A 5 3484.600 1.000 0.100E-03
0.1655 -.3864E-01 0.000 0.000 0.000
-.2094E-01
0.5619E-010.2366 0.3363 0.2787
0.3181E-01-.4615E-01
A 0 3756.200 1.000 0.100E-02
0.3941E-010.8069E-01 0.000 0.000 0.000 1.453
0.9555E-010.3539 0.4299 0.2937
0.1674E-010.3707E-01
A 1 3982.900 1.000 0.100E-01
-.6706E-010.4392E-01 0.000 0.000 0.000 1.811
0.1228 0.4295 0.4798 0.2599
-.6428E-01-.8414E-03
A 6 3996.000 1.000 0.100E-03
-.6188E-02-.2130 0.000 0.000 0.000 -1.430
0.3023E-010.1069 0.1187 0.4360E-01-.7901E-01-.1668
A 2 4169.300 1.000 0.100E-03
0.1375E-02-.5022E-01 0.000 0.000 0.000 -2.405
-.7805E-01-.2692 -.3005 -.1182 0.1422
0.1538E-01
A 4 4316.600 1.000 0.100E-03

-.7190E-01-.2725E-01 0.000 0.000 0.000 -.8119
0.9701E-010.3930 0.4911 0.4003 0.1400
0.1297E-02
A 6 4769.500 1.000 0.100E-03
0.1786 -.4529E-01 0.000 0.000 0.000 -1.046
-.3010E-01-.7254E-01-.2524E-010.6954E-010.7001E-01-.2979E-0
1
A 3 4784.400 1.000 0.100E-03
0.4477E-01-.3194E-01 0.000 0.000 0.000 -2.364
-.9699E-01-.3817 -.4557 -.2436 0.1245
0.2664E-01
A 7 5044.300 1.000 0.100E-03
-.9631E-02-.2137 0.000 0.000 0.000 -1.687
-.8052E-03-.1722E-01-.3781E-01-.7667E-01-.9332E-01-.1580
A 4 5257.700 1.000 0.100E-03
0.2500E-01-.5455E-01 0.000 0.000 0.000 -3.218
-.5784E-01-.2181 -.2399 -.4697E-010.2252
0.2718E-01
A 7 5652.400 1.000 0.100E-03
0.1355 -.7474E-01 0.000 0.000 0.000 -2.456
-.3603E-020.9727E-010.2359 0.3508 0.2371
-.2397E-01
A 5 5928.800 1.000 0.100E-03
0.1053 0.5812E-02 0.000 0.000 0.000 1.821
-.1462E-02-.4163E-01-.8048E-01-.1451 -.1996
-.4965E-01
A 8 6094.300 1.000 0.100E-03
0.3923E-010.2090 0.000 0.000 0.000 1.882
0.4630E-020.5008E-010.9560E-010.1240 0.8832E-010.1422
A 5 6617.000 1.000 0.100E-03
-.6317E-010.3379E-01 0.000 0.000 0.000 2.083
0.6386E-010.4339 0.6532 0.4682
-.3213E-01-.1561E-01
A 6 6767.500 1.000 0.100E-03
-.9406E-02-.3750E-01 0.000 0.000 0.000 -2.490
-.1641E-010.1382 0.3465 0.5205 0.3454
0.2526E-01
A 8 6935.800 1.000 0.100E-03
-.1808 0.6636E-01 0.000 0.000 0.000 1.377
0.4729E-010.2723 0.3742 0.2173
0.2519E-020.4984E-01
A 9 7168.300 1.000 0.100E-03
-.3357E-01-.2084 0.000 0.000 0.000 -1.867
0.1029E-02-.1122E-01-.3585E-01-.7480E-01-.8073E-01-.1387
A 6 7451.500 1.000 0.100E-03
0.1754E-01-.2573E-01 0.000 0.000 0.000 -2.411
-.1803E-01-.3241 -.5774 -.4790
0.5223E-010.3611E-01
A 7 7678.800 1.000 0.100E-03
0.4741E-02-.3452E-01 0.000 0.000 0.000 -2.292
-.6777E-010.2473E-010.2902 0.6145 0.3914
0.1991E-01
A 9 8022.500 1.000 0.100E-03
0.1792 -.7471E-01 0.000 0.000 0.000 -1.270
-.1113E-01-.4137E-01-.2513E-010.4683E-010.3714E-01-.6463E-0
1
A 10 8187.600 1.000 0.100E-03
-.1336E-01-.1695 0.000 0.000 0.000 -1.592
0.1885E-020.2440E-010.5026E-01-.4417E-02-.6144E-01-.1308
A 7 8238.600 1.000 0.100E-03
-.1118E-010.1963E-01 0.000 0.000 0.000 1.817
-.3772E-010.2567 0.6088 0.6360
0.6096E-01-.2773E-01
A 0 8685.600 1.000 0.100E-02
-.7645E-020.3241E-02 0.000 0.000 0.000
-.8076E-02
-.1086 -.1134 0.5146E-010.2521 0.1146
0.3894E-02
*END

CWW.mp

CWW modal parameters file created 10-6-03 by TK (NA-type wheel)
FACTOR MASS 4.000 ! web response positions
FACTOR DAMPING 1.000 ! 2 @ 0.1620 3 @ 0.2040 4 @ 0.2460
MIN DAMPING 0.5000E-04 ! 5 @ 0.2870 6 @ 0.3270
NODE POINT 0.43000 0.88700E-2
*MODES
A 0 0.000 248.250 0.100E-03
0.000 1.000 0.000 0.000 0.000 0.000
1.000 1.000 1.000 1.000 1.000 1.000
S 1 0.000 248.250 0.100E-03
1.000 0.000 -1.000 0.000 0.000 0.000
0.000 0.000 0.000 0.000 0.000 0.000
A 1 0.000 77.851 0.100E-03
-.5600 -.4300 -.5600 1.000 0.000 1.000
-.1620 -.2040 -.2460 -.2870 -.3270 -.3950
A 1 163.300 1.000 0.100E-01
0.3373E-010.2080 0.000 0.000 0.000 -.5836
0.2932E-020.2728E-010.6427E-010.1039 0.1453 0.1877
A 0 312.890 1.000 0.100E-02
0.6609E-020.1496 0.000 0.000 0.000 -.3248
0.5179E-020.3356E-010.5572E-010.7448E-010.1113 0.1387
A 2 417.820 1.000 0.100E-03
-.1207E-01-.2245 0.000 0.000 0.000 1.074
-.2531E-02-.1840E-01-.4113E-01-.7239E-01-.1165 -.1865
A 1 743.810 1.000 0.100E+01
0.1250 -.7601E-01 0.000 0.000 0.000 0.8714
-.1154E-01-.3202E-010.2245E-010.7228E-010.2317E-01-.4628E-01
A 2 1072.300 1.000 0.100E-03
0.1601 -.3803E-01 0.000 0.000 0.000 0.6955
-.1069E-01-.1469E-010.7147E-010.1248
0.4723E-01-.1365E-01
A 3 1085.700 1.000 0.100E-03
0.2004E-01-.2291 0.000 0.000 0.000 1.399
-.2709E-02-.1145E-01-.1403E-01-.3518E-01-.9319E-01-.1787
A 0 1626.700 1.000 0.100E-02
0.3309E-01-.8678E-01 0.000 0.000 0.000 2.253
0.2840E-010.1865 0.2897 0.2222 0.1510
-.7756E-02
A 3 1678.800 1.000 0.100E-03
0.1706 0.1485E-01 0.000 0.000 0.000 0.2313
-.3264E-020.2299E-010.1321 0.1674
0.5848E-010.2399E-01
A 1 1912.200 1.000 0.100E-01
-.2392E-01-.9733E-01 0.000 0.000 0.000 2.786
0.6240E-010.3702 0.5345 0.3486 0.1984
-.9497E-03
A 4 1922.000 1.000 0.100E-03
0.5048E-01-.2223 0.000 0.000 0.000 1.563
-.6936E-030.4253E-020.2378E-010.4884E-02-.7471E-01-.1646
A 0 2265.500 1.000 0.100E-02
-.1281 -.1375E-02 0.000 0.000 0.000 -.1525
0.3896E-010.2270 0.2747
0.8265E-01-.1757E-01-.1249E-01
A 4 2353.900 1.000 0.100E-03
0.1624 0.8002E-01 0.000 0.000 0.000 -1.116
-.3794E-01-.1861 -.1942
-.4434E-01-.2231E-010.4343E-01
A 2 2475.400 1.000 0.100E-03
0.4498E-01-.1665E-01 0.000 0.000 0.000 1.366
0.8065E-010.4864 0.7827 0.5012 0.1582
0.3047E-01
A 1 2749.900 1.000 0.100E-01
-.7716E-010.5803E-01 0.000 0.000 0.000 -2.473
0.5510E-010.3873 0.6518 0.2821 -.1583
-.3384E-01
A 0 2785.100 1.000 0.100E-02
0.4349E-010.4612E-01 0.000 0.000 0.000 -1.950
0.2197E-010.2145 0.4699 0.2657 -.1111
-.1903E-01
A 5 2842.700 1.000 0.100E-03
0.8162E-01-.2045 0.000 0.000 0.000 1.473
0.4769E-020.4842E-010.1181 0.7272E-01-.6624E-01-.1475
A 3 2847.300 1.000 0.100E-03
0.4051E-010.1846E-01 0.000 0.000 0.000 -.5791
-.7614E-01-.4521 -.7084 -.3861
-.6574E-01-.7166E-03
A 2 3181.800 1.000 0.100E-03
-.1860E-010.6964E-01 0.000 0.000 0.000 -3.291
0.3320E-010.2876 0.5763 0.2409 -.2257
-.4464E-01
A 5 3322.500 1.000 0.100E-03
0.9784E-010.7928E-01 0.000 0.000 0.000
-.9548E-01
0.1583E-010.1053 0.1925 0.1604
0.8915E-010.7428E-01
A 6 3842.000 1.000 0.100E-03
0.8099E-01-.2038 0.000 0.000 0.000 1.688
0.2026E-020.2559E-010.7001E-010.4481E-01-.5568E-01-.1378

A 4 3921.100 1.000 0.100E-03
-.5284E-01-.4587E-01 0.000 0.000 0.000 1.486
0.4303E-010.2594 0.3841 0.1856 0.1008
0.5207E-02
A 3 3958.500 1.000 0.100E-03
0.1209E-010.8192E-01 0.000 0.000 0.000 -3.858
-.1690E-01-.4380E-020.1323 -.1157E-01-.2886
-.4961E-01
A 6 4441.400 1.000 0.100E-03
-.1316 -.1006 0.000 0.000 0.000 0.6701
-.1170E-01-.1342 -.3127 -.2309
-.6700E-01-.8034E-01
A 5 4460.800 1.000 0.100E-03
-.1128 -.2688E-01 0.000 0.000 0.000 0.5460
0.2943E-010.2123 0.3126
0.7255E-010.1248E-01-.1256E-01
A 7 4848.100 1.000 0.100E-03
-.8168E-010.1847 0.000 0.000 0.000 -1.725
-.1860E-01-.1558 -.3128 -.1648 0.3290E-010.1158
A 4 4910.500 1.000 0.100E-03
-.5071E-02-.7136E-01 0.000 0.000 0.000 3.737
0.2490E-010.4709E-01-.6609E-010.7167E-010.3002
0.5533E-01
A 7 5209.700 1.000 0.100E-03
-.4151E-01-.1111 0.000 0.000 0.000 0.7018
-.3653E-01-.3353 -.6742 -.3563
-.7320E-01-.8488E-01
A 6 5448.700 1.000 0.100E-03
0.8503E-010.4167E-01 0.000 0.000 0.000 -.5977
-.3014E-01-.3449 -.6502 -.1994
0.7528E-020.2460E-01
A 5 5903.900 1.000 0.100E-03
0.8384E-010.9608E-01 0.000 0.000 0.000 -3.548
-.3993E-01-.1610 -.1215 -.1078 -.2484
-.1912E-01
A 7 5955.300 1.000 0.100E-03
0.1135 0.3760E-01 0.000 0.000 0.000 1.259
-.4245E-02-.1485 -.3588 -.1037E-010.2004
0.8456E-01
A 8 6009.500 1.000 0.100E-03
-.4635E-010.1947 0.000 0.000 0.000 -1.774
0.1567E-010.1242 0.2528 0.1428 0.6023E-010.1220
A 8 6890.700 1.000 0.100E-03
-.1472 -.9730E-01 0.000 0.000 0.000 1.095
0.2494E-02-.7969E-02-.1108 -.1948
-.4517E-01-.6833E-01
A 6 6979.800 0.500 0.100E-03
-.3227E-02-.4627E-01 0.000 0.000 0.000 3.538
0.4595E-010.1154 -.3984E-010.1353 0.3384
0.7118E-01
A 9 7059.900 1.000 0.100E-03
-.6019E-010.2002 0.000 0.000 0.000 -1.894
0.1235E-010.6982E-010.1355 0.9806E-010.5971E-010.1178
A 8 7256.900 1.000 0.100E-03
0.3381E-010.4000E-01 0.000 0.000 0.000 -.1876
-.5743E-01-.2802 -.6098 -.4961
-.3055E-010.3500E-01
A 7 7956.800 1.000 0.100E-03
0.1424E-01-.2008E-01 0.000 0.000 0.000 1.927
0.3410 0.6529 -.2825 0.1756 0.3065
0.4437E-01
A 0 8000.200 1.000 0.100E-02
0.2801E-010.9900E-02 0.000 0.000 0.000 -.7670
0.3195 0.6003 -.2170
0.8911E-010.3536E-01-.1538E-01
A 9 8064.500 1.000 0.100E-03
0.9706E-010.6166E-01 0.000 0.000 0.000 0.1622
-.1150 -.4842E-010.1681 -.3269
-.2007E-010.7673E-01
A 10 8085.000 1.000 0.100E-03
0.6547E-01-.1378 0.000 0.000 0.000 1.330
0.2204 0.5037 -.1870 -.1844
-.2141E-01-.9160E-01
A 10 8122.600 1.000 0.100E-03
-.2641E-010.1369 0.000 0.000 0.000 -1.296
0.2886 0.7008 -.1233 -.1744
0.5393E-010.6383E-01
A 1 8146.500 1.000 0.100E-01
0.6994E-010.6135E-01 0.000 0.000 0.000 -3.178
0.3413 0.6038 -.3308 -.9650E-01-.1723
-.3917E-01
A 9 8187.600 1.000 0.100E-03
-.1059 -.6306E-01 0.000 0.000 0.000 0.5608
-.8905E-010.6322E-010.3596 -.4140 -.1878
-.4910E-01
A 2 8301.000 1.000 0.100E-03
-.3118E-010.8050E-02 0.000 0.000 0.000
-.1932E-01
-.2409 -.4926 0.1958 0.1007
-.5179E-01-.2767E-01
A 3 8341.700 1.000 0.100E-03
0.1628E-020.9145E-02 0.000 0.000 0.000 -.1149
-.3063 -.8092 0.1470 0.3928
0.1273E-01-.2666E-02

```
A        4      8861.000        1.000 0.100E-03
0.3148E-010.1398E-01 0.000        0.000        0.000       0.2142
0.9663E-010.4423                                    0.6699E-01-.3381
-.1162E-010.4061E-01
A        9      9101.000        1.000 0.100E-03
0.1170E-01-.4880E-03 0.000        0.000        0.000       2.540
-.1670          -.3570          0.1540          0.1779          0.2519
0.7878E-01
A       11      9144.900        1.000 0.100E-03
0.5860E-01-.1881        0.000        0.000        0.000       1.748
-.2888E-02-.3472E-01-.3082E-010.2921E-01-.4124E-01-.1052
A        5      9244.400        1.000 0.100E-03
-.1701E-010.3209E-01 0.000        0.000        0.000      -.4195
0.3049E-010.2286E-01-.3770E-020.2531
0.6180E-010.2666E-02
*END
```

C CALCULATION PROCEDURE

C1 Calculation procedure

In order to carry out the calculations for the TWINS validation, the following procedure has been employed.

- the TWINS calculations have been performed using a "unit roughness" excitation.
- train speeds in the range 50-150km/h have been used in the TWINS calculations.
- post-processing is carried out using Matlab and Excel, in which a standard roughness spectrum is added to the noise or vibration spectra predicted with the TWINS model, in 1/3 octave bands.

In this procedure, the reference roughness spectra and the effect of train speed on noise components are checked in following sections.

C2 Reference roughness

In order to evaluate noise and vibration with the TWINS model, a roughness spectrum should be input to the calculations. However, wheel and rail roughnesses have not been measured for the measurement campaign. In this report, a standard roughness spectrum from European wheels/rails is used instead for the TWINS calculations [C1]. Figures C1-C2 show the reference roughness spectra of the wheel and rail. The reference rail roughness is the maximum level measured at three sites and two rails at each site. The reference wheel roughnesses are the average results of 34 tread braked wheels and 37 disc braked wheels. Also shown for comparison are the roughness spectra of the wheel and rail measured at one Japanese railway line (not JR1 track) and two wheels [C3-C4].

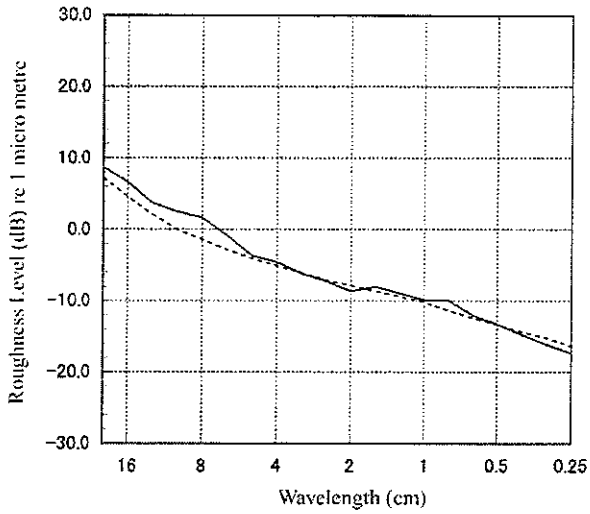

Figure C1 Rail roughness spectrum [C1, C3]

——— *: reference rail,* - - - - - *: rail at JR line*

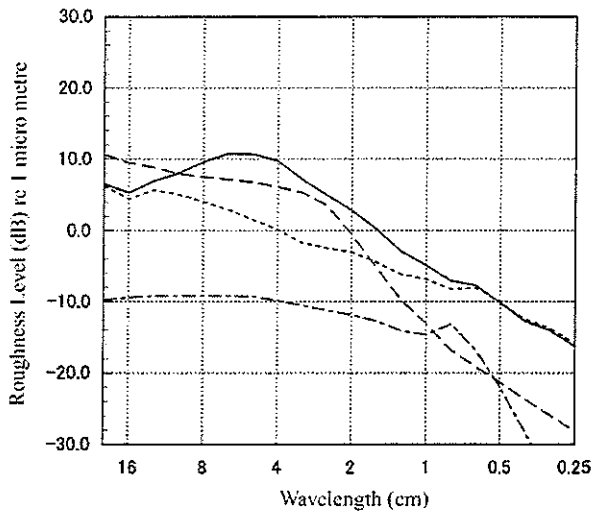

Figure C2 Rail roughness spectrum [C1, C4]

——— *: tread braked wheel (cast iron block),*

····· *: disc braked wheel,*

- - - - - *: tread braked wheel (cast iron block, JR),*

—·—·· *: disc braked wheel (JR)*

The reference rail roughness can be seen to be comparable to that from the Japanese railway line, and the reference rail roughness is appropriate for the TWINS calculations. For the wheel, the reference roughness spectra are different from those obtained for Japanese wheels. However, each roughness measurement for the Japanese wheels is obtained from only one wheel. The reference spectra are obtained by averaging the results of 30 or more wheels, and would be more reliable for the TWINS validation.

Roughness with wavelength comparable and shorter than the contact patch length is attenuated in its excitation of the wheel/rail system. Figure C3 shows the filtering effect used in [C2].

The wheel and rail roughness spectra are combined with the contact filter. This is because a roughness spectrum should include the effect of contact filtering for the TWINS calculations, as the filter effect is not added by TWINS. Figure C4 shows the combined filtered wheel/rail roughness spectra.

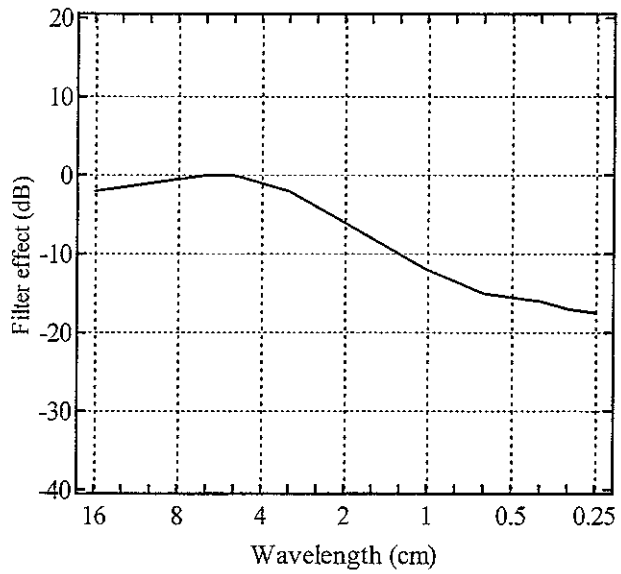

Figure C3 Assumed contact filter [C2]

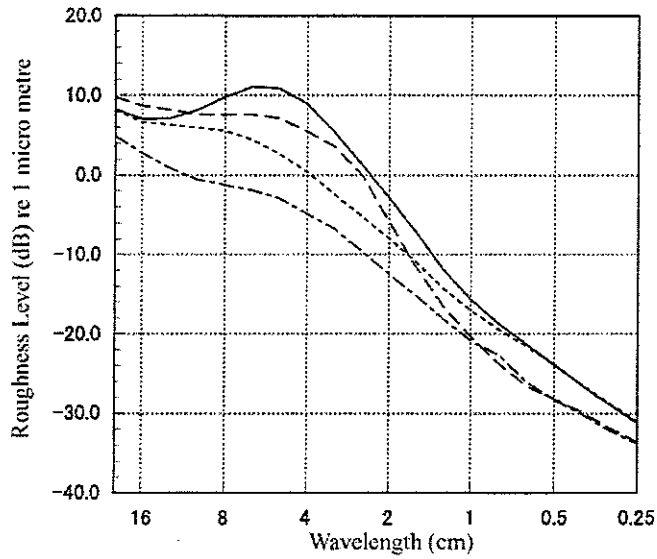

Figure C4 Combined wheel/rail roughness spectra after contact filtering [C1]

——: block braked wheel + rail, ·····: disc braked wheel + rail,

- - - - -: block braked wheel (JR) + rail (JR), —·—··: disc braked wheel (JR) + rail (JR)

The TWINS calculations have been carried out for each speed at intervals of 10 km/h in the range 50-150 km/h, using the roughness shown in Figure C4. However, as the roughness spectra shown in Figure C4 cover only the wavelength range 0.25-20 cm, they are not sufficient to carry out the TWINS calculations in the whole of speed range 50-150 km/h. Therefore, the roughness spectra are extrapolated logarithmically in two wavelength range

(λ >20 cm and λ < 0.25 cm, λ :wavelength), as shown in Figure C5.

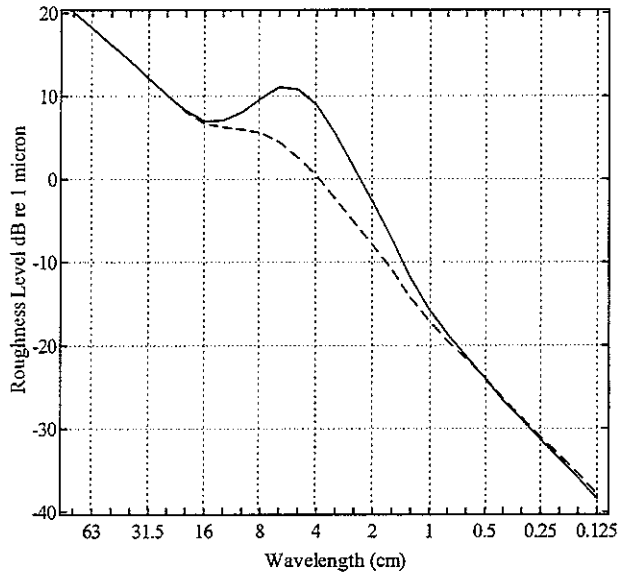

Figure C5 Extended wheel/rail roughness spectra after contact filtering

——: block braked wheel + rail, - - - - -: disc braked wheel + rail,

In order to estimate the roughness spectra in 1/3 octave bands corresponding to each train speed in the range 50-150 km/h, the following procedure was used:

(1) roughness power in one band is divided by the corresponding bandwidth into narrow-band estimates.

(2) wavelength components are transformed into frequency components by using train speed

(3) frequency components corresponding to each 1/3 octave band are added together.

This method might not be wholly appropriate, since the narrow band roughness spectra obtained by this procedure are completely different from the actual spectra (the calculated narrow band spectra are in step form). However they are converted again to 1/3 octave bands, since TWINS output data are given in 1/3 octave bands. The differences in 1/3 octave bands between the calculated and measured roughness spectra are expected to be small. Therefore, the roughness spectra calculated with this method should be acceptable.

Figures C6-C7 show the combined wheel/rail roughness spectra in the speed range 50-150 km/h for tread-braked and disc braked wheels. It can be seen that the whole roughness spectra shift to the right as the train speed is higher.

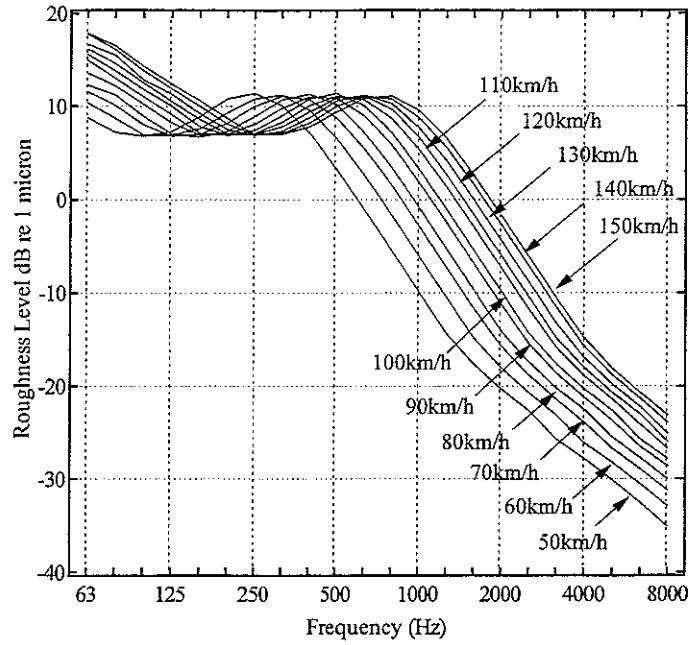

Figure C6 Combined wheel/rail roughness spectra for each train speed (tread braked wheel + rail, 50-150km/h)

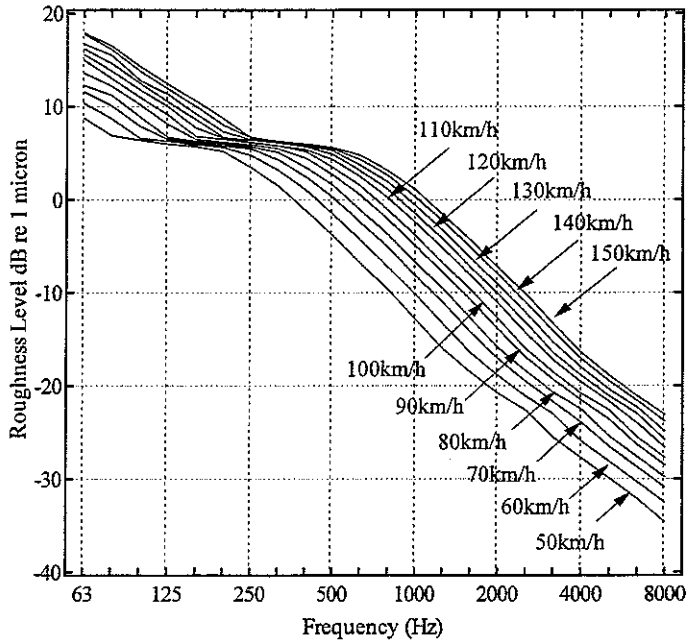

Figure C7 Combined wheel/rail roughness spectra for each train speed (disc braked wheel + rail, 50-150km/h)

C3 Contact filter

The contact filter effect shown in Figure C3 corresponds to the case of wheel radius of 0.46 m [C1-C2]. In this report, the TWINS calculations must be carried out for two different wheel radii, 0.43 m and 0.405 m (see table B9). The contact filter depends on the wheel radius. It might be better to estimate the contact filter effect corresponding to each wheel radius. However, as rail and wheel roughnesses have not been measured in the measurement campaign, the contact filter effect cannot be calculated from the TWINS model. Therefore, it is necessary to calculate the contact filter effects corresponding to the two wheel radii by shifting frequency components.

Figure C8 shows the contact filter effect from reference [C5]. This was obtained from a set of DPRS analyses on different roughness data and is considered more reliable than the earlier analysis in reference [C2]. In this section, the contact filter shown in Figure C8 is used, since the effects of wheel radius on the contact filter effect have been estimated in [C5]. As the contact filter spectrum covers the frequency range 125-10000 Hz only, the frequency range is not sufficient to estimate the contact filter effects corresponding to other wheel radii. Therefore, the contact filter spectrum is extrapolated logarithmically in two frequency ranges (f>10000 Hz and f<125 Hz, f: frequency). Figure C8 also shows the extrapolated contact filter spectrum.

In order to obtain the contact filter effects corresponding to wheel radii of 0.405m and 0.43 m, the following procedure has been used:

(1) the spectrum in one band is divided by the corresponding bandwidth into a narrow-band spectrum.

(2) frequency components are shifted by using wheel dimensions.

(3) for each wheel radius, frequency components corresponding to each 1/3 octave band are taken, and are added together.

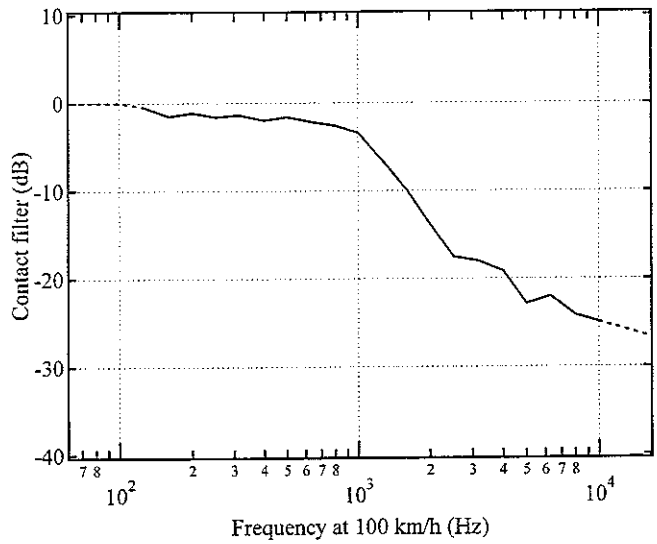

Figure C8 Contact filter effect for 0.46m wheel radius [C6]

In the procedure, it is important how the frequency components are shifted. The relationship between major semi-axis, a, and minor semi-axis, b, in contact zone for elliptical point contacts case is shown in [C6].

$$a/b \approx (R'/R'')^{\frac{3}{2}} \qquad \text{(C1)}$$

$$c = (ab)^{\frac{1}{2}} = \left(\frac{3PR_e}{4E^*}\right)^{\frac{1}{3}} F_1\left(R'/R''\right) \qquad \text{(C2)}$$

$$\frac{1}{R'} = \frac{1}{R_{11}} + \frac{1}{R_{21}} \qquad \text{(C3)}$$

$$\frac{1}{R''} = \frac{1}{R_{12}} + \frac{1}{R_{22}} \qquad \text{(C4)}$$

where P is the wheel load, E^* is the plane strain elastic modulus, R' and R'' are major and minor relative radii of curvature and R_e is the equivalent radius of curvature, $R_e = (R'R'')^{\frac{1}{2}}$. The parameter, F_1, depends on R' and R'', and is tabulated in [C6]. R_{11} and R_{12} are wheel rolling radius and wheel transverse radius respectively, and R_{21} and R_{22} are rail rolling radius ($=\infty$) and rail transverse radius respectively.

It is assumed that

$$F_1\left(R'/R''\right) \approx const. \qquad \text{(C5)}$$

This assumption will be acceptable, since the value of R'/R'' used in [C2] is nearly equal to that used in this report. Then,

$$a \propto R'^{\frac{1}{2}} R''^{-\frac{1}{6}}. \qquad \text{(C6)}$$

Therefore, as the contact patch length determines the wavelength at which the contact filter effects are effective, frequency components are shifted by using equation (C6).

The frequency shifting method might not be appropriate, since the narrow band filter spectra obtained by the method are completely different from the actual spectra (the calculated narrow band spectra are in step form). However, Figure C9 shows the contact filter effect obtained for various wheel radii, which can be seen to be plausible.

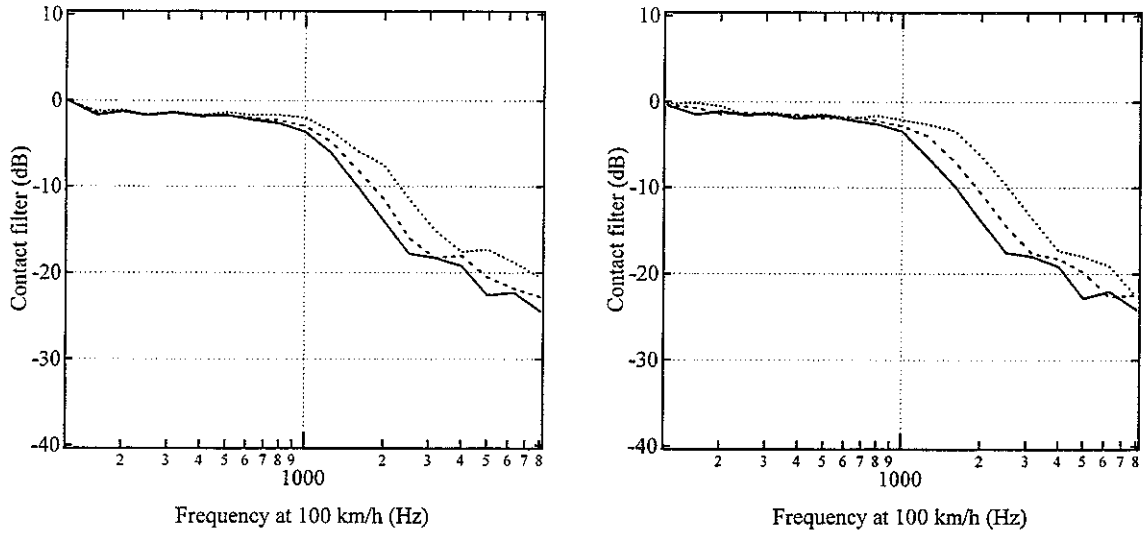

(a) Average results from DPRS model [C5] (b) results from frequency shifting method

Figure C9 Contact filter due to various wheel radii.

(: 460 mm radius wheel, : 327 mm radius wheel, : 180 mm radius wheel, R_{12}=6.7e5 mm, R_{22}=300 mm)

From Figure C9, it can be seen that the results from frequency shifting method (right-hand figure) show good agreement with the average results from DPRS model (left-hand figure). Therefore, it is confirmed that the frequency shifting method gives reliable results. Figure C10 shows the contact filter effect of the two radii (0.405 m, 0.43 m) relative to the results of wheel radius of 0.46 m.

It is found that the effect is mostly less than 0.2 dB below 1000 Hz. Above 1000 Hz, the

contact filter effects are affected by the variation of wheel radius, and have deviations of up to 2 dB. However, the relative difference above 1000 Hz has not been taken into account in the TWINS calculations. The wheel/rail roughness has an error margin of about +/-3 dB [C5]. As the relative difference is smaller than this, the relative difference is not significant.

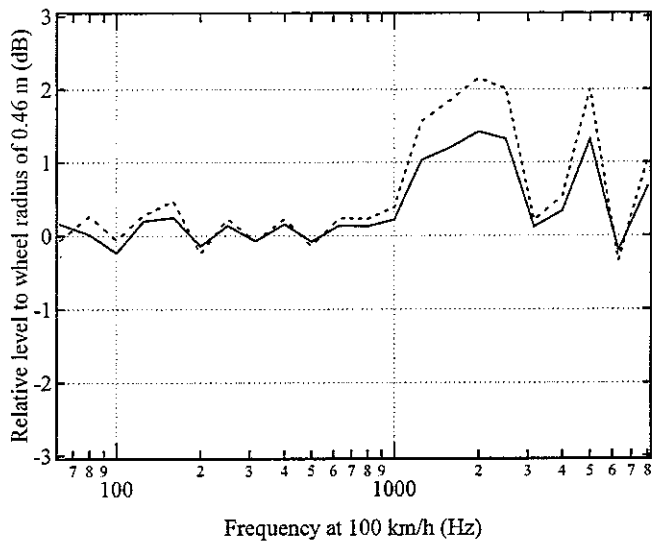

Figure C10 Predicted contact filter effect relative to result of reference wheel (reference wheel (R_{11}=460 mm, R_{12}=6.7e5 mm, R_{22}=300 mm), ——— : wheel 1 (R_{11}=430 mm, R_{12}=-800 mm, R_{22}=600 mm), ------- : wheel 2 (R_{11}=405 mm, R_{12}=-900 mm, R_{22}=600 mm))

C4 Train speed

The train speeds are used for the estimation of the wheel rotation and creep force coupling in the TWINS calculations. The rotation of a wheel leads to a splitting of the resonance peaks associated with a mode having nodal diameters ($n \geqq 1$) into two peaks.

It is important to confirm the influence of train speed on noise and vibration predictions in advance. Two effects on the noise prediction are investigated for the CW-wheel/JR1-track case:

- effect of ignoring wheel rotation effects on total noise prediction (i.e. setting speed = 0 for wheel receptance)
- effect of ignoring train speed on total noise prediction (i.e. using a single speed for all calculations)

Figure C11 shows the effect of ignoring the wheel rotation effects on the noise predictions. It is found that the effect is mostly less than 1 dB in 1/3 octave bands for the total noise. However, the wheel component is affected more than the rail and sleeper components, and has deviations of up to 4 dB. Therefore, train speed should be used for the estimation of the wheel rotation, and the inclusion of the wheel rotation effect could make better results.

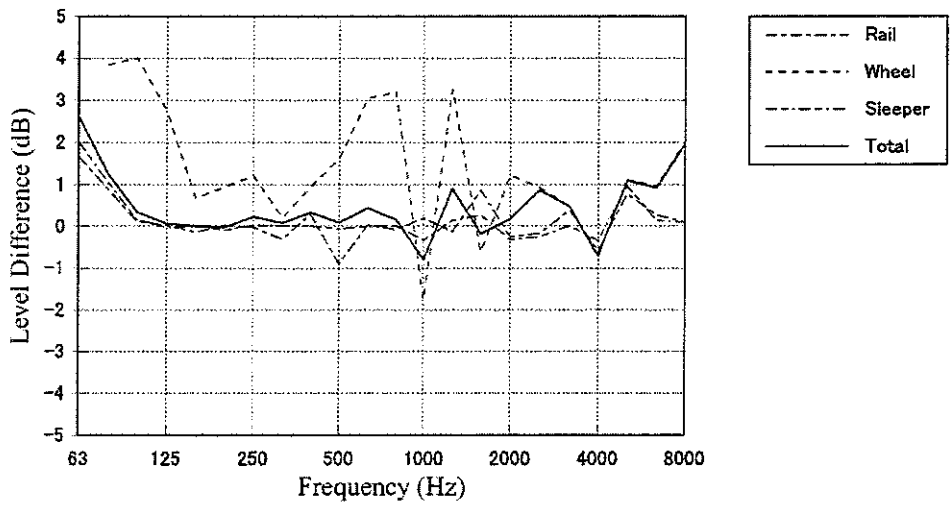

Figure C11 Effect of ignoring wheel rotation on noise components (CW-wheel, JR1-track, 150km/h, rodel, bi-bloc sleeper)

Figure C12 shows the effect of ignoring train speed on the total noise predictions. The effect can be seen to be less than 1 dB. Figure C13 shows the effect on the separate wheel

and rail components. It is also found that the effects of the wheel and rail components are less than 1dB. Therefore, in order to save computational effort, it might be better to carry out TWINS calculations by using one single speed (e.g. 100km/h). However, to obtain more reliable results, the TWINS calculations have been carried out for each speed at intervals of 10 km/h in the range 50-150 km/h in this report.

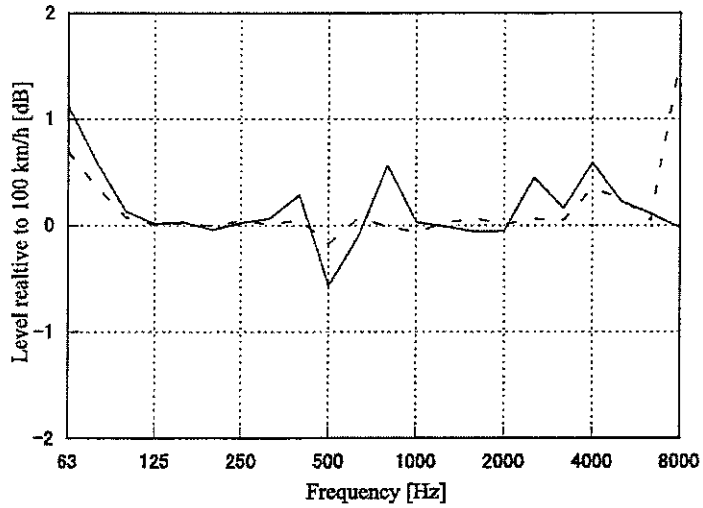

Figure C12 Effect of ignoring train speed on total noise

(——: 150km/h, -----: 50 km/h, CW-wheel, JR1-track, rodel, unit roughness excitation, wheel rotation, bi-bloc sleeper)

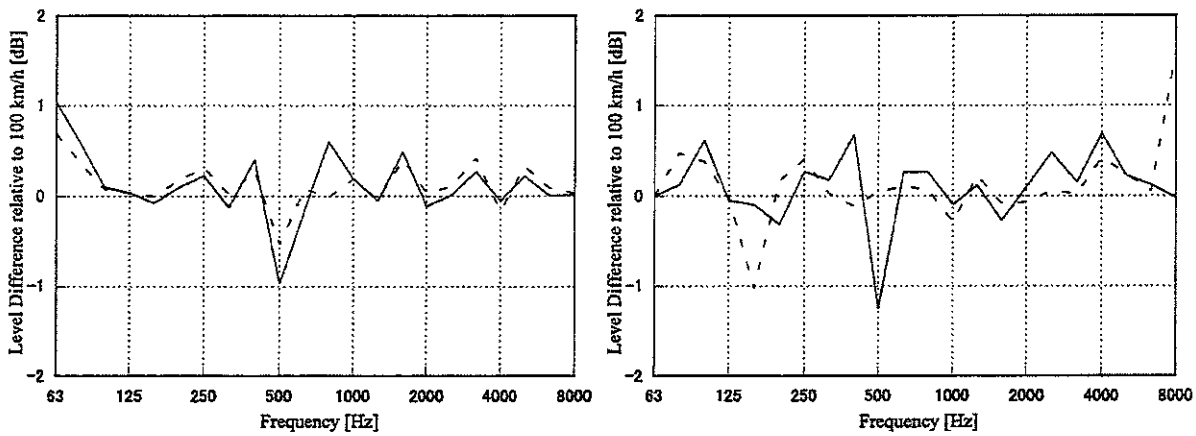

(a) rail noise (b) wheel noise

Figure C13 Effect on rail and wheel noise components of ignoring train speed

(——: 150km/h, -----: 50 km/h, CW-wheel, JR1-track, rodel, unit roughness excitation, wheel rotation, bi-bloc sleeper)

C5 Distribution of measured results

The measured result is not generally constant and the values vary in a certain range, even if the train speed is constant. Before presenting predictions, it is useful to check the deviations of the measurement data, which will give the criterion of the accuracy in the predictions.

It could be useful to use the standard deviation of the measured results as a criterion for the validation. It can be considered that the TWINS model gives adequate predictions as long as the differences between measured and predicted levels fall within a range of plus/minus one standard deviation of the measured results. Table C1 shows the standard deviations of the measured results for each wheel type and train speed. From Table C1, the predictions of the TWINS model can be considered to show a good agreement with the measurements as long as differences between measured and predicted levels are smaller than +/-1.5 dB for the noise and +/-2 dB for the rail vibration.

Table C1 Standard deviations of measured results (JR1 track, overall A-weighted level)

Data	Rail vibration [a]					Noise				
Velocity (km/h)	70	100	110	120	Δ [c]	70	100	110	120	Δ
A	0.5 (4)[b]	2.5 (9)	2.5 (20)	---	2.3 (33)	0.9 (4)	1.8 (9)	2.8 (20)	---	2.3 (33)
B	---	1.9 (7)	2.9 (15)	---	2.6 (22)	---	---	---	---	---
C	---	1.0 (12)	1.4 (7)	1.0 (2)	1.1 (21)	---	1.5 (12)	1.0 (7)	1.5 (2)	1.3 (21)
AW	---	0.2 (5)	0.6 (5)	---	0.4 (10)	---	0.3 (5)	0.4 (5)	---	0.4 (10)
BW	1.3 (6)	1.4 (12)	1.9 (50)	2.0 (22)	1.8 (90)	---	---	---	---	---
CW	0.9 (9)	1.7 (14)	2.2 (47)	2.6 (37)	2.2 (107)	1.0 (9)	1.7 (14)	2.1 (47)	1.1 (37)	1.6 (107)

a) The rail vibration is presented in the form of A-weighted velocity levels in the vertical direction.

b) Numerical value put in brackets stands for the number of sampled data.

c) Δ is derived from the following equation,

$$\Delta = \sum_i \frac{N_i \Delta_i}{N},$$

where N_i is the number of the sampled data for each train speed, Δ_i is the standard deviation corresponding to N_i and N is the total of the sampled data.

C6 Calculation parameters

In this section the parameters used in the TWINS calculations are summarized.

C6.1 Excitation and interaction parameters

Excitation parameter

- "unit roughness" excitation

Interaction parameters

- Degree of freedom: LX, LY
- max. level increment: 3
- offsets: all 0
- R_{11}: 0.405 (for A and B wheels), 0.43 (for C, AW, BW and CW wheels)
- R_{12}: -0.9 (for A, B and C wheels), -0.8 (for AW, BW and CW wheels)
- R_{22}: 0.6 (for 60-type rail)
- static load: 50000N
- Young's modulus: 2.1e+11
- Poisson constant: 0.3
- train speed: 50-150 km/h (10 km/h intervals)
- creepages: all 0

C6.2 Radiation parameters

Wheel radiation

- calculated radiation efficiencies

Rail radiation

- The TUB model is used to calculate transfer functions from vertical and lateral motions to noise, for 60-type rail profile.

Sleeper radiation

- "baffled plate" model

Sound pressure calculations

•ground reflection: No

•integration length:

20.0 (for two adjacent bogies),

10.0 (for the first bogie of a leading coach or the second bogie of a rear coach)

•wheelsets:

4 (for two adjacent bogies),

2 (for the first bogie of a leading coach or the second bogie of a rear coach)

•wheels per axle: 1 (take into account only nearside wheels and rail)

•receiver positions:

x=-0.4 (height below contact point), y=1.431 (distance from near rail)

•source height (rail): 0.07 (below contact point)

•source height (sleeper): 0.2 (below contact point)

References

[C1] Thompson, D.J. Definition of the reference roughness, *ISVR contract report*, 1997.

[C2] Thompson, D. J. Vincent, N. et al. Railway rolling noise: Validation of the TWINS model, *Vibratec/TNO report 072-21*, November 1993.

[C3] Sunaga, Y. Measurements of rail roughness, *draft document*, June 2003.

[C4] Obara, T. Measurements of wheel roughness, *draft document*, June 2003.

[C5] Thompson, D.J. The influence of the contact zone on the excitation of wheel/rail noise. *Proceeding of 8th International Workshop on Railway Noise*. 2001.

[C6] Johnson, K.L. Contact mechanics. Cambridge: Cambridge University Press

D GLOBAL COMPARISONS

D1 Continuous track model with bi-bloc sleeper

This section presents calculations of noise carried out using:

- the continuous track model (rodel model)
- bi-bloc sleeper
- calculated track decay rates

Figure D1.1 shows the total noise predicted minus measured noise in dB(A). Most of the results are in the range +/-1.5 dB(A). The predictions show good agreement with the measured results. However, the results are somewhat under-predicted.

Figure D1.2 shows the relative contributions of wheel, rail and sleeper to the predicted total level in dB(A).

Figure D1.3 shows the relative contributions of wheel, rail and sleeper of each wheel/track combination compared with the results corresponding to the A-type wheel/JR1 track combination. The relative contribution of each noise component can be seen to be independent of train speed. For the rail, the relative contributions are in the range +/-1 dB(A), and this means that the noise components of the rail are comparable in the three wheel/track combinations considered here. The relative contributions of the sleeper are also in the range +/-1 dB(A). For the wheel, the sound generated by the CW-wheel is greater than those of the other wheels.

Figure D1.4 shows the relative noise of each wheel to the A-type wheel in dB(A). The changes in relative noise of each wheel do not depend on train speed. C-type wheel is quieter than the others.

Figure D1.5 shows predicted noise plotted against measured noise in terms of overall A-weighted levels. The individual points represent one of the 4 wheel/track combinations. The solid line corresponds to the mean difference between predictions and measurements (which is -0.9 dB(A)). The dashed lines show a range of +/- one standard deviation (which is 2.6 dB(A)). It is shown that the overall trends are predicted well by the rodel model.

In order to illustrate the spectral variation, the difference between predicted and measured noise spectra should be constructed for each wheel/track combination and each train speed. Figure D1.6 shows the spectral differences as the mean and a range of +/- one standard

deviation for all cases. The predicted result can be seen to be under-predicted below 1000 Hz, and be better above 1000 Hz. There is a significant under-prediction below 250 Hz. This is because, as the sound measurements were made close to the track, the measured results were affected by wind, which is generated during train pass-by, at the low frequencies.

Figure D1.7 shows the total predicted sound pressure level minus measured level for each wheel/track combination and each train speed. In Figure D1.7(d), it is found that the difference does not depend on train speed.

Figures D1.8-D1.9 show the separate components of noise from rail, wheel and sleeper. The measured spectra are also shown for comparison. It is clear that the sleeper is the dominant source at low frequencies, up to 500 Hz, and the wheel is the predominant source above 2000 Hz. In the middle frequencies, the dominant component in the total noise depends on the wheel type. For A and C wheels, the rail becomes dominant in the middle frequencies. On the other hand, for AW and CW wheels, the wheel has almost the same contribution to the total noise as the rail has between 1000 and 2000 Hz.

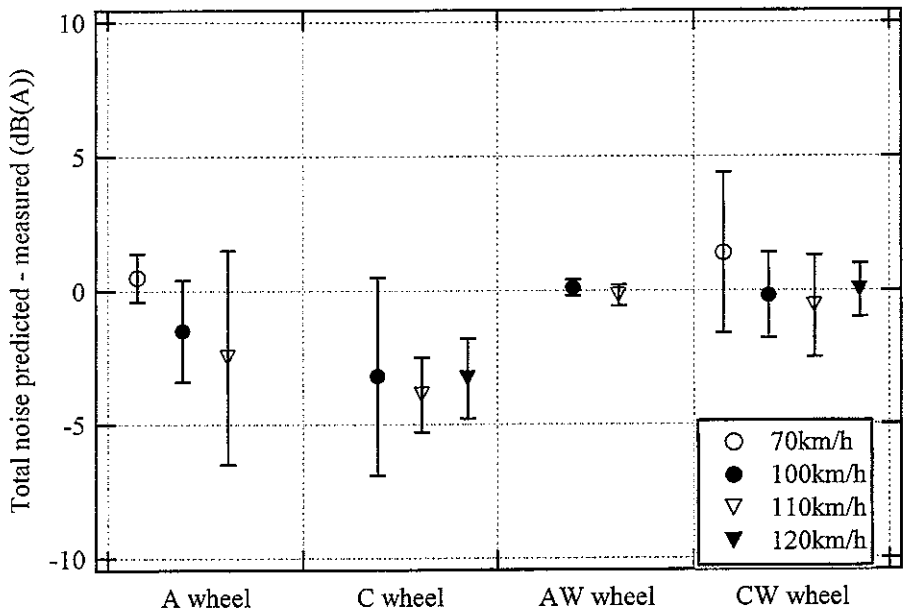

Figure D1.1 Total Predicted noise minus measured noise in dB(A) using rodel model (bi-bloc sleeper) Results are shown for each speed (70, 100, 110 and 120 km/h).

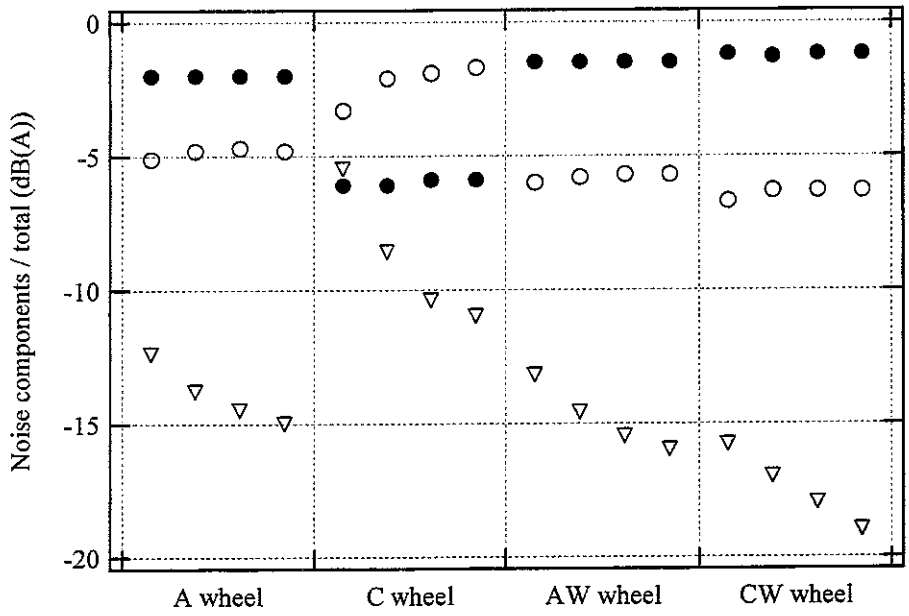

Figure D1.2 Predicted noise components from rail (○), wheel (●) and sleeper (▽) using rodel model (bi-bloc sleeper), minus predicted total noise in dB(A)
Results are shown for each speed (70, 100, 110 and 120 km/h).

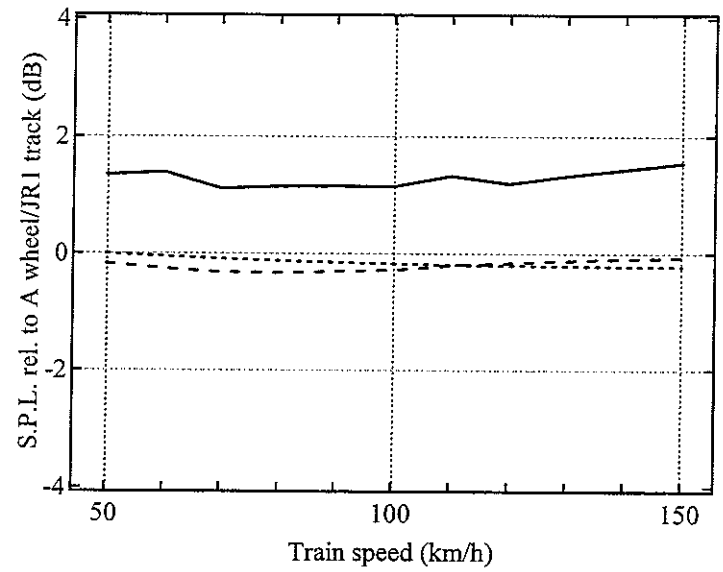

(a) AW wheel / JR1 track

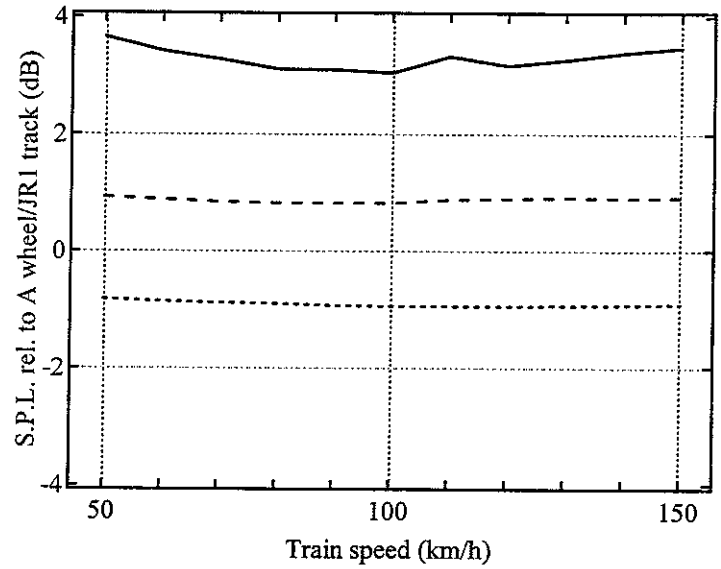

(b) CW wheel / JR1 track

Figure D1.3 Predicted noise components from rail, wheel and sleeper relative to A-wheel/JR1-track (rodel, bi-bloc sleeper, ------- :rail, ——— :wheel, - - - - :sleeper)

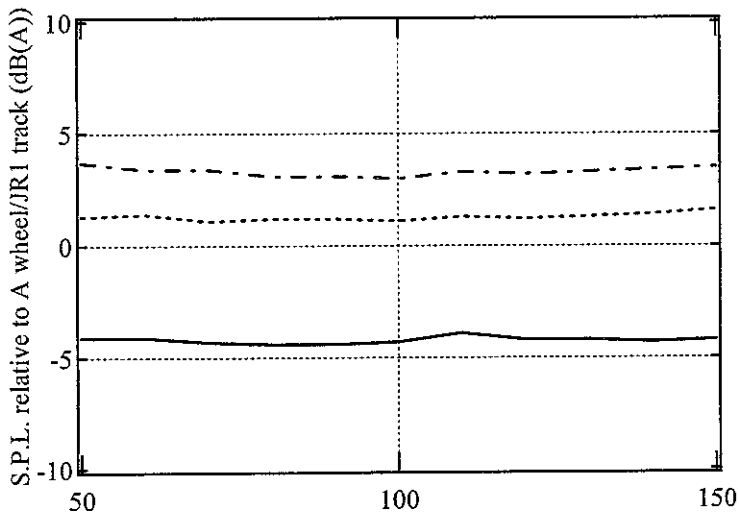

(a) Disk braked wheel/ JR1 track

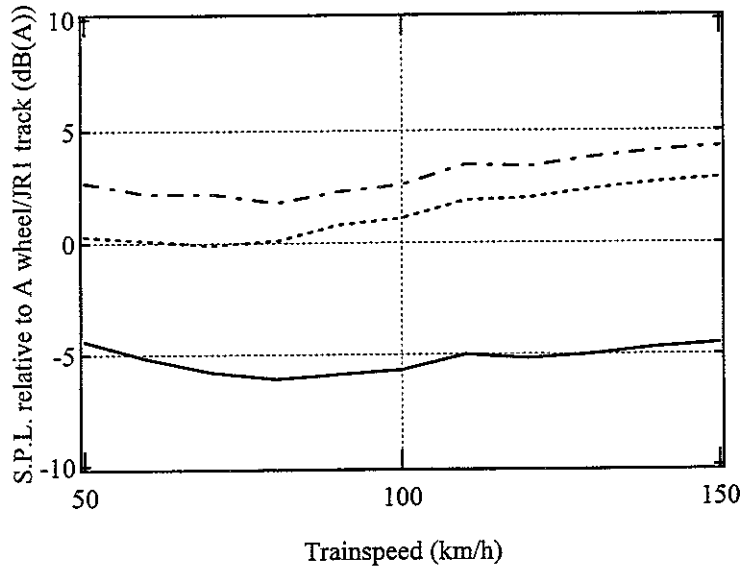

(b) Tread braked wheel/ JR1 track

Figure D1.4 Predicted wheel noise relative to A-wheel/JR1-track

(rodel, bi-bloc sleeper, ——— :C wheel, ------- :AW wheel, – – – :CW wheel)

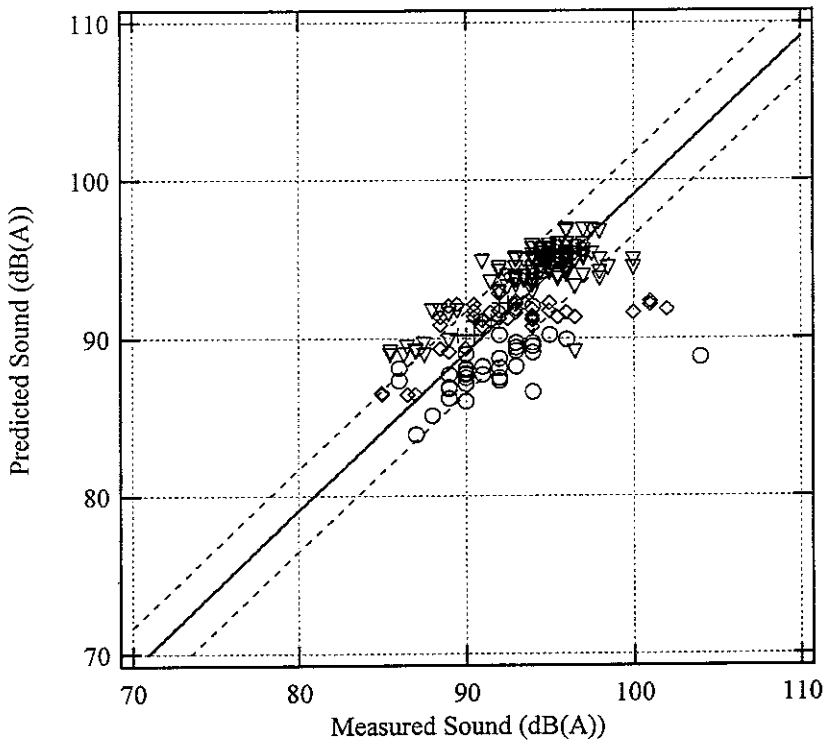

Figure D1.5 Predicted noise plotted against measured noise for all cases (rodel, bi-bloc sleeper)

◇: A-type wheel, ○: C-type wheel,

+: AW-type wheel, ▽: CW-type wheel

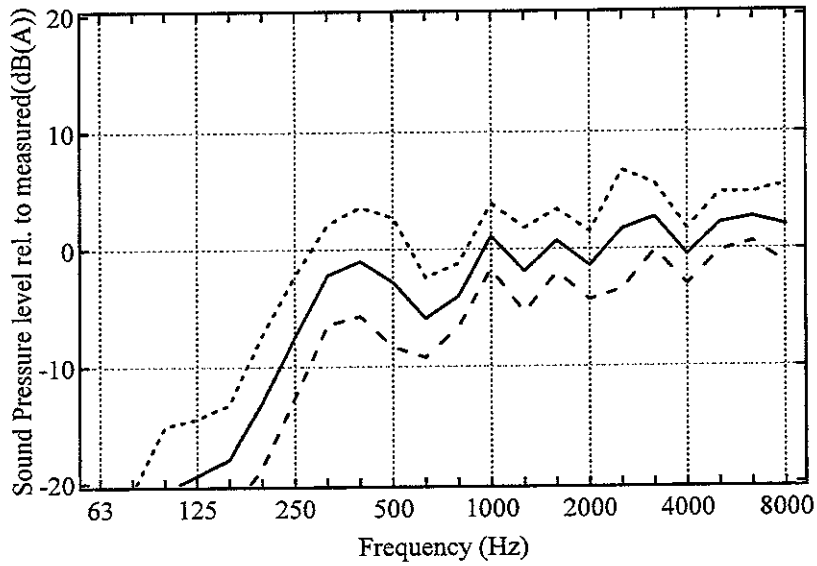

Figure D1.6 Average difference between predicted and measured noise spectra for all cases (rodel, bi-bloc sleeper, —— :mean, ----- :mean+std deviation,- - - :mean-std deviation)

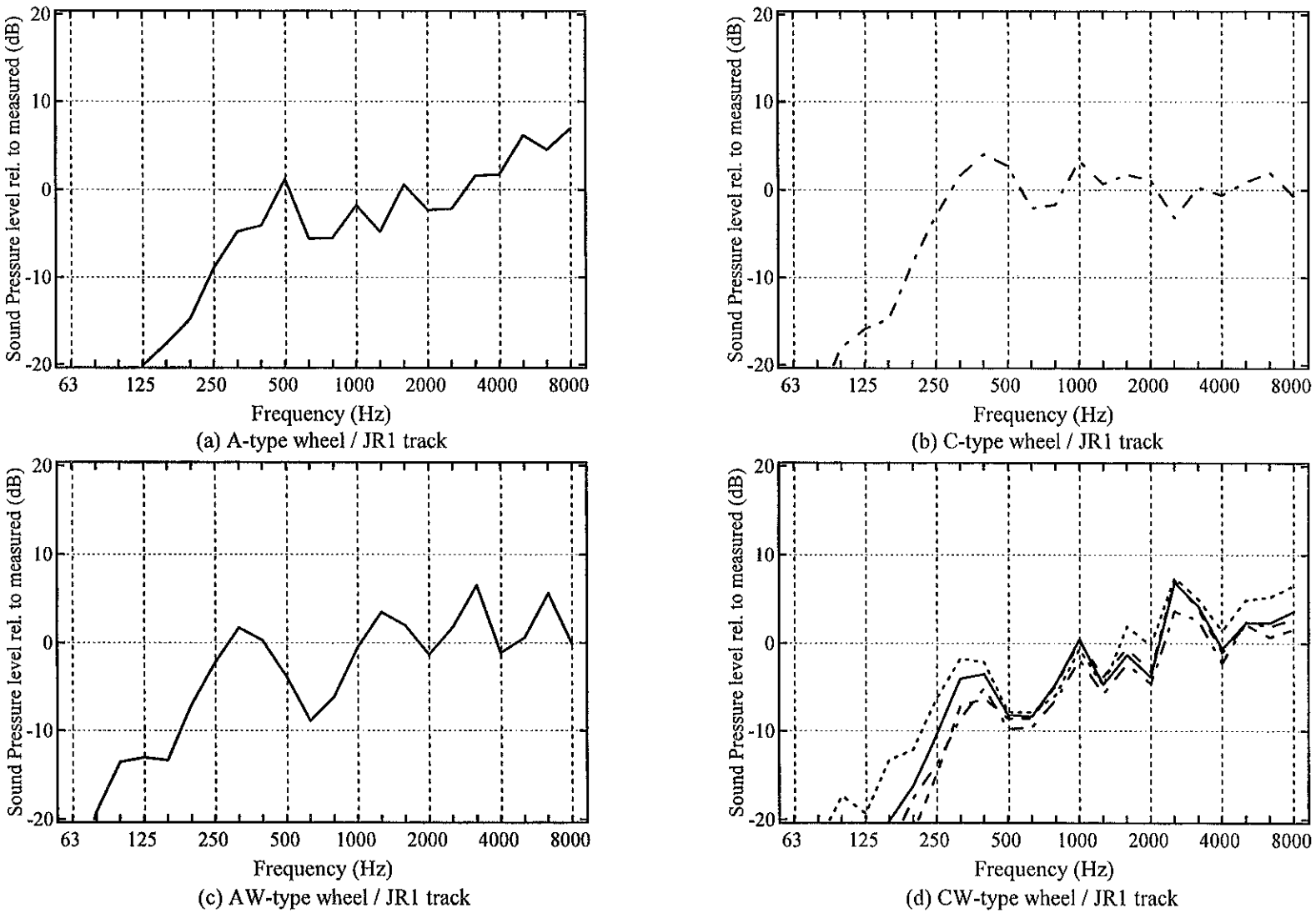

(a) A-type wheel / JR1 track

(b) C-type wheel / JR1 track

(c) AW-type wheel / JR1 track

(d) CW-type wheel / JR1 track

Figure D1.7 Predicted noise minus measured noise for each wheel using rodel model
(JR1 track, bi-bloc sleeper,····· :70 km/h,– – – :100 km/h,—— :110 km/h,- - - :120 km/h)

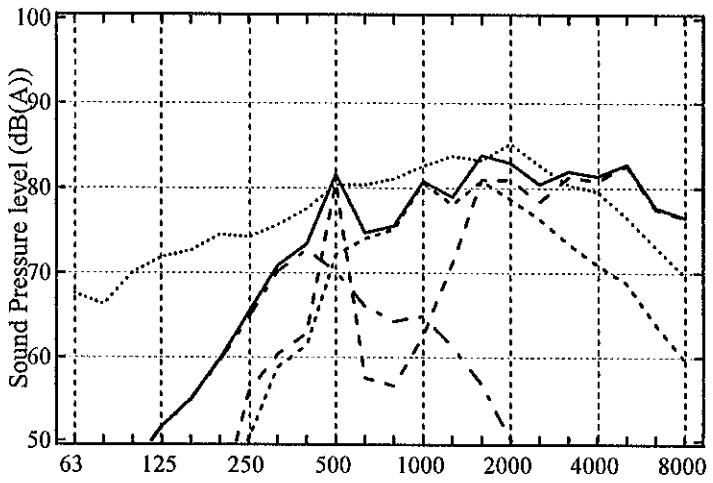

(a) A-type wheel / JR1 track (110km/h)

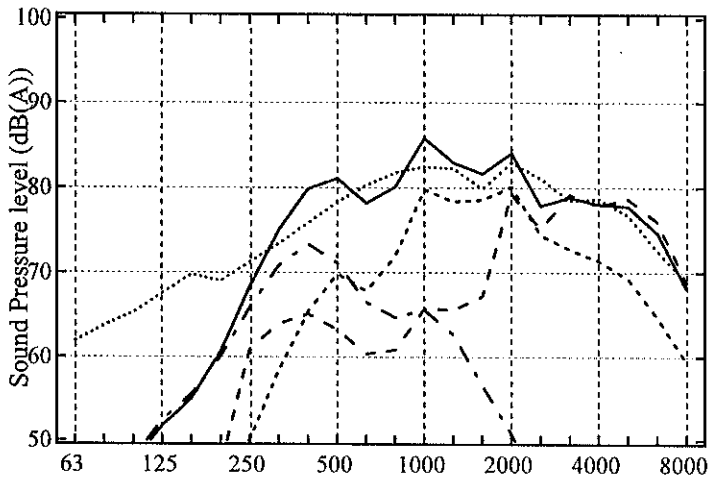

(b) C-type wheel / JR1 track (100 km/h)

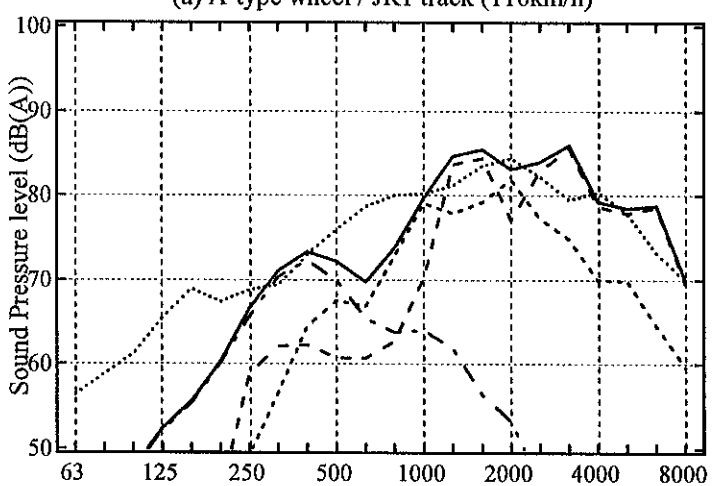

(c) AW-type wheel / JR1 track (110 km/h)

Figure D1.8 Predicted noise and measured noise for each wheel using rodel model

(JR1 track, bi-bloc sleeper, ····· :measured noise, —— :predicted noise,------ :rail, - - :wheel, - - :sleeper)

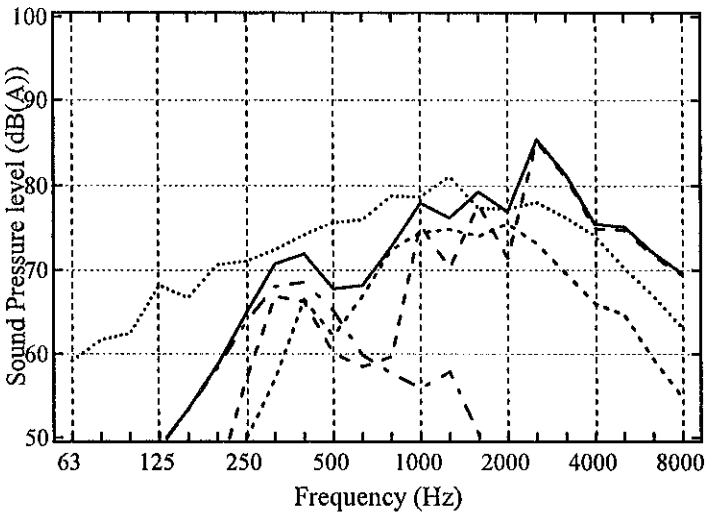

(a) CW-type wheel / JR1 track (70km/h)

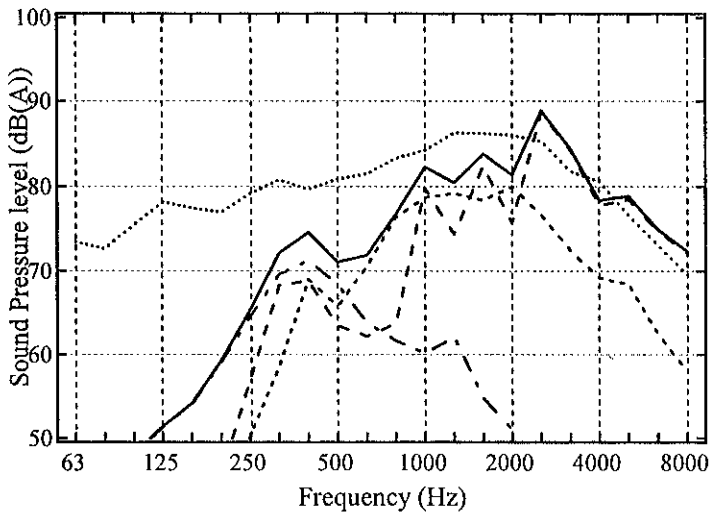

(b) CW-type wheel / JR1 track (100 km/h)

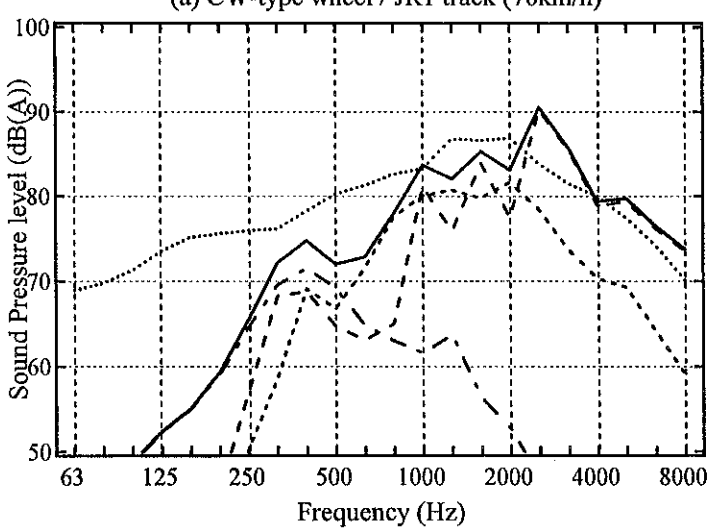

(c) CW-type wheel / JR1 track (110 km/h)

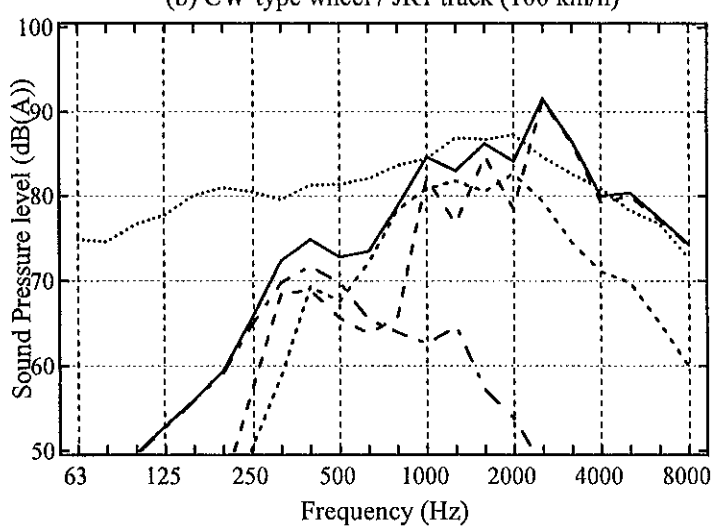

(d) CW-type wheel / JR1 track (120 km/h)

Figure D1.9 Predicted noise and measured noise for each wheel using rodel model

(JR1 track, bi-bloc sleeper, ····· :measured noise, ——— :predicted noise,- - - - - :rail, - - - :wheel, - - - :sleeper)

D2 Periodic track model with bi-bloc sleeper

This section presents calculations of noise carried out using:

- the periodic track model (tinf model)
- bi-bloc sleeper
- calculated track decay rates

Figure D2.1 shows the total noise predicted minus measured noise in dB(A). It can be seen that most of the results are over-predicted. The results of the tinf model show poor agreement with the measured results. Comparing with Figure D1.1, the results of the tinf model can be seen to be higher than those of rodel. This is probably due to the fact that, as the predictions of the tinf model are carried out at mid-span only, the vibration amplitude of rail component predicted with the tinf model is higher than that of the rodel model. It might be better that the calculations are carried out at many excitation points within a sleeper span, and subsequently the results are averaged. In addition, the rail noise is over-predicted at high frequencies due to the fact that rail damping cannot be entered into tinf.

Figure D2.2 shows the relative contributions of wheel, rail and sleeper to the predicted total level in dB(A).

Figure D2.3 shows the relative contributions of wheel, rail and sleeper of each wheel/track combination compared with the results corresponding to the A-type wheel/JR1 track combination. In the tinf model, the changes in relative contribution of each noise component do not depend on train speed. The relative changes in the contributions of the rail and sleeper are in the range +/-1 dB(A). For the wheel, the sound radiation of the CW-wheel is again greater than those of the other wheels.

Figure D2.4 shows the relative noise of each wheel to the A-type wheel in dB(A). It can be seen that C-type wheel is less than the other wheels.

Figure D2.5 shows predicted noise plotted against measured noise in terms of overall A-weighted levels. The individual points represent one of the 4 wheel/track combinations. The solid line corresponds to the mean difference between predictions and measurements (which is +1.6 dB(A)). The dashed lines show a range of +/- one standard deviation (which is 2.4 dB(A)). The results of the tinf model show worse agreement with the measured results

than the results of rodel.

Figure D2.6 shows the spectral differences as the mean and a range of +/- one standard deviation for all cases. Comparing with the results of the rodel model shown in Figure D1.6, it can be seen that the tinf model gives worse predictions, with a peak around 315 Hz and a trough around 630 Hz. These features occur because the sleeper vibration is not modelled adequately (at these frequencies the sleeper vibration is the dominant source). The result is also worse below 250 Hz. This is again due to the fact that the measured results were contaminated by wind noise. At high frequencies, the results are considerably over-predicted.

Figure D2.7 shows the total predicted sound pressure level minus measured level for each wheel/track combination and each train speed.

Figures D2.8-D2.9 show the separate components of noise from rail, wheel and sleeper.

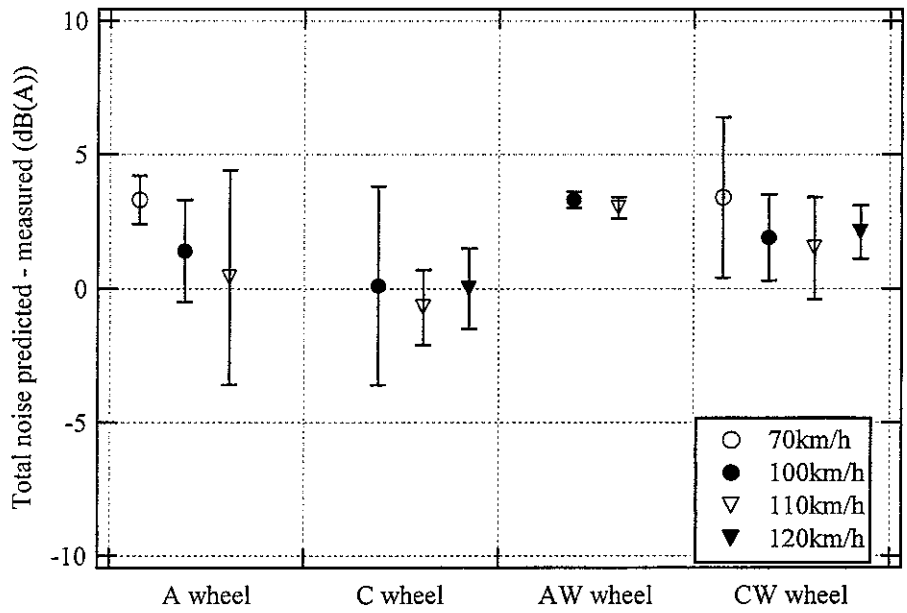

Figure D2.1 Total Predicted noise minus measured noise in dB(A) using tinf model (bi-bloc sleeper) Results are shown for each speed (70, 100, 110 and 120 km/h).

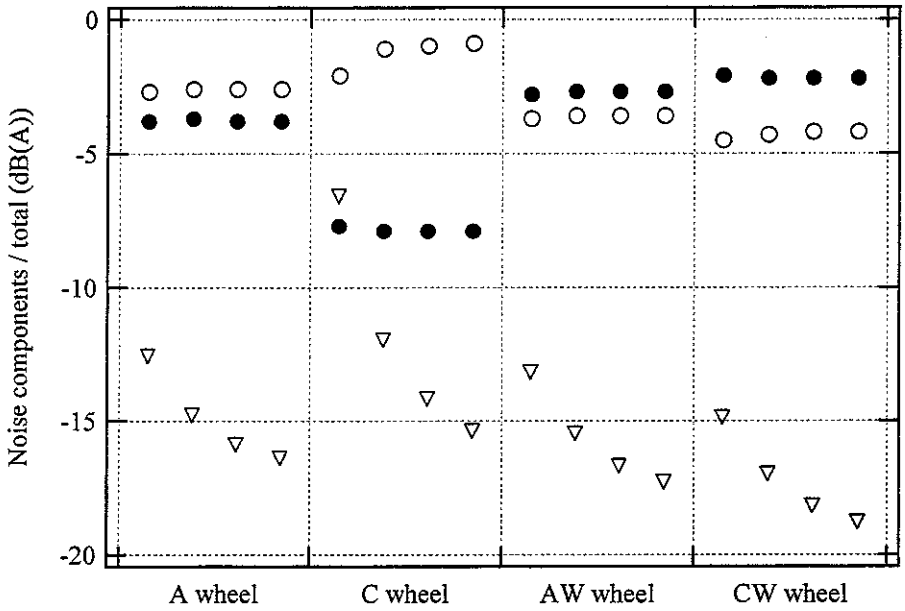

Figure D2.2 Predicted noise components from rail (○), wheel (●) and sleeper (▽) using tinf model (bi-bloc sleeper) minus predicted total noise in dB(A).
Results are shown for each speed (70, 100, 110 and 120 km/h).

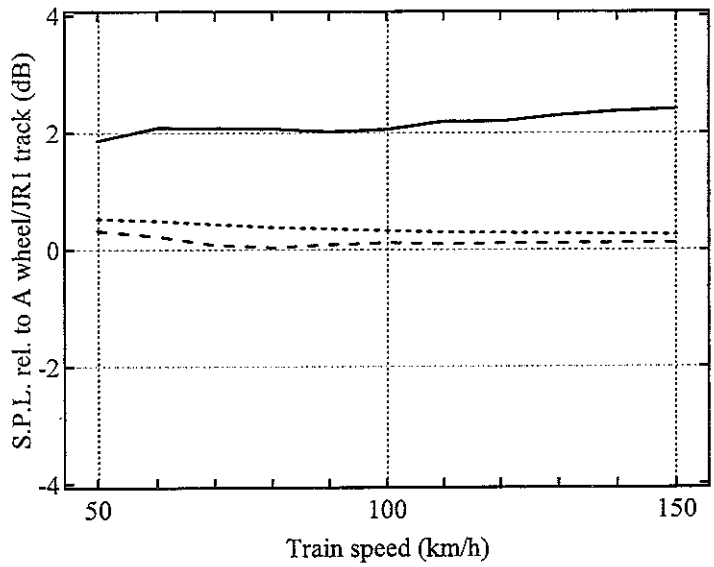

(a) AW wheel / JR1 track

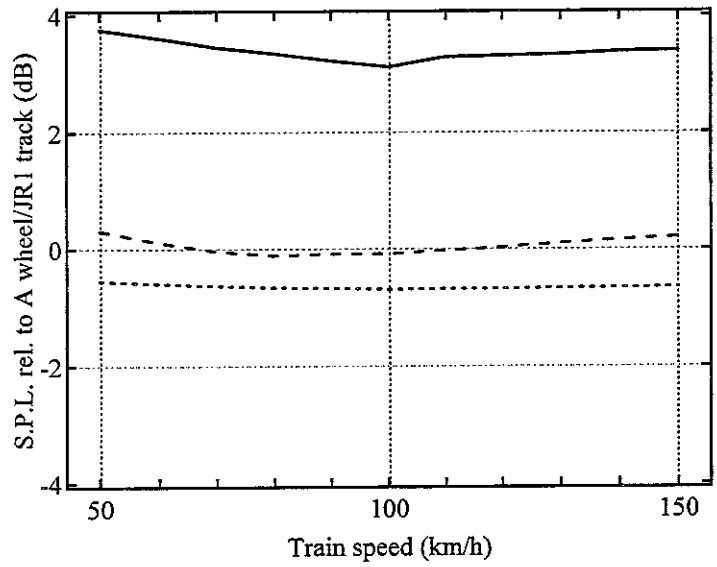

(b) CW wheel / JR1 track

Figure D2.3 Predicted noise components from rail, wheel and sleeper relative to A-wheel/JR1-track (tinf, bi-bloc sleeper, ·····:rail, ——— :wheel, - - - -:sleeper)

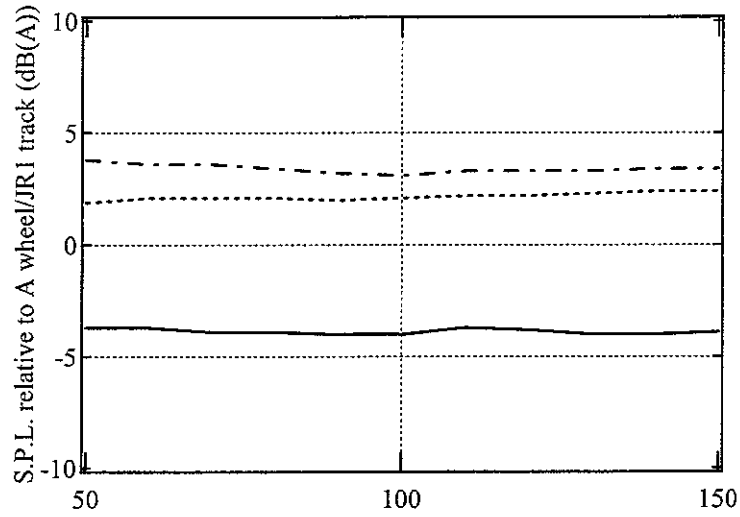

(a) Disk braked wheel/ JR1 track

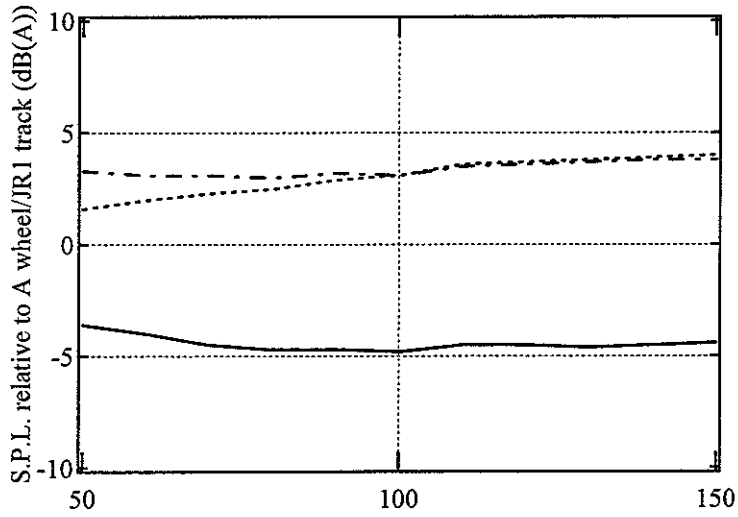

(b) Tread braked wheel/ JR1 track

Figure D2.4 Predicted wheel noise relative to A-wheel/JR1-track

(tinf, bi-bloc sleeper, ——— :C wheel, ····· :AW wheel, – – – :CW wheel)

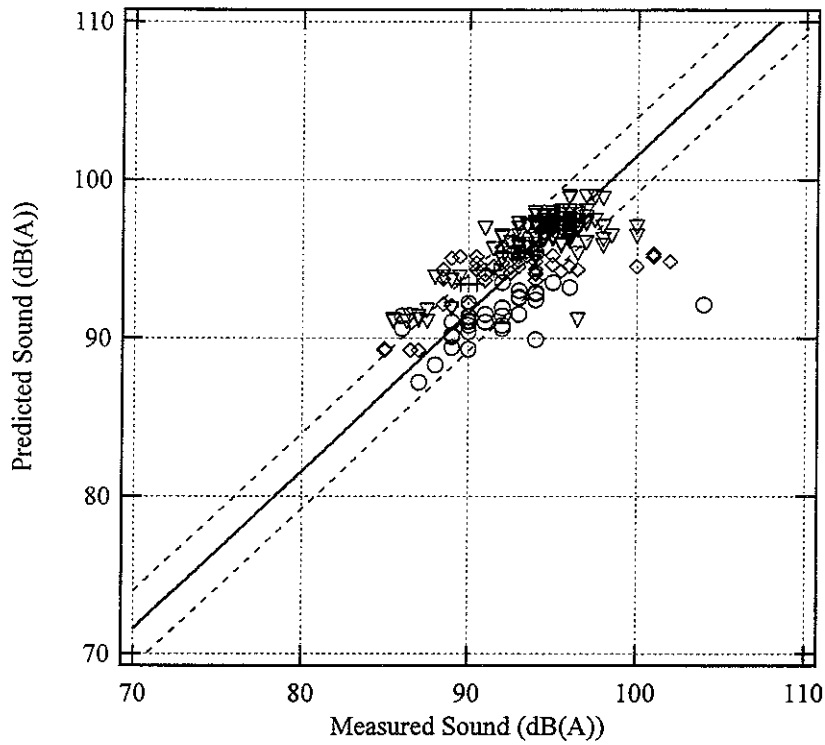

Figure D2.5 Predicted noise plotted against measured noise for all cases (tinf, bi-bloc sleeper)

◇: A-type wheel, ○: C-type wheel,
+: AW-type wheel, ▽: CW-type wheel

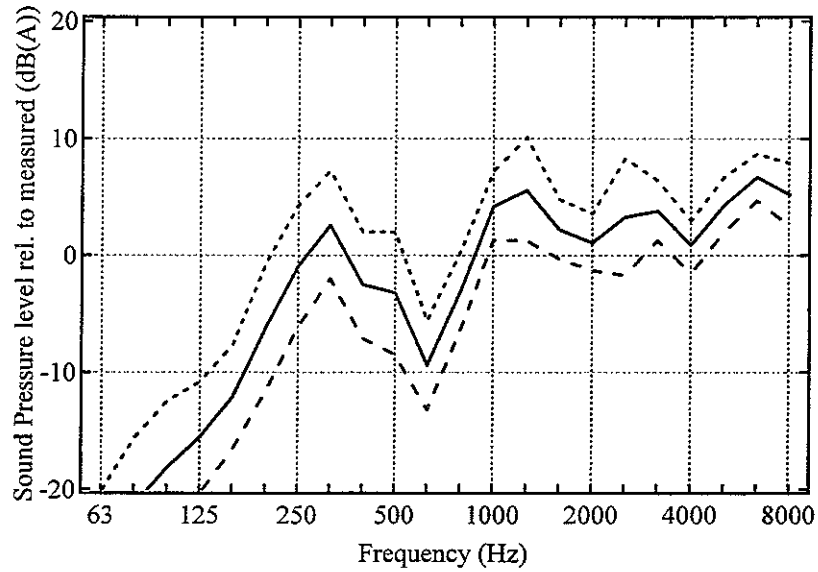

Figure D2.6 Average difference between predicted and measured noise spectra for all cases (tinf, bi-bloc sleeper, ——:mean, ----- :mean+std deviation, - - - :mean-std deviation)

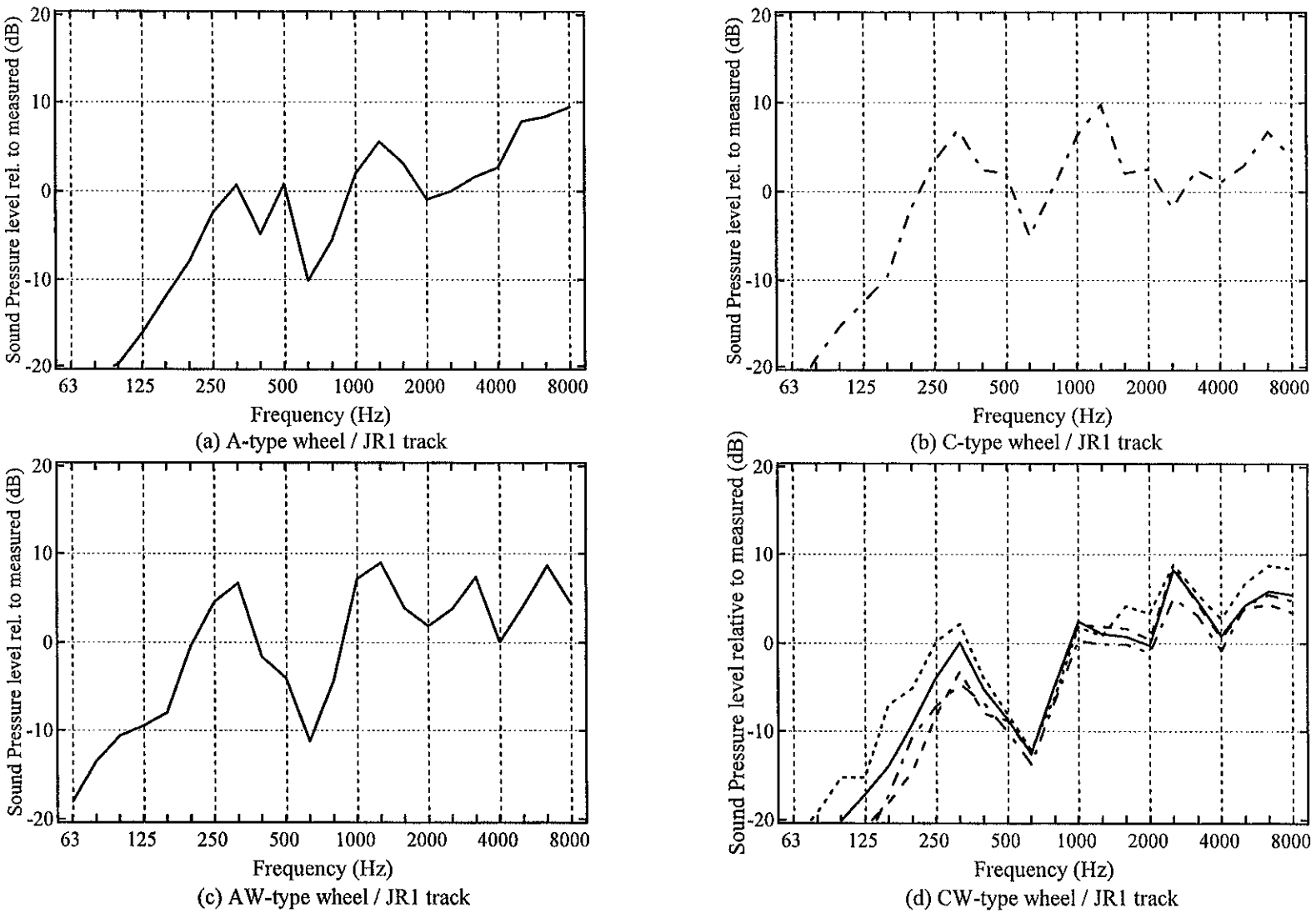

Figure D2.7 Predicted noise minus measured noise for each wheel using rodel model
(JR1 track, bi-bloc sleeper, ·····:70 km/h,– – :100 km/h,——:110 km/h,- - - :120 km/h)

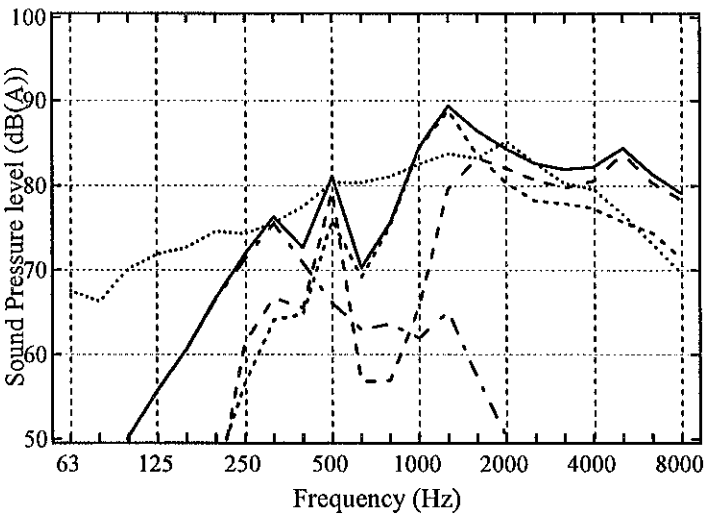

(a) A-type wheel / JR1 track (110km/h)

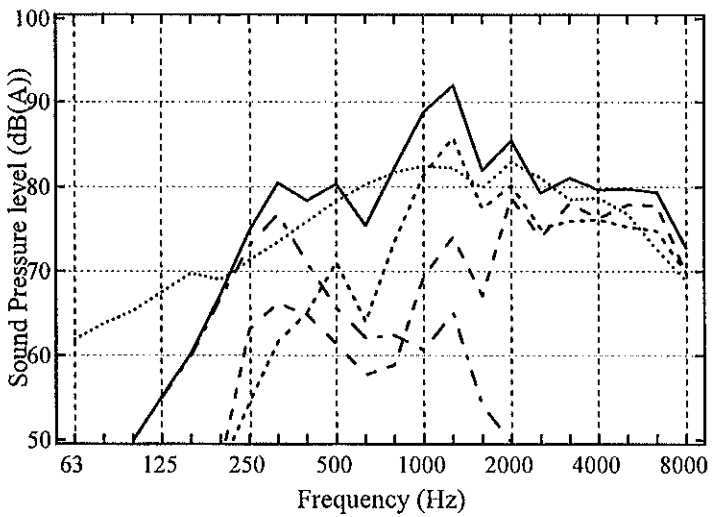

(b) C-type wheel / JR1 track (100 km/h)

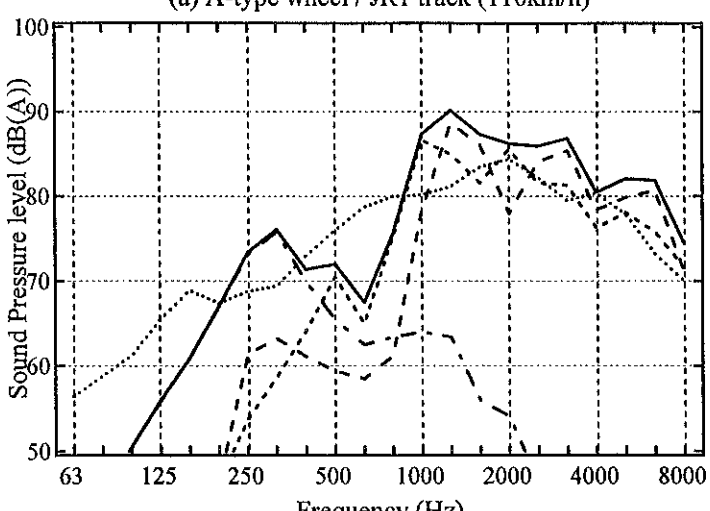

(c) AW-type wheel / JR1 track (110 km/h)

Figure D2.8 Predicted noise and measured noise for each wheel using tinf model

(JR1 track, bi-bloc sleeper, ····· :measured noise, —— :predicted noise,------ :rail, - - :wheel, - - :sleeper)

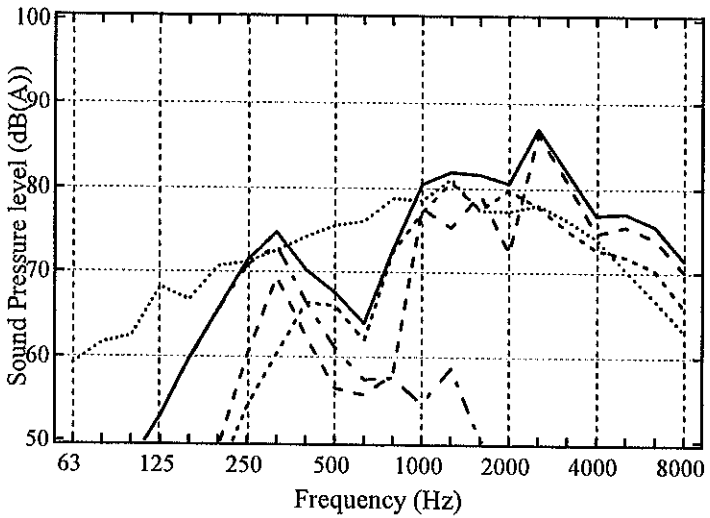

(a) CW-type wheel / JR1 track (70km/h)

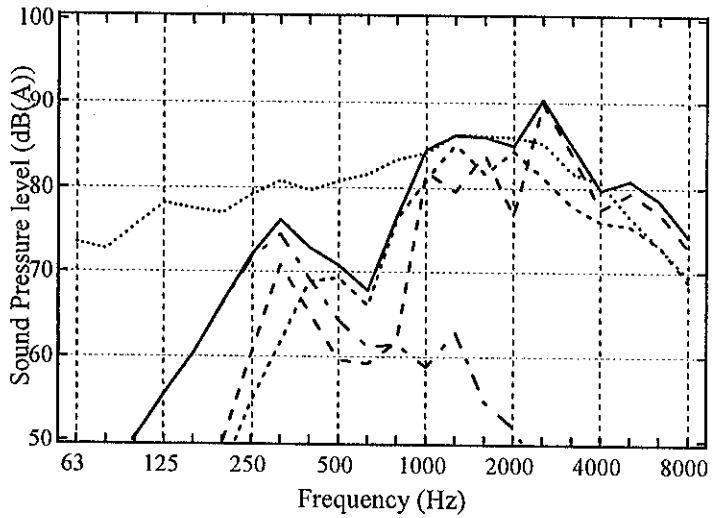

(b) CW-type wheel / JR1 track (100 km/h)

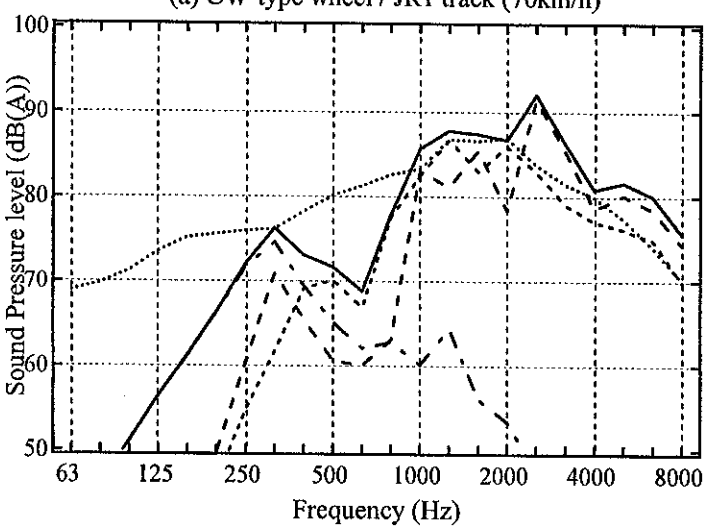

(c) CW-type wheel / JR1 track (110 km/h)

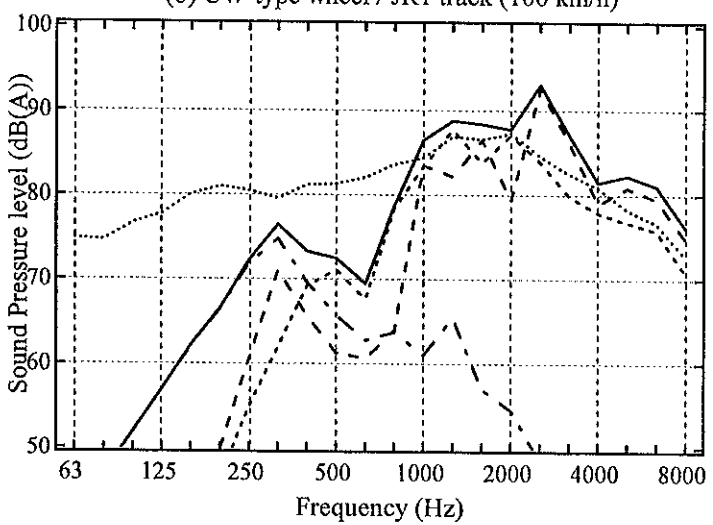

(d) CW-type wheel / JR1 track (120 km/h)

Figure D2.9 Predicted noise and measured noise for each wheel using tinf model

(JR1 track, bi-bloc sleeper, ····· :measured noise, —— :predicted noise,----- :rail, - - :wheel, - - - :sleeper)

D3 Continuous track model with mono-bloc sleeper

This section presents calculations of noise carried out using:

- the continuous track model (rodel model)
- modal sleeper model
- frequency dependent ballast stiffness model.
- calculated track decay rates

In this section, two models (the modal sleeper model and the frequency-dependent ballast stiffness model) are brought into the rodel model. These models should improve the predictions at low frequencies, where the sleeper vibration is dominant.

Figure D3.1 shows the total noise predicted minus measured noise in dB(A). Almost all of the results fall in the range +/- 2 dB(A). A comparison of Figures D1.1 and D3.1 shows that the results of the rodel model with mono-bloc sleeper are closer to zero than those of the rodel model with bi-bloc sleeper. The rodel model with mono-bloc sleeper thus gives better predictions. The introduction of these two models has clearly improved the predictions.

Figure D3.2 shows the relative contributions of wheel, rail and sleeper to the predicted dB(A) level.

Figure D3.3 shows the relative contributions of wheel, rail and sleeper of each wheel/track combination to the results of the A-type wheel/JR1 track combination. The global trend of each noise component is similar to that shown in figure D1.3.

Figure D3.4 shows the relative noise of each wheel to the A-type wheel in dB(A). The results show similar trends to those shown in Figures D1.4.

Figure D3.5 shows predicted noise plotted against measured noise in terms of overall A-weighted levels. The individual points represent one of the 4 wheel/track combinations. The solid line corresponds to the mean difference between predictions and measurements (which is +0.3 dB(A)). The dashed lines show a range of +/- one standard deviation (which is 2.4 dB(A)). The mean difference can be seen to be close to zero. Therefore, it is confirmed that the improved model gives better overall predictions fitting closely to the measured results.

Figure D3.6 shows the spectral differences as the mean and a range of +/- one standard deviation for all cases. Comparing with Figure D1.6, the predicted results can be seen to be

closer to zero, and the shape of the results is improved above 250 Hz. The average difference is slightly reduced from -0.9 to -0.8 dB in the whole frequency range of 250-8000 Hz, while the average standard deviation of the results is not changed (3.5 dB). Below 250 Hz, the result is still poor, since the measured results were contaminated by wind noise.

Figure D3.7 shows the total predicted sound pressure level minus measured level for each wheel/track combination and each train speed.

Figures D3.8-D3.9 show the separate components of noise from rail, wheel and sleeper. These results show similar trends to those shown in Figures D1.8-1.9.

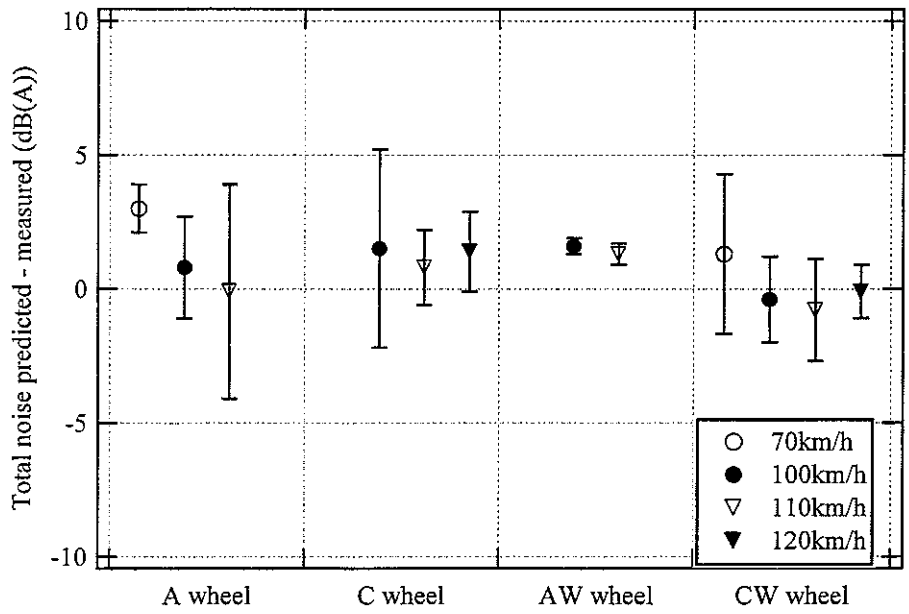

Figure D3.1 Total Predicted noise minus measured noise in dB(A) using rodel model (mono-bloc sleeper) Results are shown for each speed (70, 100, 110 and 120 km/h).

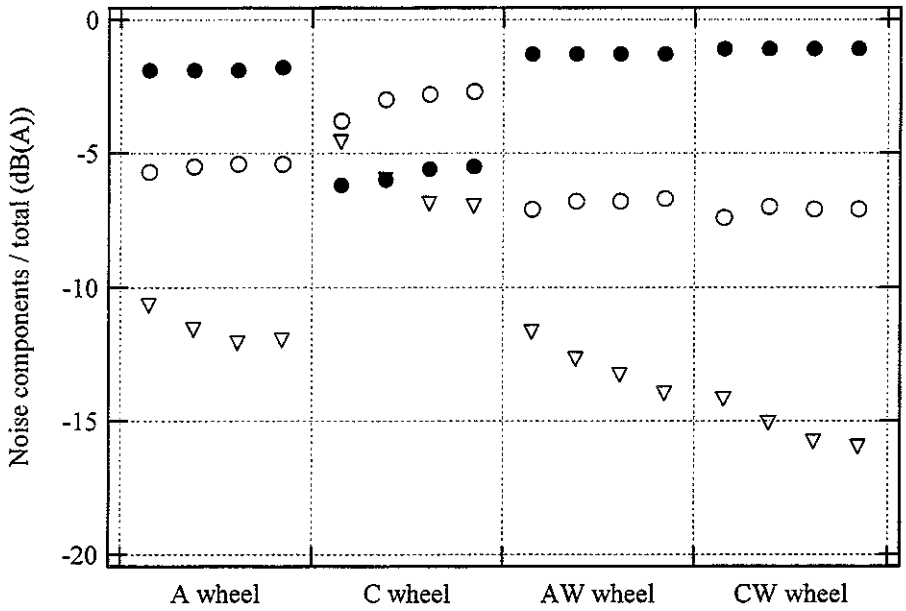

Figure D3.2 Predicted noise components from rail (○), wheel (●) and sleeper (▽) using rodel model (bi-bloc sleeper) minus predicted total noise in dB(A).
Results are shown for each speed (70, 100, 110 and 120 km/h).

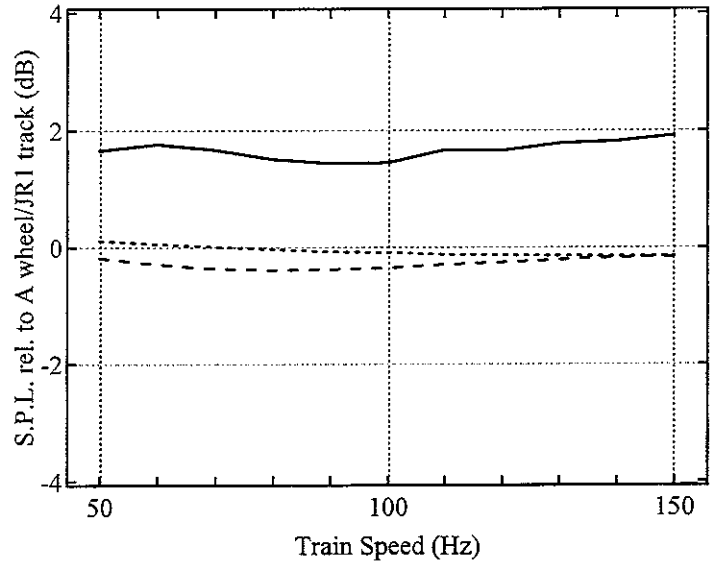

(a) AW wheel / JR1 track

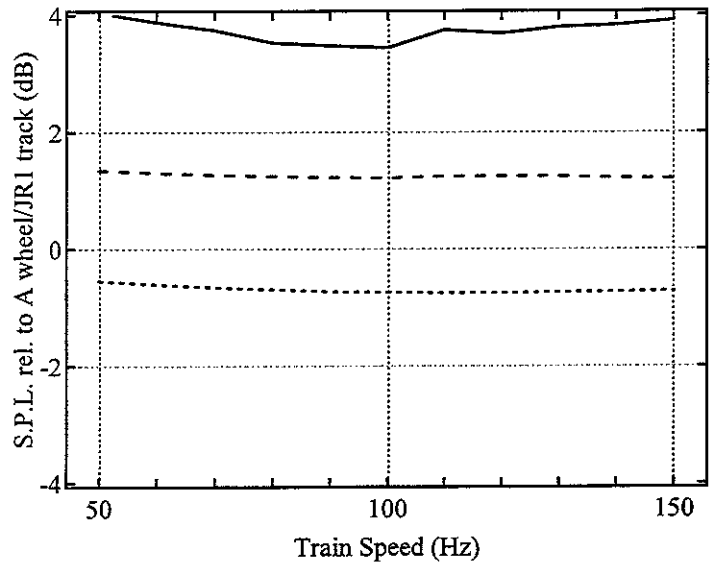

(b) CW wheel / JR1 track

Figure D3.3 Predicted noise components from rail, wheel and sleeper relative to A-wheel/JR1-track (rodel, mono-bloc sleeper, ····· :rail, —— :wheel, - - - - :sleeper)

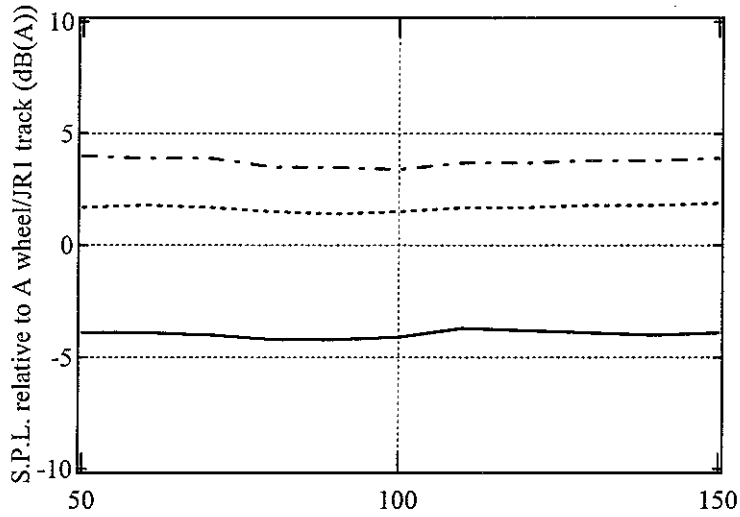

(a) Disk braked wheel/ JR1 track

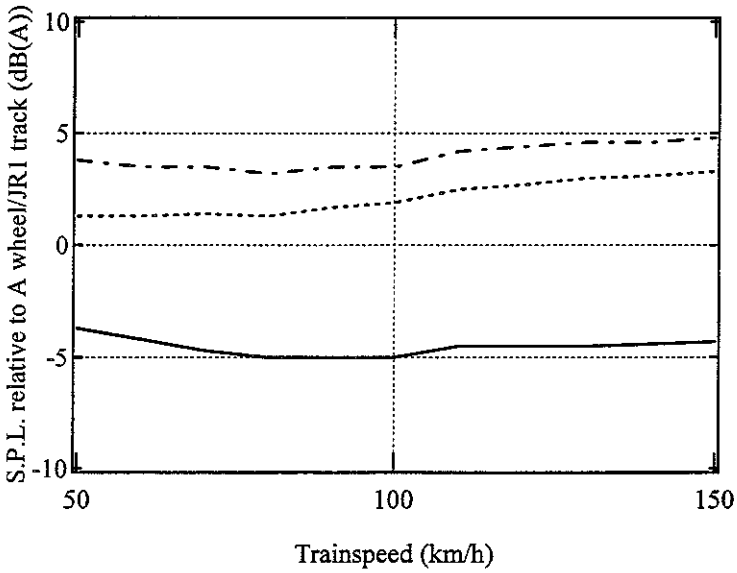

(b) Tread braked wheel/ JR1 track

Figure D3.4 Predicted wheel noise relative to A-wheel/JR1-track

(rodel, mono-bloc sleeper, ——— :C wheel, ------- :AW wheel, – – – :CW wheel)

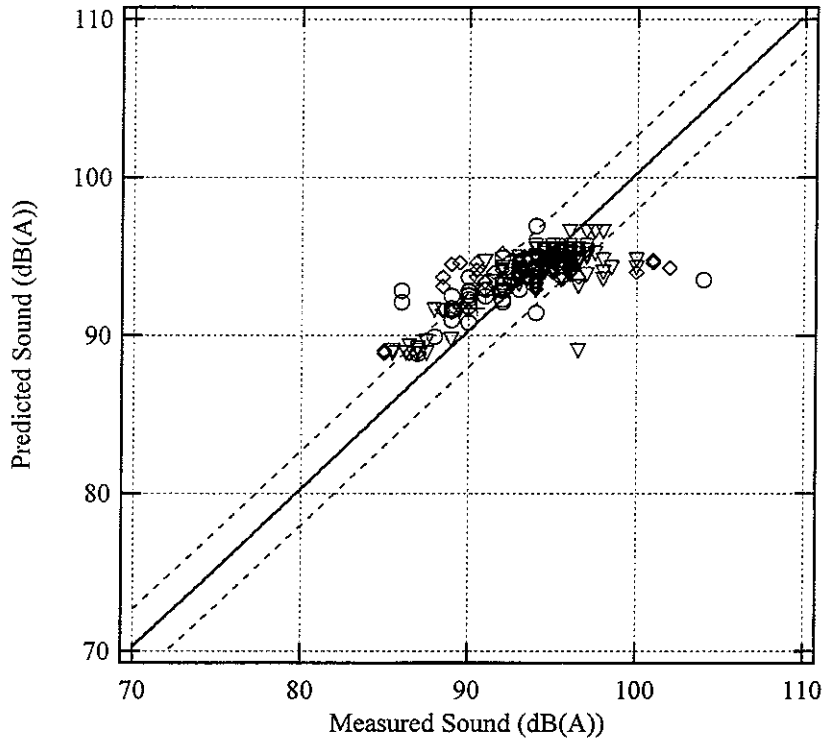

Figure D3.5 Predicted noise plotted against measured noise for all cases (rodel, mono-bloc sleeper)

◇: A-type wheel, ○: C-type wheel,

+: AW-type wheel, ▽: CW-type wheel

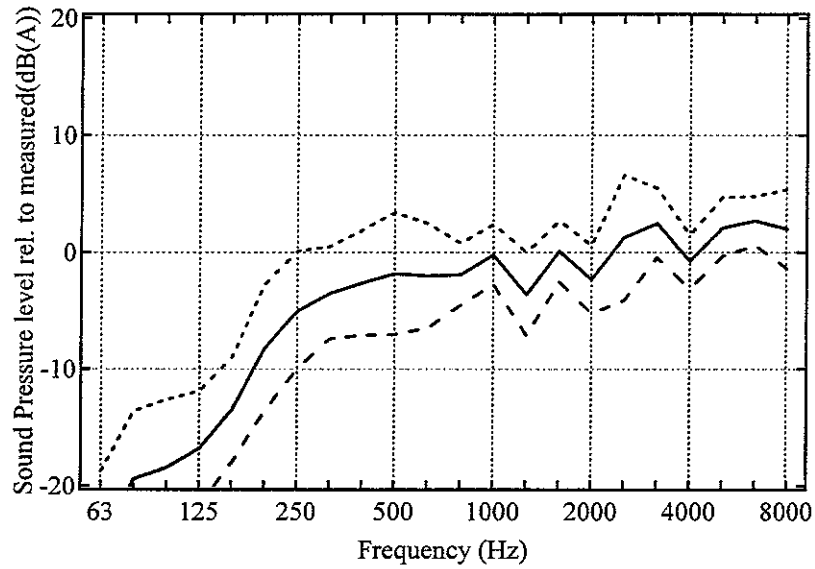

Figure D3.6 Average difference between predicted and measured noise spectra for all cases (rodel, mono-bloc sleeper, ——:mean, ----- :mean+std deviation,- - - :mean-std deviation)

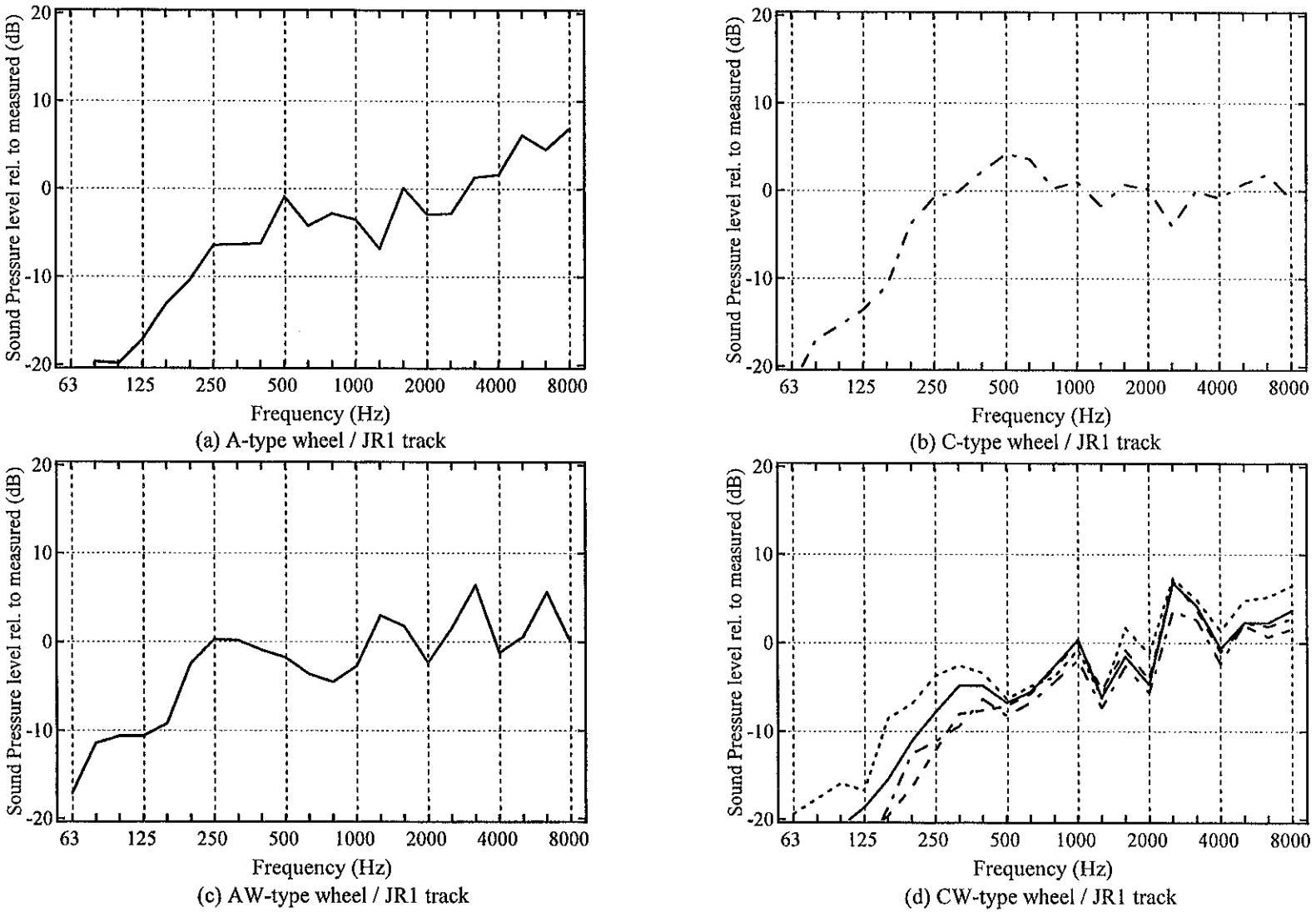

(a) A-type wheel / JR1 track

(b) C-type wheel / JR1 track

(c) AW-type wheel / JR1 track

(d) CW-type wheel / JR1 track

Figure D3.7 Predicted noise minus measured noise for each wheel using rodel model
(JR1 track, mono-bloc sleeper, ····· :70 km/h, – – :100 km/h, ——— :110 km/h, – – – :120 km/h)

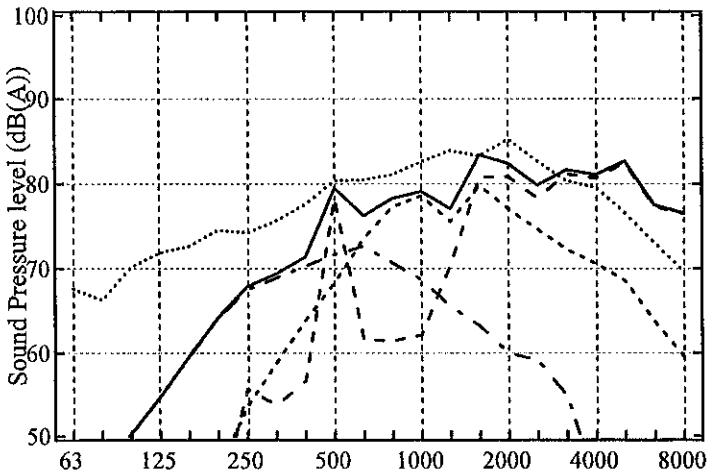

(a) A-type wheel / JR1 track (110km/h)

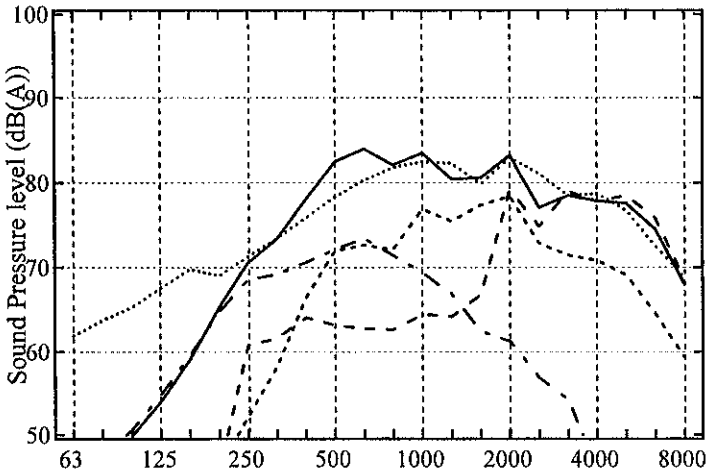

(b) C-type wheel / JR1 track (100 km/h)

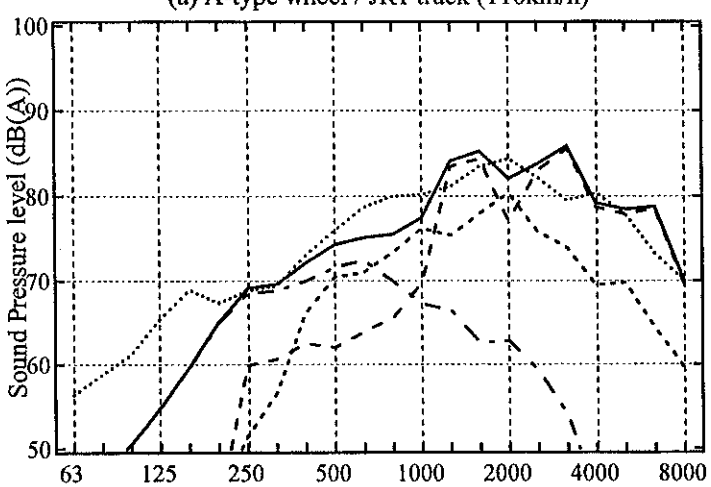

(c) AW-type wheel / JR1 track (110 km/h)

Figure D3.8 Predicted noise and measured noise for each wheel using rodel model

(JR1 track, mono-bloc sleeper, ····· :measured noise, —— :predicted noise, ----- :rail, - - :wheel, - - - :sleeper)

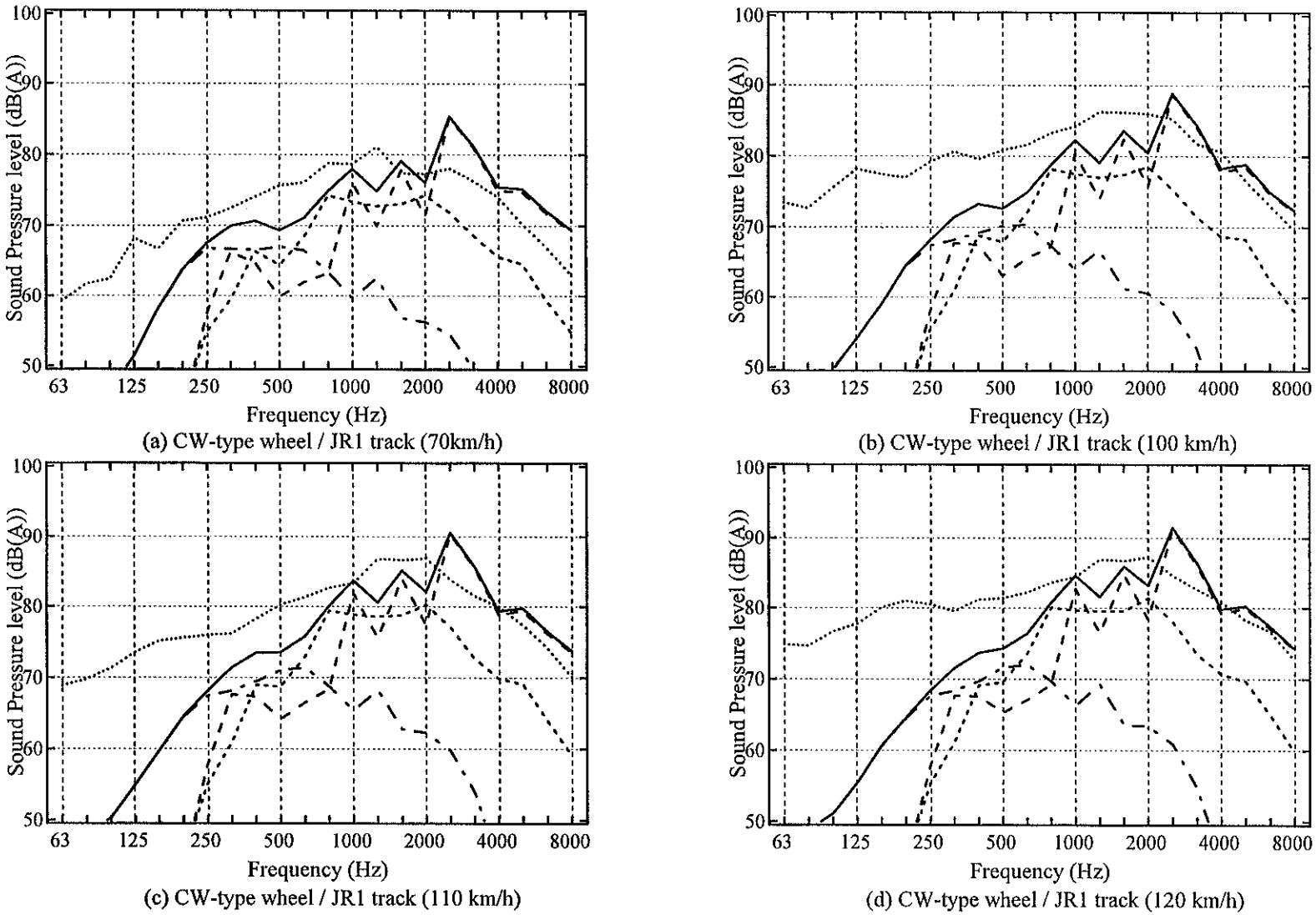

(a) CW-type wheel / JR1 track (70km/h)

(b) CW-type wheel / JR1 track (100 km/h)

(c) CW-type wheel / JR1 track (110 km/h)

(d) CW-type wheel / JR1 track (120 km/h)

Figure D3.9 Predicted noise and measured noise for each wheel using rodel model

(JR1 track, mono-bloc sleeper, ····· :measured noise, —— :predicted noise, ----- :rail, - - :wheel, - - :sleeper)

D4 Periodic track model with modal sleeper

This section presents calculations of noise carried out using:

- the periodic track model (tinf model)
- modal sleeper model
- frequency dependent ballast stiffness model.
- calculated track decay rates

In this section, the two models (the modal sleeper model and the frequency-dependent ballast stiffness model) are also introduced to the tinf model.

Figure D4.1 shows the total noise predicted minus measured noise in dB(A). It is clear that the predictions are too high, and show poor agreement with the measured results. Comparing Figure D4.1 with Figure D3.1, the mean of the predictions is higher than that of the improved rodel model. This is probably due to the fact that the predictions of the tinf model are carried out at mid-span only and the fact that rail damping cannot be entered into tinf. Comparing Figure D4.1 with Figure D2.1, it is found that the influence of the introduction of the two models depends on wheel/track combination. The results of AW and CW wheels are improved, but the results of A and C wheels become worse.

Figure D4.2 shows the relative contributions of wheel, rail and sleeper to the predicted dB(A) level.

Figure D4.3 shows the relative contributions of wheel, rail and sleeper of each wheel/track combination to the results of the A-type wheel/JR1 track combination. This results show similar trends to the results shown in Figure D2.3.

Figure D4.4 shows the relative noise of each wheel to the A-type wheel in dB(A).

Figure D4.5 shows predicted noise plotted against measured noise in terms of overall A-weighted levels. The individual points represent one of the 4 wheel/track combinations. The solid line corresponds to the mean difference between prediction and measurements (which is +1.7 dB(A)). The mean difference is similar to the results predicted with the tinf model with bi-bloc sleeper (which is +1.6 dB(A)). The dashed lines show a range of +/- one standard deviation (which is 2.4 dB(A)).

Figure D4.6 shows the spectral differences as the mean and a range of +/- one standard deviation for all cases. Comparing with Figure D3.6, the shape of the results is improved,

and the peak at 315 Hz has been eliminated. However, the results are under-predicted below 1000 Hz, and over-predicted at high frequencies.

Figure D4.7 shows the total predicted sound pressure level minus measured level for each wheel/track combination and each train speed.

Figures D4.8-4.9 show the separate components of noise from rail, wheel and sleeper.

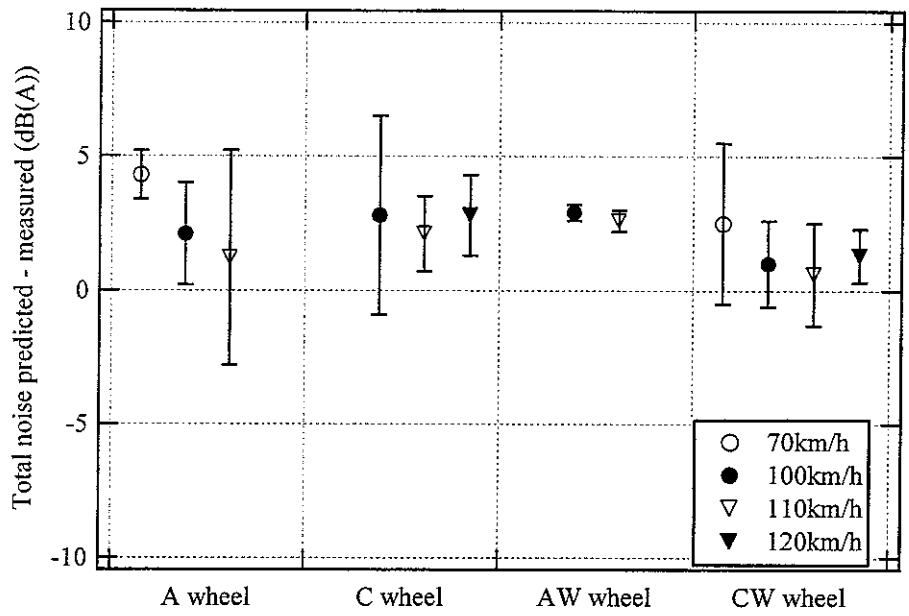

Figure D4.1 Total Predicted noise minus measured noise in dB(A) using tinf model (mono-bloc sleeper) Results are shown for each speed (70, 100, 110 and 120 km/h).

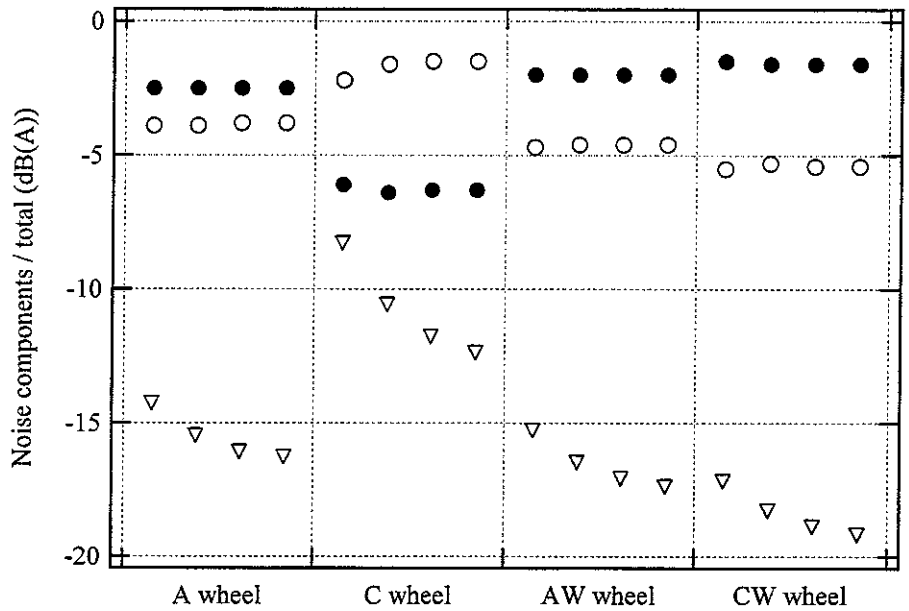

Figure D4.2 Predicted noise components from rail (○), wheel (●) and sleeper (▽) using tinf model (mono-bloc sleeper) minus predicted total noise in dB(A). Results are shown for each speed (70, 100, 110 and 120 km/h).

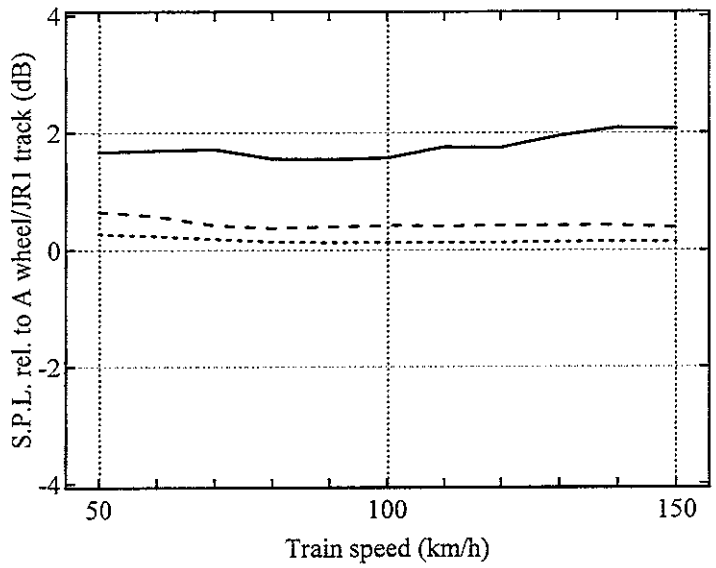

(a) AW wheel / JR1 track

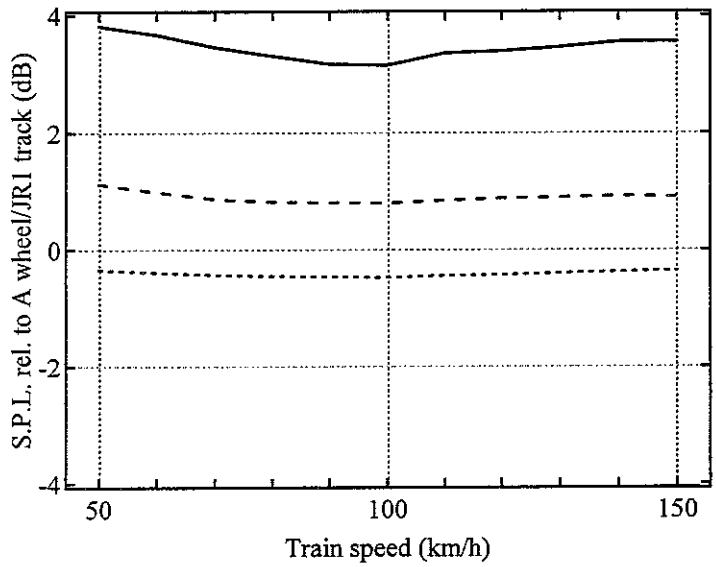

(b) CW wheel / JR1 track

Figure D4.3 Predicted noise components from rail, wheel and sleeper relative to A-wheel/JR1-track (tinf, mono-bloc sleeper, -------:rail, —— :wheel, - - - - :sleeper)

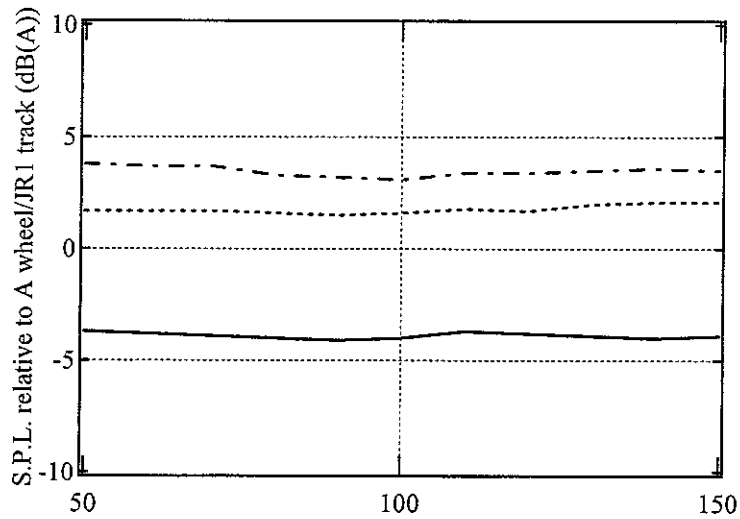

(a) Disk braked wheel/ JR1 track

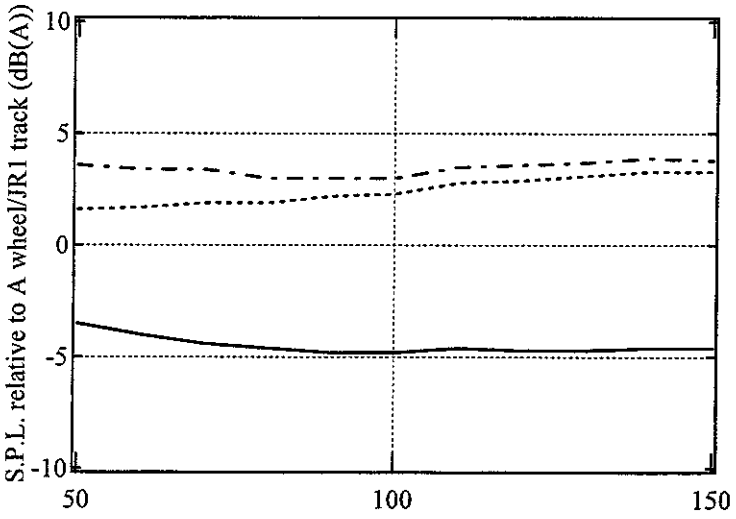

(b) Tread braked wheel/ JR1 track

Figure D2.4 Predicted wheel noise relative to A-wheel/JR1-track

(tinf, mono-bloc sleeper, ——— :C wheel, ------- :AW wheel, – - – :CW wheel)

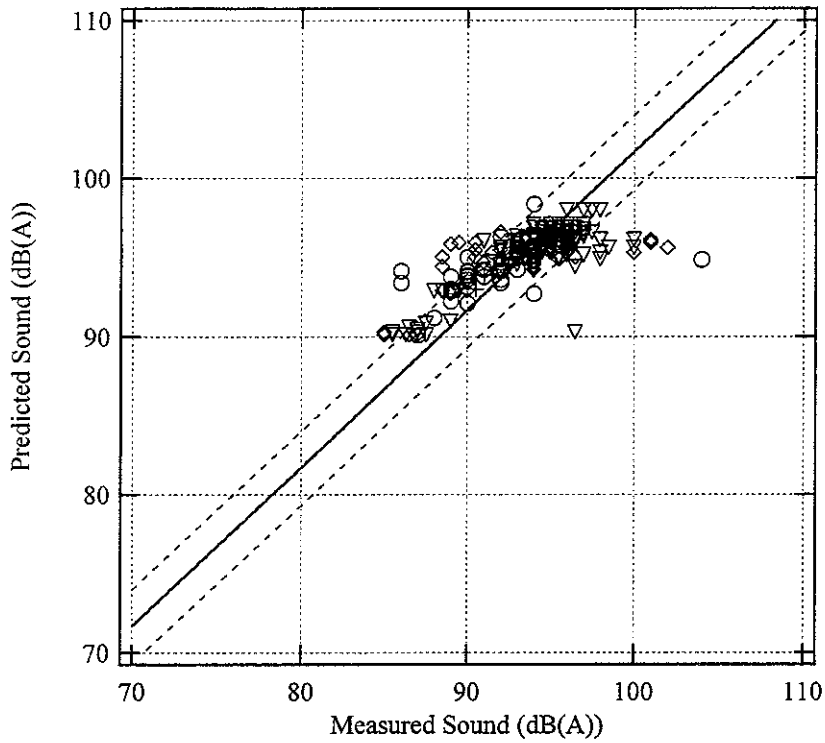

Figure D4.5 Predicted noise plotted against measured noise for all cases (tinf, mono-bloc sleeper)

◇: A-type wheel, ○: C-type wheel,

+: AW-type wheel, ▽: CW-type wheel

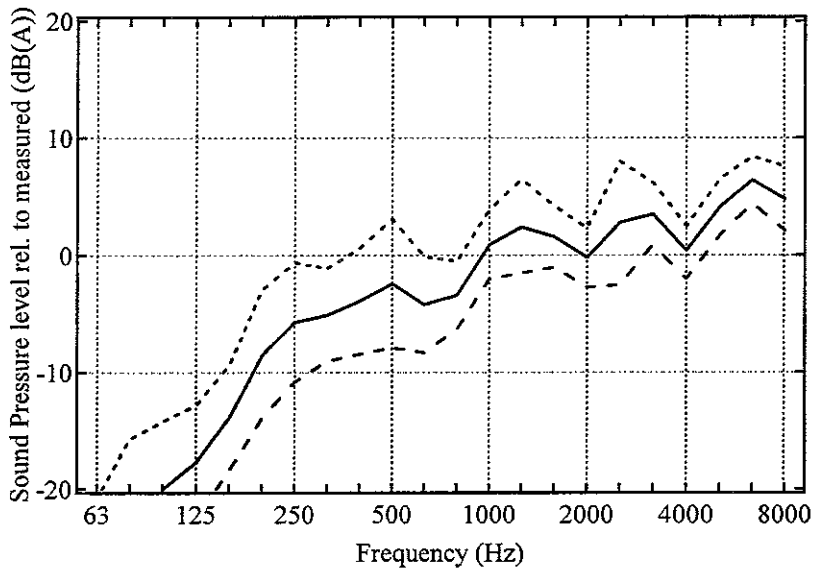

Figure D4.6 Average difference between predicted and measured noise spectra for all cases (tinf, mono-bloc sleeper, ——:mean, ----- :mean+std deviation,- - - :mean-std deviation)

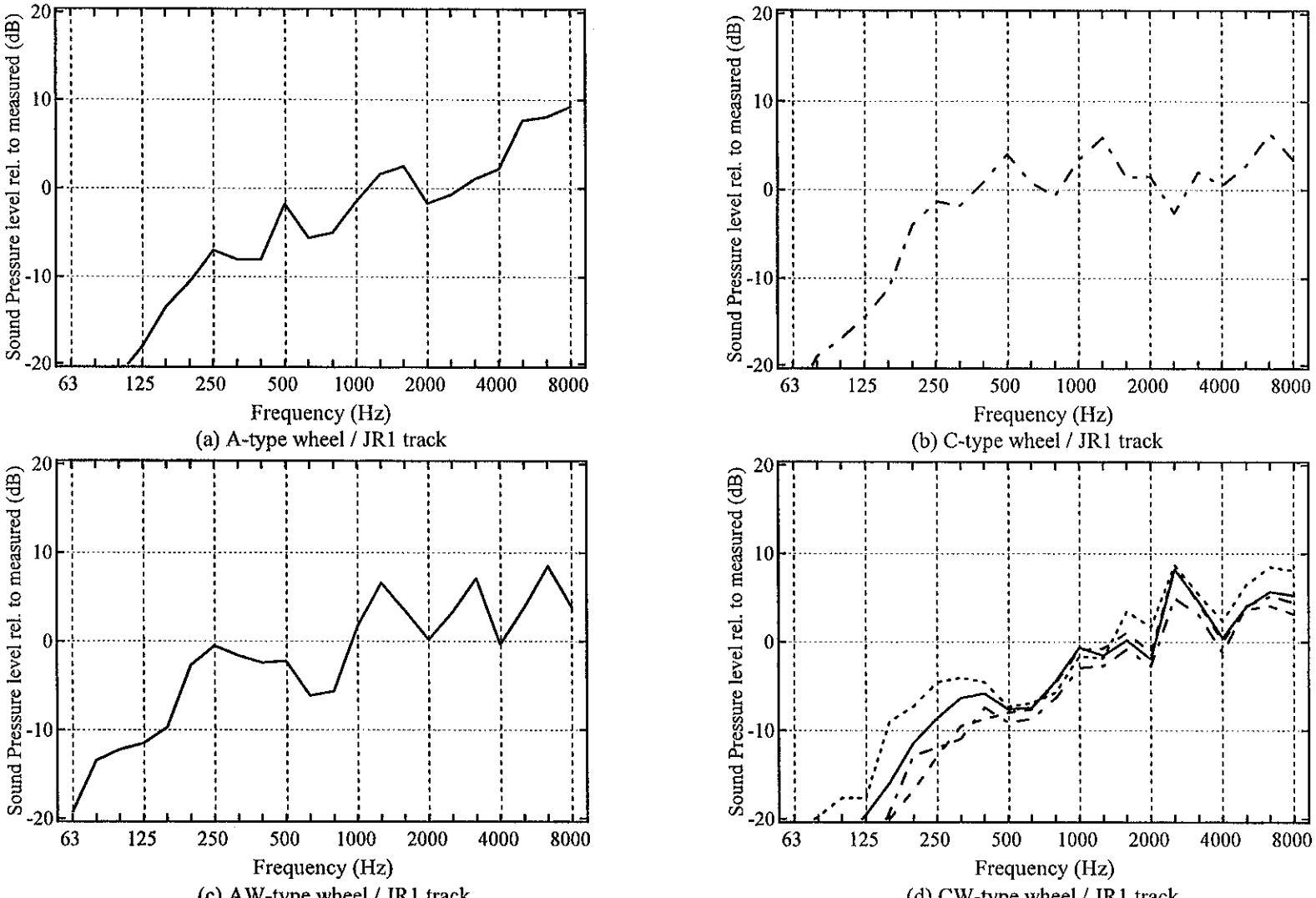

(a) A-type wheel / JR1 track

(b) C-type wheel / JR1 track

(c) AW-type wheel / JR1 track

(d) CW-type wheel / JR1 track

Figure D4.7 Predicted noise minus measured noise for each wheel using rodel model
(JR1 track, mono-bloc sleeper,------ :70 km/h,– – – :100 km/h, ——:110 km/h, - - - :120 km/h)

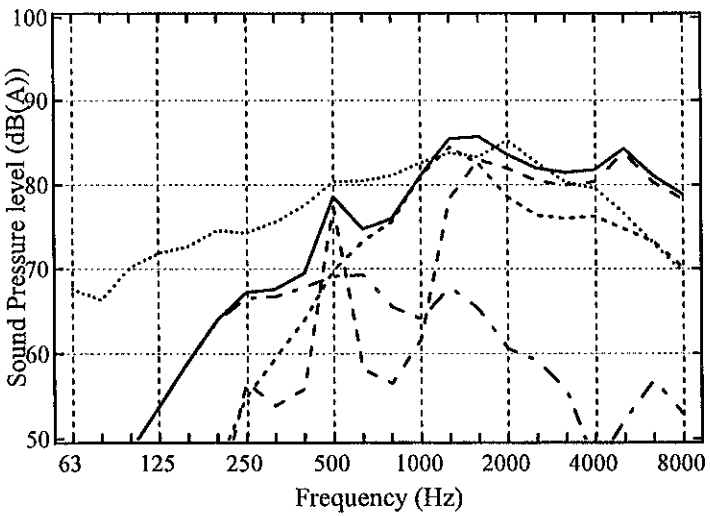

(a) A-type wheel / JR1 track (110km/h)

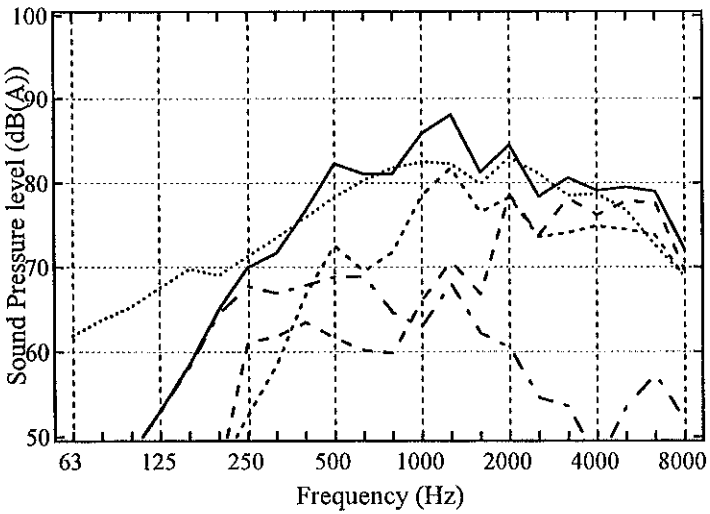

(b) C-type wheel / JR1 track (100 km/h)

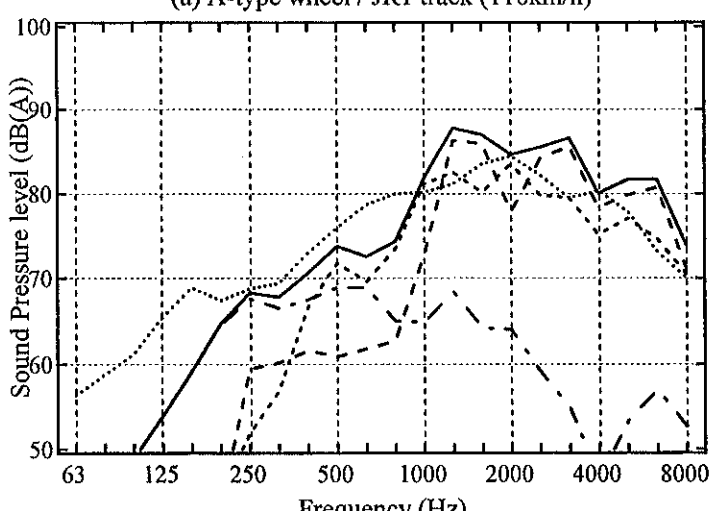

(c) AW-type wheel / JR1 track (110 km/h)

Figure D4.8 Predicted noise and measured noise for each wheel using tinf model

(JR1 track, mono-bloc sleeper, ····· :measured noise, —— :predicted noise, ----- :rail, – – :wheel, – – – :sleeper)

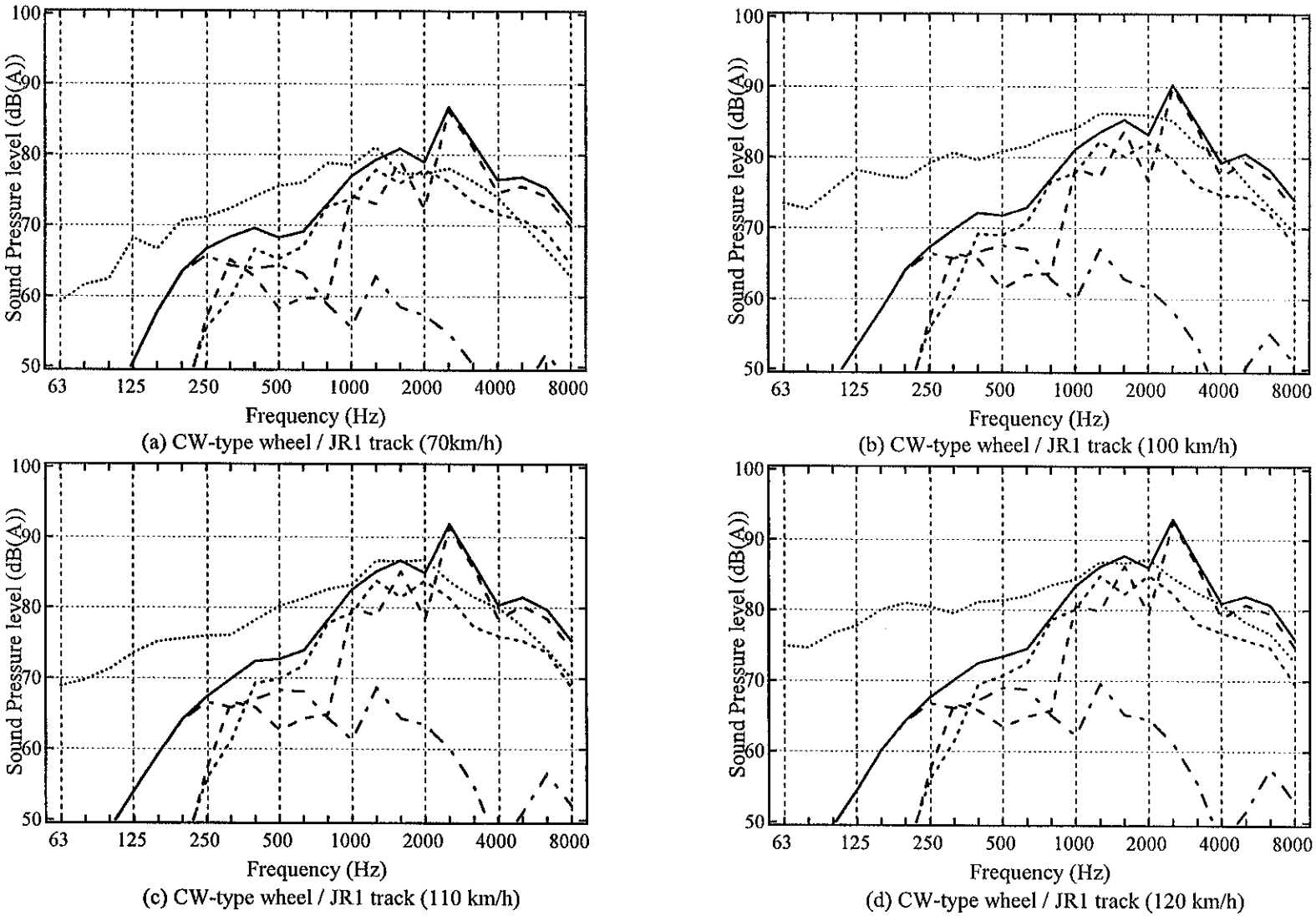

(a) CW-type wheel / JR1 track (70km/h)

(b) CW-type wheel / JR1 track (100 km/h)

(c) CW-type wheel / JR1 track (110 km/h)

(d) CW-type wheel / JR1 track (120 km/h)

Figure D4.9 Predicted noise and measured noise for each wheel using tinf model

(JR1 track, mono-bloc sleeper, ····· :measured noise, —— :predicted noise, ----- :rail, - - :wheel, - - :sleeper)

E INTERMEDIATE COMPARISONS

E1 Rail vibration predicted with rodel and tinf models with bi-bloc sleeper

This section presents calculations of rail vibration carried out using:

- the continuous track model (rodel model) and the periodic track model (tinf model)
- bi-bloc sleeper
- calculated track decay rates

Figure E1.1 shows the vertical rail vibration velocity level predicted with each model minus measured level for each combination in dB(A). The rodel model gives better predictions closer to 0. However, it is clear that most of the results predicted with both models are greater than 0 dB. The predictions of the tinf model should be close to the measured results, since the predictions are carried out at the same position where the measurements are made. However, the results of the tinf model show poor agreement with the measured results. This is related to the fact that rail loss factor is neglected in the tinf model.

Figures E1.2 and E1.4 show predicted rail vibration velocity level plotted against measured level in the vertical direction in terms of overall A-weighted levels. The individual points represent one of the 6 wheel/track combinations. The solid line corresponds to the mean difference between predictions and measurements (mean + 0.9 dB for the rodel model and 4.8 dB for the tinf model). The dashed lines show a range of +/- one standard deviation (standard deviations of 2.8 dB in each case).

Figures E1.3 and E1.5 show the spectral differences as the mean and a range of +/- one standard deviation for all cases. For the rodel model, the result is closer to 0 with an over-prediction around 250 Hz and an under-prediction around 500 Hz. These features, also seen in the noise, are due to the fact that the sleeper vibration is not modelled adequately, and these features could be eliminated by an introduction of the modal sleeper and frequency dependent ballast stiffness models. For the tinf model, the predicted results can be seen to be over-predicted. The mean is between about +3dB(A) and +13 dB(A), and the results vary significantly below 1000 Hz. This is also mainly due to the inadequacy of the model of the sleeper vibration.

Figures E1.6-E1.9 show the total predicted rail vibration level minus measured level in

vertical direction for each wheel/track combination and each train speed. Most of the results show an over-prediction around 250 Hz and an under-prediction around 500 Hz. In Figures E1.7 and E1.9, the differences tend to be generally independent of train speed.

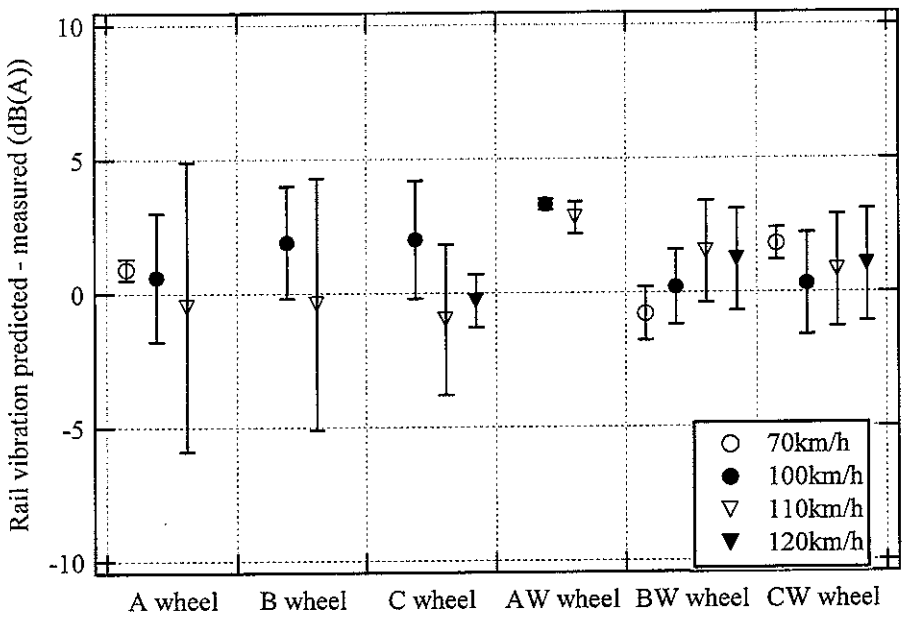

(a) rodel model (vertical direction, bi-bloc sleeper)

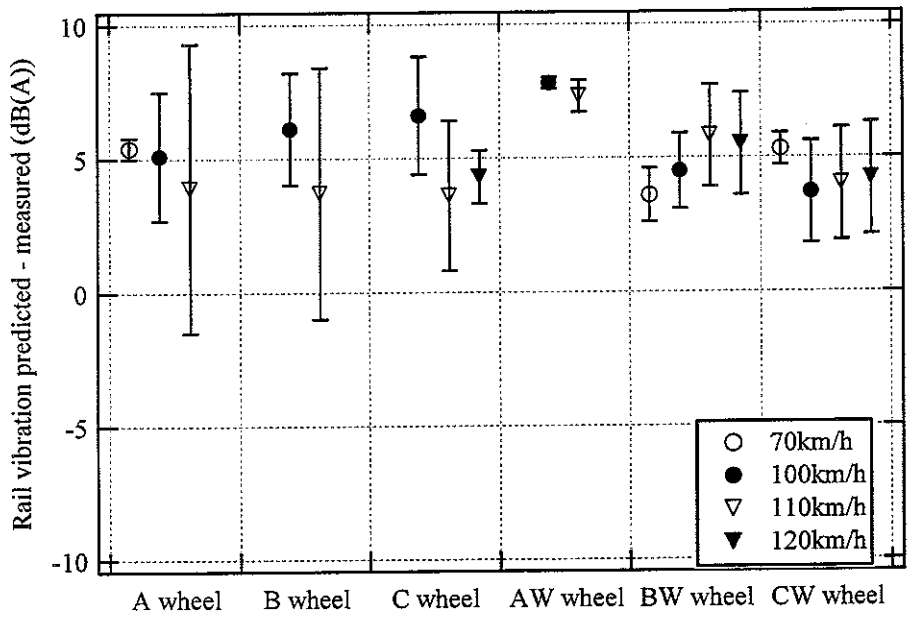

(b) tinf model (vertical direction, bi-bloc sleeper)

Figure E1.1 Total Predicted rail vibration vibration minus measured rail vibration velocity in dB(A) Results are shown for each speed (70, 100, 110 and 120 km/h).

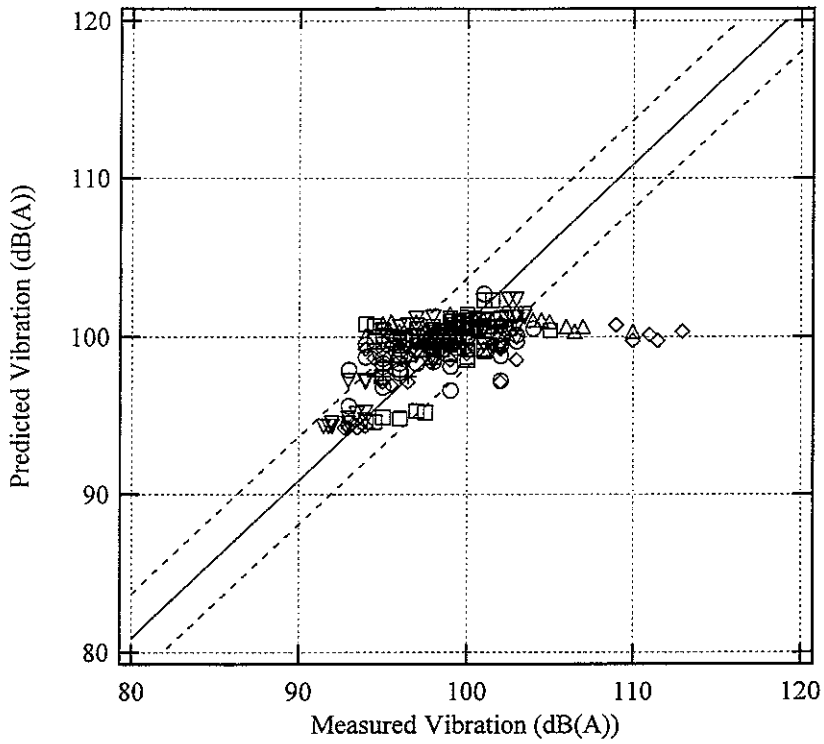

Figure E1.2 Predicted rail vibration velocity plotted against measured rail vibration velocity for all cases (vertical direction, rodel, bi-bloc sleeper)

◇: A-type wheel, △: B-type wheel, ○: C-type wheel,
+: AW-type wheel, □: BW-type wheel ▽: CW-type wheel

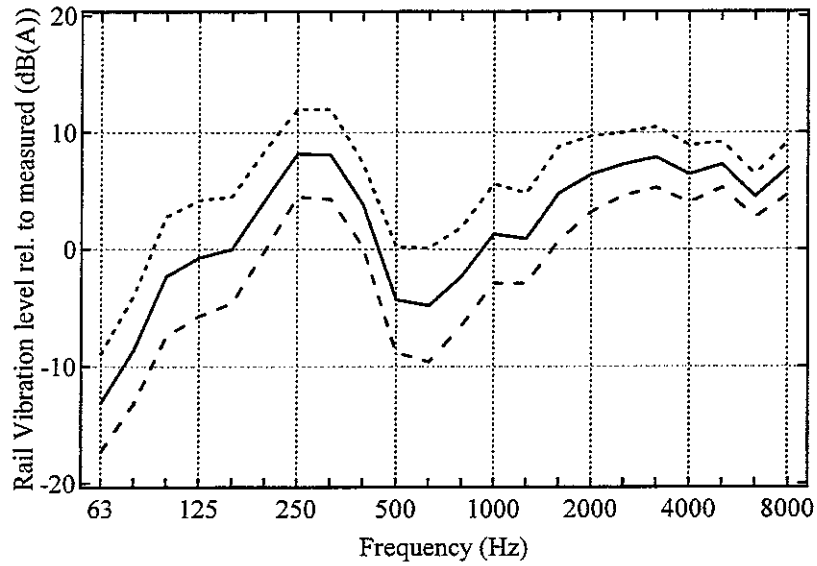

Figure E1.3 Average difference between predicted and measured rail vibration velocity spectra for all cases (rodel, bi-bloc sleeper, —— :mean, ----- :mean+std deviation,- - - :mean-std deviation, vertical direction)

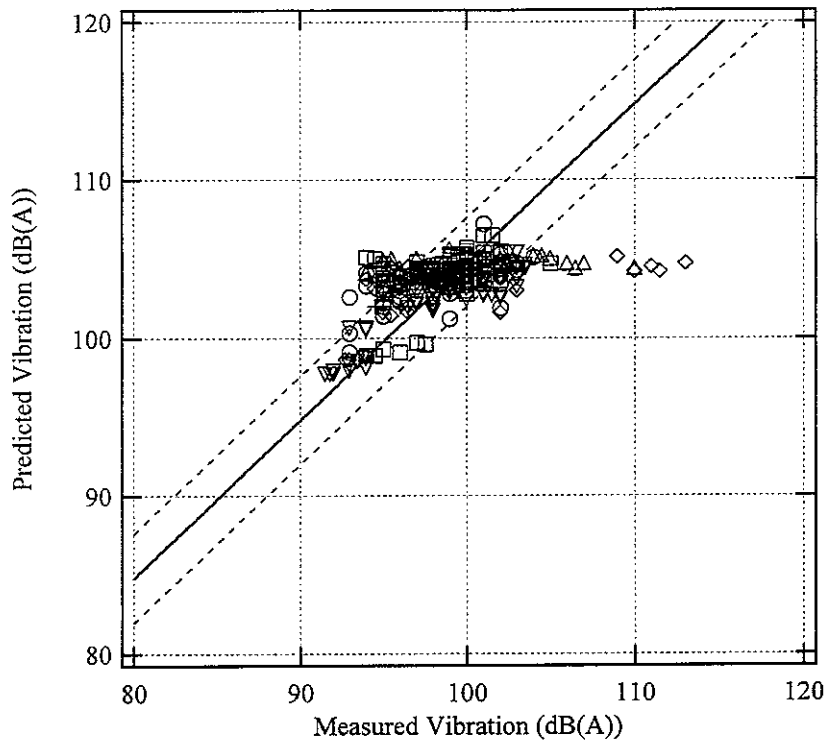

Figure E1.4 Predicted rail vibration velocity plotted against measured rail vibration velocity for all cases (vertical direction, tinf, bi-bloc sleeper)

◇: A-type wheel, △: B-type wheel, ○: C-type wheel,
+: AW-type wheel, □: BW-type wheel ▽: CW-type wheel

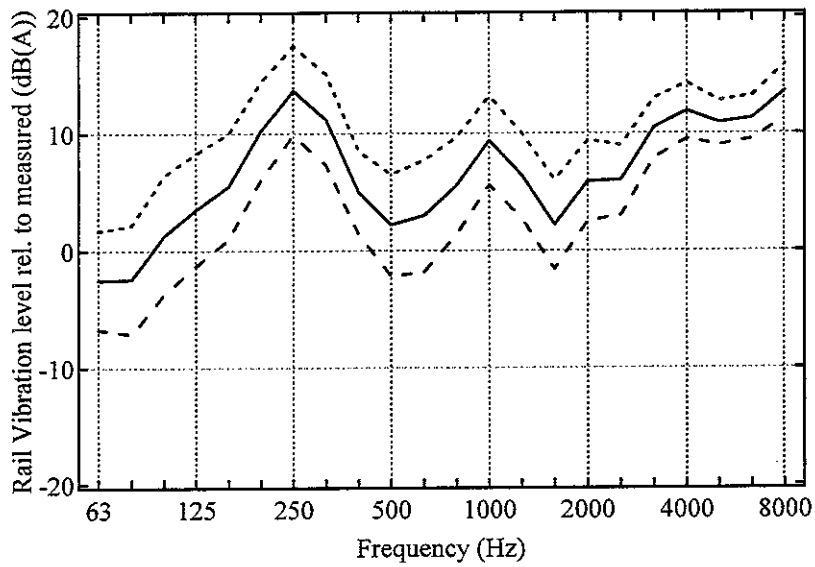

Figure E1.5 Average difference between predicted and measured rail vibration vibration spectra for all cases (tinf, bi-bloc sleeper, ——:mean, -----:mean+std deviation,- - - :mean-std deviation, vertical direction)

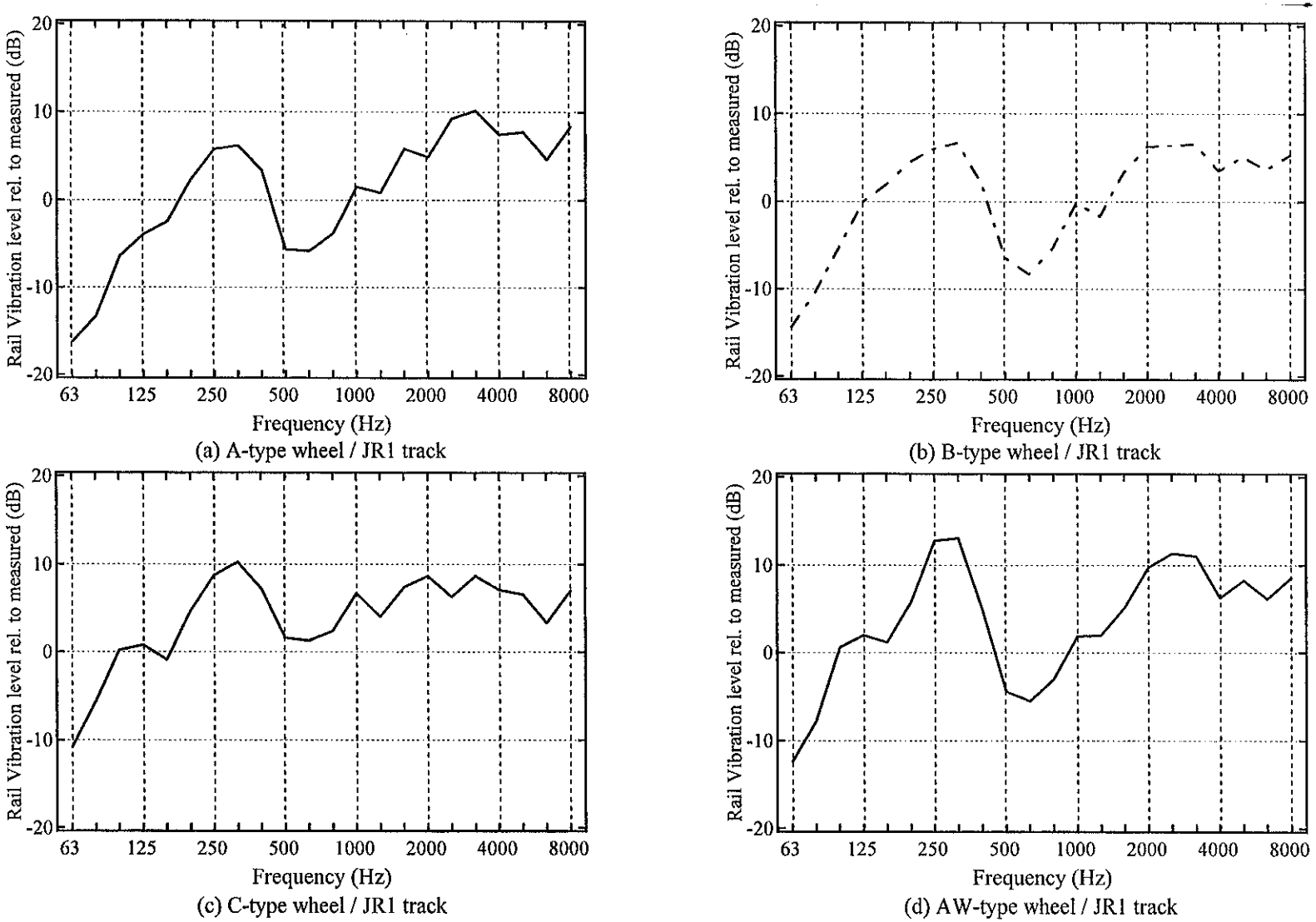

Figure E1.6 Predicted rail vibration velocity minus measured rail vibration velocity for each wheel using rodel model (JR1 track, bi-bloc sleeper, ------:70 km/h,– – –:100 km/h,——:110 km/h,– – –:120 km/h, virtical direction)

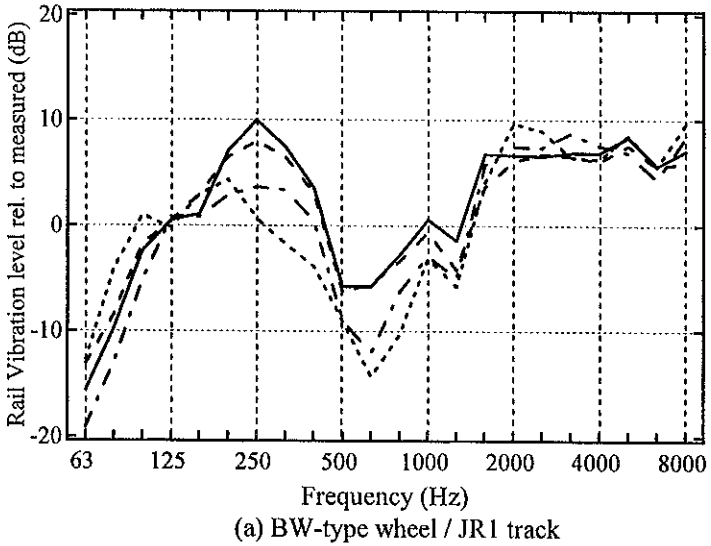

(a) BW-type wheel / JR1 track

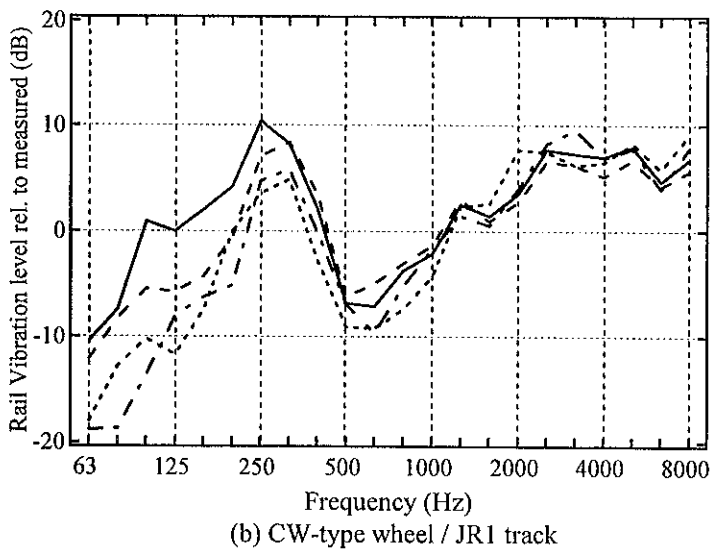

(b) CW-type wheel / JR1 track

Figure E1.7 Predicted rail vibration velocity minus measured rail vibration velocity for each wheel using rodel model (JR1 track, bi-bloc sleeper, ·····:70 km/h,– – :100 km/h,—— :110 km/h,– – – :120 km/h, virtical direction)

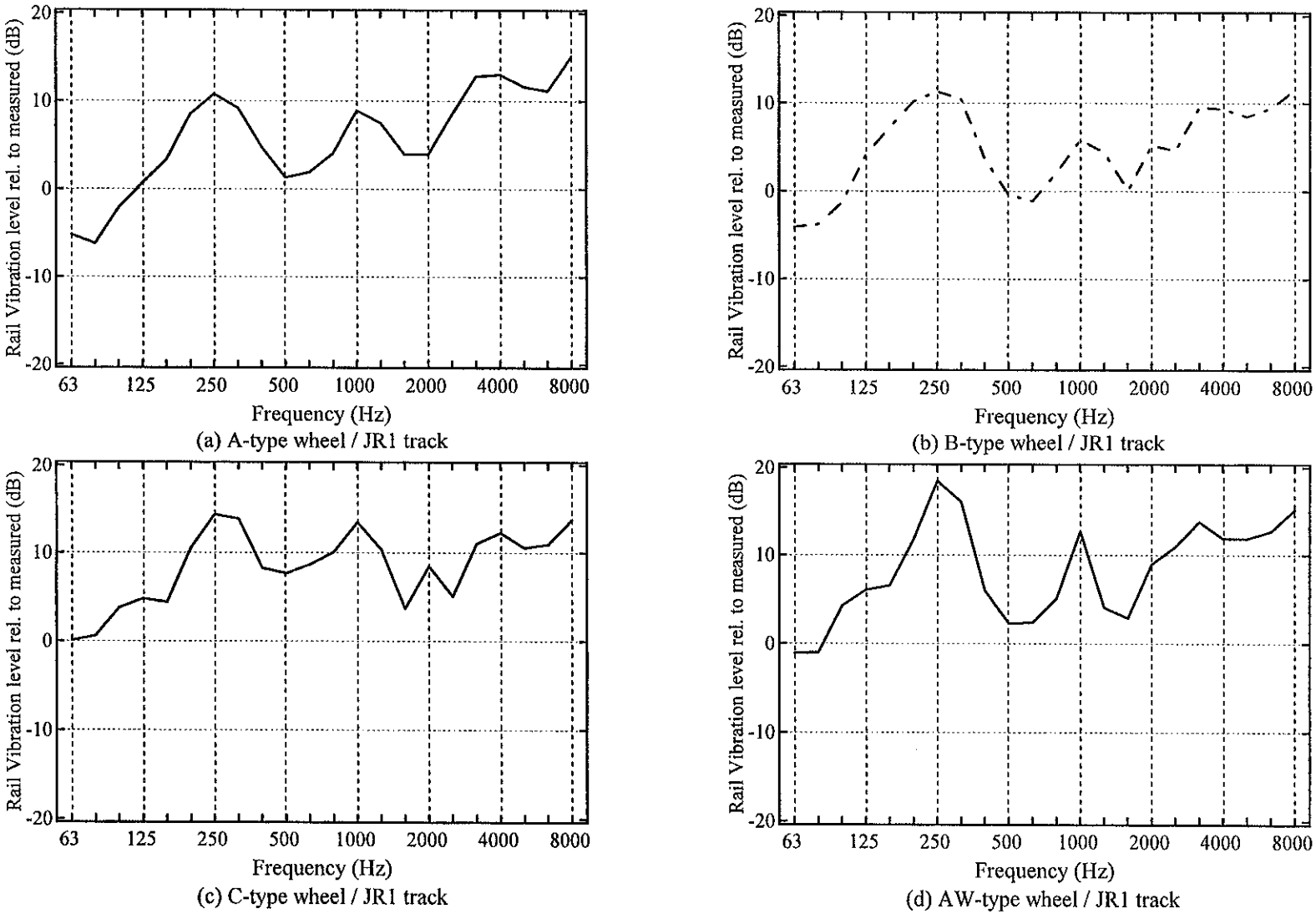

Figure E1.8 Predicted rail vibration velocity minus measured rail vibration velocity for each wheel using tinf model (JR1 track, bi-bloc sleeper, ·····:70 km/h,– – –:100 km/h,——:110 km/h,– – –:120 km/h, virtical direction)

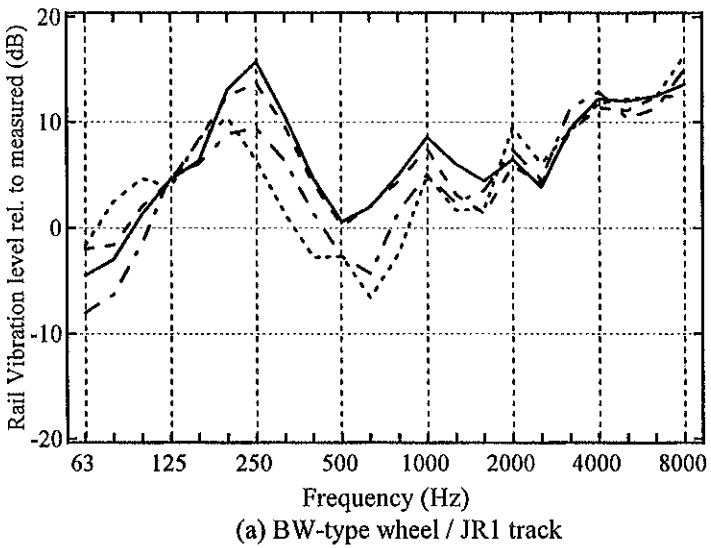

(a) BW-type wheel / JR1 track

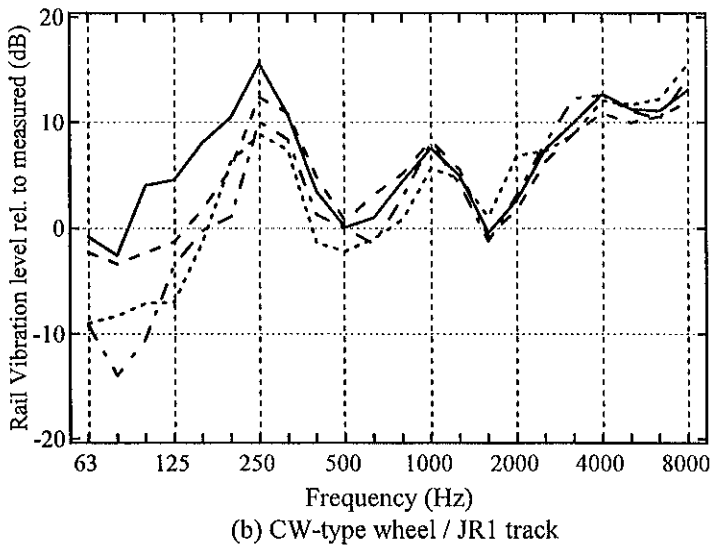

(b) CW-type wheel / JR1 track

Figure E1.9 Predicted rail vibration velocity minus measured rail vibration velocity for each wheel using tinf model (JR1 track, bi-bloc sleeper, ------:70 km/h,– – –:100 km/h,——:110 km/h,- - -:120 km/h, virtical direction)

E2 Rail vibration predicted with rodel and tinf models with mono-bloc sleeper

This section presents calculations of rail vibration carried out using:

- the continuous track model (rodel model) and the periodic track model (tinf model)
- modal sleeper model
- frequency dependent ballast stiffness model
- calculated track decay rates

In this section, the modal sleeper model and the frequency-dependent ballast stiffness model are introduced into the TWINS model.

Figure E2.1 shows the vertical rail vibration velocity level predicted with each model minus measured level for each wheel/rail combination in dB(A). The mean is reduced from +0.9 dB(A) to -0.5 dB(A) for the rodel model, and from +4.8 dB(A) to +2.6 dB(A) for the tinf model. It is clear that the results of both models are improved by using the two additional models. The results of the rodel model are closer to 0 than those of the tinf model. This is again because rail loss factor is neglected in the tinf model.

Figures E2.2 and E2.4 show predicted vertical rail vibration velocity level plotted against measured level in terms of overall A-weighted levels. The individual points represent one of the 6 wheel/track combinations. The solid line corresponds to the mean difference between predictions and measurements (mean -0.5 dB for the rodel model and +2.6 dB for the tinf model). The dashed lines show a range of +/- one standard deviation (standard deviations of 2.8 dB in each case).

Figures E2.3 and E2.5 show the spectral differences as the mean and a range of +/- one standard deviation for all cases. Comparing with Figures E1.3 and E1.5, the shape of the results is much improved and the peak at 250 Hz has been eliminated. However, the results are over-predicted. For the rodel model, an under-prediction is found in the frequency range 800-1250 Hz. This under-prediction is probably due to the phenomena associated with the pinned-pinned resonance around 1000 Hz. The rodel model cannot predict the pinned-pinned resonance correctly, since the rodel model has a continuous support.

Figures E2.6-E2.9 show the total predicted rail vibration level minus measured level in vertical direction for each wheel/track combination and each train speed.

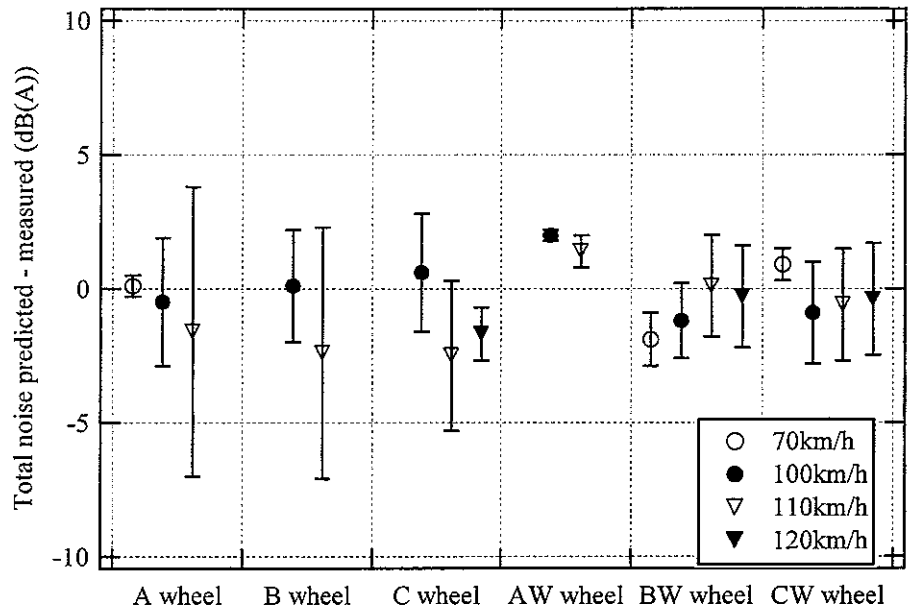

(a) rodel model (vertical direction,mono-bloc sleeper)

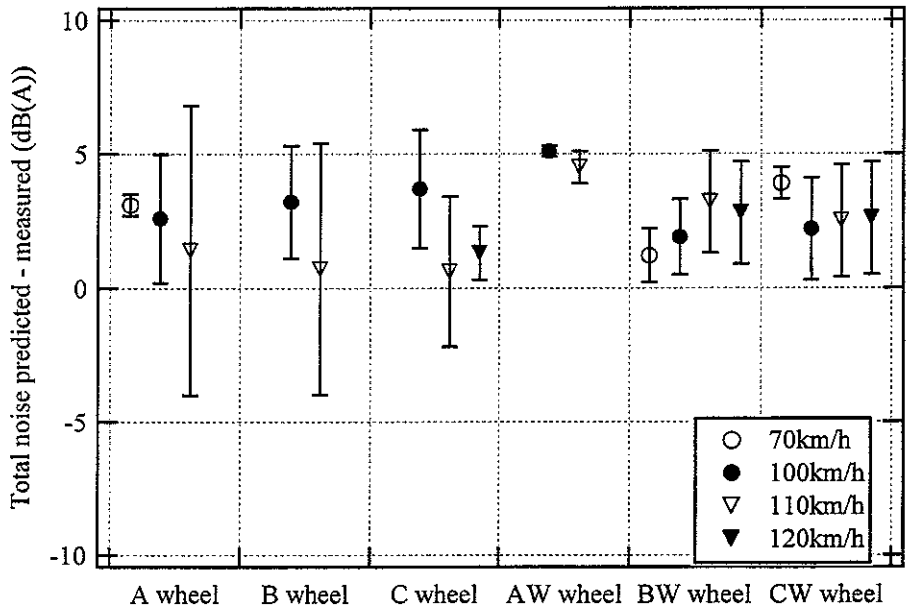

(b) tinf model (vertical direction, mono-bloc sleeper)

Figure E2.1 Total Predicted rail vibration velocity minus measured rail vibration velocity in dB(A) Results are shown for each speed (70, 100, 110 and 120 km/h).

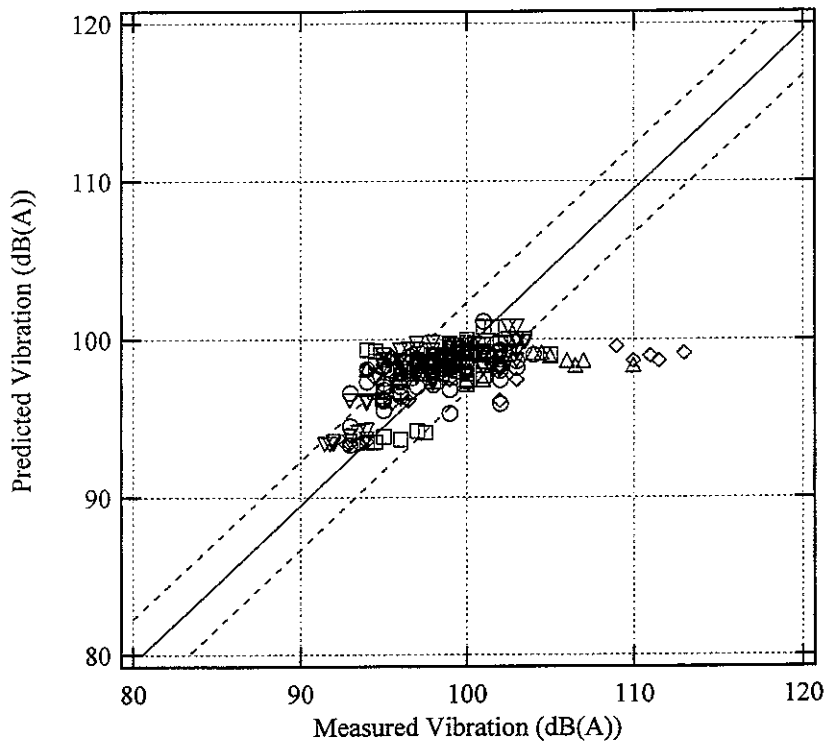

Figure E2.2 Predicted rail vibration vibration plotted against measured rail vibration vibration for all cases (vertical direction, rodel, mono-bloc sleeper)

◇: A-type wheel, △: B-type wheel, ○: C-type wheel,

+: AW-type wheel, □: BW-type wheel ▽: CW-type wheel

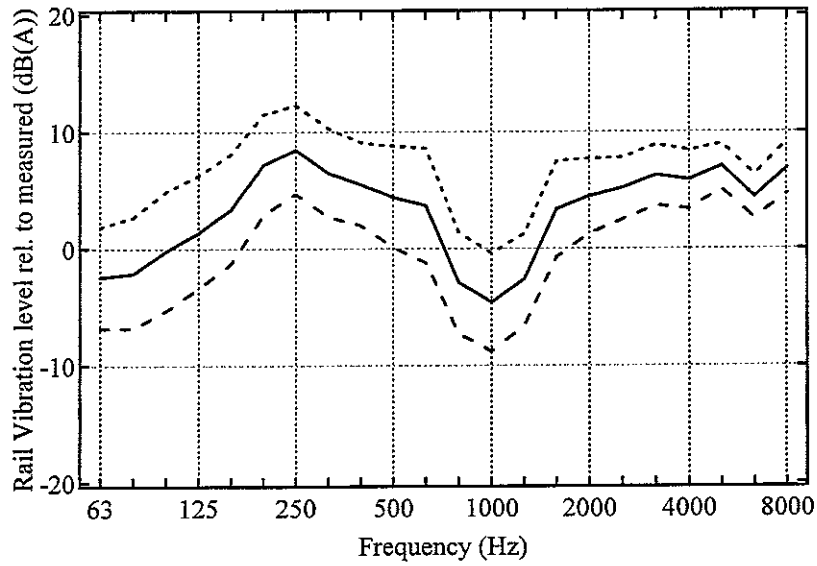

Figure E2.3 Average difference between predicted and measured rail vibration velocity spectra for all cases (rodel, mono-bloc sleeper, ——:mean, ----- :mean+std deviation,- - - :mean-std deviation, vertical direction)

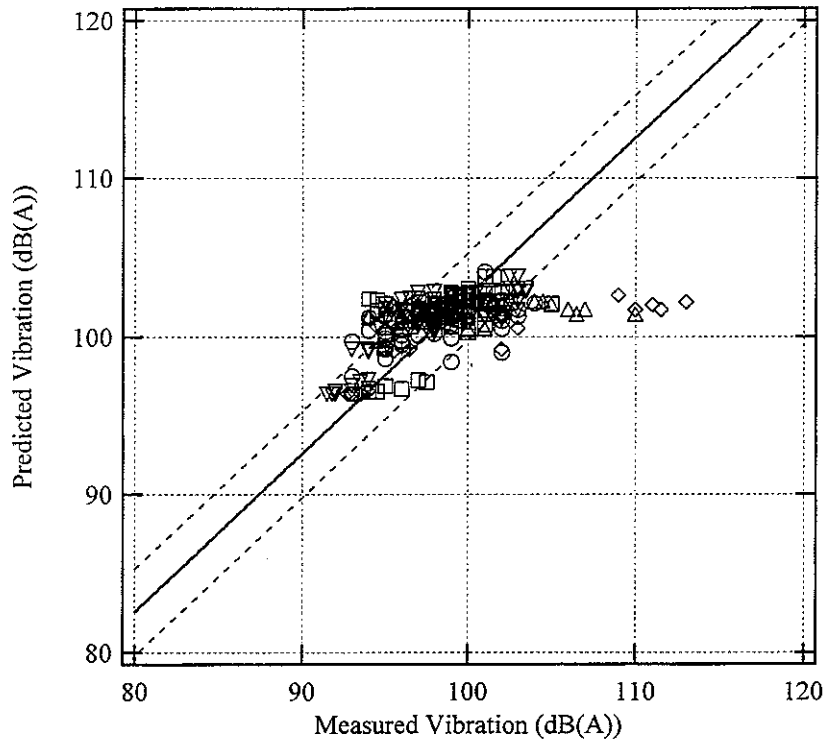

Figure E2.4 Predicted rail vibration velocity plotted against measured rail vibration velocity for all cases (vertical direction, tinf, mono-bloc sleeper)

◇: A-type wheel, △: B-type wheel, ○: C-type wheel,
+: AW-type wheel, □: BW-type wheel ▽: CW-type wheel

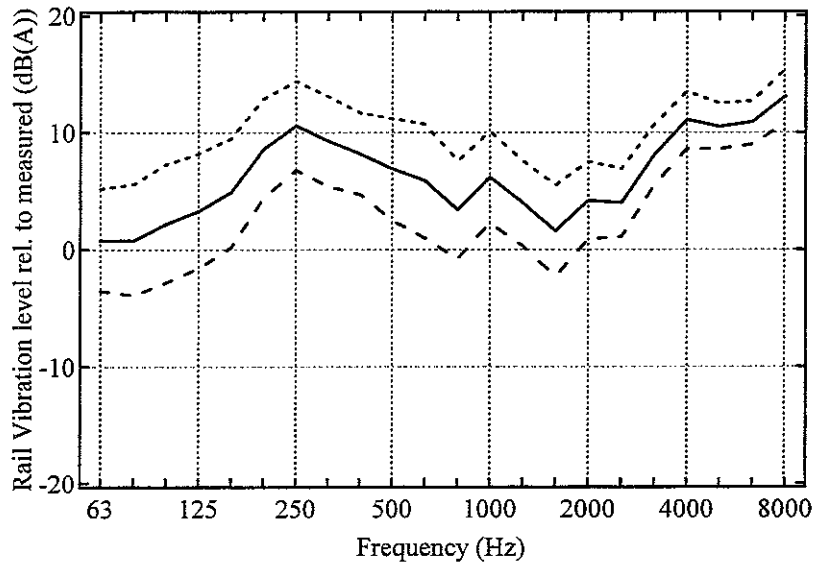

Figure E2.5 Average difference between predicted and measured rail vibration velocity spectra for all cases (tinf, mono-bloc sleeper, —— :mean, ----- :mean+std deviation,- - - :mean-std deviation, vertical direction)

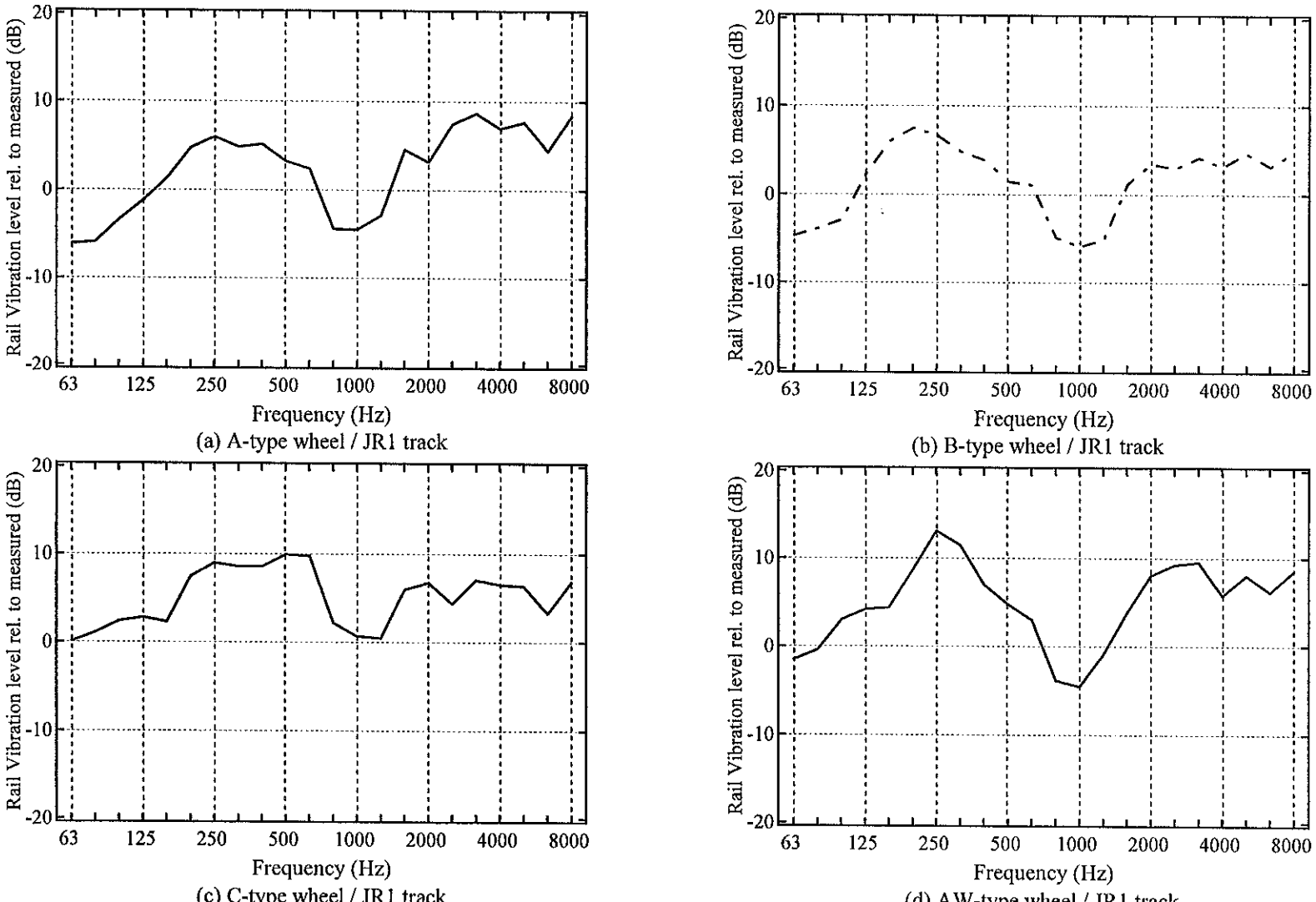

Figure E2.6 Predicted rail vibration velocity minus measured rail vibration velocity for each wheel using rodel model (JR1 track, mono-bloc sleeper, ····· :70 km/h, - - :100 km/h, —— :110 km/h, - - :120 km/h, virtical direction)

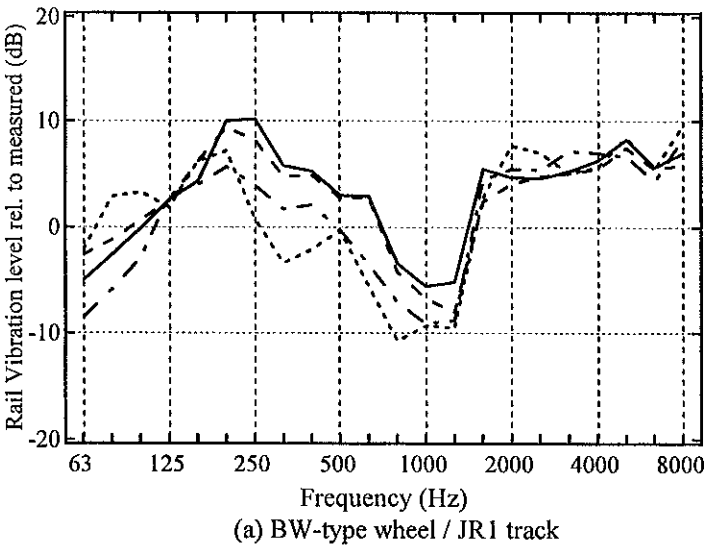

(a) BW-type wheel / JR1 track

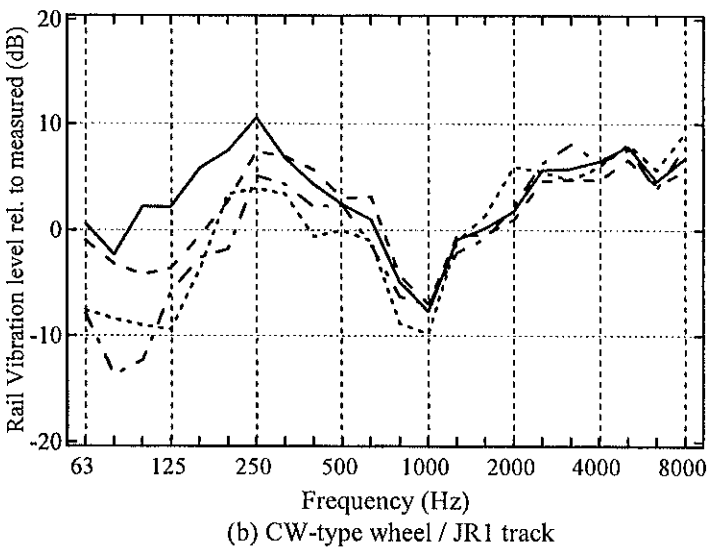

(b) CW-type wheel / JR1 track

Figure E2.7 Predicted rail vibration velocity minus measured rail vibration velocity for each wheel using rodel model (JR1 track, mono-bloc sleeper,····· :70 km/h,– – – :100 km/h,—— :110 km/h,– – – :120 km/h, virtical direction)

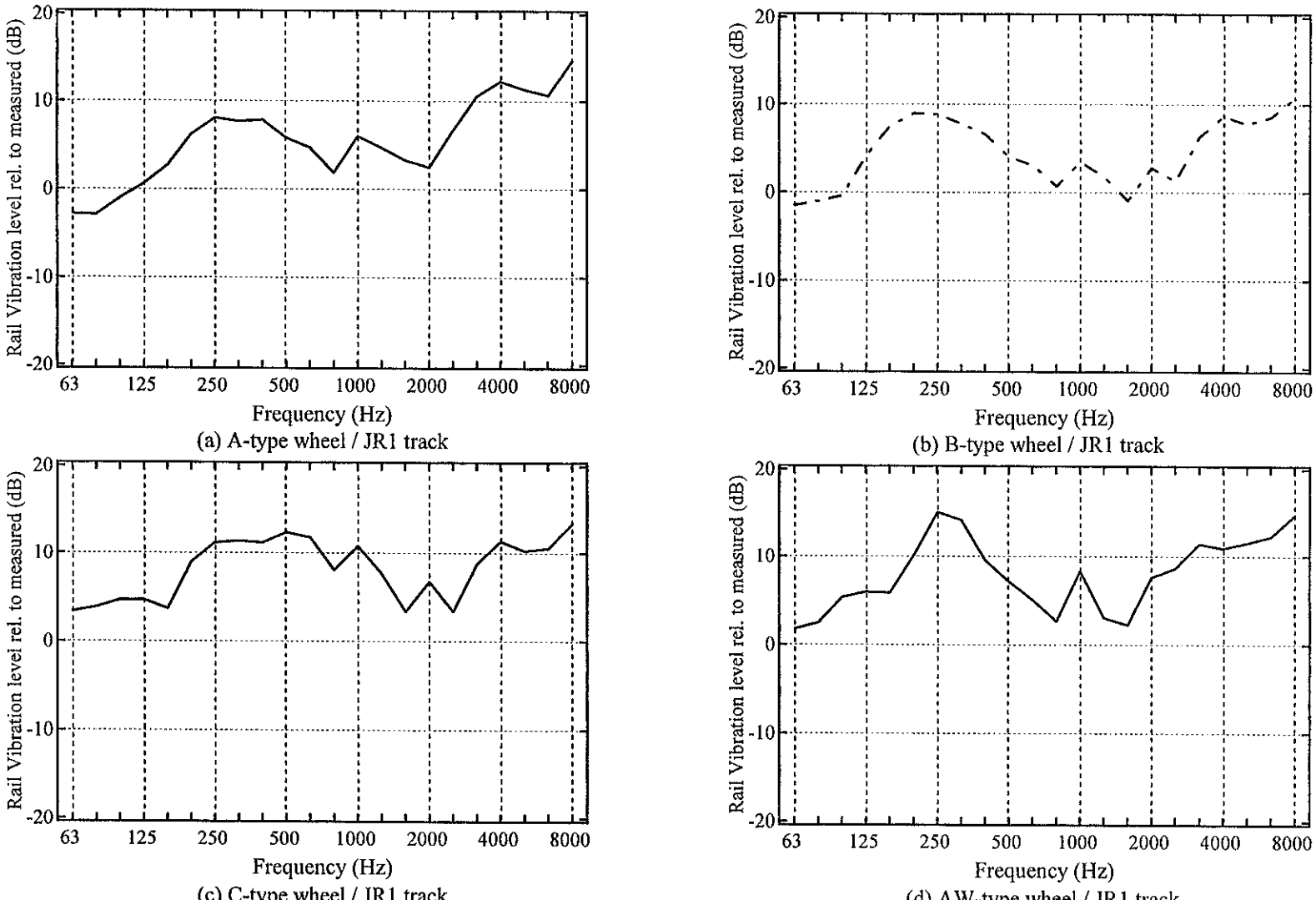

Figure E2.8 Predicted rail vibration velocity minus measured rail vibration velocity for each wheel using tinf model (JR1 track, mono-bloc sleeper,····· :70 km/h,– – :100 km/h,—— :110 km/h,– – :120 km/h, virtical direction)

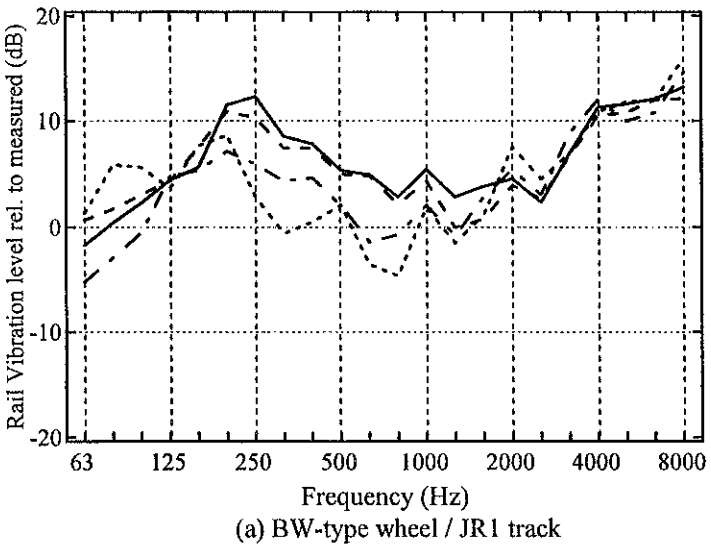

(a) BW-type wheel / JR1 track

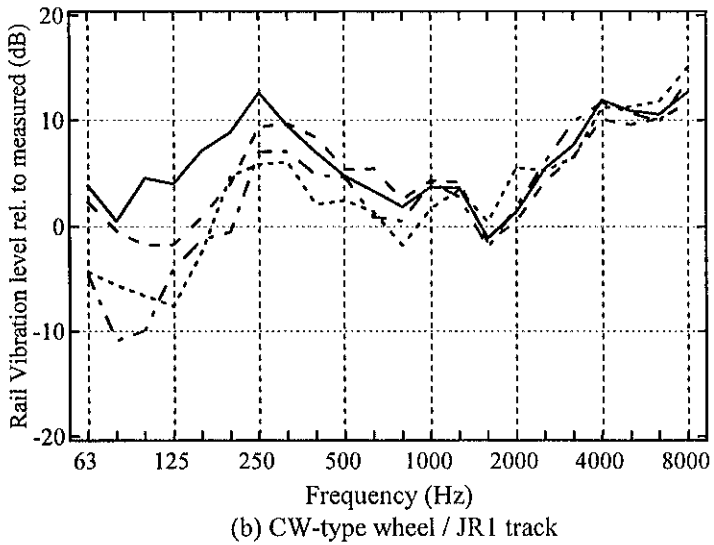

(b) CW-type wheel / JR1 track

Figure E2.9 Predicted rail vibration velocity minus measured rail vibration velocity for each wheel using tinf model (JR1 track, mono-bloc sleeper,------ :70 km/h, - - :100 km/h,—— :110 km/h, - - :120 km/h, virtical direction)

F SUPPLEMENTARY STUDIES

F1 Effect of axle load on contact filter effect

The size of the contact zone between the wheel and the rail depends on wheel load. The contact patch length determines the wavelength on which the contact filter has a significant effect. Therefore, in order to make TWINS predictions correctly, the contact filter effect corresponding to wheel load condition should be determined.

Figure F1 shows the spectrum of the contact filter from reference [F1]. This was determined using a DPRS analysis on several sets of roughness data. The spectrum covers the frequency range 125-10000 Hz. However, the spectrum is not sufficient to estimate the contact filter corresponding to other axle load conditions, since frequency components are shifted by changing wheel load condition. Therefore, the contact filter spectra are extrapolated logarithmically in two frequency ranges (f>10000 Hz and f<125 Hz, f: frequency), also shown in Figure F1.

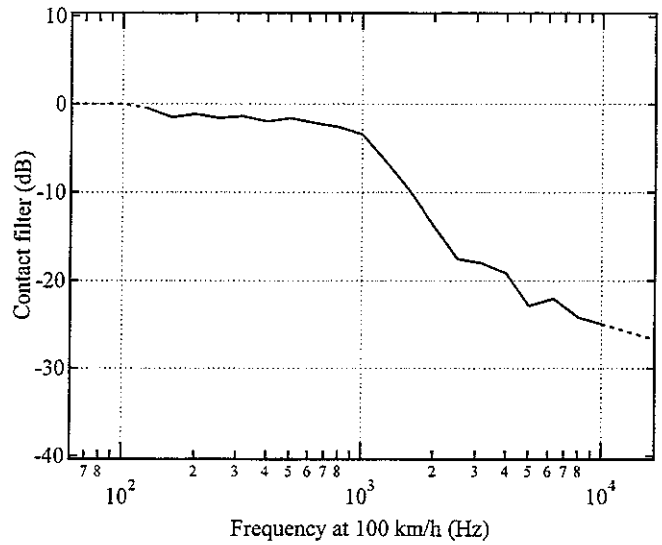

Figure F1 Contact filter effect (wheel load: 50000 N) [F1]

In order to obtain the contact filter for each wheel load condition, the following procedure has been used:

(1) filtering effect in each band, shown in Figure F1, is divided by the corresponding bandwidth into narrow bands.

(2) frequency components are shifted in relation to the one-third power of wheel load, $P^{1/3}$.

(3) for each wheel radius, frequency components corresponding to each 1/3 octave band are added together.

In the procedure, it is important that frequency components are shifted correctly. The relationship between major semi-axis, a, and minor semi-axis, b, of the contact zone for elliptical point contacts is given in [F2].

$$a/b \approx (R'/R'')^{\frac{3}{2}} \qquad \text{(F1)}$$

$$c = (ab)^{\frac{1}{2}} = \left(\frac{3PR_e}{4E^*}\right)^{\frac{1}{3}} F_1(R'/R'') \qquad \text{(F2)}$$

$$\frac{1}{R'} = \frac{1}{R_{11}} + \frac{1}{R_{21}} \qquad \text{(F3)}$$

$$\frac{1}{R''} = \frac{1}{R_{12}} + \frac{1}{R_{22}} \qquad \text{(F4)}$$

where P is the wheel load, E^* is the plane strain elastic modulus, R' and R'' are major and minor relative radii of curvature and R_e is the equivalent radius of curvature, $R_e = (R'R'')^{\frac{1}{2}}$. The parameter, F_1, depends on R' and R'', and is tabulated in [F2]. R_{11} and R_{12} are wheel rolling radius and wheel transverse radius respectively, and R_{21} and R_{22} are rail rolling radius ($=\infty$) and rail transverse radius respectively. The relationship between the contact length and the wheel load is derived from equations (F1)-(F4). Then,

$$a \propto P^{\frac{1}{3}}. \qquad \text{(F5)}$$

As the contact patch length determines the wavelength at which the contact filter rolls off, frequency components should be shifted by using equation (F5).

Figure F2 shows the contact filter effect due to various loads by shifting frequency components.

In Figure F2, it can be seen that the results predicted by shifting frequency components show similar trends to the average results from DPRS model. Therefore, it is confirmed that the method gives reliable contact filter effects.

Figure F3 shows the contact filter effect relative to the results of a load of 50000 N. These relative differences should be included in the TWINS calculations in order to estimate the effect of axle load on noise and rail vibration.

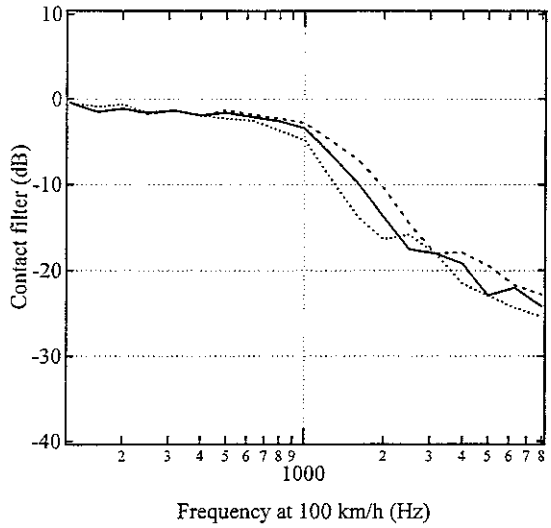

(a) Average results from DPRS model [F1]

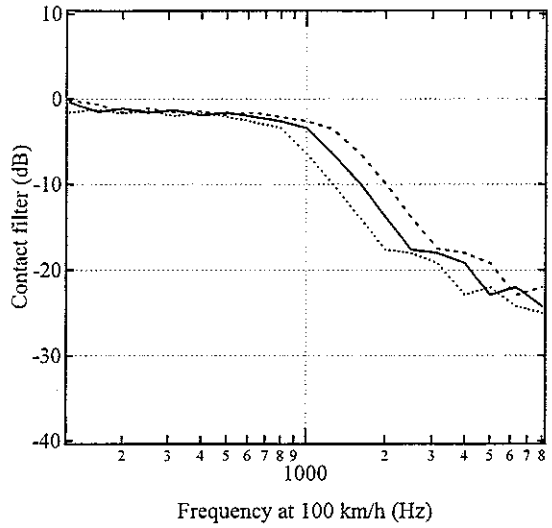

(b) Results from frequency shifting method

Figure F2 Contact filter of various loads. (—— :50000N, ---- :25000N, ... :100000N)

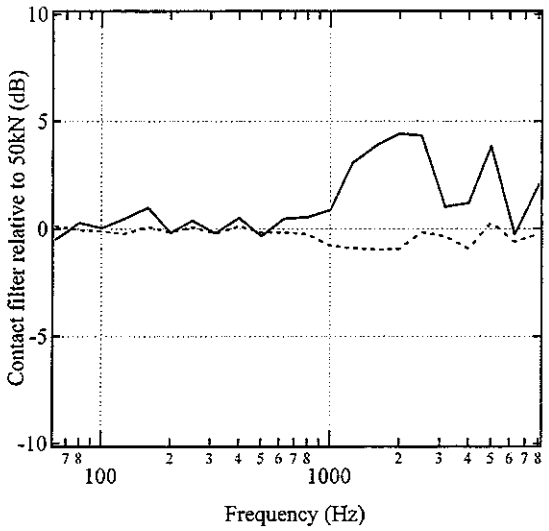

(a) Freight A

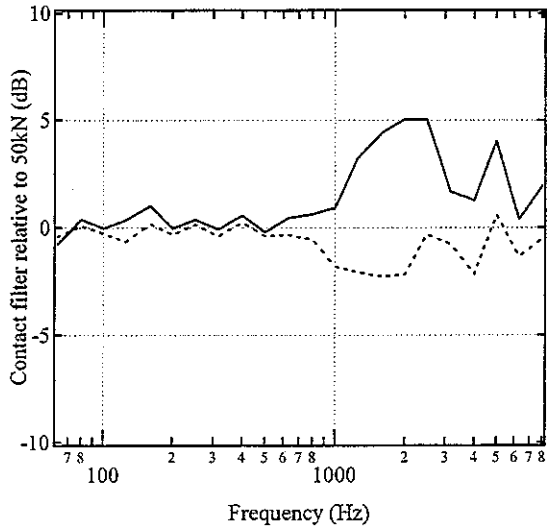

(b) Freight B

Figure F3 Predicted contact filter effect relative to result of a wheel load of 50000N

(Freight A: 23000N (_____), 64000N (.....), Freight B: 21500N (_____), 81500N (.....))

F2 Global comparison

This section presents calculations of noise and rail vibration carried out using:

- the continuous track model (rodel model)
- modal sleeper model
- a "unit roughness" excitation
- frequency dependent ballast stiffness model.
- calculated track decay rates
- calculating with a single speed (100 km/h)

In this section, only the rodel model with mono-bloc sleeper model is used only. This is because the rodel model gives better predictions than the other models (see Appendices D-E). In order to save computational effort, the TWINS calculations are carried out for a single speed (see Appendix C).

Figure F4 shows the results plotted against train speed in terms of overall A-weighted levels. For the predicted noise, it is clear that the overall levels increase with increasing train speed, and that the overall levels are lower when the wheel load is increased. The predictions show similar trends to the measurements. However, the predictions are somewhat higher. This is probably due to the fact that the standard roughness spectrum used in this report is different from the roughness spectrum calculated from the actual wheel/rail roughnesses of JR2 track (see Appendix C2).

Figures F5-F8 show the predicted noise spectra for each train speed (80, 100 and 110 km/h). The measured results are also shown for comparison. It is found that the result shows an under-prediction below 1600 Hz, and an over-prediction above 1600 Hz. This is again probably due to the inconsistency of the two wheel/rail roughness spectra. Below 125 Hz, the predictions show a significant under-prediction. This is because, as the sound measurements were made close to the track, the measured results would be contaminated by wind noise during train pass-by.

Figure F9 shows the predicted difference in overall A-weighted levels between the two wheel load conditions. The measured results are also shown for comparison. For the predicted noise, the differences are in the range 1-2.5 dB, and appear to be independent of train speed. This indicates that a heavier wheel load should give a lower noise level. For

the measured noise, the overall levels are also reduced by increasing the wheel load. However, as the train speed increases, the differences are smaller

The spectral variations between the two wheel load conditions should be constructed for each train speed. It is noted that, in the TWINS calculations, the effect of the wheel/rail roughnesses on the differences in frequency between the two wheel load conditions can be excluded, if the difference is calculated at one train speed. The differences depend on the contact filter and normal load effects, which are induced by the increase of the wheel load. The differences are equal to the differences between the contact filter and normal load effects.

Figures F10-F11 show the differences in noise between the two wheel load conditions. In order to compare the predictions with the measurements, it is important to concentrate on the results from 125 Hz upwards, since the measured results would be affected by wind noise below 125 Hz. For the predictions of Freight A, it is clear that the difference is less than 1 dB below 1000 Hz, and is of an order of up to 2 dB above 1000 Hz. Comparing with the measurements, the predictions show similar trends above 1000 Hz. However, below 1000 Hz, the predictions show poor agreement with the measurements. Some points may be responsible for this.

- the wheel/rail roughness profile may have changed gradually during the running tests (the running tests were carried out over a period of two weeks).
- other vehicle components may radiate noise (e.g. rattling noise from bogies and goods on cars).
- track non-linearities may modify the track noise under preload.

Figures F12-13 show the spectral differences in contact filter and normal load effects between the two wheel load conditions. It is clear that, below 800 Hz, the noise components are not much affected due to the contact filter and normal load effects. Above 1000 Hz, the contact filter effect can be seen to have greater influence on the noise components than the normal load effect does. As the wheel load is increased, the whole contact filter curve is shifted to the left (see Figure F2). The frequency at which the contact filter effect is effective reduced with increasing wheel load. The contact filter effect is significantly changed above 1000 Hz, and hence reduces the noise above 1000 Hz.

Figures F18-F19 show the differences in rail vibration velocity between the two wheel

load conditions. For the results of Freight A, a comparison of the predictions and measurements shows that the global trends are well predicted above 125 Hz. This indicates that the wheel/rail roughness profile would remain unchanged during the running tests, and other vehicle components would radiate noise.

For the results of Freight B, the predicted noise and rail vibration show poor agreement with the measurements.

References

[F1] Thompson, D.J. The influence of the contact zone on the excitation of wheel/rail noise. *Proceeding of 8th International Workshop on Railway Noise.* 2001.

[F2] Johnson, K.L. Contact mechanics. Cambridge: Cambridge University Press

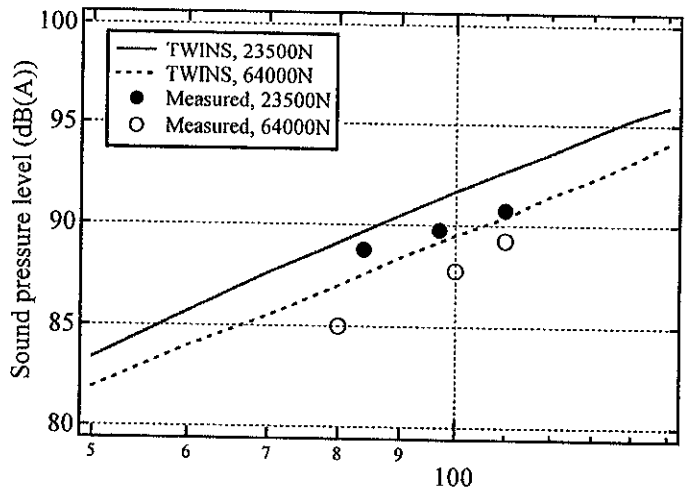

(a) Noise, Freight A

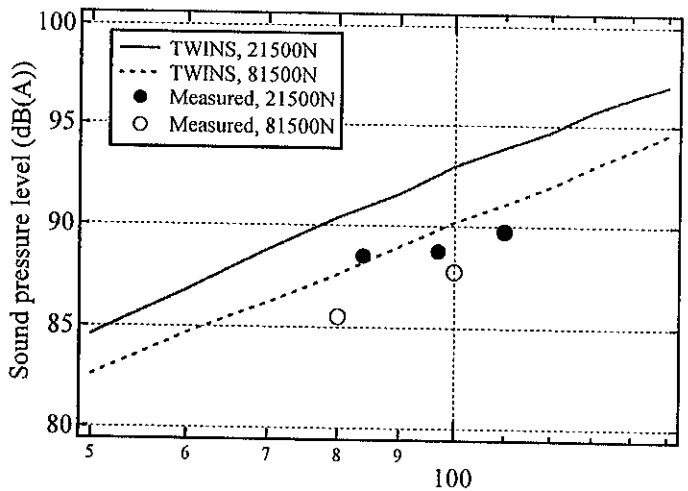

(b) Noise, Freight B

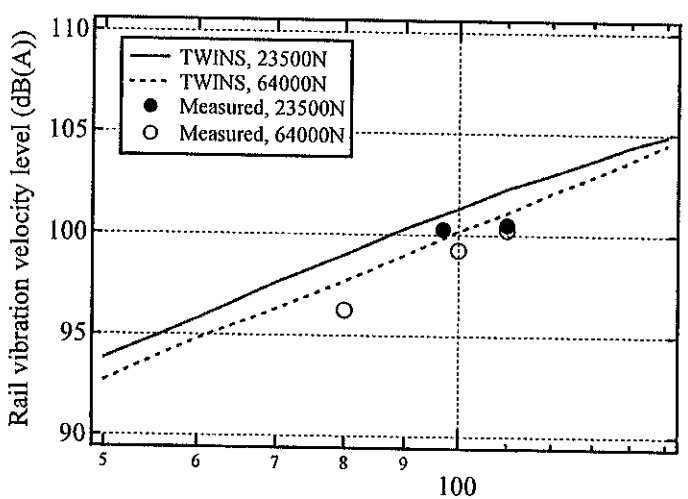

(c) Rail vibration velocity, Freight A

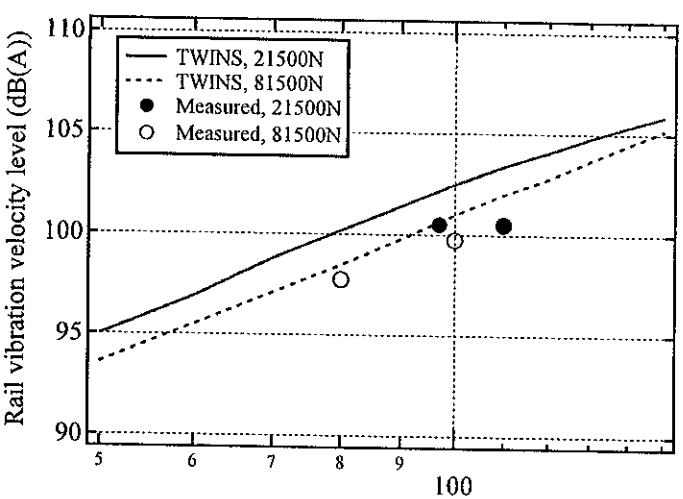

(d) Rail vibration velocity, Freight B

Figure F4 Overal level plotted aginst train speed (rodel, mono-bloc sleeper)

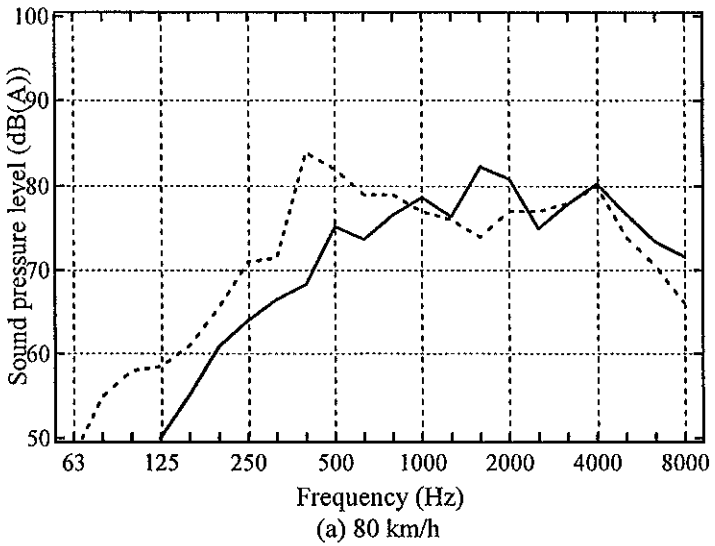

(a) 80 km/h

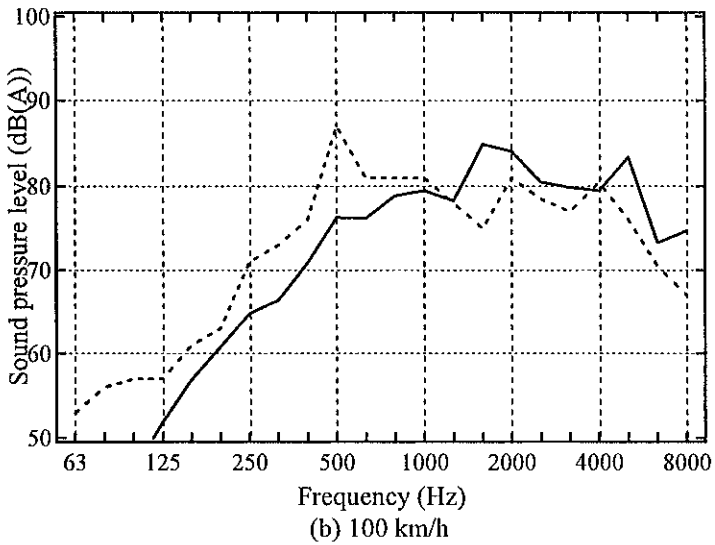

(b) 100 km/h

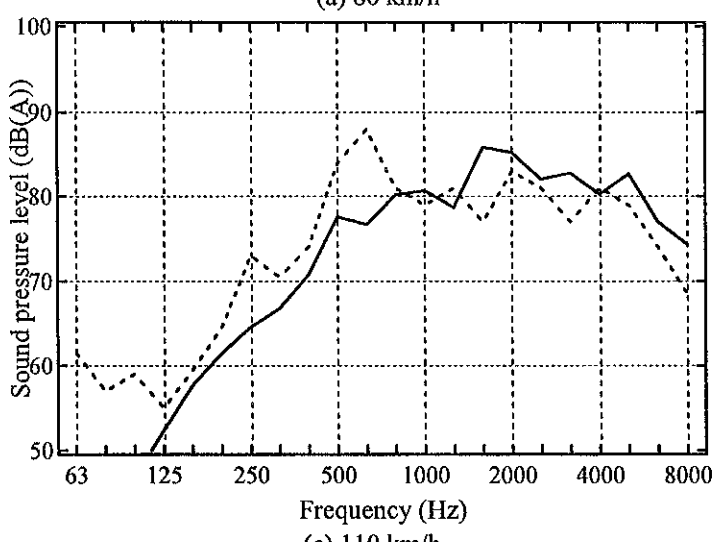

(c) 110 km/h

Figure F5 Predicted noise and measured noise for each train speed using rodel model

(Freight A, 23500N, JR2 track, mono-bloc sleeper, ——:predicted noise,------ :measured noise)

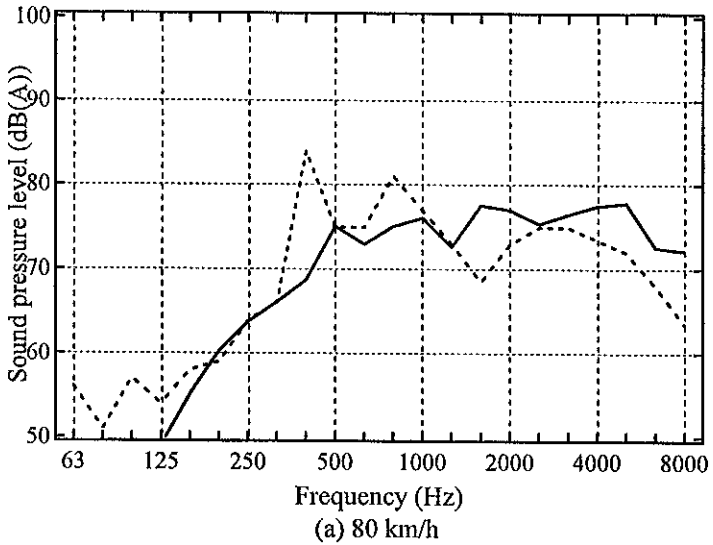

(a) 80 km/h

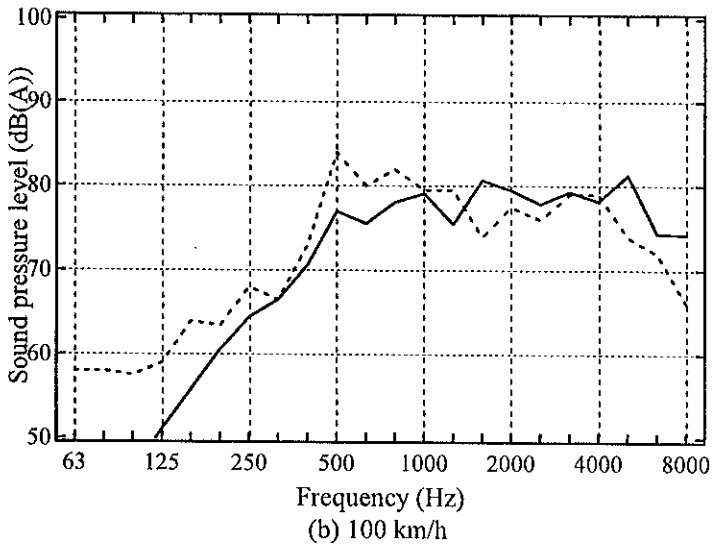

(b) 100 km/h

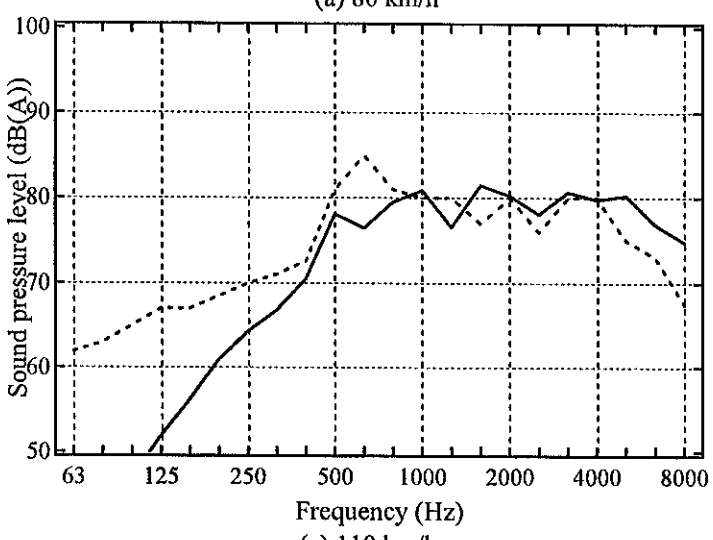

(c) 110 km/h

Figure F6 Predicted noise and measured noise for each train speed using rodel model

(Freight A, 64000N, JR2 track, mono-bloc sleeper, ——:predicted noise, ------ :measured noise)

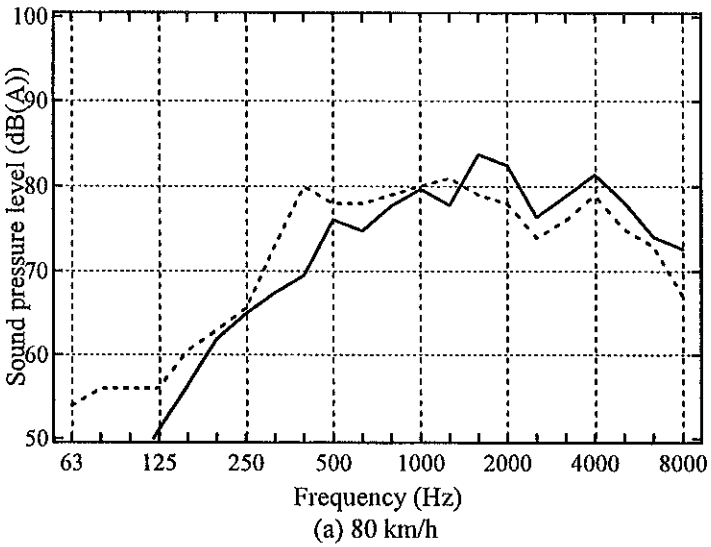

(a) 80 km/h

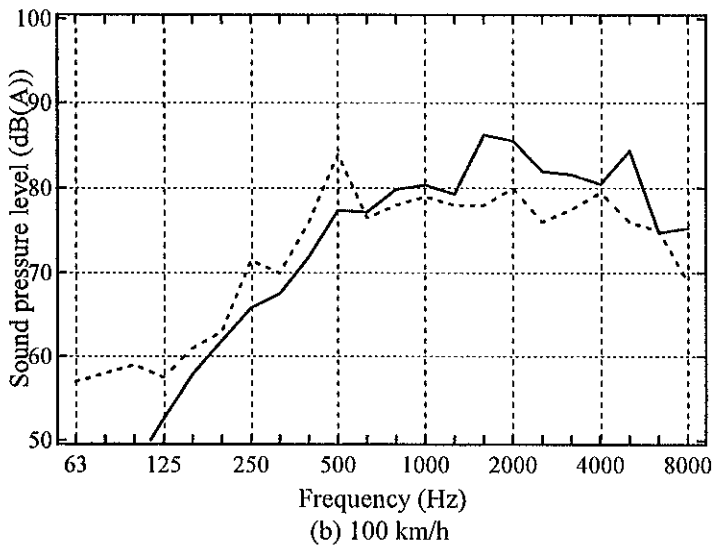

(b) 100 km/h

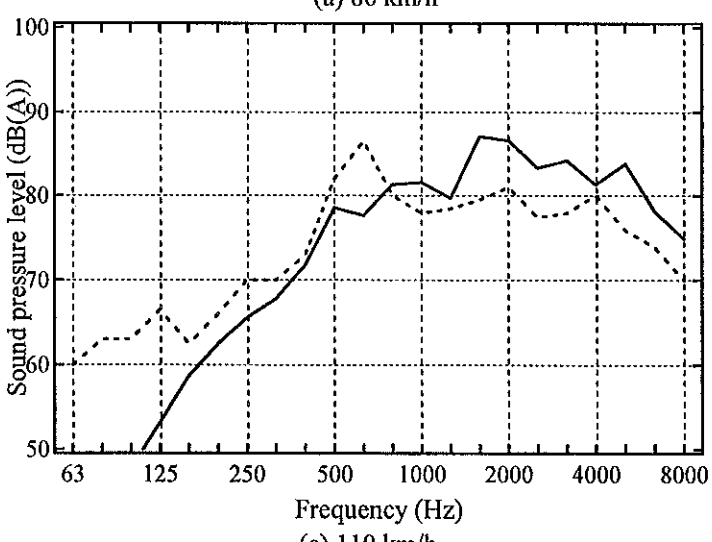

(c) 110 km/h

Figure F7 Predicted noise and measured noise for each train speed using rodel model

(Freight B, 21500N, JR2 track, mono-bloc sleeper, ——:predicted noise, ------ :measured noise)

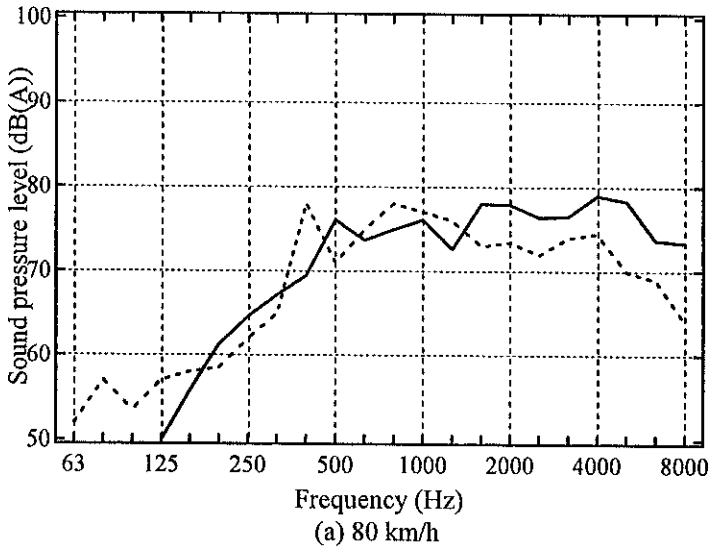

(a) 80 km/h

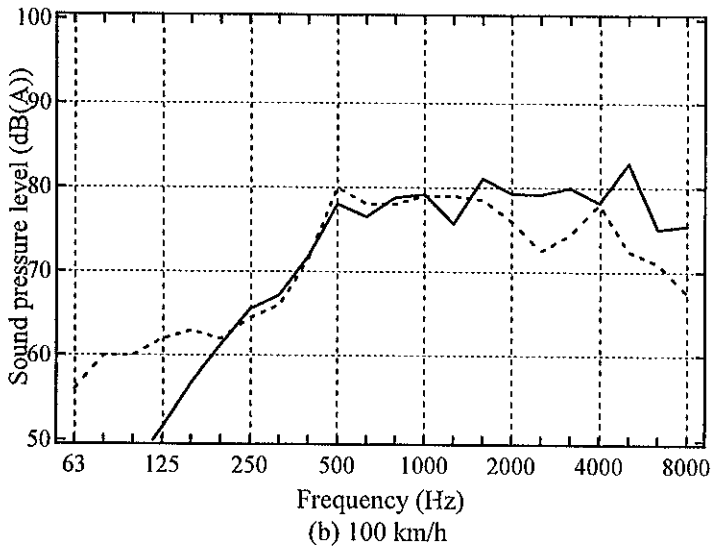

(b) 100 km/h

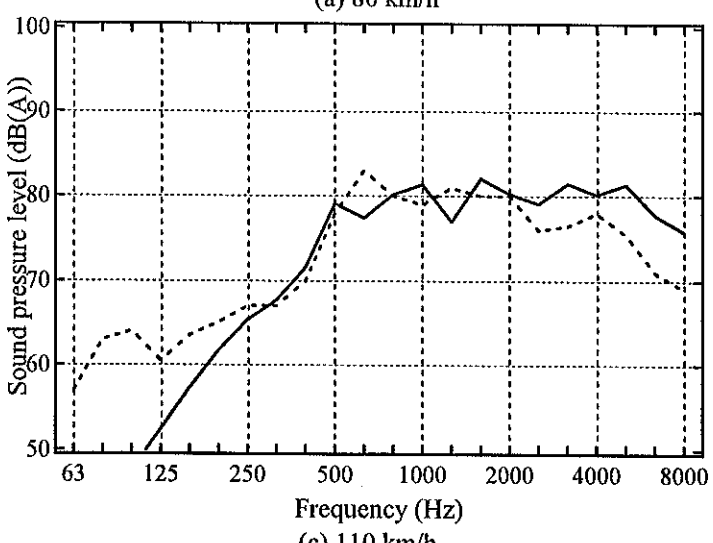

(c) 110 km/h

Figure F8 Predicted noise and measured noise for each train speed using rodel model

(Freight B, 81500N, JR2 track, mono-bloc sleeper, ——:predicted noise, ------ :measured noise)

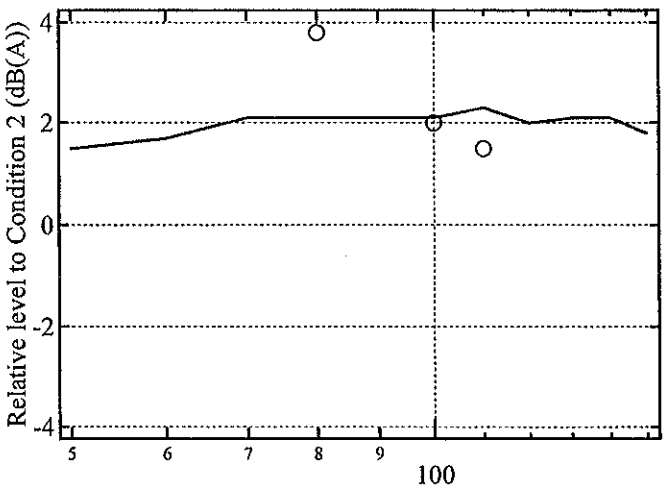

(a) Noise, Freight A

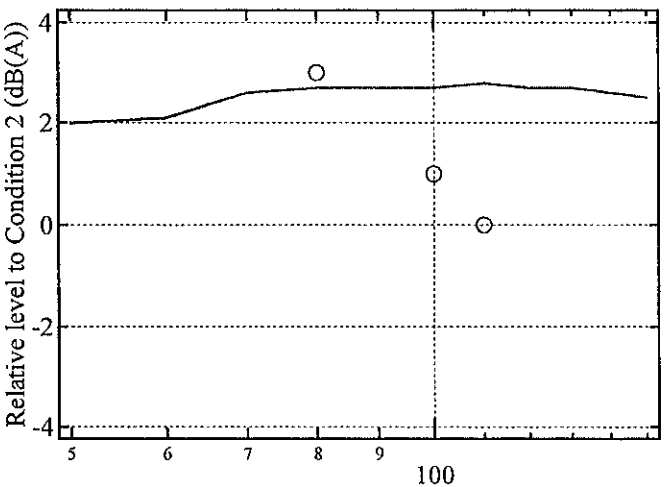

(b) Noise, Freight B

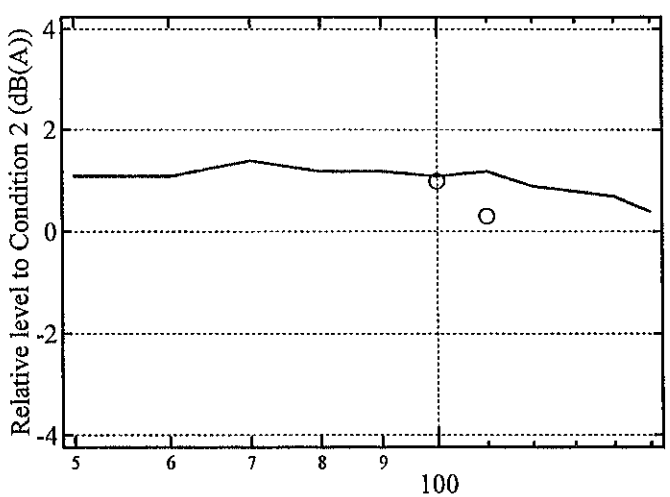

(c) Rail vibration velocity, Freight A

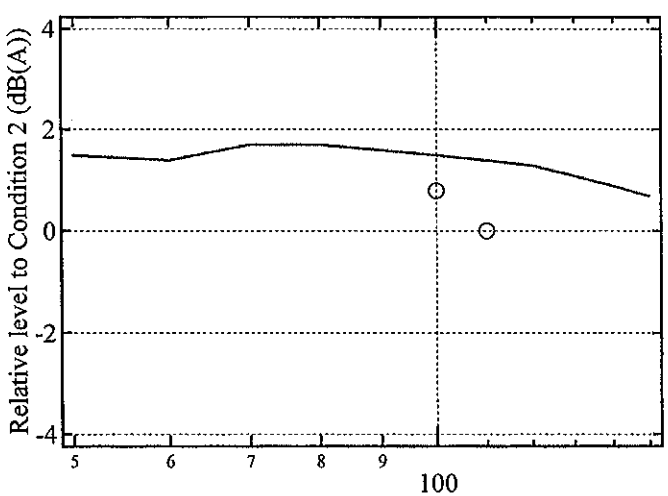

(d) Rail vibration velocity, Freight B

Figure F9 Difference in dB(A) between two axle load conditions

(rodel, mono-bloc sleeper, ——:TWINS, O:Measured results, Freight A: 23500N(Cond.1), 64000N(Cond.2), Freight B: 21500N(Cond.1), 81500N(Cond. 2))

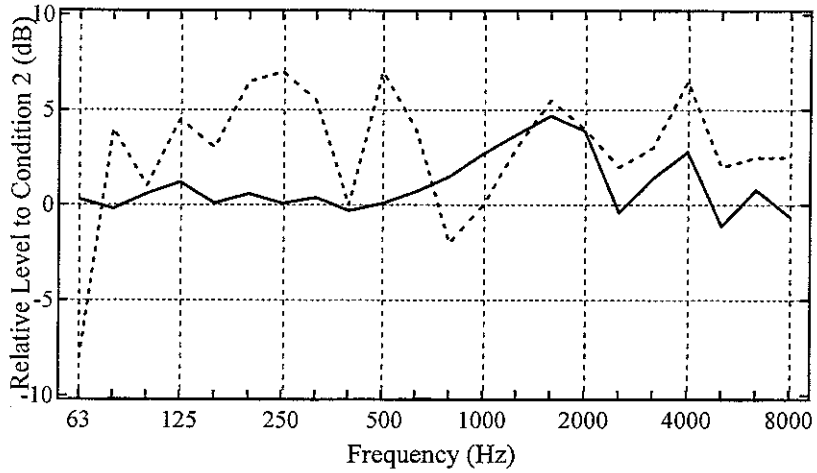

(a) Train speed: 80(km/h)

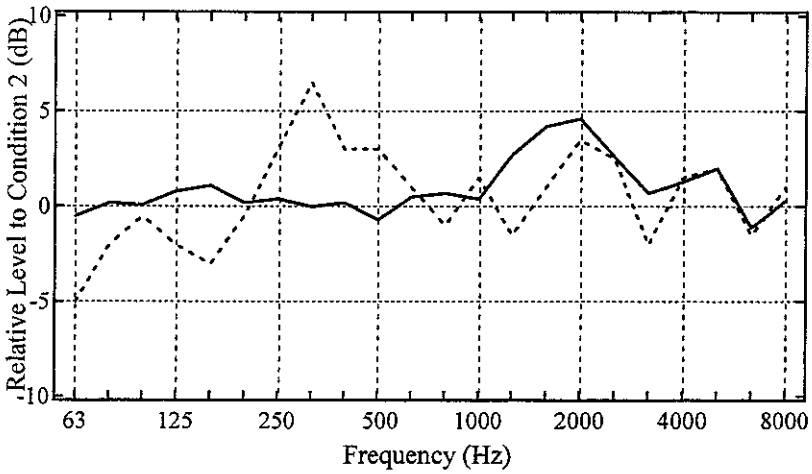

(b) Train speed: 100(km/h)

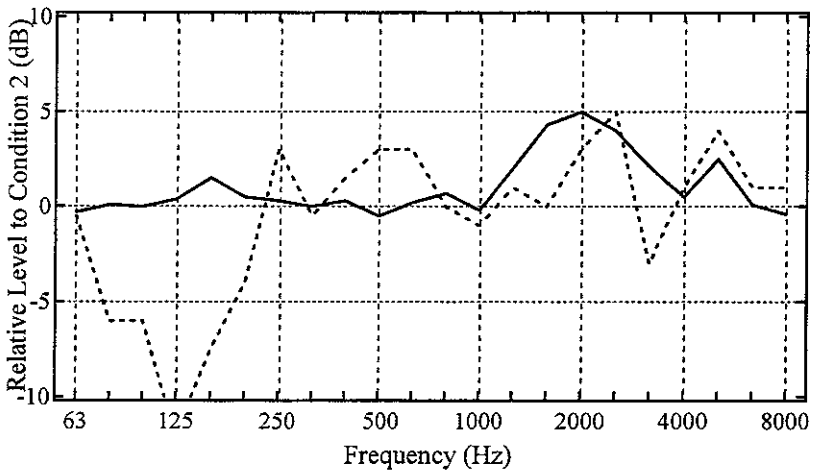

(c) Train speed: 110(km/h)

Figure F10 Difference in noise spectra between two axle load conditions (Freight A, Condition 1: 23500N, Condition 2: 64000N, rodel, mono-bloc sleeper, —:TWINS, ----:Measured results)

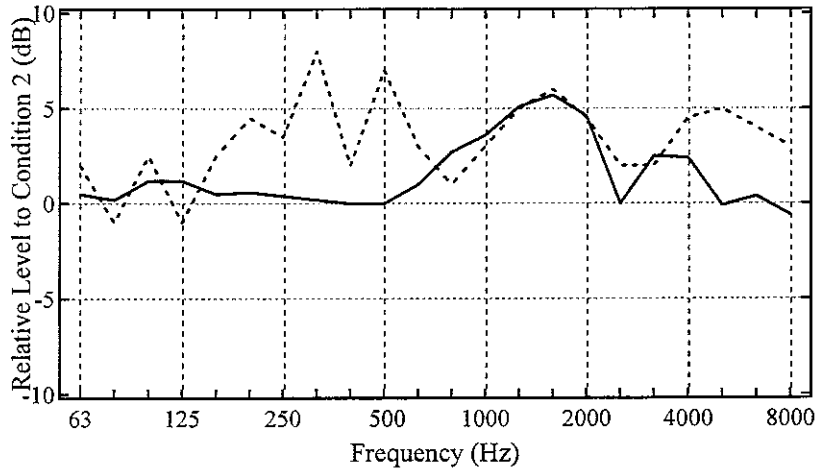

(a) Train speed: 80(km/h)

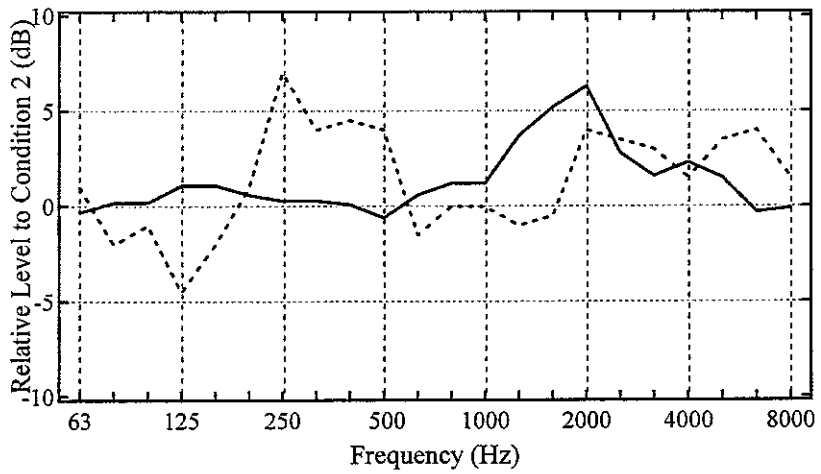

(b) Train speed: 100(km/h)

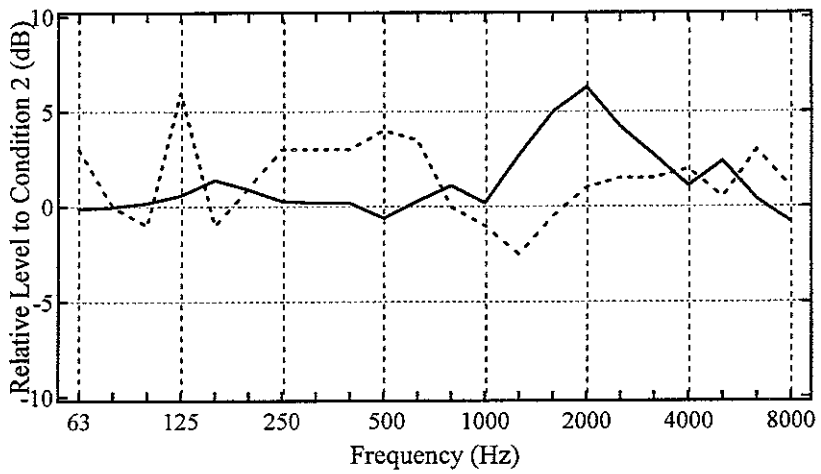

(c) Train speed: 110(km/h)

Figure F11 Difference in noise spectra between two axle load conditions (Freight B, Condition 1: 21500N, Condition 2: 81500N, rodel, mono-bloc sleeper, ——:TWINS, ----:Measured results)

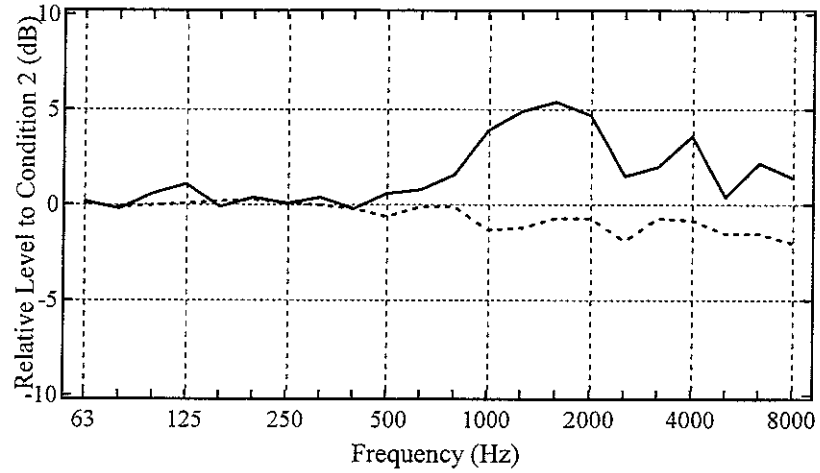

(a) Train speed: 80(km/h)

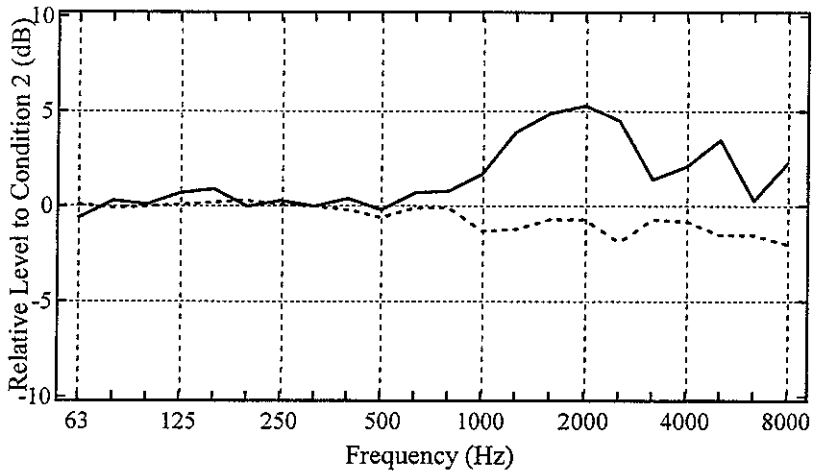

(b) Train speed: 100(km/h)

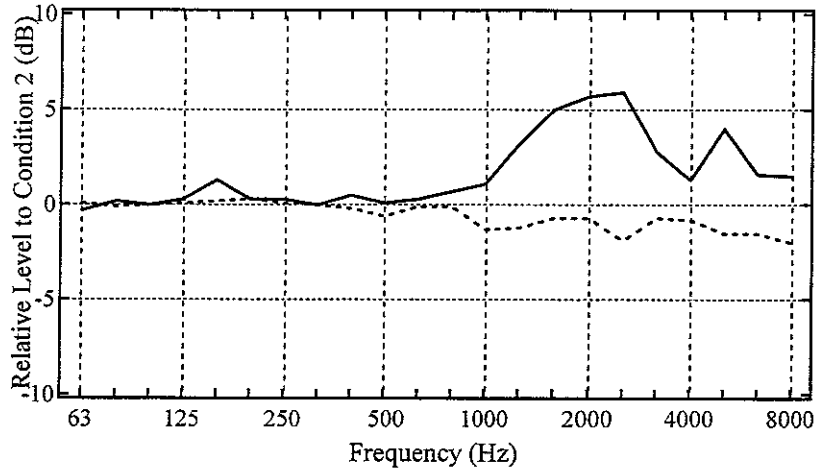

(c) Train speed: 110(km/h)

Figure F12 Difference in contact filter and normal load effects
(Freight A, Condition 1: 23500N, Condition 2: 64000N, rodel, mono-bloc sleeper,
—:Contact filter, ----:Normal load)

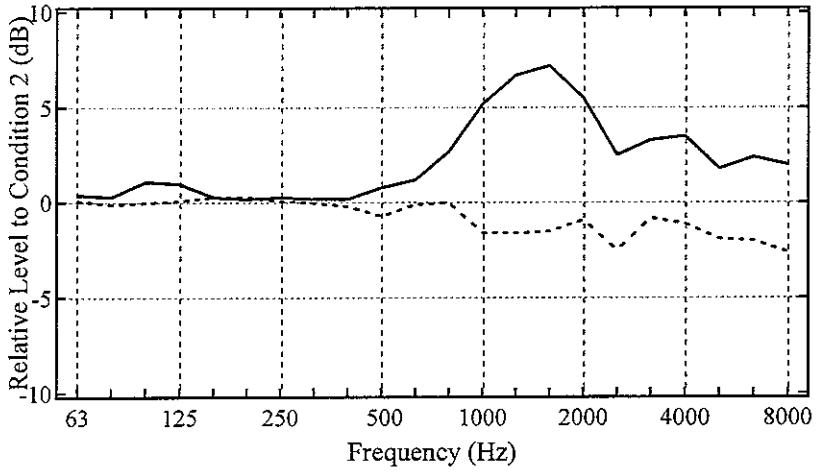

(a) Train speed: 80(km/h)

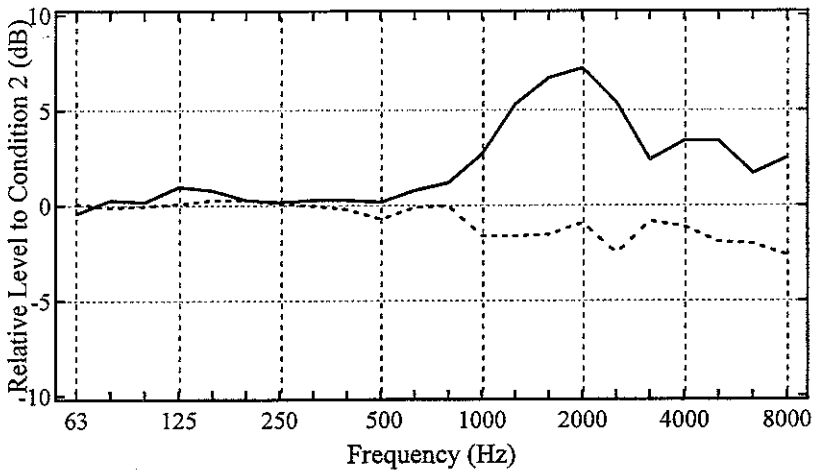

(b) Train speed: 100(km/h)

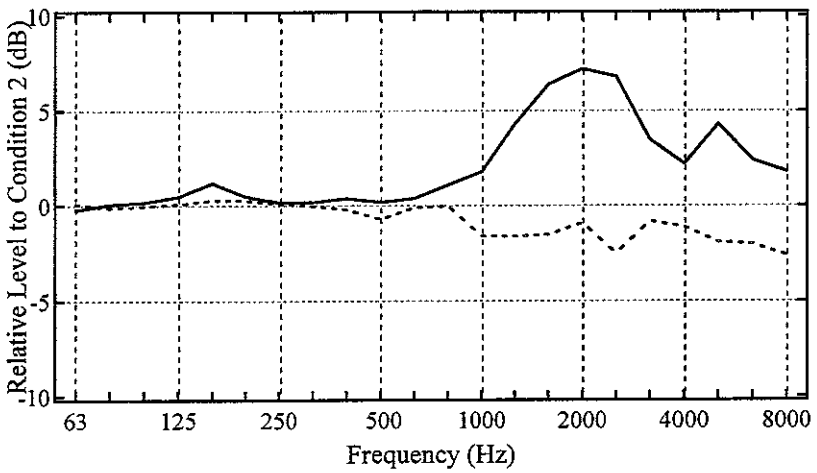

(c) Train speed: 110(km/h)

Figure F13 Difference in contact filter and normal load effects
(Freight B, Condition 1: 21500N, Condition 2: 81500N, rodel, mono-bloc sleeper,
——:Contact filter, ----:Normal load)

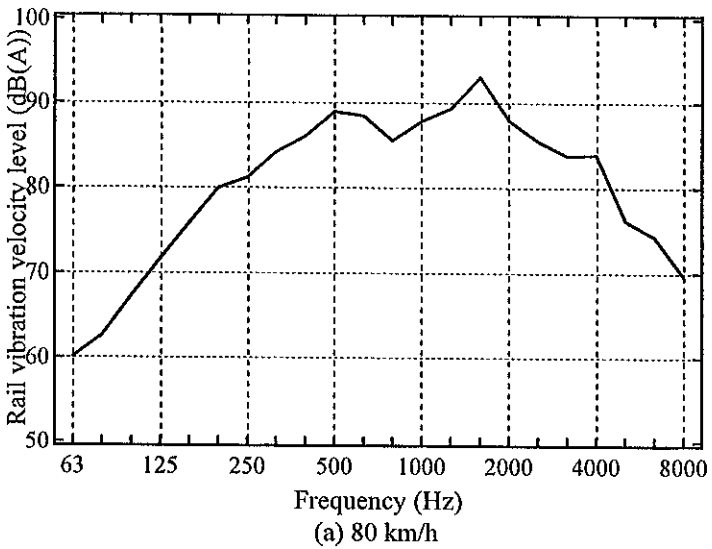

(a) 80 km/h

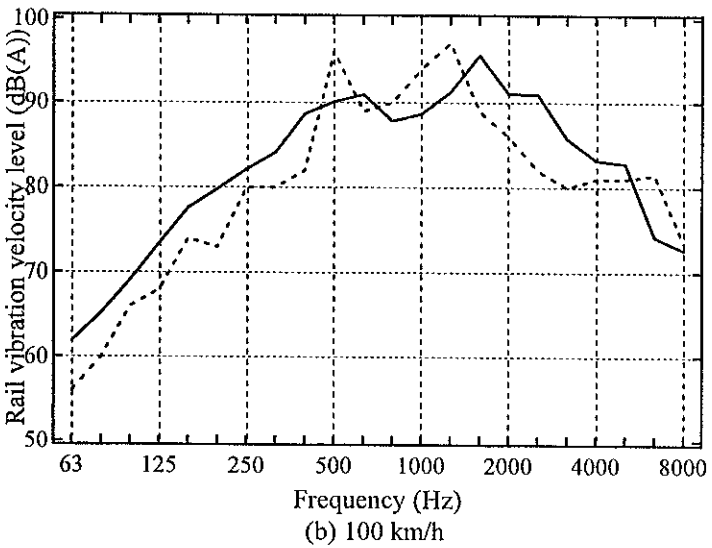

(b) 100 km/h

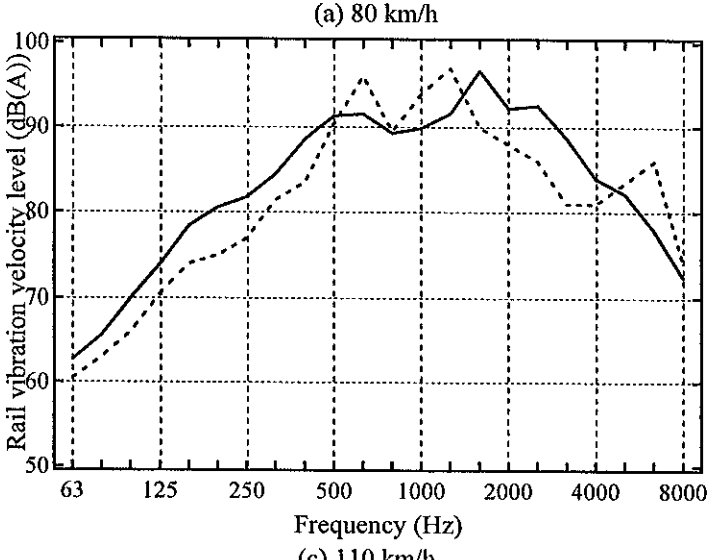

(c) 110 km/h

Figure F14 Predicted rail vibration velocity and measured rail vibration velocity for each train speed using rodel model (Freight A, 23500N, JR2 track, mono-bloc sleeper, ——:predicted,------ :measured, vertical direction)

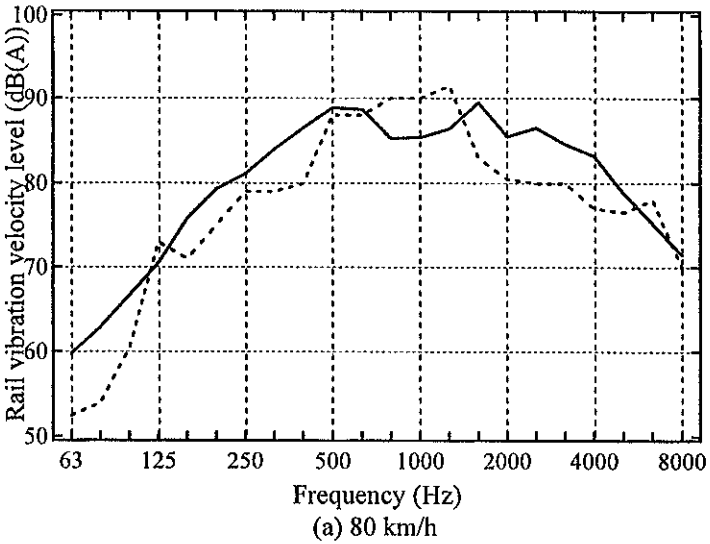

(a) 80 km/h

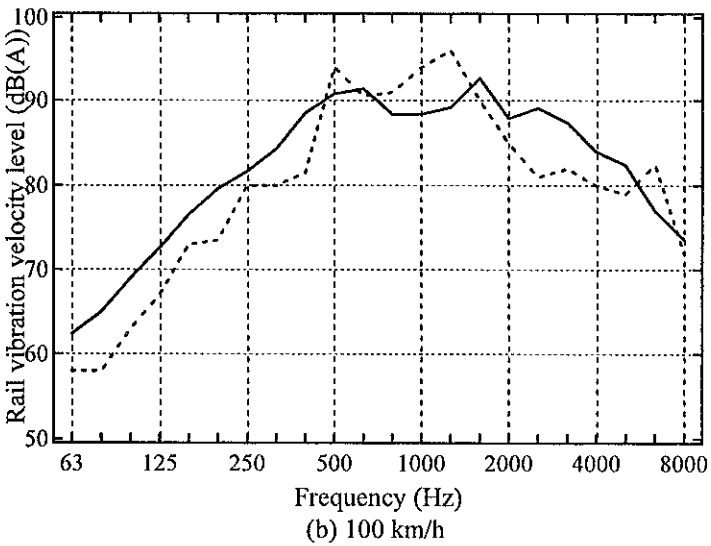

(b) 100 km/h

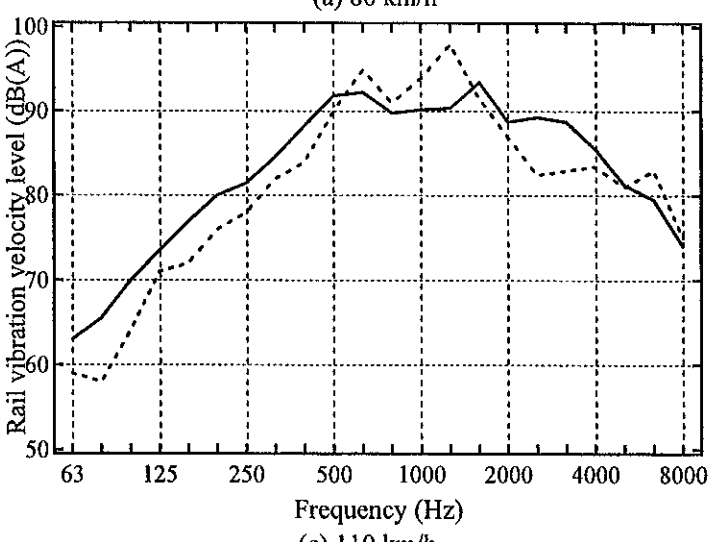

(c) 110 km/h

Figure F15 Predicted rail vibration velocity and measured rail vibration velocity for each train speed using rodel model (Freight A, 64000N, JR2 track, mono-bloc sleeper, ——:predicted,------ :measured, vertical direction)

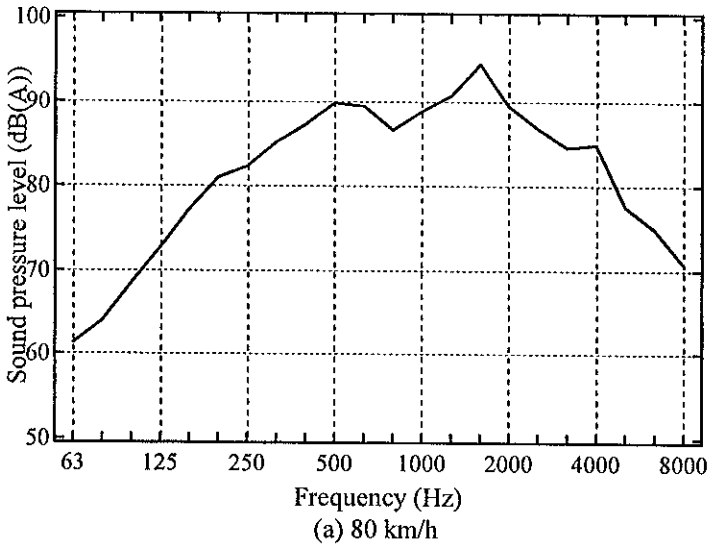

(a) 80 km/h

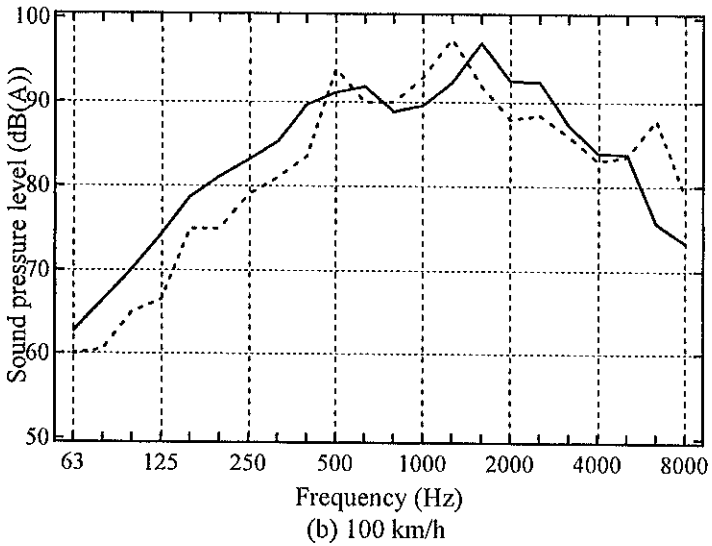

(b) 100 km/h

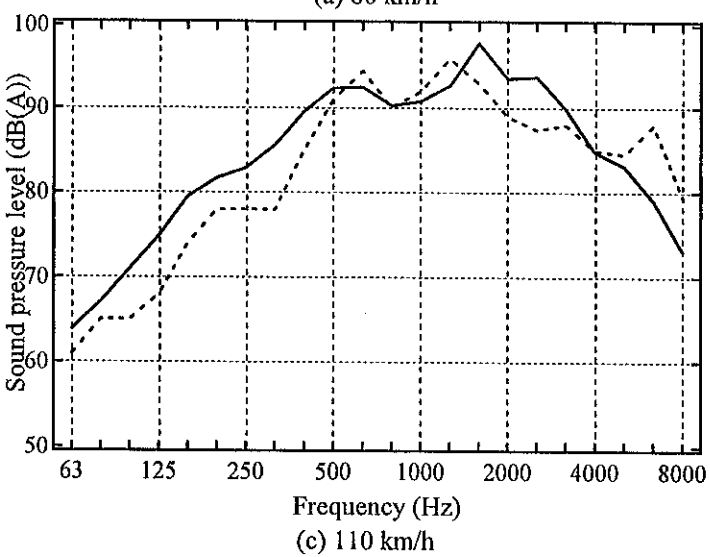

(c) 110 km/h

Figure F16 Predicted rail vibration velocity and measured rail vibration velocity for each train speed using rodel model (Freight B, 21500N, JR2 track, mono-bloc sleeper, ——:predicted,------ :measured, vertical direction)

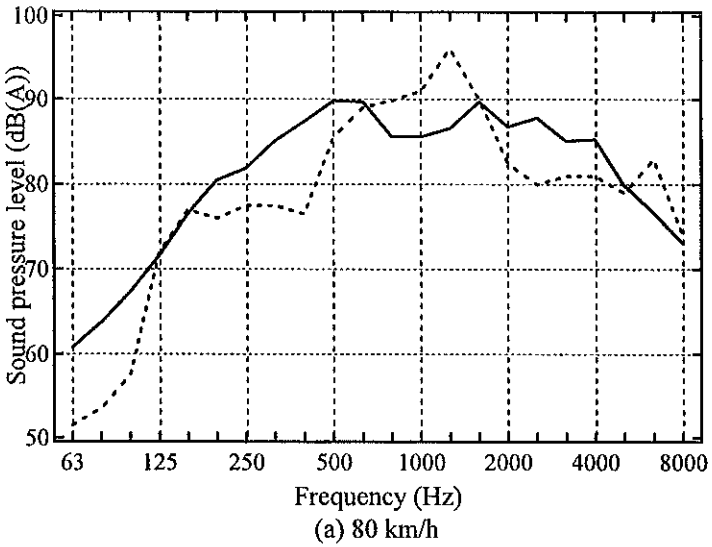

(a) 80 km/h

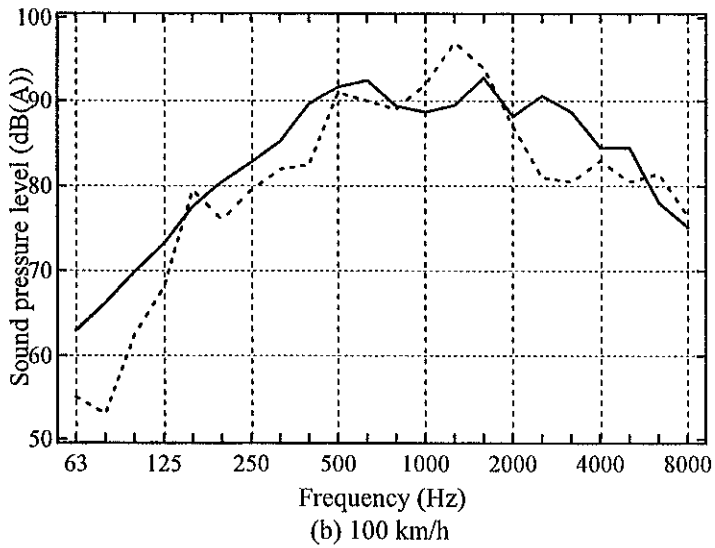

(b) 100 km/h

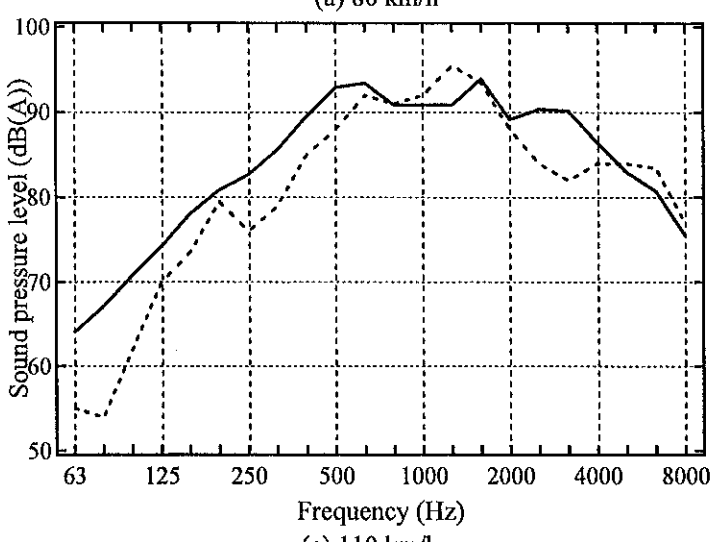

(c) 110 km/h

Figure F17 Predicted rail vibration velocity and measured rail vibration velocity for each train speed using rodel model (Freight B, 81500N, JR2 track, mono-bloc sleeper, ——:predicted,------ :measured, vertical direction)

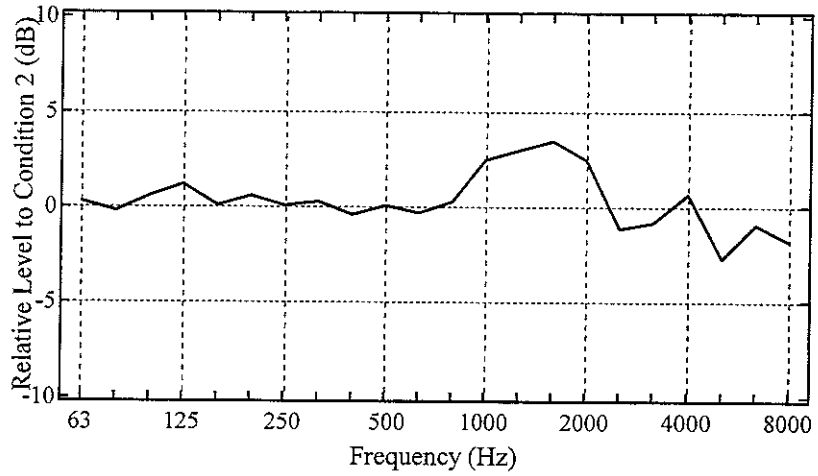

(a) Train speed: 80(km/h)

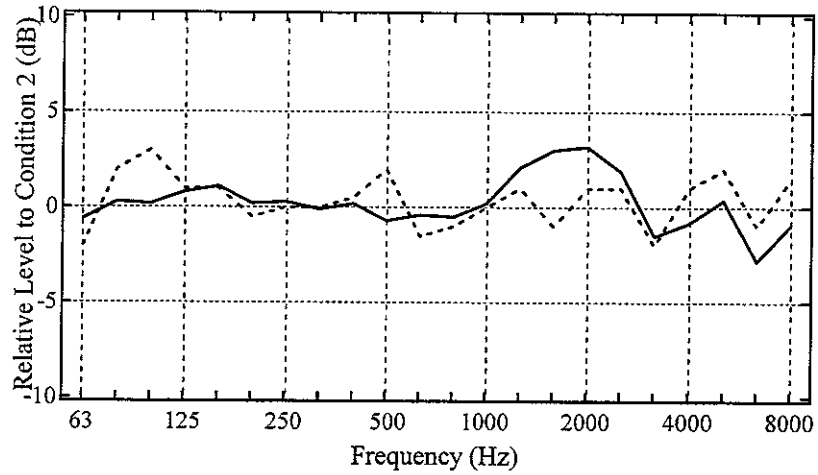

(b) Train speed: 100(km/h)

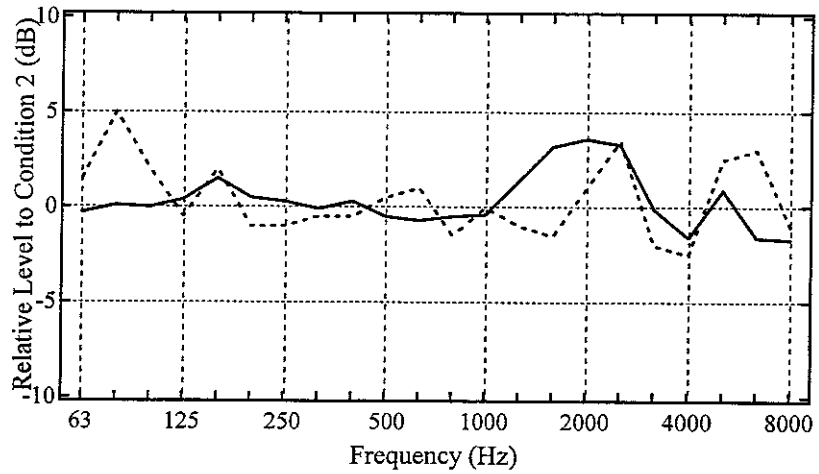

(c) Train speed: 110(km/h)

Figure F18 Difference in rail vibration spectra between two axle load conditions (Freight A, Condition 1: 23500N, Condition 2: 64000N, rodel, mono-bloc sleeper, —:TWINS, ----:Measured results, rail vibration velocity, vertical direction)

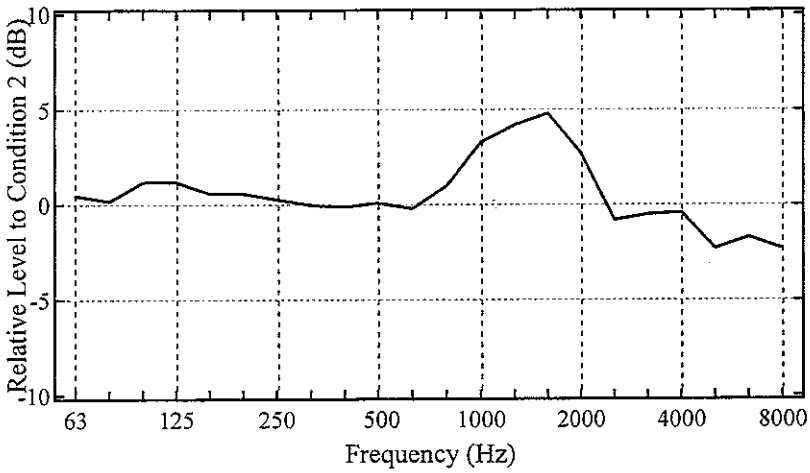

(a) Train speed: 80(km/h)

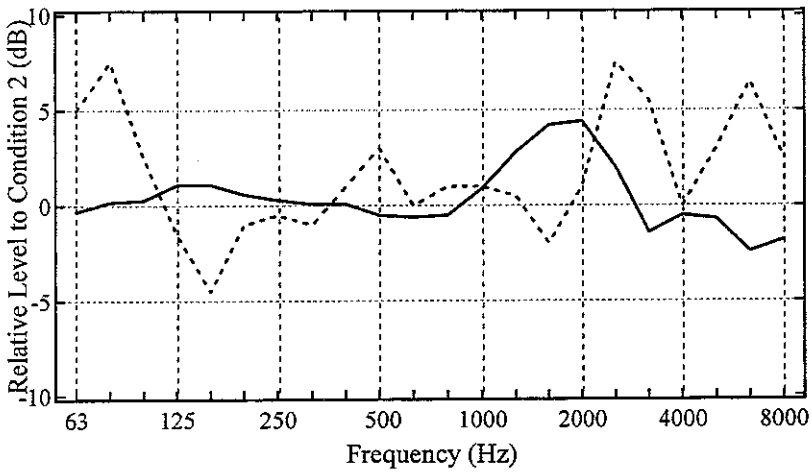

(b) Train speed: 100(km/h)

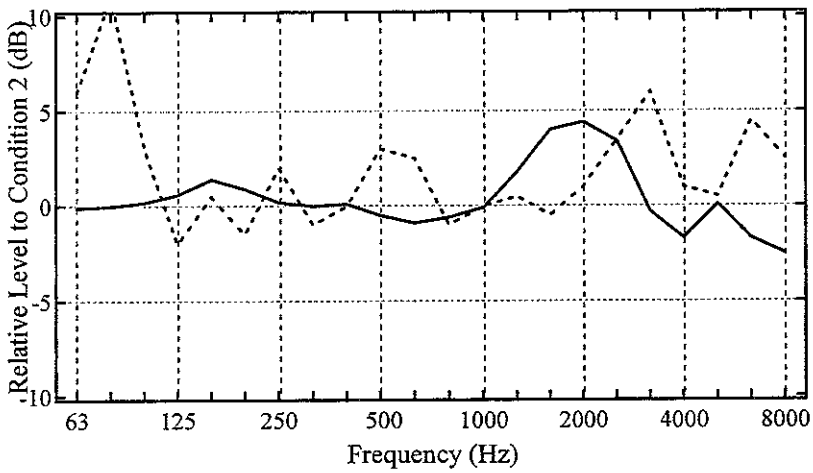

(c) Train speed: 110(km/h)

Figure F19 Difference in rail vibration spectra between two axle load conditions (Freight B, Condition 1: 21500N, Condition 2: 81500N, rodel, mono-bloc sleeper, —:TWINS, ----:Measured results, rail vibration velocity, vertical direction)